PART A
FUNDAMENTALS OF HETEROGENEOUS PHOTOCATALYSIS

AND

PART B
CONSEQUENCES OF INORGANIC AND ORGANIC UV SUNBLOCKS ON DNA

Angela Salinaro

A Thesis
in the
Department of Chemistry and Biochemistry

Presented in Partial Fulfillment of the Requirements
for the Degree of Doctor of Philosophy at
Concordia University
Montreal, Quebec, Canada

May 2001

ABSTRACT

Part A
Fundamentals of Heterogeneous Photocatalysis

Part B
Consequences of Inorganic and Organic UV Sunblocks on DNA.

Angela Salinaro, Ph.D.
Concordia University, 2001

Titanium dioxide is a highly photoactive catalyst used extensively to abate and detoxify polluted waters, air, and soils. It is also commonly employed in commercial sunscreen lotions as a physical filter to block UVA/UVB sunlight radiation, designed to protect people from sunburns and skin cancers. The thesis is two-dimensional. Part A deals with fundamental studies of photocatalysis. Part B addresses more practical considerations of the use of titanium dioxide in suncreams.

The thesis addresses the fundamentals of Heterogeneous Photocatalysis to provide additional understanding of the activity of TiO_2, and of the (primary) events occurring during the photocatalytic process. A protocol is developed for measuring photochemical quantum yields, Φ, in heterogeneous media. Turnover quantities and the nature of photocatalysis are treated mathematically. The spectral dependence of quantum yields and wavelength-dependent selectivities of photocacatalysts are examined for the first time. Of import,

reactions occurring at the TiO_2 particle surface involve hot charge carriers that do not relax down the conduction and valence band electronic manifolds as fast as conventional wisdom had predicted.

Further, the thesis focuses on the genotoxic effects of TiO_2 on DNA. The spectroscopic features of TiO_2, make it an excellent UVA/UVB sunblock. We demonstrate that, when commercial TiO_2 specimens are illuminated with UV radiation, hydroxyl radicals are generated, which. damage supercoiled DNA plasmids and human skin cells as evidenced by single- and double-strand breaks, and kill yeast cells. Passivation of the titania particle surface reduces the photoactivity, of titanium dioxide with profound impact on the photooxidation of phenol. Also, damage to DNA, human skin cells and yeast cells is dramatically attenuated by modified titania samples, thus making them safer for use in sunscreen lotions. Moreover, the modified specimens completely retain their UVB/UVA absorption characteristics.

Contrary to manufacturers claims, commercial sunscreen lotions exposed to simulated sunlight are not photostable. Preliminary spectroscopic and photochemical studies on active ingredients in various solvents are reported. Results indicate that the organic chemical UV filters photodegrade on exposure to simulated sunlight in relatively short time. The nature of the solvent and the presence of oxygen influence the photodegradation. Formation of singlet oxygen is suspected.

PERSONAL ACKNOWLEDGMENTS

A great blessing of the PhD program has been the opportunity to work with a number of talented and generous people, who have taught me and provided assistance in seeing this research project through. First and foremost, I would like to thank Prof. Nick Serpone, my "mentor", whom I regard as the "Father of Heterogeneous Photocatalysis".I have learned immensely from his comments, feedback and steady guidance. Thanks to him, I had the opportunity to spend two fruitful summers (1998 and 1999) in the Department of Biochemistry at Oxford University messing around with DNA, yeast cells, and the like.

During the last four years, my fellow researcher and colleague at Concordia, Dr. Alexei Emeline, has contributed significantly to my understanding the "physics" and "maths" behind photocatalysis. Most important, he is not a mere colleague - he is a good friend. Alexei has also provided invaluable advice and insights that have helped me better appreciate the more general, overall aspects of physics and chemistry. I am also grateful to Dr. Ryabchuck of St. Petersburg State University, Russia, for his contribution to the overall appreciation of photocatalysis.

I consider myself very fortunate to have had the opportunity to collaborate with Dr. John Knowland's students and associates at Oxford. They have broadened my horizons by introducing me to the genteel world of biochemistry in short time. Rosemary Dunford, Melanie Gulston, and Robin Parson have provided solid support in assisting with some of the experiments and for providing companionship during my stay at Oxford. I am also grateful to Dr. Knowland for letting me taste some of the traditional life at the prestigious Pembroke College in the beautiful city of Oxford.

Many thanks to Prof. Hidaka and Dr. Horikoshi of Meisei University, Tokyo, for their assistance with some of the X-ray and FT-IR measurements on our titanium dioxide specimens. I am also thankful to Concordia's Mr. Bert Patterson for some X-ray experiments and to Prof. LevanMao and David Ohayo for the BET experiments on some of the titanium dioxide specimens. I also wish to thank my friends Alessandra and Parvin who have provided critical help in enhancing the quality of the graphics and pictures.

Finally, I thank my family (Anna Maria, Umberto, and Maurizio) for being the reference point through the many storms in my life. Their love has kept "the ship on course". Lastly, but certainly not least, my deepest gratitude goes to my father Nino, for having strongly supported and believed in me through all the years to become a scientist.

PROFESSIONAL ACKNOWLEDGMENTS

This thesis enterprise is written in a manuscript-based style, with chapters either already published as full journal articles, or soon to be submitted for publication. Consequently, some of the references and parts of the discussion/text may seem repetitive, but that is the ultimate result of this approach. As well, some symbols defining a given parameter may differ from one chapter to another. Nonetheless, each chapter is self-contained so that the interested reader will not need to perform undue aerobic exercises.

Several people have intellectually contributed, and as is often the case have also contributed in some of the experiments because a few of the techniques used and/or the required sophisticated instrumentations were either not accessible or not available in house. It is appropriate therefore to acknowledge their specific contribution(s). In our group, Dr. Emeline provided much of the theoretical backdrop for Chapter 5 and to some extent for Chapter 4, whereas Chapter 1 formed the basis of a larger review article of Prof. Serpone's introductory plenary lecture given recently at the Cairo Conference (April 3-8, 2001) on Applied Photochemistry. Chapters 2 and 3 are based entirely on the thesis author's experimental work and significant intellectual discussions held within Prof. Serpone's group and with the other co-authors regarding the nature of photocatalysis. In Chapter 7 the author's contribution was no less significant; our Japanese collaborators assisted with the X-ray determination of the anatase/rutile ratios and Dr. Knowland's student (Rosemary Dunford) provided the biochemical assays. I am indeed grateful for their contribution and collaboration that have made the enterprise more enjoyable.

Chapter 1

A. Emeline, A. Salinaro, V.K. Ryabchuk, and N. Serpone, "Photo-Induced Processes in Heterogeneous Photocatalysis. From Photoexcitation to Interfacial Chemical Transformations", *International Journal of PhotoEnergy*, **in press** (2001).

Chapter 5

A.V. Emeline, A. Salinaro, and N. Serpone, N., "Spectral Dependence and Wavelength Selectivity in Heterogeneous Photocatalysis. I. Experimental Evidence from the Photocatalyzed Transformation of Phenols", *J. Phys. Chem. B*, **104**, 11202 - 11210 (2000).

Chapter 4

N. Serpone, A. Salinaro, A. Emeline, and V.K. Ryabchuk, "Turnovers and Photocatalysis. A Mathematical Description", *J. Photochem.Photobiol. A: Chem.*, **130**, 83-94 (2000).

Chapter 2

N. Serpone and A. Salinaro,"Terminology, Relative Photonic Efficiencies, and Quantum Yields in Heterogeneous (solid/liquid and solid/gas) Photocatalysis. Part I: Suggested protocol"; *Pure & Appl. Chem.*, **71**, 303-320 (1999).

Chapter 3

A. Salinaro, A.V. Emeline, J. Zhao, H. Hidaka, V.K. Ryabchuk, and N. Serpone, "Relative Photonic Efficiency and Quantum Yields in Heterogeneous (Solid/Liquid) Photocatalysis. Part II: Experimental determination of Quantum Yields", *Pure & Appl. Chem.*, **71**, 321-335 (1999).

Chapter 7

R. Dunford, A. Salinaro, L. Cai, N. Serpone, S. Horikoshi, H. Hidaka and J. Knowland "Chemical Oxidation and DNA Damage Catalyzed by Inorganic Sunscreens", *FEBS, Letters*, **418**, 87-90 (1997).

À mon père Nino Salinaro

qui me disait dans les moments les plus

difficiles de ma vie

la phrase du célèbre poète Alfieri:

"Volli, sempre volli, fortissimamente volli".

Ces paroles firent de moi une femme forte d'esprit

et m'encouragèrent à poursuivre mes objectifs

avec amour.

Papa, je ne t'oublierai jamais!

Ta fille adoree Angela

Table of Contents

List of Figures

Chapter 1

Chapter 2

Chapter 3

Chapter 6

Chapter 10

List of Tables

Chapter 1

HETEROGENEOUS PHOTOCATALYSIS

GENERAL INTRODUCTION

1. HISTORICAL BACKGROUND

Heterogeneous Photocatalysis has been examined and explored extensively as a potentially viable alternative technology to classical "best" technologies for both environmental detoxification and for energy production [1]. Both fundamental and applied investigations have been pursued over the last two decades. This technology employs illuminated semiconductor particulate materials, e.g. TiO_2, as photocatalysts to produce both reducing and highly oxidizing species on the particle surface poised to unleash redox processes in aqueous media, many of which would not otherwise be possible by normal chemical means.

Indeed heterogeneous photocatalysis has seen its initial development with the several studies in the late 1970s to early 1980s [2] which explored ways to photogenerate clean alternative fuels (e.g. dihydrogen from water) with the realization that processes carried out

with organized assemblies afforded some advantages over homogeneous processes. Semiconductor materials provided several interesting features toward this end, not least of which was chemical stability and the possibility to modify the semiconductor particle surface, itself possessing good catalytic characteristics, by addition of functional or bifunctional catalysts (e.g. Pt and RuO_2) to improve the overall catalytic functions and to accentuate process kinetics.

In the last two decades Serpone's laboratory has made significant contributions to heterogeneous photocatalysis both in (a) demonstrating the general usefulness of photocatalysis [3] and in its development [4] toward a viable technology with potential attributes in energy conversion and in resolving environmental issues. together with (b) efforts to unravel and understand the events occurring at the particle surface and at the particle/solution interface by application of various time-resolved methods (e.g. picosecond laser spectroscopy [5] and pulse radiolysis [6]). In essence. the principal focus of Serpone's laboratory has been to follow the course of events from the initial interaction of the UV/visible photons with the semiconductor material. to the interfacial events. to product formation (in the case of fuel generation), to the mineralization of environmental polluting organic substances to carbon dioxide and water, and to the removal of toxic or precious and/or strategic metals from waste waters, ground waters, and industrial discarded waste effluents.

Several issues hampered the progress in the fundamental understanding and the underlying issues of heterogeneous photocatalysis with semiconductor particulates [7-9]:

namely,the description of such terms as (i) photocatalysis (i.e., what is photocatalysis?), (ii) turnover quantities (viz., turnover numbers, turnover rates and turnover frequencies; liberally used but too often incorrectly), (iii) quantum yields (here also too often misused), and (iv) the utilization of the Langmuir-Hinshelwood kinetic model to describe the mineralization process kinetics and to associate it automatically as "proof" of the concept or notion that reactions take place at the surface of the photocatalyst particle without any corroborating independent evidence to that effect. In fact, for item (iv) it suffices to note briefly that process kinetics, as too often reported in heterogeneous photocatalysis, are model independent and are simply manifestations of saturation-type kinetics commonly observed even in homogeneous phase processes.

Much of the discussions in the 1990s on the heterogeneous photocatalytic mineralization of organic contaminants, mediated by titania particulates (mostly in the anatase form), centered on the mechanistic details to improve the photocatalytic activity of the photocatalyst, and to understand the role and importance of ***free*** versus ***surface-bound*** oxidizing radicals (e.g., •OH radicals) on the one hand and *versus* direct hole oxidation on the other. It was clear by the mid-1990s that if the potential of TiO_2 as the photocatalyst material in photocatalytic processes was to be maximized, a better understanding of the chemical nature of the photogenerated electrons and holes, and of the role(s) these species played in heterogeneous reactions at the TiO_2/solution interface was required. Despite the many efforts since the early 1990s [10], the mechanistic details of the photocatalyzed oxidative degradation of organic substances remains nonetheless a matter of current debate.

especially the initial events/processes that occur on interaction of the photons with the photocatalyst particle in the bulk and at the surface.

Consequently, it is relevant and instructive to examine very briefly some of the recent work undertaken in the LPASECM laboratory related to some of the issues raised above and germane to our fundamental understanding of the events occurring in heterogeneous photocatalysis involving semiconductor and insulator materials. In this regard, the first part of the thesis addresses some of the relevant problems in heterogeneous photocatalysis and provides possible solutions to fundamental questions.

2. GENERAL CONSIDERATIONS OF PROCESS EFFICIENCIES IN METAL-OXIDE PHOTOCATALYSTS

Of all the metal oxides, the titanium dioxide semiconductor TiO_2 has been investigated extensively in heterogeneous photocatalysis as a means to abate and detoxify polluted waters, air and soils [11-15]. The focus of most researchers in this area (notably the groups of Fujishima at the University of Tokyo and Anpo at Osaka University in Japan, among several others) has been to develop highly photoactive TiO_2 specimens so as to boost the efficiency of the photocatalytic process. In spite of the large and excellent body of literature that demonstrates the utility of TiO_2 in such endeavors, understanding the (primary) events in photocatalysis has lagged considerably behind. In particular, a major issue has been the lack of an appropriate protocol to compare the photocatalytic activities of different photocatalysts in different heterogeneous systems and the work from the different

laboratories. Therefore, the quantitative description and characterization of photostimulated processes in such heterogeneous systems remains a matter of current interest. A protocol for measuring quantum yields of heterogeneous photocatalytic processes, Φ, was proposed in recent work [16-18] (see Chapters 2 and 3).

A few parameters have been suggested for the characterization of photocatalytic activities in heterogeneous systems. One is the photonic efficiency ξ which expresses the ratio between the rate of molecules formed or degraded in the system, dN_r/dt (molecules s^{-1}) and the rate of incident photons impinging on the system, $dN_{h\nu}(inc)/dt$ (photons s^{-1}) at some given wavelength (some workers have incorrectly taken ξ to be equivalent to the quantum yield). In other words, photonic efficiency is a reaction rate normalized to the photon flow from the light source that describes how many molecules are transformed per photon acting on the system.

Another parameter used to characterize the photochemical activity of heterogeneous systems is of course the more fundamental parameter quantum yield (Φ; eqn 1) of the

$$\Phi = \frac{\dfrac{dN_r}{dt}}{\dfrac{dN_{h\nu(abs)}}{dt}} \qquad (1)$$

photoreaction and defined in homogeneous photochemistry as the ratio between the rate of

molecules formed or converted in the system, dN_r/dt (molecules s^{-1}), and the rate of photons ***absorbed*** by the system, $dN_{h\nu}(abs)/dt$ (photons s^{-1}) at a given wavelength. Thus, Φ represents how many molecules are transformed per photon **actually absorbed**. The essential difference between photonic efficiency ξ and quantum yield Φ in heterogeneous photochemistry is that not every incident photon will necessarily act upon the heterogeneous system and initiate the chemical transformation. Consequently, and especially for weak absorption of light, although the photonic efficiency may be close to 0, the quantum yield may nevertheless reach high values. Appropriate determination of the fraction of absorbed light in heterogeneous systems has made the measurements of quantum yields a complex issue.

To establish both the photonic efficiency and the quantum yield of a photostimulated reaction in heterogeneous systems, two important conditions must be satisfied [19,20]: (i) the reaction rate must scale linearly with photon flow, and (ii) the reaction rate must be independent of the concentration of reagent. Otherwise, if both photonic efficiency and quantum yield depended on photon flow and reagent concentration, the photocatalytic activities described by ξ and Φ from different heterogeneous systems and different laboratories could not be compared. Indeed, if the reaction rate of a photocatalytic process were given by equation 2,

$$\frac{dC}{dt}(\rho,C) = (const)\ C^n\ \rho^m \qquad (2)$$

then the quantum yield of the process would be given by:

$$\Phi = \frac{\frac{dC}{dt}(\rho,C)}{A\ \rho} = (const)'\ C^{n}\ \rho^{m-1} \qquad (3)$$

where A represents the fraction of the photon flow absorbed by the heterogeneous system, ρ is the photon flow from the radiation source, and C is the concentration of the substrate undergoing conversion.

Clearly, the quantum yield is a constant only if $n = 0$ and $m = 1$. In recent work, Emeline and coworkers [19,20] established that the reaction orders m and n of the photodegradation of phenol over TiO_2 and the photostimulated adsorption of oxygen on ZrO_2 are interdependent. The reaction order m varies with reagent concentration C, whereas the order n depends on photon flow ρ. The description indicates that $m \rightarrow 1$ if $n \rightarrow 0$, whereas $n \rightarrow 1$ if $m \rightarrow 0$. The results of the kinetic studies (see Figure 1) of photostimulated processes show that the interdependence of the reaction rate can be generalised by eqn 4:

$$(\frac{dC}{dt})(\rho,C) = \frac{\alpha\ \rho\ C}{(\beta\ \rho + \gamma\ C)} \qquad (4)$$

where the coefficients α, β, and γ are independent of light intensity (and photon flow) and

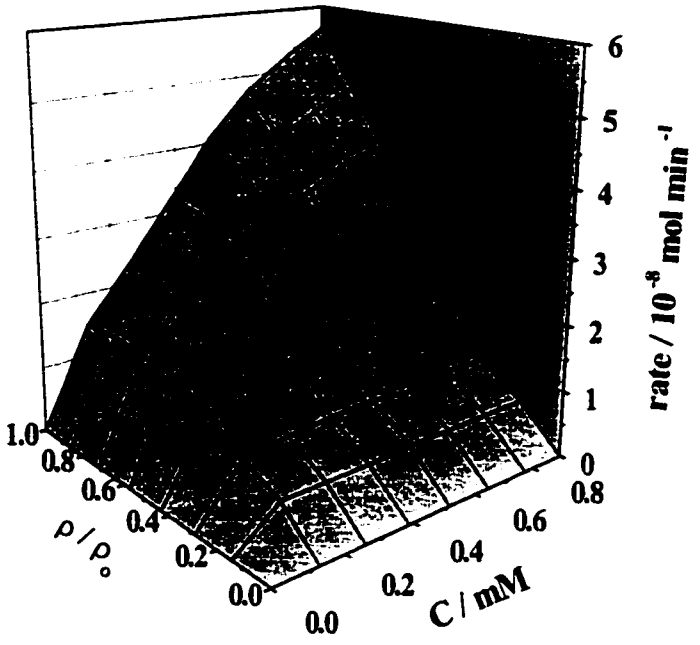

Figure 1. - Three-dimensional dependence of the rate of phenol photodegradation over TiO_2 on its concentration (C) and on photon flow (ρ/ρ_o; $\rho_o = 1.1 \pm 0.3 \times 10^{17}$ photons cm^{-2} sec^{-1} at $\lambda = 365$ nm) of the actinic light. From Emeline et al [16].

reagent concentration. Consequently, the quantum yield of a photochemical process is given by:

$$\Phi(\rho,C) = \frac{\alpha C}{A (\beta \rho + \gamma C)} \qquad (5)$$

Hence, the necessary condition to determine the highest value of the quantum yield independent of concentration and photon flow is for $\gamma C >> \beta\rho$. {Note that under such

conditions, to achieve the higher efficiency of the photocatalyst at lower concentrations of reagent requires a lower light intensity.

To gain a better understanding of the factors that determine the efficiency (quantum yield) of heterogeneous photocatalytic processes Emeline and coworkers [21] considered a theoretical approach that required consideration of both bulk and surface processes in the photocatalyst, along with primary and secondary chemical surface reactions. For simple primary surface chemical reactions in the photooxidative process, one has:

$$h_s^{\cdot} + OH_s^{-} \rightarrow \bullet OH_s \qquad k_6 \qquad (6)$$

$$\bullet OH_s + e_s^{-} \rightarrow OH_s^{-} \qquad k_7 \qquad (7)$$

$$\bullet OH_s + M \rightarrow (M\text{-}\bullet OH) \qquad k_8 \qquad (8)$$

In the steady-state approach for the concentration of surface $\bullet OH_s$ radicals and charge carriers (electrons, e_s^{-}, and holes, $h_s^{\cdot}$), the reaction rate $d[M]/dt$ was given by equation 9:

$$\frac{d[M]}{dt}(\rho,[M]) = \frac{k_6\, k_8\, [h^{\cdot}_s]\, [OH_s^{-}]\, [M]}{k_7\, [e_s] + k_8\, [M]} \qquad (9)$$

By analogy, a similar result was obtained for the photoreduction reaction with participation of such electron surface active centers as Ti^{3-} (reactions 10-12).

$$Ti^{4+}{}_s + e^- \rightarrow Ti^{3+}{}_s \qquad k_{11} \qquad (10)$$

$$Ti^{3+}{}_s + h^+ \rightarrow Ti^{4+}{}_s \qquad k_{12} \qquad (11)$$

$$Ti^{3+}{}_s + M \rightarrow Ti^{4+}{}_s + \bullet M^- \qquad k_{13} \qquad (12)$$

Reactions 8 and 12 represent the primary oxidative and reductive chemical events, respectively, of the catalytic cycle; processes 6 and 10 show the generation of surface active centers; and reactions 7 and 11 reflect the deactivation of such centers. Both generation and deactivation of surface active centers form the particular pathway of surface recombination of free carriers.

To the extent that the surface concentrations of the free carriers are proportional to the photon flow of the actinic light, equation 9 is equivalent to the experimental dependence expressed by equation 4 and demonstrates the interdependence of the reaction rate on photon flow and concentration of reagent [19]. The necessary condition $\gamma C >> \beta \rho$ to observe the higher quantum yield of the photocatalytic process is satisfied when $k_{13}[M] >> k_{12}[e_s]$, that is when the rate of chemical decay of the surface active sites is much greater than the rate of their physical recombination process. Note that at constant light intensity, which provides constant surface concentrations of free charge carriers, both equations 4 and 9 could easily be transformed into the Langmuir-Hinshelwood (LH) kinetics equation, although strictly speaking the mechanism represented by reactions 6-8 corresponds to the Eley-Rideal (ER) mechanism. For the LH pathway, the notation M in reaction 8 represents the pre-

adsorbed molecules of reagent whose concentration obeys the Langmuir adsorption isotherm. That is,

$$[M_{ads}] = \frac{[S_o]\ K[M]}{1 + K[M]} \tag{13}$$

The reaction rate expression is then [22],

$$\frac{d[M]}{dt}(\rho,[M]) = \frac{k_6\ k_8\ [h^+_s]\ [OH^-_s]\ [S_o]\ K\ [M]}{k_7\ [e_s] + (k_7\ [e_s] + k_8\ [S_o])\ K\ [M]} \tag{14}$$

Equation 14 can also be transformed into the classic LH equation at constant photon flow; it demonstrates the interdependence of the reaction rate on photon flow and on the concentration of reagent. However, in spite of the similar behavior of ER and LH kinetics, there is nevertheless a subtle difference in the approximations of the so-called apparent Langmuir constant (K_L) in the two mechanistic models [20].

$$K_L = \frac{k_8}{k_7\ [e_s]} \qquad \text{(In the ER-mechanism)} \tag{15}$$

$$K_L = \frac{(k_7\ [e_s] + k_8\ [S_o])\ K}{k_7\ [e_s]} \qquad \text{(In the LH-mechanism)} \tag{16}$$

For example, at very high photon flow (i.e., when $[e_S] \rightarrow \infty$) $K_L \rightarrow 0$ in the ER pathway, whereas $K_L \rightarrow K$ in the LH mechanism.

At sufficiently high concentration of reagent, when the chemical reaction dominates the physical pathway of the surface recombination of carriers, the reaction rate equals the rate of generation of surface active centers {e.g., surface •OH radicals for oxidative processes (eqn 17) and electron centers (Ti^{3+}) for reductive reactions} and is proportional to the surface concentration of free charge carriers of the corresponding sign. The latter can be found from

$$\left(\frac{d[M]}{dt}\right) = k_6 \, [h^{\cdot}_s] \, [OH^{-}_s] \tag{17}$$

the solution to the continuity equation under the steady-state approximation [17]:

$$\frac{\partial n(x,\ t)}{\partial t} = -\frac{\partial J_n(x,\ t)}{\partial x} - \frac{n(x,\ t)}{\tau} + G(x,\ t) = 0 \tag{18}$$

with the boundary condition given by equation 19,

$$J_s = s \, n_s \tag{19}$$

where $n(x,t)$ is the concentration of free charge carriers at a given point in space with spatial coordinates x at a given time t ; $J(x,t)$ is the flow of charge carriers caused either by diffusion or by drift; $G(x,t)$ is a time-space function of carrier photogeneration; τ is the

lifetime of carriers in the bulk of the solid; and s is a constant of the surface recombination represented by reactions 6, 7, 10, and 11.

3. FURTHER OBSERVATIONS

The conventional band model describes a semiconductor in terms of two bands (Figure 2) : the valence band which is typically composed of $2p$ orbitals of the oxide O^{2-} ions in a metal oxide semiconductor and of a conduction band typically made up of the nd orbitals of the M^{x-} ions. These two bands are separated by a forbidden band gap (E_{BG}) within which there may exist surface states (ss). These bands are also thought to consist of a very large number of closely spaced energy levels, such that when the semiconductor is illuminated with light of energy greater than the bandgap energy E_{BG} to generate free charge carriers. these carriers are expected to thermalize rapidly to the lowest energy level of the conduction band (CB) for electrons and to the "lowest energy level" of the valence band (VB) for the holes. Conventional wisdom dictates that whatever the ensuing redox reactions may be, they will take place from the lowest energy levels of a given charge carrier, and thus there should be no spectral dependence of the quantum yields or whatever other parameter is employed to assess the photon efficiencies.

Subsequent to photoexcitation then, generation of charge carriers occurs either from band-delocalized electronic states associated with the regular lattice (VB and CB), or from the intragap-localized electronic states associated with lattice irregularities or defects in the solid (ss). It is relevant to distinguish between *intrinsic* (excitonic and band-to-band

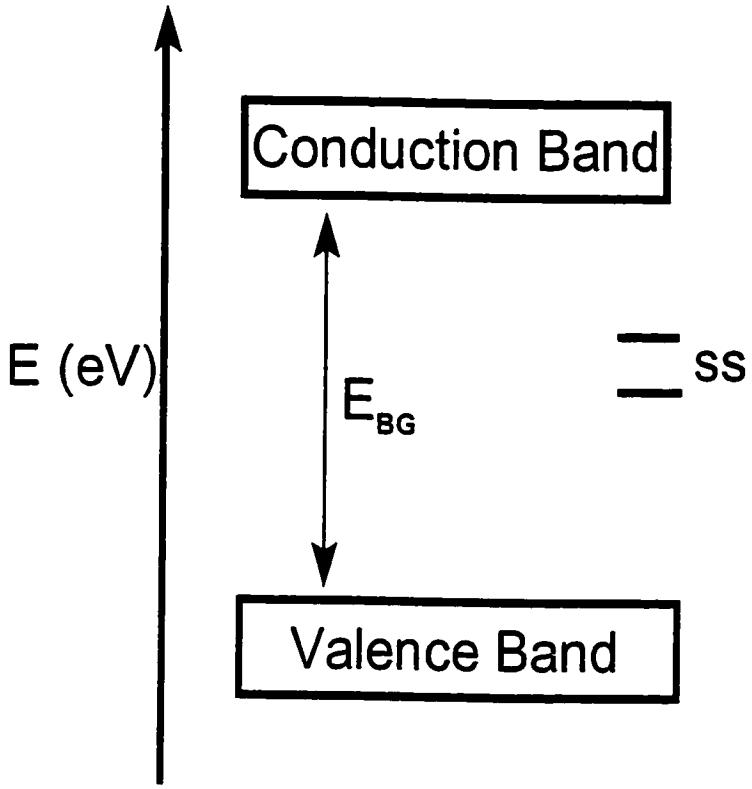

Figure 2. - Conventional view of the band model of semiconductors.

excitation) and *extrinsic* (excitation of impurities, defects, and surface states) light absorption [23]. Effects of surface absorption may also be observed because of the peculiarity of surface processes (e.g., surface reconstruction and relaxation processes, and formation of new surface structures). *Extrinsic* absorption by solids normally occurs at energies lower than for *intrinsic* absorption. {Note that *extrinsic* surface absorption is sometimes red-shifted by a few eV relative to the *intrinsic* fundamental absorption edge of wide bandgap insulators [23]}.

It is also important to recognize that the lifetime of photogenerated charge carriers, τ, is determined by a set of carrier recombination and trapping processes involving solid lattice defects, in particular anion and cation vacancies (V_a, V_c), and lattice ions in low-coordinated positions:

(20) $e + R \rightarrow R^-$ (21) $h + R^- \rightarrow R$

(22) $e + V_a \rightarrow \boldsymbol{F}$ (23) $h + V_c \rightarrow \boldsymbol{V}$

(24) $e + \boldsymbol{V} \rightarrow V_c$ (25) $h + \boldsymbol{F} \rightarrow V_a$

In the six reactions above, stages 20 and 21 describe fast electron/hole recombination through specific recombination centers R which are generally responsible for the lifetime of carriers; stages 22 and 23 represent trapping of the carriers by lattice defects such as anion vacancies V_a and cation vacancies V_c, respectively, to form the so-called ***F***- and ***V***-type color centers with corresponding new absorption bands in the spectra of the solid. Stages 24 and 25 describe the decay of color centers during irradiation due to their recombination with carriers of the appropriate sign. These processes (reactions 24 and 25) are typically slow enough to allow accumulation of photoinduced color centers in solids. After irradiation is stopped, the lifetime of newly formed photoinduced color centers is often quite long (from seconds to hours under certain conditions).

Because of the exchange of charge carriers between the bulk and the surface in a solid

photocatalyst, there is a strong co-influence between surface processes (reactions 6-8 and 10-12) and the bulk processes (stages 20-25) involving free carriers, particularly between surface chemical reactions and photoinduced coloration of solids [24-26].

Surface recombination processes are similar to those in the bulk. Some are represented by reactions 6,7 and 10,11. However, the greater defective nature of the surface, owing to specific surface defects such as corners, edges, terraces, dislocations and new near-surface structures, may lead to a greater rate of carrier recombination on the surface compared to the bulk. This decreases the concentration of carriers $\{n(x)\}$ at the near-surface space in the solid [21], leading to the diffusion of carriers $\{J_n\}$ from the bulk to the surface (eqn 26).

$$J_n = -D\frac{\partial n}{\partial x} \tag{26}$$

Another cause for the flow of carriers toward the surface or from the surface is the surface charge that causes carriers to drift and whose direction is determined by the charge of the carriers and of the surface.

$$J_n = \mu n(x)E(x) \tag{27}$$

where μ is the mobility of the carriers, and $E(x)$ refers to the electric field at a distance x from the surface. However, if the size of the photocatalyst particles is much less than the Debye

screening length, the contribution of carrier drift to carrier flow becomes negligible.

Emeline et al [21] solved the continuity equation 18 for a one-dimensional infinite plate model which considered a non-uniform function of carrier generation that obeys the Lambert-Beer law; diffusion was the major path of carrier flow to give the spatial distribution of carriers in the bulk of the solid (see Figure 3). The expression for the surface concentration of carriers was given by [21],

$$n_s = \frac{2(1 - e^{-\alpha d})\,\chi\,\rho\,\alpha\,L^2}{D\,(\tanh(\frac{d}{2L}) + \zeta)\,(1 - \alpha^2 L^2)}\,[\tanh(\frac{d}{2L})\coth(\frac{\alpha d}{2}) - \alpha L] \qquad (28)$$

where α is the absorption coefficient of the solid, d is the thickness of the plate, $L = (D\tau)^{1/2}$ is the diffusion length of carriers, and ζ is a ratio of rates of surface to bulk recombinations. Substitution of the surface concentration of carriers (eqn 28) into equation 17 for the reaction rate, followed by substitution of the resulting expression into equation 1 for the quantum yield {where $A = 2(1 - e^{-\alpha d})$ for the infinite plate irradiated from both sides} resulted in expression 29 for the quantum yield Φ of the primary surface chemical process [21]:

$$\Phi = \frac{k_{ir}\,S\,\chi\,\alpha\,L^2}{D\,(\tanh(\frac{d}{2L}) + \zeta)\,(1 - \alpha^2 L^2)}\,[\tanh(\frac{d}{2L})\coth(\frac{\alpha d}{2}) - \alpha L] \qquad (29)$$

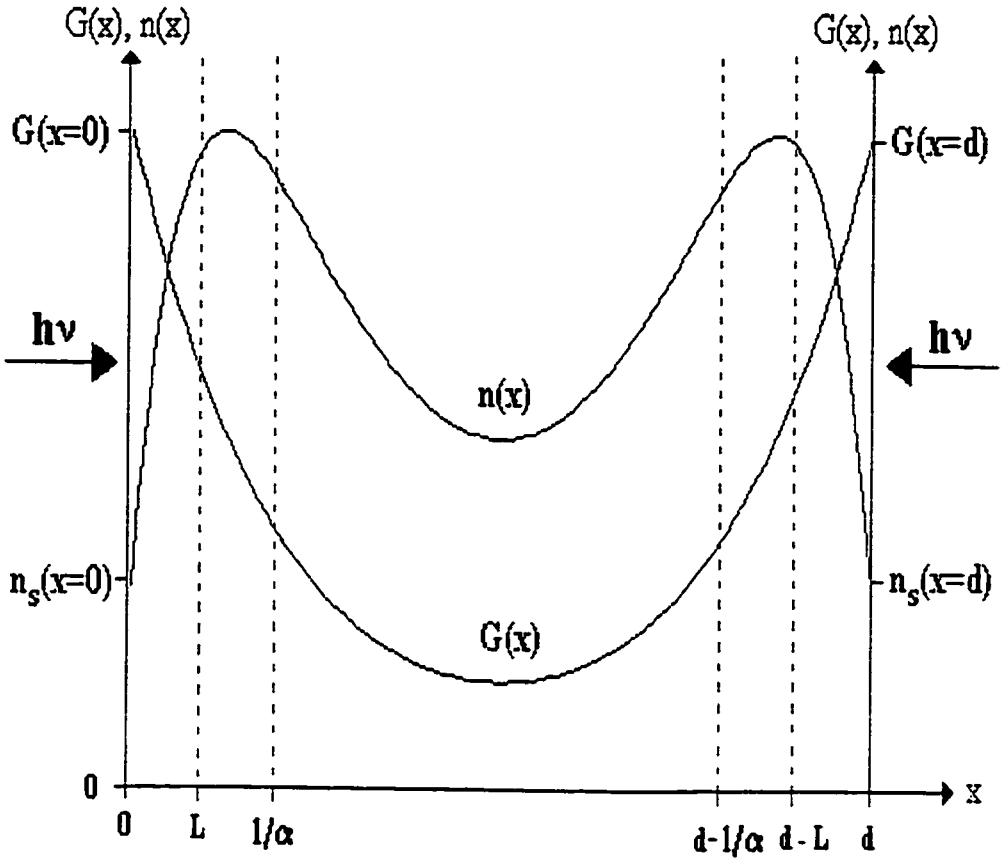

Figure 3. - Scheme of an infinite solid plate with thickness *d* irradiated uniformely from both sides. The curve *G(x)* describes a non-uniform spatial distribution of carrier photogeneration. The straight vertical lines between the surface and the bulk define a depth equal to the average diffusion length of the carriers *L* and average length $1/\alpha$ of light penetration into the bulk. The carriers generated within the diffusion length can reach the plate surfaces by diffusion migration. Those generated in the remaining part of the lattice bulk cannot take part in surface chemical processes. The curve *n(x)* represents the spatial distribution of the concentration of free charge carriers. From ref. [21].

where S is the concentration of surface active sites (e.g., surface OH^- groups or surface electron traps, Ti^{4+}) and k_{tr} corresponds to either k_6 or to k_{10}, respectively.

Equation 29 suggests that a spectral variation of the absorption coefficient α leads to a spectral variation of the quantum yield of a chemical process, and permits inferences on the conditions which determine whether the quantum yield is spectrally dependent or spectrally independent. Specifically, the quantum yield is spectrally independent in the case of very strong fundamental absorption (i.e. when $\alpha \rightarrow \infty$) and when absorption is weak (i.e. for $\alpha \rightarrow 0$) corresponding to *extrinsic* light absorption. The quantum yield is also spectrally independent in the case of light absorption by surface states. At αL comparable to unity, Φ becomes spectrally variable and grows with increasing absorption coefficient α (that is, as αL increases; see e.g. Figure 4). The reasons for such a behavior are that the spectral variations of the absorption coefficient change the number of carriers generated within the diffusion length (L) from the surface that can reach the surface and participate in surface photoreactions. For weak light absorption, the ratio of the number of such carriers to the number of absorbed photons is constant, so that the quantum yield of a surface photoreaction on a given photocatalyst depends on the ratio $d/2L$. During the growth of the absorption coefficient α, more carriers are generated within the diffusion length distance from the surface leading to an increase in the quantum yield of surface chemical reactions. For the

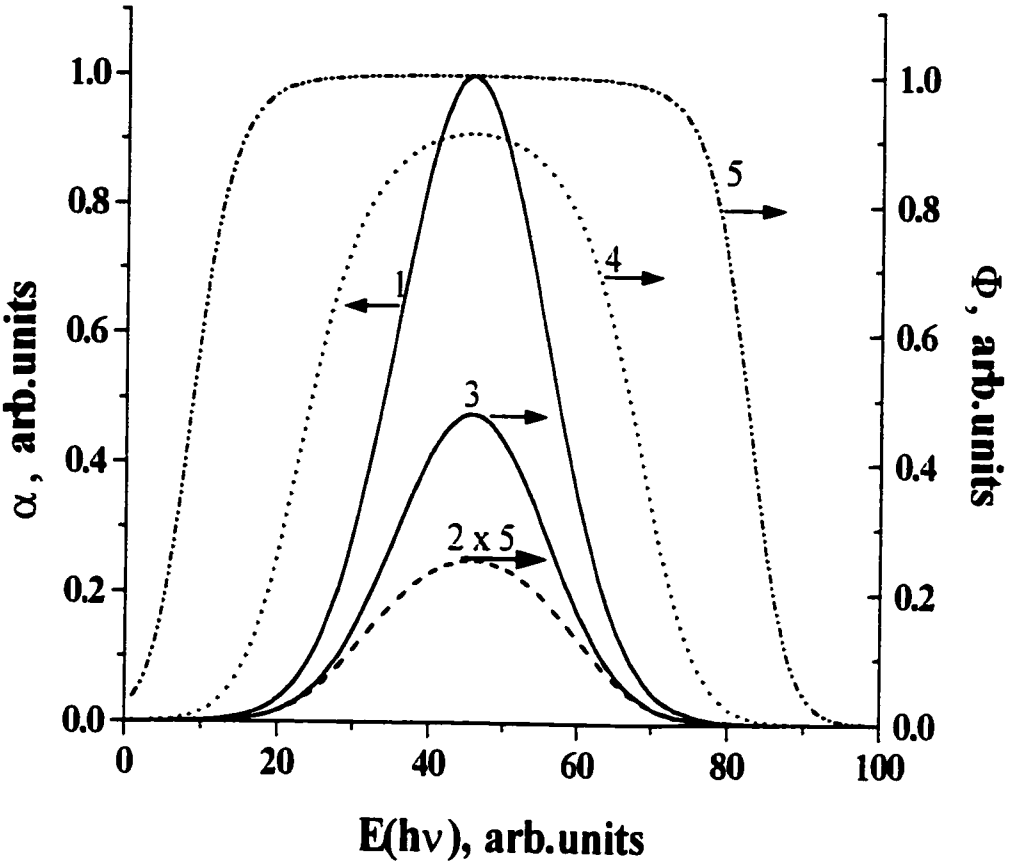

Figure 4. - Spectral dependencies of the quantum yield within a single absorption band (curve 1) for different values of the co-relationship αL: (curve 2), $\alpha L = 0.1$; (curve 3), $\alpha L = 1$; (curve 4), $\alpha L = 10$; (curve 5), $\alpha L = 1000$. From ref. [21]. {Note that curve 2 has been amplified fivefold for easier viewing}.

case of very strong absorption, all carriers are generated within the diffusion length or at the surface, and with a certain probability of participating in surface processes.

More complex events take place when the absorption spectra of solids are formed by

the overlap of several single absorption bands belonging to different types of light absorption, and that differ either (a) by their abilities to form free carriers (internal quantum yield of photoeffects, χ) and/or (b) by the properties (mobility, lifetime) of newly generated carriers. Emeline and coworkers [23] have demonstrated experimentally that cause (a) is essential for weak *extrinsic* light absorption by defects,which will lead to step-like (see for example Figures 5 and 6 below) or band-like (see for example Figures 7 and 8 below) spectral dependencies of the quantum yields whose shape is dictated by the degree of overlap of single absorption bands of different types (particularly by the degree of overlap of active and inactive light absorption). Reason (b) becomes important in the spectral range of *intrinsic* (fundamental) light absorption by the solid when the hot carriers generated at a photon energy greater than the bandgap energy are involved in surface processes. In such a case, in addition to the spectral variations of Φ caused by the spectral variation of the absorption coefficient α (see above), especially at the fundamental absorption edge, the spectral dependence of Φ may also be attributed to the spectral variation of the mobilities and lifetimes of carriers generated at different wavelengths (see eqn 29) owing to different direct and indirect band-to-band transitions that result in different initial population of the electronic states in bands. This latter factor is essential provided that communication between different sub-bands is weak enough to render fast thermalization of hot carriers unlikely. In such a case, competition between diffusion of carriers toward the surface and their energy losses are quite effective in small particles and promote the involvement of carriers with excess energy into surface processes. The latter may also affect the reactivity of surface

active sites.

In practice, the actual absorption spectrum of the photocatalyst is the result of several overlapping absorption bands of different origins (*intrinsic* bulk and surface absorption, absorption of different types of defects, and free charge carrier absorption, among others). Hence, the spectral dependence of the quantum yield of a surface photochemical reaction is expected to be a composite of the superposition of different types of photoexcitation of the solid. Accordingly, the total rate for a simple photochemical reaction, such as reaction 30, is the sum of the rates of elementary processes considering the photoexcitation in each

$$S + e^{-} \text{ (or } h^{+}) \xrightarrow{k_{tr}} S^{-} \text{ (or } S^{+}) \tag{30}$$

single absorption band separately; thus,

$$\frac{dS}{dt} = R = \Sigma_i R_i = \rho \Sigma_i A_i \Phi_i \tag{31}$$

assuming that

$$R_i = A_i \rho \Phi_i \tag{32}$$

where R_i is the rate of the elementary reaction under excitation in the i-th single absorption band, A_i is the absorbance in the i-th single absorption band, and Φ_i is the corresponding quantum yield of the reaction. Taking the total number of absorbed photons per unit time to

be given by $A\rho = \rho\Sigma_i A_i$ (where A is the total absorbance at a given wavelength) the total quantum yield is given by expression 33:

$$\Phi = \frac{R}{A\ \rho} = \frac{\Sigma_i\ A_i\Phi_i}{\Sigma_i\ A_i} \qquad (33)$$

where Φ_i can be estimated from equation 29 (and any of its simplified forms [21]) taking α as the absorption coefficient resulting from all the different types of light absorption.

In general, excitation in each of the single absorption bands differs from others by the values of the quantum yield of internal photoeffects χ, the corresponding lifetime τ and the diffusion coefficient D of the carriers (and hence by the diffusion length L) depending on the type of delocalized excitation (electrons, holes or excitons), the energy (hot or thermalized carriers) and type of excitation (direct or indirect electronic transitions), the rate of surface recombination s, and the rate constant k_{tr} of carrier trapping either by adsorbed molecules or by the "potential" surface active centers (surface defects) [21]. All these parameters must be considered in the interpretation of the spectral dependence of the quantum yield of surface photochemical processes when using equation 33.

As an example of this interpretation of the spectral dependence of the quantum yield (equation 33), Emeline and coworkers [21] considered the hypothetical absorption spectrum (curve 1) illustrated in Figure 5 in which the absorption spectrum is the result of overlap of two single Gaussian-shaped bands of equal amplitudes and half-widths (curves 2 and 3).

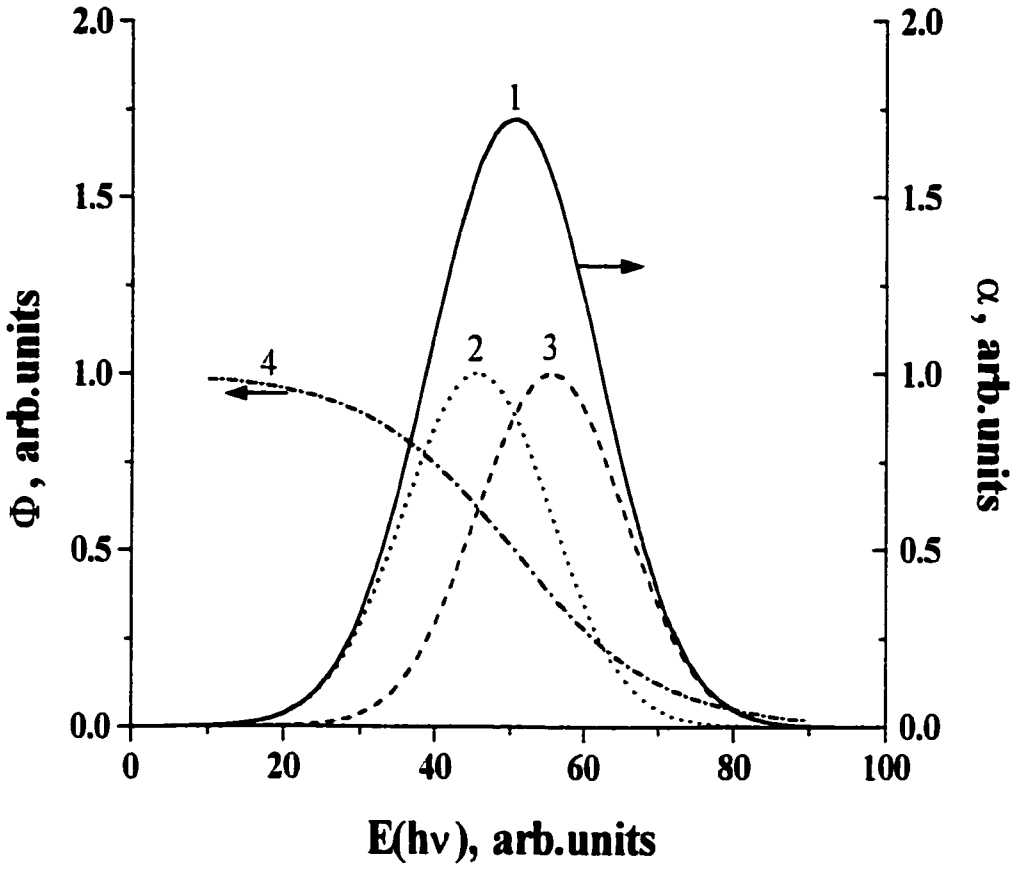

Figure 5. - Spectral dependence of the quantum yield (curve 4) within the absorption spectrum (curve 1) formed by overlap of two single absorption bands: (curve 2), band corresponding to the photochemically active light absorption; (curve 3), band corresponding to the photochemically inactive light absorption. From ref. [21].

Here, curve 2 ($\chi = 1$) is taken to be a photochemically active absorption band and curve 3 ($\chi = 0$) to be a photochemically inactive band. For the case of weak light absorption (that is, for $\alpha d << 1$), the quantum yield $\Phi(h\nu)$ remains constant within the spectral region of

the single active absorption band and within the inactive band $\{\Phi(h\nu) = 0\}$. However, for multi-band absorption (i.e. for their sum, curve 1) $\Phi(h\nu)$ would consist of two spectral regions in which the quantum yield (curve 4) is practically constant (at least initially; see Figure 5) and subsequently a "transition" region is evident where $\Phi(h\nu)$ changes with photon energy.

Experimentally, the expectation from the above discussion and from Figure 5 was corroborated by the observed spectral dependencies illustrated in Figure 6 for the quantum yield of photoadsorption of dihydrogen H_2, methane CH_4, and carbon monoxide CO, and for the photodesorption of pre-adsorbed dioxygen O_2 on scandia Sc_2O_3 [27]. {In this particular case, curve 3 is the photochemically active band, and curve 2 is the photochemically inactive band; the former corresponds to absorption by *V* centers}.

Figure 7 shows another typical situation [21]. Here the absorption spectrum (curve 1) is formed by the overlap of a photochemically active single Gaussian-like absorption band (herein considered as absorption by the surface states, curve 2), and of photochemically inactive and exponentially decaying background absorption (considered herein as absorption by the crystal bulk, curve 3). For surface light absorption [21], the quantum yield is constant (curve 5) within the single band of light absorption by the surface states provided that this type of light absorption only occurs in a given spectral region. However, if account is taken of the total light absorption (curve 1) resulting from the overlap of the active band (curve 2)

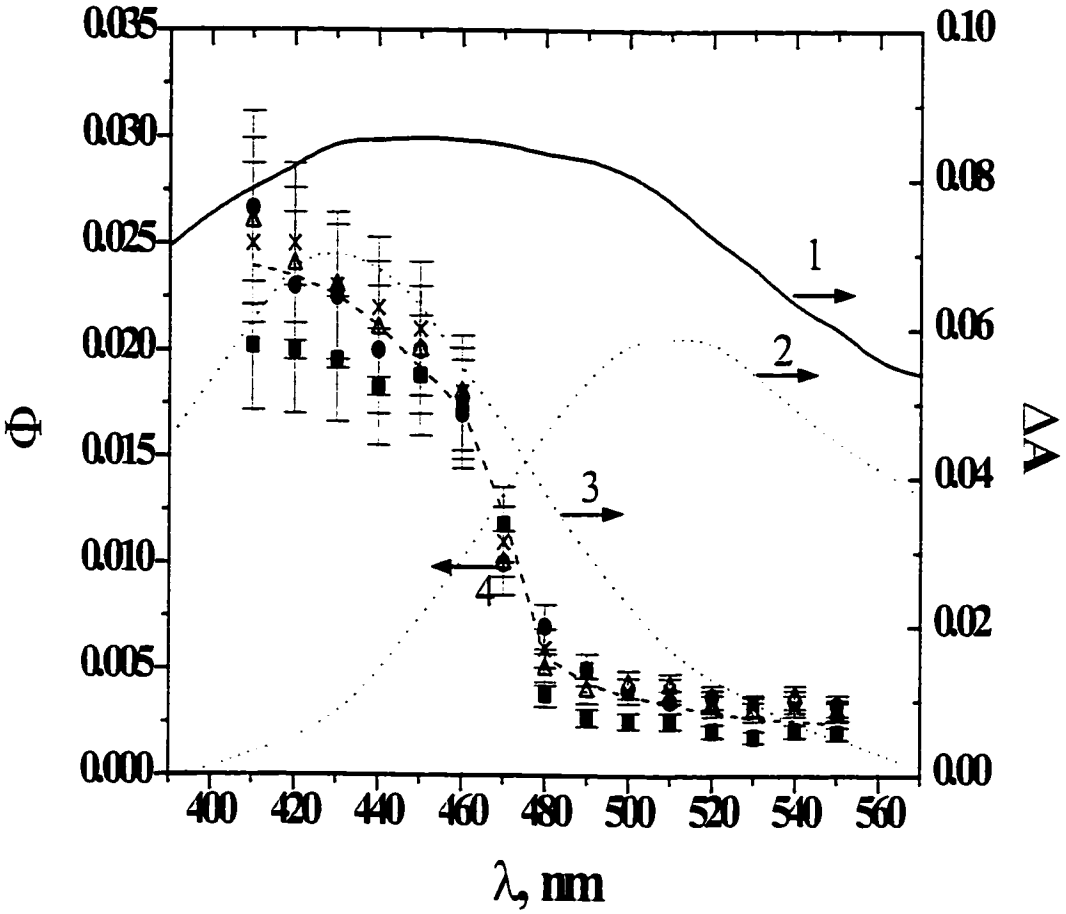

Figure 6. - Spectral dependencies of quantum yields of photoadsorption of hydrogen (▲), methane (X) and carbon monoxide (●) and photodesorption of pre-adsorbed oxygen (■) on Sc_2O_3 within the spectral absorption region of photogenerated color centers (curve 1). Spectra 2 and 3 demonstrate the overlap of the two active single Gaussian-shaped absorption bands in the given spectral region (see Figure 5). The calculated spectral dependence of the quantum yields of surface photoprocesses in the given spectral region is presented by curve 4 (dashed line). From ref. [27].

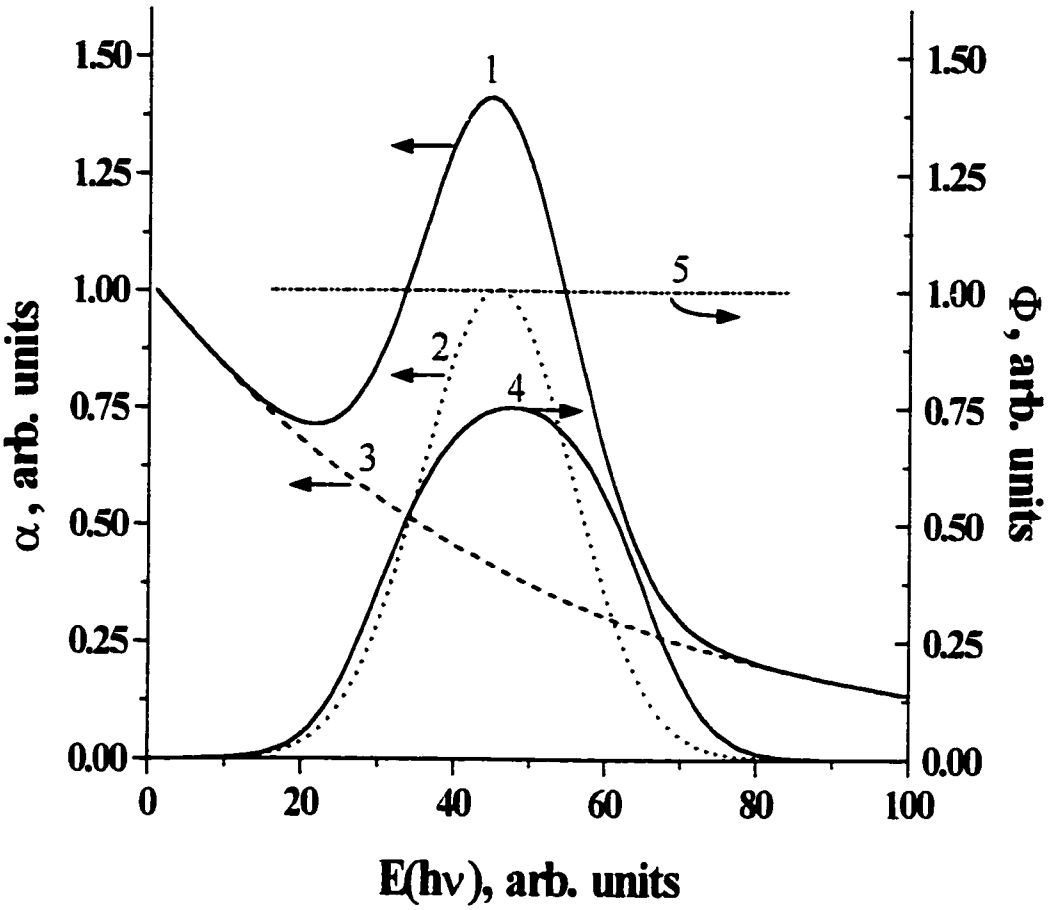

Figure 7. - Spectral dependence of the quantum yield (curve 4) when the absorption spectrum (curve 1) is formed by the overlap of a single absorption band of photochemically active light absorption (curve 2) and by a photochemically inactive background absorption (curve 3). Curve 5 represents the spectral dependence of the quantum yield provided that only the photochemically active light absorption (curve 2) takes place in a given spectral region. From Emeline and coworkers [21].

and the inactive background absorption (curve 3), and if it is further assumed that the similar to the absorption band of the active light absorption. Clearly, in the general case, an active

absorption band-like peak in the $\Phi(h\nu)$ dependence appears because of the inactive yield Φ_i for the photochemically inactive light absorption is 0 (because $\chi = 0$), then the absorption background. The shift of its maximum with respect to the maximum of the active absorption band is more significant the more abruptly the background absorption changes with wavelength. Zero shift would be observed at constant background absorption. On the other hand, the greater the inactive light absorption is the smaller the quantum yield will be. and the greater the resemblance of the shape of the $\Phi(h\nu)$ peak will be to the shape of the single absorption band provided that χ is constant. The latter should be kept in mind when a correspondence between $\Phi(h\nu)$ and $\alpha(h\nu)$ is observed.

Experimentally, the band-like spectral dependent behavior expected from the last discussion and from Figure 7 is depicted in Figure 8 for the spectral dependencies of the quantum yields for the photoadsorption of dioxygen O_2, dihydrogen H_2, and methane CH_4 on powdered TiO_2 rutile particles [23].

The conventional model of semiconductors alluded to earlier and based on the concept of continuity of carrier states within the solid's valence and conduction bands (Figure 2), which infers fast thermalization of the hot carriers, requires revisiting. For this conventional model, the free carriers involved in surface processes are indistinguishable with regard to their properties (lifetimes, mobilities, reactivities) irrespective of the energy of excitation used. Consequently, the simple band model of Figure 2 is not suitable in interpreting the spectral dependence of the quantum yields presented in Figure 8 (and

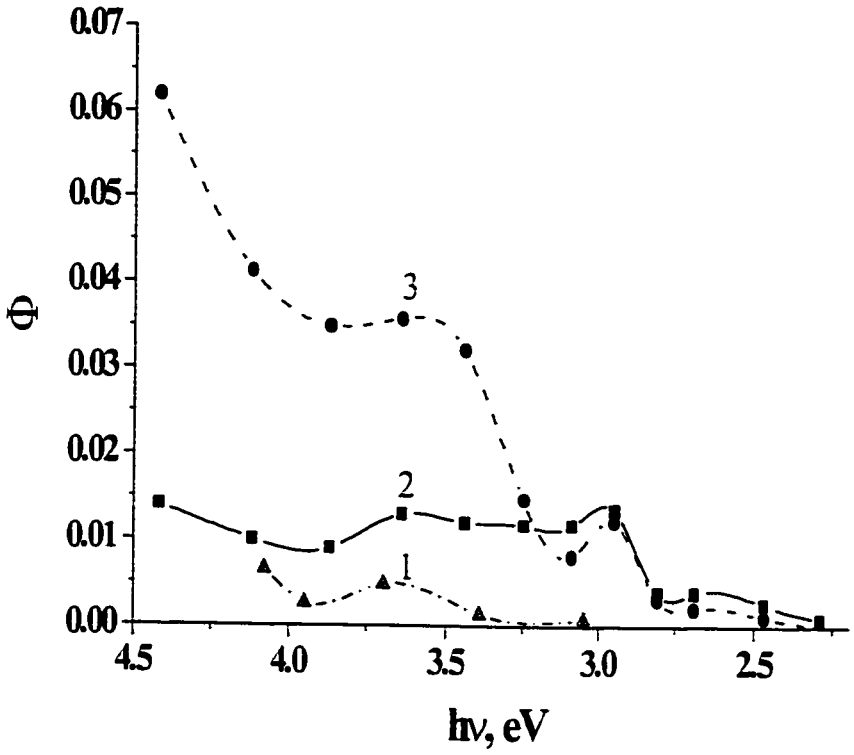

Figure 8. - Spectral dependencies of quantum yields of photoadsorption {at T = 100 K} of oxygen (1), hydrogen (2), and methane (3) on powdered TiO_2 (rutile). From ref. [23].

elsewhere in this thesis; see Chapter 5). It is obvious that one also needs to consider the possibility that the different electronic transitions (direct and indirect) caused by photoexcitation at different wavelengths will lead to different distribution(s) of the population of the electronic states in the (sub)bands (see Figure 6 in Chapter 5) depending on which type of band-to-band transition dominates at the given wavelengths. This is

expected to lead to different pathways for carrier relaxation in the momentum/energy space that will be dictated by the distribution of probabilities for carrier thermalization from the initial photoexcited states to the quasi-thermalized excited states of the carriers. Such distribution(s) will depend on the degree to which the different sub-bands occupied after photoexcitation at a given wavelength communicate with each other. Otherwise, it may lead to the different energetic states of the free carriers and thus to their different kinetic behavior (lifetimes, mobilities, and rate constants of reactions 20-25). In other words, photocarriers generated at the different wavelengths of photoexcitation corresponding to the different electron transitions (different absorption bands within the fundamental absorption region) have a different probability of initiating surface chemical reactions that result in the spectral dependence of the quantum yield.

Another consequence of the solution to the continuity equation 18 is the possibility of analysing the factors that lead to the spectral selectivity of photocatalysts [21]. In particular, the ability of photocatalysts to promote either reductive or oxidative surface reactions depends on the ratio between the concentrations of surface electrons and surface holes. Since surface concentrations of both types of carriers are spectrally dependent (eqn 28), their ratio is generally also spectrally dependent. This may cause a spectral variation in photocatalyst selectivity. Thus far such spectral variations of selectivity have been observed experimentally only for a very few heterogeneous systems. For example, spectral selectivity of TiO_2 was detected for the surface reaction involving (i) methane {under weak light absorption TiO_2 promotes formation of complex hydrocarbons whereas under strong light

absorption the major pathway is oxidation to CO_2 and water} [28], and (ii) for the reactivity of surface oxygen species adsorbed on KBr particles, which depends on whether excitation of the solid occurs in the *extrinsic* absorption region or in the excitonic absorption band [25]. Detailed considerations of the factors resulting from and affecting the spectral selectivity of photocatalysts may be found elsewhere [21,30] (see also Chapter 5).

4. CONCLUDING REMARKS

In this introductory Chapter, we have briefly raised some of the issues that have generally hampered faster progress in the fundamental understanding of heterogeneous photocatalysis and most importantly of the photocatalyst materials, and have examined recent theoretical considerations and predictions that involve quantum yields, which reflect the efficiency of photons absorbed by metal-oxide particles. From these considerations, we noted that on the basis of a simple one-dimensional model and the continuity equation solved by Emeline and coworkers [21], some predictions could be made regarding the spectral dependence of photonic efficiencies and quantum yields. As well, the experimental evidence from other work [23] demonstrates that indeed surface reactions taking place on metal-oxide systems do show a spectral dependence, something totally unexpected from the conventional band model of semiconductors. Clearly, there is a need to revisit this conventional model in light of this and other recent reports in the literature (see ref. [30] and references therein). Subsequent Chapters in this thesis address some of the issues that remain under debate in heterogeneous photocatalysis, namely (i) a description of process efficiencies

{Chapters 2 and 3}, (ii) a description of turnover quantities {Chapter 4}, and (iii) the spectral dependency of quantum yields and photonic efficiencies, together with wavelength selectivity of photocatalysts {Chapter 5}.

5. REFERENCES

[1]. D.M. Blake, "*Bibliography of Work on the Heterogeneous Photocatalytic Removal of Hazardous Compounds from Water and Air (update No. 2)*", January 1997. NREL/TP-430-22197, National Renewable Energy Laboratory, Golden, Colorado.

[2]. See for example, M.A. Fox and M.T. Dulay, *Chem.Rev.*, **93**, 341 (1993).

[3]. See for example: (a) N. Serpone and E. Pelizzetti, "Solar Photochemical Remediation of Air and Water", in *Photoconversion of Solar Energy - Photochemical and Photoelectrochemical Approaches* , M.D. Archer and A.J. Nozik, Eds., Imperial College Press, London, 2001, volume III, Chapter 16.

(b) N. Serpone, "Heterogeneous photocatalytic technology for the detoxification of photographic processing effluents", in *Imaging on the Information Superhighway*, Society for Imaging Science & Technology, Springfield. VA, 1995. pp.186-189.

(c) N. Serpone, "Solar Photochemistry and heterogeneous photocatalysis: A convenient and practical utilization of sunlight photons, in *Photochemical Energy Conversion*, J. Norris Jr., and D. Meisel, Eds., Elsevier, Amsterdam, Holland. 1989, pp. 297-315.

[4]. See for example: (a) H. Al-Ekabi and N. Serpone, "Kinetic studies in heterogeneous photocatalysis I. Degradation of chlorinated phenols in aerated aqueous solutions over TiO_2 supported on a glass matrix", *J. Phys. Chem.*, **92**, 5726 (1988).

(b) N. Serpone, E. Borgarello, and E. Pelizzetti, "The semiconductor particle as a photoelectrochemical cell and its application to photocatalysis", *Proceedings from the Symposium on Photoelectrochemistry and Electrosynthesis on Semiconducting Materials*, D.S. Ginley, A. Nozik, N.Armstrong, K. Honda, A. Fujishima, T. Sakata. and T. Kawai, Eds., The Electrochemical Society, Inc., Pennington, N.J., vol. 88-14, 1988, pp 1-8.

(c) N. Serpone and E. Pelizzetti, "Fundamental studies into the primary events in photocatalysis employing CdS and TiO_2 semiconductors Photoluminescence,laser

flash photolysis, and pulse radiolysis", in *Homogeneous and Heterogeneous Photocatalysis*, E. Pelizzetti and N. Serpone, Eds., Reidel Publ.Co., Dordrecht, Holland, pp 51-90, 1986.

(d) M. Barbeni, E. Pramauro, E. Pelizzetti, E. Borgarello, M. Gratzel, and N. Serpone, "Photodegradation of 4-chlorophenol catalyzed by titanium dioxide particles", *Nouv. J. Chim.*, **8**, 547 (1984).

[5]. See for example: (a) J. Moser, M. Gratzel, D.K. Sharma, and N. Serpone, "Picosecond time resolved studies of photosensitized electron injection in colloidal semiconductors", *Helv. Chim. Acta*, **68**, 1686 (1985).

(b) N. Serpone, "Application of picosecond absorption and luminescence spectroscopy. The mapping of primary events in photochemistry and photocatalysis", in *Photoelectrochemistry, Photocatalysis and Photoreactors*, M. Schiavello, Ed., Reidel Publ.Co., Dordrecht, Holland, pp 351-372, 1985.

(c) G. Rothenberger, J. Moser, M. Gratzel, N. Serpone, and D.K. Sharma, "Charge carrier trapping and recombination dynamics in small semiconductor particles", *J. Am. Chem. Soc.*, **107**, 8054 (1985).

(d) N. Serpone, D.K. Sharma, J. Moser, and M. Gratzel, "Reduction of acceptor relay species by conduction band electrons of colloidal titanium dioxide. Light induced charge separation in the picosecond time domain", *Chem. Phys. Letters*, **136**, 47 (1987).

(e) P. Maruthamuthu, D.K. Sharma, and N. Serpone, "Subnanosecond Relaxation Dynamics of 2,2'-azino(3-ethylbenzothiazoline-6-sulfonate) and Chlorpromazine in the Presence and Absence of TiO_2 Colloids", *J. Phys. Chem.*, **99**, 3636 (1995).

(f) N. Serpone, D. Lawless, R. Khairutdinov, and E. Pelizzetti, "Subnanosecond relaxation dynamics of nanosized TiO_2 colloids (R = 1.0 to 13.4 nm). Relevance to heterogeneous photocatalysis", *J. Phys. Chem.*, **99**, 16655 (1995).

[6]. See for example: (a) R. Terzian, N. Serpone, and M.A. Fox, "Primary radicals in the photooxidation of aromatics - Reaction of xylenols with •OH, N_3• and H• Radicals:

Formation and characterization of dimethylphenoxyl, dihydroxydimethylcyclohexadienyl, hydroxydimethylcyclohexadienyl radicals", *J. Photochem. Photobiol.A: Chem.*, **90**, 125 (1995).

(b) J.M. Warman, M.P. de Haas, P. Pichat, and N. Serpone, "The Effect of iso-Propanol on the Surface Localization and Recombination of Conduction Band Electrons in Degussa P25 TiO_2; A Pulse Radiolytic Time-Resolved Microwave Conductivity Study", *J. hys. hem.*, **95**, 8858 (1991).

(c) R. Terzian, N. Serpone, R.B. Draper, M.A. Fox, and E. Pelizzetti, "Pulse Radiolysis of Pentahalophenols: Formation, Kinetics, and Properties of Pentahalophenoxyl and Dihydroxypentahalocyclohexadienyl Radicals", *Langmuir*, 7, 3081 (1991).

(d) D. Lawless, N. Serpone, and D. Meisel, "Semiconductor Photophysics. 6. The role of OH radicals and trapped holes in photocatalysis. A pulse radiolysis study", *J. Phys. Chem.*, **95**, 5166 (1991).

[7]. N. Serpone, E. Pelizzetti, and H. Hidaka, in "Photochemical Conversion and Storage of Solar Energy (IPS9)". Z.W. Tian and Y. Cao, Eds., International Academic Publishers, Academica Sinica, Beijing, China, pp. 33-74 (1993).

[8]. N. Serpone, E. Pelizzetti, and H. Hidaka, "*Identifying Primary Events and the Nature of Intermediates Formed During the Photocatalyzed Oxidation of Organics Mediated by Irradiated Semiconductors*", in **Photocatalytic Treatment of Water and Air**, D.F. Ollis and H. Al-Ekabi, Eds., Elsevier Amsterdam, The Netherlands, (1993).

[9]. N. Serpone, R. Terzian, D. Lawless, P. Kennepohl, and G. Sauve, *J.Photochem. Photobiol. A:Chem.*, **73**, 11 (1993).

[10]. N. Serpone, *Res. Chem. Intermed.*, **20**, 953 (1994).

[11]. N. Serpone and E. Pelizzetti, Eds., "*Photocatalysis – Fundamentals and Applications*", Wiley-Interscience, New York, **1989**.

[12]. M. Schiavello, Ed., "*Photocatalysis and Environment. Trends and Applications*", Kluwer Academic Publisher, Dordrecht, 1987.

[13]. T.L. Rose, B.E. Conway, O.J. Murphy, and E.J. Rudd, Eds., "*Water Purification by Photocatalytic, Photoelectrochemical, and Electrochemical Processes*", The Electrochemical Society, Pennington, N.J., 1994.

[14]. D.F. Ollis and H. Al-Ekabi, Eds. "*Photocatalytic and Purification and Treatment of Water and Air*", Elsevier Science, Amsterdam, 1993.

[15]. E. Pelizzetti and M. Schiavello, Eds."*Photochemical Conversion and Storage of Solar Energy*", Kluwer, Dordrecht, 1991.

[16]. N. Serpone and A. Salinaro, *Pure Appl.Chem.*, **71**, 303 (1999).

[17]. A. Salinaro, A.V. Emeline, J. Zhao, H. Hidaka, V.K. Ryabchuk, and N. Serpone, *Pure Appl.Chem.*, **71**, 321 (1999).

[18]. N. Serpone, *J. Photochem. Photobiol. A:Chem.*, **104**, 1 (1997).

[19]. A.V. Emeline, A.V. Rudakova, V.K. Ryabchuk, and N. Serpone, *J. Phys. Chem.*, **102**, 10906 (1998).

[20]. A.V. Emeline, V.K. Ryabchuk, and N. Serpone, *J.Photochem. Photobiol. A:Chem.*, **133**, 89 (2000).

[21]. A.V. Emeline, V.K. Ryabchuk, and N. Serpone, *J. Phys.Chem. B.*, **103**, 1316 (1999).

[22]. N. Serpone, A.V. Emeline, A. Salinaro, and V.K. Ryabchuk, Proc. IPS-2000, Snowmass, Colorado, July 2-August 4, 2000.
See e.g., the website: http://www.nrel.gov/ips2000/lectures/Serpone.PDF

[23]. A.V. Emeline, G.N. Kuzmin, D. Purevdorj, V.K. Ryabchuk, and N. Serpone, *J. Phys. Chem.B*, **104**, 2989 (2000).

[24]. A.V. Emeline, G.V. Kataeva, A.S. Litke, A.V. Rudakova, V.K. Ryabchuk, and N. Serpone, *Langmuir*, **14**, 5011 (1998).

[25]. A.V. Emeline, S.V. Petrova, V.K. Ryabchuk, and N. Serpone, *Chem. Mater.*, **10**, 3484 (1998).

[26]. V.K. Ryabchuk and G.V. Burukina, *Sov. J. Phys. Chem.*, **65**, 1621 (1991).

[27]. A.V. Emeline, E.V. Lobyntseva, V.K. Ryabchuk, and N. Serpone, *J.Phys.Chem.,B*, **103**, 1325 (1999).

[28]. G.N. Kuzmin, M.V. Knatko, and S.V. Kurganov, *React. Kinet. Catal. Letters*, **23**, 313 (1983).

[29]. V.K. Ryabchuk, L.L. Basov, and Yu. P. Solonitsin, *Sov. J. Chem. Phys.*, **8**, 1475 (1989).

[30]. A.V. Emeline, A. Salinaro, and N. Serpone, *J. Phys. Chem. B*, **104**, 11202 (2000).

Chapter 2

TERMINOLOGY, RELATIVE PHOTONIC EFFICIENCY, AND QUANTUM YIELDS IN HETEROGENEOUS PHOTOCATALYSIS. PART I: *SUGGESTED PROTOCOL*

Summary

The term *photocatalysis* is one amongst several in a quagmire of labels used to describe a photon-driven catalytic process; a simple description of photocatalysis is proposed herein. Other labels such as *quantum yield* and/or *quantum efficiency* used in solid/liquid and solid/gas heterogeneous photocatalytic systems to express process efficiencies have come to refer (incorrectly) to *the ratio of the rate of a given event to the rate of* ***incident*** *photons impinging on the reactor walls and typically for broadband radiation.* There is no accord on the expression for process efficiency. At times quantum yield is defined; often, it is ill-defined and more frequently how it was assessed is not described. This has led to much confusion in the literature, not only because of its different meaning from homogeneous photochemistry, but also because the description of photon efficiency precludes comparison of results from different laboratories owing to variations in light sources, reactor geometries, and overall experimental conditions. The previously reported quantum yields are in fact *apparent*

quantum yields, i.e. *lower limits* of the true quantum yields. We address this issue and argue that any reference to *quantum yields* or *quantum efficiencies* in a heterogeneous medium is inadvisable until the number of photons ***absorbed*** by the light harvester (the photocatalyst) is known. A practical and simple alternative is proposed for general use and in particular for processes employing complex reactor geometries: the concept of ***relative photonic efficiency*** (ξ_r) is useful to compare process efficiencies using a given photocatalyst material (e.g. TiO_2) and a given standard test molecule (e.g. phenol). A quantum yield can subsequently be calculated since $\Phi = \xi_r \Phi_{phenol}$, where Φ_{phenol} denotes the quantum yield for the photocatalyzed oxidative transformation of phenol used as the standard secondary actinometer and Degussa P-25 TiO_2 as the standard photocatalyst. For heterogeneous suspensions (only), an additional method to determine quantum yields Φ is also proposed.

1. INTRODUCTION

Heterogeneous photocatalysis describes a process whereby illumination of a semiconductor particulate (CdS, TiO_2, ZnO, WO_3,...) with UV-visible light suitable to its bandgap energy ($\geq E_g$) ultimately generates thermalized conduction band electrons (e^-) and valence band holes (h^+) which, subsequent to their separation and other competitive photochemical and photophysical decay channels (see below), are poised at the particulate/solution interface ready to initiate redox chemistries. The energy level at the bottom of the conduction band (LUMOs) reflects the reduction potential of the photo-electrons, whereas the uppermost level of the valence band (HOMOs) is a measure of

the oxidizing ability of the photo-holes. The flatband potenial, V_{fb}, fixed by the nature of the material and by the proton exchange equilibria, determines the energy of the two charge carriers at the interface. Hence, reductive and oxidative processes for adsorbed couples with redox potentials more positive and more negative than the V_{fb} of the conduction and valence bands, respectively, can be driven by surface-trapped e^- and h^+ carriers. Figure 1 illustrates a fraction of the complex sequence of events that may take place in a semiconductor photocatalyst.

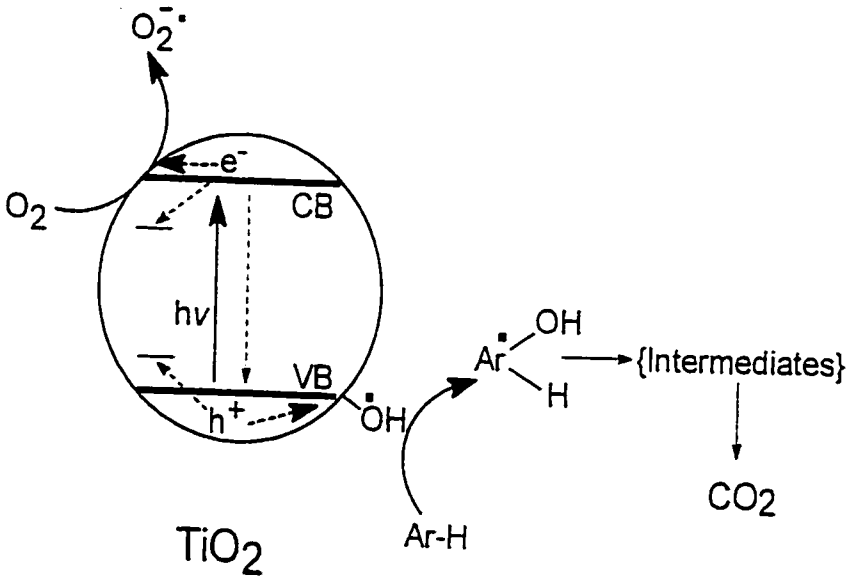

Figure 1.- Sequence of photophysical and photochemical events taking place upon irradiation of a TiO_2 particle in an air-equilibrated aqueous dispersion with $h\nu$ greater than E_g together with secondary reactions of the oxidized Ar-H to total mineralization to CO_2.

Taking TiO_2 as an example, initially, irradiation of the semiconductor particle generates a bound electron/hole pair (the exciton), which can either recombine or dissociate to give a conduction band electron and a valence band hole. These separated charge carriers may also recombine, migrate to the surface while scanning several shallow traps (anion vacancies and/or Ti^{4+} for the electrons; and oxygen vacancies or other defect sites for the hole). On the surface, both charge carriers scan the surface visiting several sites to reduce adsorbed electron acceptors (A_{ads}) and to oxidize adsorbed electron donors (D_{ads}) in competition with surface recombination of the surface trapped electrons and holes (e^-_{st} and h^+_{st}) to produce light emission and/or phonon emission. In an air-equilibrated aqueous dispersion, oxygen is omnipresent on the particle surface and acts as an electron acceptor. whereas OH^- groups and H_2O molecules are available on the particle surface as electron donors to yield the strongly oxidizing •OH radicals. Note that under certain conditions. photooxidations of some substrate S can also take place to produce the cation radical $S^{+\bullet}$ as one of the primary species and ultimately an oxidized product {for an extensive report on this aspect the reader should consult the work of Fox and Dulay [4a] and the more recent review by Li and Wang [4b]}. Trapping of electrons and holes in pristine naked TiO_2 colloids (size = a few nm) takes place in less than ca. 30 ps [1-3]. At concentrations of organic pollutant substrates normally found in the environment (a few tens of mg L^{-1}) the •OH radicals are the primary oxidizing entities to produce, in the case of an aromatic substance. the corresponding •OH-adduct (a cyclohexadienyl radical [5]) that ultimately breaks down into a variety of intermediate products on the way to total mineralization to carbon dioxide.

The function of photo-excited semiconductor particulates then is to act as pools of electrons and holes which can be exploited in several multi-electron transfer processes [4]. Thus:

$$TiO_2 \xrightarrow{h\nu} TiO_2(e^-/h^+) \rightarrow e^-_{cb} + h^+_{vb} \quad \text{(generation/separation)} \quad (1)$$

$$e^-_{cb} + h^+_{vb} \rightarrow e^-_{tr} + h^+_{tr} \quad \text{(lattice and/or surface trapping)} \quad (2)$$

$$e^-_{cb} + h^+_{vb}\,(\text{and/or } h^-_{tr}) \rightarrow \text{recombination} \quad (h\nu' \text{ and phonon emission}) \quad (3)$$

$$e^-_{cb}\,(\text{and/or } e^-_{tr}) + h^+_{vb} \rightarrow \text{recombination} \quad (h\nu'' \text{ and phonon emission}) \quad (4)$$

$$e^-_{tr} + h^+_{tr} \rightarrow \text{recombination} \quad (h\nu''' \text{ and phonon emission}) \quad (5)$$

$$Ti\text{-}{}^{\bullet}OH + RH \rightarrow \rightarrow \rightarrow \text{....photooxidations} \quad (6a)$$

$$e^-_{tr} + \text{compound} \rightarrow \rightarrow \rightarrow \text{....photoreductions} \quad (6b)$$

where e^-_{tr} is a trapped electron (e.g., as Ti^{3+}) and h^+_{tr} is a trapped hole denoted here [3,6] as a surface-bound •OH radical, i.e. as Ti-$^{\bullet}$OH. Close examination of the field discloses gaps in our understanding of the basic elements that underlie heterogeneous photocatalysis.

Issues that require a collective fundamental understanding of heterogeneous photocatalysis are the description of (i) photocatalysis, (ii) quantum yields, and (iii) turnover numbers, rates and frequencies.

2. PHOTOCATALYSIS

A suitable description of the term ***photocatalysis***, whether in homogeneous or

heterogeneous media, seems to elude acceptance as attested by the spectrum of specific labels used to describe a variety of mechanistic possibilities for a given process [7,8]. We have adopted the view [8] that the terminology *photocatalysis* refers simply to a catalytic reaction involving light absorption by a catalyst or by a substrate [9,10], although there is no universal agreement on an appropriate definition. Without reference to a special or specific mechanism, photocatalysis has also been described [7] as *the acceleration of the rate of a photoreaction by the presence of a catalyst*; further, as a label to indicate that *a catalyst may accelerate the photoreaction by interaction with a substrate either in its ground state or in its excited state and/or with the primary photoproduct, depending on the mechanism of the photoreaction.* This description also encompasses [11] *photosensitization*, yet such a process, defined officially [9] as *a process by which a photochemical or photophysical alteration occurs in one molecular entity as a result of initial absorption of radiation by another molecular entity - the photosensitizer*, is by no means necessarily catalytic without the knowledge of the turnover number and/or quantum yield. The issue seems to rest entirely on the role of the photons. Where in a process the quantum yield is **greater than one** (as occurs in photoreactions involving radicals) the process may be considered *catalytic in photons*, and where the quantum yield is **less than or equal to one**, the process may be taken as being *non-catalytic in photons*.

In an excellent account, Salomon [12] proposed that a broad definition of photocatalysis should be divided operationally into two distinct classes: (1) ***photogenerated catalysis***, and (2) ***catalyzed photolysis***. The former implicates only ground states of the

catalyst and the substrate in the catalytic step, which is thermodynamically spontaneous (exoergic). In the latter, either the nominal catalyst or the substrate, or both, are in an excited state during the catalytic step. Later, Kutal [7,13] clarified and illustrated Salomon's formal schemes, and Hennig [14] suggested consistent labels that applied to observed experimental evidence. This led to the appearance of a quagmire of mechanism-specific labels: (i) ***photo***catalysis [10,11,15], (ii) ***photogenerated*** catalysis [12], (iii) ***catalyzed*** photolysis [12], (iv) ***photoinduced*** catalytic reactions [14], (v) ***stoichiometric photogenerated*** catalysis [12], (vi) ***photo-assisted*** catalysis [14,16], (vii) ***catalyzed*** photoreactions [13,17], (viii) ***catalyzed*** photochemistry [13], (ix) ***sensitized*** photoreactions [13,14], (x) ***photosensitized*** reactions [15], and (xi) ***"substance-assisted(-catalyzed)"*** photoreactions [18]. Here the word "substance" refers to a transition metal complex or to a semiconductor if dealing in the field of heterogeneous photocatalysis. Unquestionably, this quagmire of labels can only lead to confusion. As echoed by Kisch [11], a definition to be useful must be such as to facilitate communication amongst researchers in the different areas of chemistry, as the principal aim of chemists is to discover novel chemical transformations through (photo)catalysis. We summarize in the scheme below Salomon's classification; for an elaborate account and illustration of these various labels the work of Chanon and Chanon is worth consulting [10].

To the extent that many of the labels alluded to pertain to a specific mechanism, the label becomes useful only in so far as the mechanism of the chemical transformation is reliable and until such time as the mechanism has not been revised by more recent experimental evidence [8]. This calls immediate attention to the usage of the less descriptive

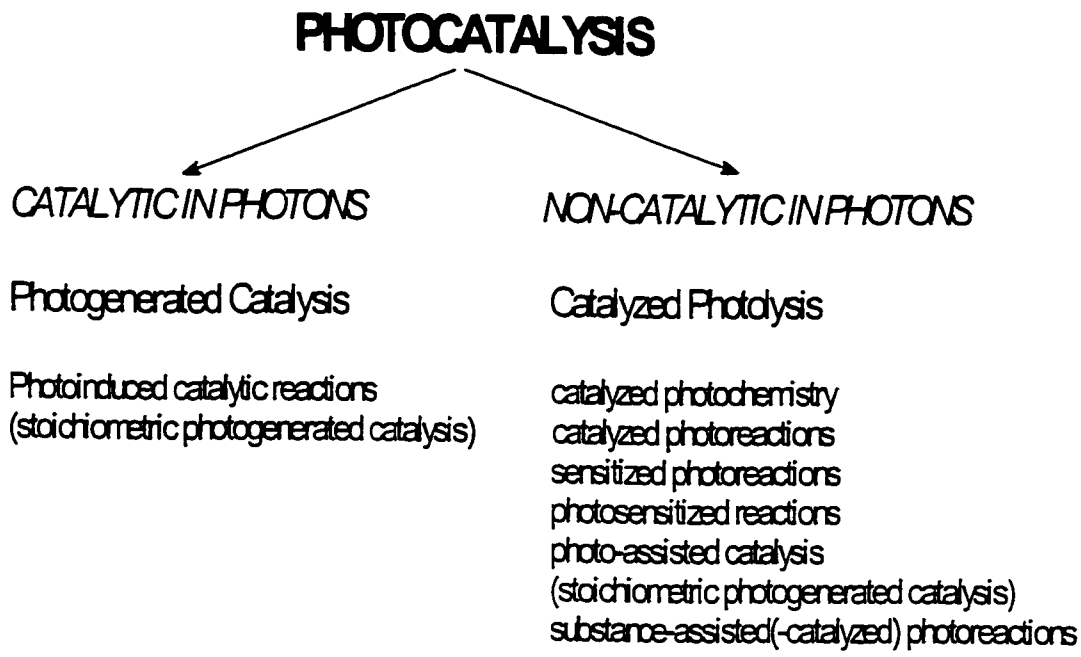

and recommended (albeit unfulfilling) label *photocatalysis* to denote simply a process that is ***photon-driven*** and is ***catalytic*** upon establishing the turnover number of the given process to demonstrate that the process is indeed catalytic [8]. For a process to be labeled catalytic, the turnover number must be greater than unity. Unfortunately, the expression *turnover number* has its own limitations in heterogeneous photocatalysis. Problems associated with its description shall be taken up in a later chapter [19].

3. EFFICIENCIES IN AN INDUSTRIAL ENVIRONMENT

In an industrial environment where the efficiency of a given process is a significant component to determine its economic viability, Bolton *et al* [20] have proposed the Figures of Merit "*Electrical Energy per Order*" (*EE/O*) and "*Electrical Energy per Unit Mass*

(*EE/M*). Braun [21] has proposed the figure of merit "*Energetic Efficiency of Degradation*" (*EED*) given as mg L^{-1} of organic carbon in a given solution volume irradiated per kilowatt-hour (kWh) of electrical energy used, or the more recent suggestion of using volume-corrected efficiencies (mg C per kWh) [22], to afford comparisons between the different methods of water treatment technologies. This presumably includes the analytical procedure into any comparison between different processes, different reactors, and different light sources, among others. Just like the *EE/O*, the *EED* is useful in an economic analysis of various given processes.

In practical oxidative degradations, as envisaged in water treatment technologies, not only is the simple disappearance of the pollutant relevant but conversion of total organic carbon (TOC) into inorganic carbon CO_2 is also important. The pertinent process is the complete mineralization of all organic carbons to insure that the substrate(s) and any intermediate product(s) formed during the degradative process have also been degraded [23]. In some cases, conversion to an innocuous product may be acceptable (e.g., atrazine to cyanuric acid [24]) if the end product is environmentally friendly.

Unfortunately, the *EE/O*, *EE/M*, *EED*, and other figures of merit do not provide that fundamental quantity that describes the extent to which the absorbed photon (the efficiency) contributes to drive a certain event. In homogeneous photochemistry, this parameter is the quantum yield, Φ. We therefore seek to define and experimentally attain something identical in heterogeneous photocatalysis. It should be noted that *EE/O* and *EE/M* scale with Φ^{-1} [20].

4. QUANTUM YIELD IN HOMOGENEOUS PHOTOCHEMISTRY

We begin by recalling the meaning of quantum yield in homogeneous photochemistry and the constraints under which it is measured.

Knowledge of the **quantum yield** (defined as *the number of defined events which occur per photon absorbed by the system* OR *as the amount (mol) of reactant consumed or product formed per amount (einstein) of photons absorbed* [9]) is central to homogeneous photochemistry. Photochemists routinely determine quantum yields of reactant disappearance, product formation, light emission, and of various other events occurring in some photochemical process. Many of these events have been examined in great detail by several laboratories, and the reported quantum yield data are precise and reproducible [25].

Ferrioxalate {$[Fe(C_2O_4)_3]^{3-}$, for UV and visible region to ~ 500nm}, Reinecke's salt {$[Cr(NH_3)_2(SCN)_4]^-$; for the visible region}, uranyl oxalate {$[UO_2(C_2O_4)_2]^{2-}$ for the UV region}, and more recently Aberchrome 540 {for the 310-370 nm and the 436-546 nm ranges} [9,25,26] are typical secondary standards used to measure the photon flow incident on the photolytic cell {for details of the experimental protocols, appropriate references [9,25-27] may be consulted}. These substances are the *chemical actinometers* because the product quantum yield is rather insensitive to temperature changes, and to changes in reactant concentration, photon flow, and the wavelength of the absorbed light. Procedures are well established and analysis of products is simple and precise [25]. Utilization of such actinometric substances has simplified determination of the photon flow compared to the earlier more tedious radiometric procedures [9,26]. Placing the actinometer in the same

photolysis cell used for the subsequent photochemical study, while maintaining the same optical train, avoids corrections for differences between the fraction of incident light ***reflected*** from the front window of the photolysis cell if different cells were used.

If the photochemical reaction of the actinometer (Ac) is the simple reaction 7

$$\mathrm{Ac} \rightarrow \mathrm{B} \tag{7}$$

and Ac is the ***only*** substance that absorbs light at the wavelength of irradiation λ, the rate $R_{Ac,\lambda}$ at which photons are absorbed by Ac (photon flow) will then be given by:

$$R_{Ac,\lambda} = R_{o,\lambda}\left(1 - 10^{-A_\lambda^{Ac}}\right) \qquad \text{(photons min}^{-1}\text{ or einstein min}^{-1}\text{)} \tag{8}$$

where A_λ^{Ac} is the absorbance of Ac at wavelength λ. Operationally, $A_\lambda^{Ac} \geq 2$ during the entire irradiation period t to ensure that the light harvester collects ≥99% of the photon flow, such that $R_{Ac,\lambda} \approx R_{o,\lambda}$; here $R_{o,\lambda}$ is the incident photon flow from the irradiation source given by [25,26]:

$$R_{o,\lambda} = \frac{n_B}{\Phi_B\, t\left(1 - 10^{-A_\lambda^{Ac}}\right)} \qquad \text{(photons min}^{-1}\text{)} \tag{9}$$

where n_B is the number of product molecules formed from the irradiated actinometer and t is the time(s) of irradiation. Thus, actinometry allows determination of the incident photon flow for a system of *specified geometry* and in a *well-defined spectral domain* [26]. Typically, good stirring of the actinometric solution needs to be maintained during irradiation, and the photolysis cell should contain no particulate matter that might reflect or scatter light as this would have a detrimental effect on the precision and accuracy of the quantum yield determination. Practical detailed procedures for determining quantum yields in homogeneous media are available elsewhere [9,25-27].

When polychromatic radiation is used there is an added complication in the measurements of quantum yields since the action spectrum in the spectral region of interest (λ_1 to λ_2) to the reaction being examined must be known. In such case, we can define a wavelength-averaged quantum yield from λ to $\lambda + d\lambda$ as:

$$\Phi_{poly} = \frac{\int_{\lambda_1}^{\lambda_2} R_{o\lambda}\, \Phi(\lambda)\, d\lambda}{\int_{\lambda_1}^{\lambda_2} R_{o\lambda}\, d\lambda} \qquad (10a)$$

When the action spectrum is unknown, Braun *et al.* [26] suggested usage of the term ***quantum efficiency***, η, to indicate:

$$\eta = \frac{\text{Amount of reactant consumed or product formed in the bulk phase}}{\text{Amount of photons absorbed over the spectral range } (\lambda_1 \text{ to } \lambda_2) \text{ used during the reaction period.}} \qquad (10\ b)$$

In general $\eta \neq \Phi$. As well, note the different meaning that η takes as given by Braun *et al* [26] from that given by a recent IUPAC Glossary of Terms in Photochemistry [9], which uses η to be the efficiency of a step. In the present context, η is best referred to as the *photo-efficiency* of a process over the spectral range (λ_1 to λ_2) of interest. When Φ_λ is independent of λ over the spectral range λ_1 to λ_2, then $\eta = \Phi_{poly}$.

In any description of quantum yield in heterogeneous photocatalysis, it will be useful to employ simple methods (procedures) that use the most basic of instrumentation to define a parameter such that the heterogeneous photocatalytic data from various laboratories can be evaluated and compared.

5. SUGGESTED PROTOCOL IN HETEROGENEOUS PHOTOCATALYSIS

5.1. General Considerations

The heterogeneous photocatalysis literature reports *quantum yields* and in other cases *quantum efficiencies* incorrectly. It needs to be stressed that it is the number of photons ***absorbed*** by and ***not incident*** to the contents in the photolysis cell that initiate and drive a photocatalytic process. Until the rate of absorption of photons has been adequately assessed, reference to ***quantum yield*** {or ***quantum efficiency***, also used by photochemists} in

heterogeneous photocatalysis can only continue the confusion in the literature (however, see Chapter 2). The term quantum yield becomes useful only if it has the identical meaning to the photochemical quantum yield (symbolized by Φ) in homogeneous phase.

In measurements of photons absorbed by the semiconductor light harvester, the extent of light scattered or reflected by the particulate matter in the dispersion cannot be neglected. All molecules are both light absorbers and light scatterers depending on the nature of the medium. Light collecting particles having large refractive indices may not, in principle, absorb all the photons impinging on the dispersion. Such significant losses, too often of unkown quantity and too often neglected, should *a priori* preclude usage of the term ***quantum yield*** in a heterogeneous medium, unless scattering is adequately accounted for. Clearly, there is a need to explore simpler alternatives in heterogeneous photocatalysis to express process efficiencies that ultimately can be related to a parameter implicating the photons absorbed. Any proposed procedure must be simple and amenable to common instrumentation normally available in most (photo)catalysis laboratories.

5.2. Quantum Yields

In heterogeneous photocatalysis, *quantum yield* has heretofore been taken to describe the number of molecules converted relative to the total number of photons ***incident*** on the reactor walls for an undefined reactor geometry and for polychromatic radiation. In fact, the quantum yield, Φ_λ, as done above for homogeneous photochemistry must express the moles of reactant consumed or product formed in the bulk phase, n, to the amount (i.e., einstein)

of photons at wavelength λ absorbed by the photocatalyst, n_{ph}, (eqn 11) [25].

$$\Phi_{\lambda} = \frac{\text{Amount (mol) of reactant consumed or product formed in the bulk phase}}{\text{Amount (einstein) of photons at wavelength } \lambda \text{ absorbed by the photocatalyst}} \qquad (11a)$$

$$\Phi_{\lambda} = \frac{n}{n_{ph}} \qquad (11b)$$

Alternatively, we may define the quantum yield using the initial rate R^{in} of the reaction and the rate of photons *impinging on*, and *absorbed by* the reaction system as is common practice in homogeneous photochemistry. Thus,

$$\Phi_{\lambda} = \frac{R^{initial}}{R_{o,\lambda}} \qquad (11c)$$

Analogous descriptions have been proposed for heterogeneous systems [26,28,29]. No particular difficulties are encountered in homogeneous media. In a heterogeneous system, the relationship in equation 11 has been extended, modified and applied in an analogous fashion [18,30-32]. Because the number of absorbed photons, n_{ph} , is experimentally difficult to estimate owing to reflection, scattering (see below), transmission (for transparent colloidal sols) and absorption by the suspended particulates, usage of the term *quantum yield* referenced to ***incident*** photons in heterogeneous photocatalysis has only engendered

confusion in the literature. Some methods to determine n_{ph} have appeared [30-33].

To the extent that the numerator in equation 11c expresses the rate of reaction, Φ_λ depends on the reactant concentration. However, as correctly noted by Braun and co-workers [26] and recently emphasized by Cabrera *et al.* [33], only for a zero-order reaction is Φ_λ uniquely defined at the given wavelength λ. In homogeneous photochemistry, the problem is normally overcome by determining Φ_λ at small (less than ~10%) conversions of reactants, a point not often respected in heterogeneous photocatalysis where the focus is usually complete mineralization (100% transformation to CO_2) of the substrate, at least in studies of environmental interest that focus on the total elimination of organic pollutants in water.

Additional considerations suggest that the photochemically defined *quantum yield* would be difficult to describe experimentally in heterogeneous media [33] particularly for complex reactor geometries. Consequently, so-called quantum yields thus far reported in the literature are but *apparent* or *lower limits* of the true quantum yield, since scattered light has not been accounted for [29]. In defining equation 11, we must also recognize that semiconductor-assisted photooxidations take place on the surface of the solid catalyst (see Figure 1), and thus the catalytic properties of the catalyst surface are important as the course of reactions depends highly on the characteristics of the surface on light activation. For example, usage of two TiO_2 photocatalysts obtained from different sources, or from different batches from the same source, can give different intermediate products and different distributions of intermediates under otherwise identical experimental conditions [34]. This

calls attention to the necessity of reporting the characteristics of the photocatalyst [18,29,32]. Moreover, a distinction should be noted between (i) light-activated steps (from photon absorption to formation of •OH radicals on the particle surface) related to the quantum yield, and (ii) the ensuing catalytic steps in the photocatalyzed process (includes adsorption/desorption and reaction of the •OH radicals with the adsorbed substrate) which depend highly on the surface properties of each photocatalyst. This distinction will be difficult to delineate experimentally when assessing process efficiencies. Quantum yields reported in this article do not delineate between the photochemical and catalytic processes.

The numerator in equation 11c expresses the rate of a catalyzed heterogeneous reaction* in heterogeneous photocatalysis which is related to the number of catalytically surface active sites [18]; unfortunately, these are also not experimentally attainable [8]. To bypass this difficulty, the number of active sites has often been replaced [35] by (i) the surface area of the catalyst, (ii) the mass of the catalyst or (iii) by the number of surface OH^- groups on the photocatalyst such as TiO_2 [30-32]. None of these suggestions, however, describe the actual heterogeneous rate since measuring the surface area for a somewhat porous catalyst (for example) comprises both the external and internal surfaces [33]; this internal surface may not be useful in some catalytic events. Also, not all the surface sites occupied by OH^- groups are necessarily catalytically active [8], especially since there may

* The units that describe a heterogeneous reaction are typically cm^{-3} min^{-1} for both the numerator and denominator in eqn 11. However, since the intent is on how many mol of reactant (or product) molecules have reacted (or been produced), description of the reaction in homogeneous terms is satisfactory and in no way changes the arguments.

be different kinds of OH^- groups (two in titania). Finally, depending on the reactor geometry, particle aggregation, and stirring, not all the BET catalyst surface (Brunauer-Emmett-Teller measurements in the dry state) may be accessible to the substrate being photoconverted.

Therefore a simple alternative method of comparing process efficiencies for equal absorption of photons is desirable and is herein proposed for heterogeneous photocatalysis. But first the extent of light scattered in a heterogeneous medium, such as a TiO_2/water system, is worth consideration.

5.3. Scattering Effects

The factor that most markedly complicates the measurements of the number (or rate) of absorbed quanta by a semiconductor photocatalyst is the non-negligible extent of light scattered by the particles in the dispersion. This can reach. according to some accounts. 13% to 76 % of the total incident photon flow [30]. Using the photodegradation of trichloroethylene in a TiO_2 slurry, Cabrera *et al* [33] confirmed some of these findings noting that only about 15% (Aldrich anatase TiO_2) of the radiation measured by homogeneous actinometry inside a reactor was effectively absorbed. They concluded that radiation flow measurements at the reactor entrance, or homogeneous actinometry inside the reactor volume can be very misleading and scattering effects are important.

In this regard, a metal oxide material with a high refractive index (e.g. TiO_2 anatase and/or rutile) may not, in principle, absorb all the incident photon flow from a given source (however, see refs. [36-38]) as the irradiance of light scattered, E_{sc}, by the suspension

depends on the refractive indices of the scattering molecule/particle (n_1), the surrounding medium (n_o) and other factors. In the diagram below [39]:

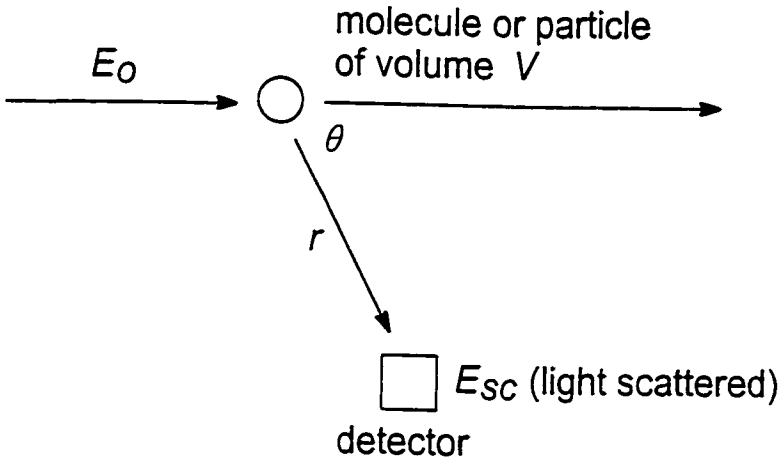

where E_o is the incident light irradiance (W m^{-2} or mW cm^{-2}).

$$\frac{E_{sc}}{E_o} = \frac{N_p(\frac{n_1}{n_o})^4 \; P(\Theta) \; V^2}{\lambda^4 \; r^2} \qquad (12)$$

The ratio E_{sc}/E_o illustrates the difficulty. The fraction of scattered light (E_{sc}/E_o) by a molecule/particle scatterer depends on the number of particles (N_p), on the square of the volume V [hence on the sixth power of the radius] of the particle, on the factor {$P(\theta)$} that accounts for the scattering from different parts of the same particle and on the fourth power of the ratio of the refractive indices (n_1 / n_o), and finally depends inversely on the fourth

power of the wavelength (λ) and on the square of the distance (r) of the detector from the scatterer.

For the materials making up a typical system in heterogeneous photocatalysis, n_o is 1.33 for H_2O and n_1 is 1.5-1.7 for glass, 3.87 for rutile TiO_2, and ~ 2.5-3 for anatase TiO_2, all at 365 nm [40,41]. If $n_1 \gg n_o$, the extent of scattered light is negligible as commonly noted in absorption spectroscopy of dilute solutions relative to the case when $n_1 > n_o$ for which the light will be highly scattered. The percentage of photons absorbable by TiO_2 seems to be around ~ 50 to 65% in some cases [40,42]. Evidence for this scattering effect is presented in the subsequent Chapter 3 [43].

5.4. Photonic Efficiencies

One of the objectives of the work in Serpone's laboratory in the past decade has been to describe a protocol to standardize process efficiencies of degradation of various organic substrates for a given set of conditions. Any method proposed should circumvent the inherent difficulties encountered in the precise evaluation of the number of quanta absorbed by the photocatalyst (e.g., titania), difficulties with utilization of different light sources, different reactor geometries and other unspecified factors by referring all the results to an equivalent experiment carried out under identical conditions for a standard process.

Photonic efficiency (ξ) was used earlier [44] to describe the number or moles of reactant molecules transformed or product molecules n formed divided by the number or

einsteins of photons at a given wavelength incident on the reactor cell (flat parallel windows) n_{ph}. Alternatively, the photonic efficiency may be determined by relating the ***initial rate*** of substrate degradation to the ***rate of incident photons*** reaching the reactor as obtained by actinometry. {**Usage of ξ is not recommend because it is basically what the literature has been incorrectly reporting as a *quantum yield* whose values have little, if any meaning in describing process efficiencies (see above)**}. The term photonic efficiency was suggested earlier [34,44] simply to avoid the confusion between heterogeneous and homogeneous photochemistry; in the latter. quantum yield is defined precisely.

One final point is worth noting about photonic efficiencies. Experiments carried out to show the dependence of initial rates of disappearance of the organic substrate, $R^{initial}$, as a function of the loading of the light harvesting photocatalyst TiO_2 typically show a functionality analogous to that of the Langmuir-Hinshelwood model; i.e., the dependence of $R^{initial}$ on $[TiO_2]$ can be described by:

$$R^{initial} = \frac{A\ [TiO_2]}{(1 + B'\ [TiO_2])} \qquad (13a)$$

where A and B' are constants. To the extent that the photon flow $R_{0,\lambda}$ remains constant for a given experiment, the functionality of photonic efficiency ξ will follow a similar behavior; thus,

$$\xi = \frac{\xi_{lim}\ C\ [TiO_2]}{(\xi_{lim} + C\ [TiO_2])} = \frac{R^{initial}}{R_{o,\lambda}} \qquad (13b)$$

where ξ_{lim} is the limiting photonic efficiency for large loadings of TiO_2 and C is a constant. This observation will have interesting consequences for heterogeneous dispersions (see below).

We now describe the steps needed to determine a photonic efficiency for a heterogeneous dispersion for later use (see below), even though in absolute terms ξ has little meaning:

1. Determine the photon flow $R_{o,\lambda}$ for the light source by actinometry using appropriate actinometric substances {see above} and the protocols in refs. [25,26].

2. Determine the initial rates, $R^{initial}$, of photoconversion of the organic substrate RH for a range of concentrations of RH at constant loading of the Degussa P-25 TiO_2 photocatalyst (initially, we suggest a loading of ca. 2 g L^{-1}).

3. From the plot of $R^{initial}$ versus [RH] for constant TiO_2 loading and for constant light irradiance E_o determine the concentration range of RH that defines the plateau of the relationship analogous to that of equation 13a ([TiO_2] is replaced by [RH]). Our experience with

aromatic substrates suggests 20 mg L^{-1} may fall in this range. However, this may change depending on the substrate because of a connectivity between light irradiance of the lamp source used and the concentration of the substrate dependence of $R^{initial}$. That is, a change in the concentration of the organic substrate changes the light irradiance dependence of $R^{initial}$ as noted in both solid/gas and solid/liquid systems [45].

4. Choose a concentration of RH in this plateau, then determine the range of the photocatalyst TiO_2 loading which also defines the plateau of the plot of $R^{initial}$ versus $[TiO_2]$, equation 13a, to ascertain that the loading of TiO_2 suggested in item (2) indeed falls in the range.

5. Photonic efficiencies may then be calculated employing the relationship $\xi = R^{initial} / R_{o,\lambda}$ for which not all the photon flow $R_{o,\lambda}$ is absorbed because of scattering and other effects.

5.5. Relative Photonic Efficiency

To avoid unnecessary errors and the necessity of stipulating reactor geometry and light source, together with the properties (e.g. size, surface area) of the photocatalyst material used, the earlier suggested protocol [8,34,44] further defined an efficiency that could be used to compare experiments within the same laboratory or with other laboratories and that would be reactor-independent: the ***relative photonic efficiency***, symbolized as ξ_r and analogous to a relative quantum yield (note: in heterogeneous media, usage of the former terminology is preferred) and thus related to an acceptable standard process, a standard photocatalyst

material [34], and a standard "secondary actinometer" in photocatalyzed processes. In the experimental description of a *relative photonic efficiency* [8,34,44], the effects of reactor geometry, light source, and photocatalyst properties remained constant in assessing ξ_{rel} [44].

The concept of relative photonic efficiency affords comparison of process efficiencies for the photodegradation of aromatic substrates and avoids unnecessary confusion with the terminology appropriately defined in homogeneous photochemistry. Moreover, ξ_r is applicable to whatever heterogeneous medium used: (i) for dispersions, (ii) for cases where the photocatalyst is immobilized on a support, and (iii) is also applicable to solid/gas as is for solid/solution media.

These relative process efficiencies are obtained by relating the ***initial rate*** of substrate degradation, $R^{initial}$(substrate), to the ***initial rate of phenol degradation,*** $R^{initial}$(phenol), for constant incident photon flow $R_{o,\lambda}$ reaching the reactor (note that the same reactor and reactor geometry must be used for both the substrate and phenol). That is,

$$\xi_{rel} = \frac{\dfrac{R^{initial}(substrate)}{R_{o,\lambda}}}{\dfrac{R^{initial}(phenol)}{R_{o,\lambda}}} \qquad \frac{(mol\ min^{-1}/einstein\ min^{-1})}{(mol\ min^{-1}/einstein\ min^{-1})} \qquad (14)$$

or

$$\xi_{rel} = \frac{R^{initial}(substrate)}{R^{initial}(phenol)} \qquad (15)$$

where both (initial) rates are obtained under otherwise ***exact identical conditions***.

Although there is no strict need to measure the photon flow, $R_{o,\lambda}$, of a given light source to estimate ξ_{rel} as defined above, it should nevertheless be determined and reported when experimentally feasible (certain reactor geometries may preclude such measurements).

A preliminary report suggested the feasibility of this concept [44] using Degussa P-25 TiO_2. The results were encouraging even under broadband AM1 simulated sunlight radiation. More extensive studies [34,46] confirmed the usefulness of ξ_{rel}. The initial photoconversion of phenol was chosen, and is herein recommended for aromatics as the standard process and Degussa P-25 TiO_2, a material used extensively by several workers, as the standard photocatalyst [34]. The choice of phenol is dictated by the recognition that the molecular structure of phenol is present in many organic pollutants and, like many of these, is degraded by an oxidative rather than a reductive pathway.

To be useful, ξ_{rel} values should not depend on light irradiance and reactor geometry, and on such other parameters as pH, photocatalyst loading, substrate concentration, and temperature. Indeed, in determining ξ_{rel}, one must chose a concentration of the organic substrate RH being examined such that the initial rate of photodegradation of RH is no longer dependent on [RH] (for constant loading of photocatalyst). Once this appropriate [RH] is chosen from the plateau of the plot of $R^{initial}$ versus [RH] (see above protocol for ξ), an optimal concentration of TiO_2 at constant [RH] can also be assessed from the plateau of the plot of $R^{initial}$ versus [TiO_2] (see above protocol and eqn 13a). Hence, experiments must be

carried out to determine the conditions under which relative photonic efficiencies become independent of light irradiance E_o, or else the value(s) of ξ_{rel} will depend on E_o and its usefulness becomes tenuous. In earlier work [34] loadings of 2 g L^{-1} for TiO_2 and 20 mg L^{-1} for phenol and for other organic substrates were used.

The method of *relative photonic efficiencies* being proposed [34] presents the advantage of simplicity and affords a means by which other investigators can compare their results with those of others. Measurements of ξ_{rel} require no added special instrumentations other than those already available in most photochemical and catalysis laboratories.

In heterogeneous photocatalysis, the total mineralization or disposal of a pollutant, and the identification of the various intermediate species produced in their course to the ultimate oxidation product(s) CO_2 and H_2O is of primary concern. It would also be useful to assess the ξ_{rel} for these processes, particularly the mineralization of total organic carbon, TOC [21]. A recent study [47] demonstrated that, at least for one case examined, the relative efficiency of the disappearance of phenol using two entirely different, industrially available titania photocatalysts is identical to the relative efficiency for the complete mineralization of phenol into carbon dioxide. That is, $\xi_{rel} = 0.25 \pm 0.03$ for the (initial) disappearance of phenol with the Hombikat UV-100 TiO_2 specimen (Degussa P-25 TiO_2 was the standard photocatalyst); for the corresponding fundamentally more important TOC degradation process $\xi_{rel} = 0.27 \pm 0.03$ [47].

The efficiencies ξ_{rel} reported earlier [34] and in part reproduced here referred

specifically to substrate disappearance and demonstrated the general applicability of the proposed method. Although ξ_{rel} were given for substituted phenols, the concept of *relative photonic efficiencies* is by no means restricted to these species; ξ_{rel} is also applicable to other aromatic substances with the only constraint being that phenol be the standard substrate against which all ξ_{rel} are reported (experimental conditions should be reported for such efficiencies to be useful). The effects of variations in light irradiance (13 to 100% where 100% is 190 mW cm^{-2}), reactor geometry, pH (3 to 6), temperature (12 to 68°C), concentration of organic substrate (40 to 800 μM), and loading of photocatalyst material TiO_2 (0.2 to 2 g L^{-1}) on the *relative photonic efficiency* were examined for 2-methylphenol, 2,4-dimethylphenol, and 4-chlorophenol [34]. Additionally, ξ_{rel} of other organic substrates were determined at specified conditions. In the case of the photodegradation of aliphatic substrates, a different secondary actinometer may be needed and recommended; a good process and substance is the photodegradation of formic acid.

Ultimately, these ξ_{rel} can be converted to the photochemically defined quantum yield Φ once the true quantum yield for phenol, Φ_{phenol}, for a given photocatalyst has been determined (see below): whence,

$$\Phi = \xi_{rel} \Phi_{phenol} \qquad (16)$$

Recent laser work from the LPASECM laboratory noted that Φ is likely to be around 10% for the TiO_2 photocatalyst [3].

6. QUANTUM YIELDS IN HETEROGENEOUS PHOTOCATALYSIS

6.1 Earlier attempts

Apparent quantum yields (i.e., *photonic efficiencies*) based on the total number of photons incident on the reactor for the disappearance of various organic substrates have been reported at 365 nm for cresols and dimethylphenols [48]; they ranged from 0.0076 to 0.010 and from 0.0060 to 0.015, respectively {2 g L^{-1} TiO_2 and 20 mg L^{-1} of organic substrate}. Analogous efficiencies were reported for phenol {0.006; 100 μM; 1 g L^{-1} TiO_2} [49], for 4-chlorophenol {0.015; 8 g L^{-1} TiO_2; $\lambda > 320$ nm} [37], for H_2 formation {0.01; reduction of water} [50], and hydrogenolysis of methylacetylene $CH_3C{=}CH$ {0.0012} [51]. The range in these values is rather general. By contrast, for the disappearance of 1-propanol and propanal [36,37] *apparent quantum yields* converged to unity for the pure substrates. The authors noted that these yields are true quantum yields and that there is efficient competition between substrate oxidation and electron/hole recombination. At the rather large concentrations of ~ 0.10 to 0.12 M of 1-propanol, the reported quantum yield was ~0.80. The inference was that charge carrier recombination had essentially been shut off. Taking phenol as an example substrate, it would be surprising that even at very high concentration formation of the oxygen-centered radicals {$O_2^{-\bullet}$, $HO_2\bullet$ and $\bullet OH$} and subsequent primary oxidation of phenol by these species, or directly by "holes", would be so efficient (unitary efficiencies) as to totally preclude radiative and nonradiative recombination of the exciton and its dissociated conduction band electrons and valence band holes. The quantum yield of the primary oxidation of phenol to produce the corresponding cyclohexadienyl radical (or

equivalent) and the subsequent intermediate products is more likely to be less than unity in dilute phenolic solutions.

In heterogeneous media, quantum yield is best described in a manner identical to that described in homogeneous photochemistry (see above). It suffices only to determine the number of absorbed photons or the fraction of light absorbed by the solid photocatalyst. Some attempts have been noted by Schiavello and co-workers [30-32], Cassano and co-workers [33], and by Valladares and Bolton [52]. The latter authors found $\Phi = 0.056$ for the photobleaching of methylene blue. The quantum yield of •OH radical formation for an Aldrich TiO_2 anatase sample that was used to convert methanol to formaldehyde was 0.040 [42].

We have used a modified integrating sphere method (see ref. [43]), otherwise identical to that used in [42], to determine the fraction of light absorbed by a Degussa P-25 TiO_2 sample (see above) later used as the standard photocatalyst sample to determine the quantum yield for the photooxidative conversion of phenol, Φ_{phenol}, taken as the standard process and test molecule, respectively. This Φ_{phenol} was then used to convert reported relative photonic efficiencies ξ_{rel} [34] to quantum yields of photooxidation of other organic substrates (eqn. 16 and Table 1).

6.2 Determination of Quantum Yields

6.2.1 Method of relative photonic efficiency

Given the relationship in equation 16 and the relative photonic efficiency ξ_{rel} of a

Table 1.- Experimental RelativePhotonic Efficiencies (ξ_{rel}) and Calculated Quantum Yields (Φ) for the Initial Photooxidative Degradation of Various Organic Substrates (~ 200 μM) in Air- Equilibrated Aqueous TiO_2 (Degussa P-25 TiO_2; 2 g L^{-1}; pH ~ 3) Dispersions.

Substrate	Relative Photonic Efficiency(ξ_{rel}) [1]	Quantum Yields $\Phi_x = \xi_{rel}\,\Phi_{phenol}$
Phenol [2]	1.0	0.14 ± 0.02
2-Methylphenol	1.2 ± 0.1	0.17 ± 0.02
3-Methylphenol	1.3 ± 0.1	0.18 ± 0.02
4-Methylphenol	1.6 ± 0.1	0.22 ± 0.02
2,3-Dimethylphenol	2.0 ± 0.2	0.28 ± 0.03
2,4-Dimethylphenol	2.7 ± 0.1	0.37 ± 0.03
2,5-Dimethylphenol	2.3 ± 0.1	0.32 ± 0.03
2,6-Dimethylphenol	3.0 ± 0.2	0.42 ± 0.04
3,4-Dimethylphenol	2.5 ± 0.2	0.35 ± 0.04
3,5-Dimethylphenol	1.6 ± 0.2	0.22 ± 0.02
2,3,5-Trimethylphenol	2.8 ± 0.4	0.39 ± 0.04
2-Chlorophenol	1.2 ± 0.1	0.17 ± 0.02
3-Chlorophenol	1.0 ± 0.1	0.14 ± 0.02
4-Chlorophenol	1.2 ± 0.1	0.17 ± 0.02
2,4-Dichlorophenol	1.0 ± 0.1	0.14 ± 0.02

[1] N. Serpone, G. Sauve, R. Koch, H. Tahiri, P. Pichat, P. Piccinini, E. Pelizzetti, and H. Hidaka, *J.Photochem. Photobiol. A:Chem.*, **94**, 191 (1996).

[2] Standard substrate

given photocatalytic process, there remains to determine the actual quantum yield for the degradation of phenol Φ_{phenol} to obtain the quantum yields for other aromatic substrates RH. The quantum yield for the disappearance of phenol in an aqueous dispersion of Degussa P-25

TiO_2 at low loadings of titania upon irradiation at 365 ± 10 nm was Φ_{phenol} (365 nm) = 0.14 ± 0.02 [43]. The low TiO_2 loadings were necessitated in the determination of the photon flow actually absorbed by the photocatalyst {see Part II [43] in Chapter 3}.

Table 2.- Experimental Relative Photonic Efficiencies (ξ_{rel}) and Calculated Quantum Yields (Φ) for the Initial Photooxidative Degradation of Phenol (~ 200 μM) in Air-Equilibrated Aqueous Dispersions with Various TiO_2 Particulates (2 g L^{-1}; pH ~ 3) .

Titania, TiO_2	**Relative Photonic Efficiency** (ξ_{rel}) [1]	**Quantum Yields** $\Phi_{TiO2} = \xi_{rel}\,\Phi_{P\text{-}25}$
Degussa P-25 [2,3]	1.0 ± 0.1	0.14 ± 0.02
Baker & Adamson	0.38 ± 0.02	0.053 ± 0.002
Tioxide	1.9 ± 0.1	0.26 ± 0.03
Sargent-Welch	2.1 ± 0.1	0.29 ± 0.03
Fluka AG	2.2 ± 0.2	0.30 ± 0.03
Hombikat UV-100 [3]	0.25 ± 0.02	0.035 ± 0.003

[1] N. Serpone, G. Sauve, R. Koch, H. Tahiri, P. Pichat, P. Piccinini, E. Pelizzetti, and H. Hidaka, *J. Photochem. Photobiol. A: Chem.*, **94**, 191 (1996).

[2] Standard titania.

[3] Degussa P-25 TiO_2 was a gift from Degussa Canada Ltd.; it consists of two crystalline phases ~80% anatase and ca. 20% rutile and contains traces of SiO_2, Al_2O_3, HCl and Fe; it is non-porous with a BET specific surface area of ca. 55 $m^2\,g^{-1}$; crystallites range between 25 and 35 nm in size (dia.). The Hombikat UV-100 TiO_2 was a gift from Sachtleben Chemie GmbH (Germany); it is 100% anatase with a particle size (dia.) less than 10 nm; it is porous and has a BET specific surface area of ca 186 $m^2\,g^{-1}$.

The quantum yields for the photooxidation of other organic substrates (Tables 1) and of phenol using other photocatalyst materials (Table 2), experiments done under otherwise identical conditions were subsequently estimated from $\Phi = \xi_{rel}\,\Phi_{phenol}$ (Table 1) or from

$\Phi_{TiO2} = \xi_{rel} \Phi_{P25}$ (Table 2) using the appropriate relative photonic efficiencies reported {where Φ_{TiO2} is the quantum yield for the initial photodegradation of phenol using a different TiO_2 batch and Φ_{P25} is the quantum yield for the initial photodegradation of phenol using the standard Degussa P-25 TiO_2 specimen}.

To obtain relative photonic efficiencies, the following is recommended:

6. Determine the initial rate of disappearance (or loss of or conversion of) of phenol, $R^{initial}$(phenol), in mol min^{-1}. (A zero-order reaction).

7. Determine the initial rate of disappearance of (or loss of or conversion of) the substrate being examined, $R^{initial}$(substrate), also in mol min^{-1} and obtained under otherwise exact identical conditions as the initial rate in (6).

8. The relative photonic efficiency ξ_{rel} can subsequently be determined as indicated in equation 15, namely

$$\xi_{rel} = R^{initial}(\text{substrate}) / R^{initial}(\text{phenol}).$$

9. Given the quantum yield for the initial photodegradation of phenol Φ_{phenol} = 0.14 ± 0.02 (at 365 nm) calculate the quantum yield for the initial photodegradation of the organic substrate under examination (also at 365 nm irradiation) as indicated in equation 16.

6.2.2. Method of photonic efficiency

We commented in Section 5.4 about the interesting consequence of the limiting photonic efficiency (see eqn. 13b). Taking up equation 13b again in the following form:

$$\xi = \frac{\xi_{lim}\ C\ [TiO_2]}{(\xi_{lim} + C\ [TiO_2])} = \frac{R^{initial}}{R_{o,\lambda}} \qquad (13b)$$

we note that for the case where $C[TiO_2] >> \xi_{lim}$, i.e. for high loading in photocatalyst TiO_2, we obtain $\xi_{lim} = R^{in} / R_{o,\lambda}$, which is exactly the definition of the quantum yield Φ (see eqn 11c) if the whole photon flow $R_{o,\lambda}$ impinging on the reactor system is totally absorbed by the photocatalyst TiO_2 at high loadings. Under these conditions, the limiting photonic efficiency for irradiation at a given wavelength λ will reflect the true quantum yield of the process at the same wavelength; that is $\xi_{lim} = \Phi_{\lambda}$. Note that if the $R^{initial}$ data are obtained under broadband radiation in the wavelength range λ_1 to λ_2 and the integrated photon flow is determined in the same wavelength range, then $\xi_{lim} = \Phi_{poly}$.

10. Determine the photonic efficiency as indicated in protocols (1) to (5) in section 5.4 for various photocatalyst loadings at a given wavelength; we recommend obtaining several data points at the lowest loadings possible in the range 0.05 to 1 g L^{-1} with as much precision as possible in each of the data points, and subsequently an additional data set at loadings greater than 1 g L^{-1} (for Degussa P-25

TiO_2 we used up to 4 g L^{-1}) to describe a complete curve as per equation 13b.

11. Plot these photonic efficiencies versus TiO_2 loadings, in g L^{-1}, as indicated by equation 13b (see Figure 2 for an example).

12. Subsequently, plot the linear transform ξ^{-1} *versus* $[TiO_2]^{-1}$ (eqn. 17); the ξ_{lim} is given by the intercept (as ξ^{-1}_{lim}; see equation 17 and insert to Figure 2 for an example). The precision in ξ_{lim} and thus in Φ_λ will be greatly improved and more consistent quantum yields achieved the greater the body of data obtained experimentally is.

$$\frac{1}{\xi} = \frac{1}{\xi_{lim}} = \frac{1}{C\ [TiO_2]}$$

Figure 2 illustrates the photonic efficiencies as a function of various Degussa P-25 TiO_2 loadings for the initial photodegradation of phenol for a dispersion irradiated at 365 nm; the initial set of rate data between 0.05 and 0.50 g L^{-1} loading used to determine the quantum yield for phenol is that reported in Table 1 of Part II [43] (see Chapter 3). The insert illustrates the linear transform of the whole Langmuirian type curve; the intercept gives the limiting photonic efficiency at high titania loadings: $\xi_{lim} = 0.12 = \Phi$. This value is remarkably identical to the quantum yield assessed directly $\Phi = 0.14 \pm 0.02$ thus supporting the notion that at very high titania loadings all of the photon flow is absorbed.

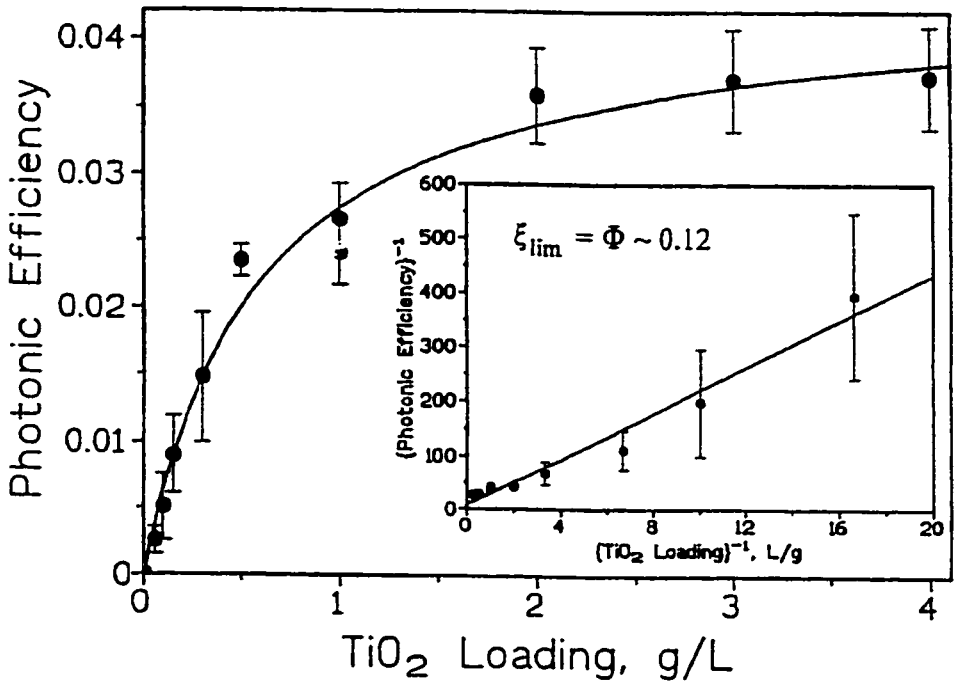

Figure 2.- Dependence of the photonic efficiencies ξ for the initial photodegradation of phenol on the loading of Degussa P-25 titania [TiO_2] for irradiation at the wavelength 365 ± 10 nm. The insert depicts the linear transform plotted as ξ^{-1} versus $[TiO_2]^{-1}$. The intercept from the linear transform gives the limiting photonic efficiency ξ_{lim}. For conditions, see text.

In an independent set of experiments we also determined $R^{initial}$ and then estimated the photonic efficiencies ($\xi = R^{initial} / R_{0,\lambda 1-\lambda 2}$) for the photooxidation of 20 mg L^{-1} phenol with irradiated Degussa P-25 TiO_2 (0.050 to 4.0 g L^{-1} loading) in the wavelength range 300 nm to 400 nm at pH ~2 in a pyrex reactor [43]. The limiting photonic efficiency at high titania loading under these conditions was $\xi_{lim} = 0.14 \pm 0.01$, identical to the calculated Φ_λ

from equation 16.

This lends credence to the possible usage of limiting photonic efficiencies at high photocatalyst loadings to assess quantum yields. Note, however, that because ξ_{lim}, is determined by an extrapolation procedure in which the $R^{initial}$ at the lowest TiO_2 loadings bears the greatest relative error, the ξ_{lim} value will carry some uncertainty. This calls attention to obtaining good initial rate data if this method is chosen.

To further test the validity of the procedure advocated herein, i.e. $\xi_{lim} = \Phi$, we also assessed the limiting photonic efficiency for the photooxidation of 4-chlorophenol {P-25 TiO_2, 0.3 g L^{-1}; λ = 365 nm; $R_{o,365}$ = 1.9 x 10^{-6} einstein min^{-1}; 20 mg L^{-1} of 4-ClPhOH}: ξ_{lim} = 0.19 ± 0.02, in good agreement with the estimated value (eqn. 16) of Φ = 0.17 ± 0.02 in Table 1.

Additionally, we estimated the limiting photonic efficiency for the photooxidation of phenol using the Hombikat UV100 TiO_2 under conditions otherwise similar to those employed for the Degussa P-25 TiO_2 system (loading 0.10 to 5.0 g L^{-1}, pyrex reactor, pH ~2, broadband radiation 300 to 400 nm): ξ_{lim} = 0.052 ± 0.009 (correlation coefficient = 0.9899), a value in fair agreement with the estimated Φ = 0.035 ± 0.003 (see Table 2). Finally we note that the trend in the quantum yields for the photodegradation of phenol for three of the titania specimens follows the order: Fluka TiO_2 > Degussa P-25 TiO_2 > Hombikat UV-100 TiO_2 , consistent with the greater light absorption at 365 nm of these systems in this order [53].

7. CONCLUDING REMARKS

In this Chapter we have examined the common label ***photocatalysis*** that has been described in a variety of ways. No agreement appears possible on an acceptable description. We have proposed a simple, general and non-specific definition. We have also presented a potentially useful protocol, noted as *Relative Photonic Efficiencies*, ξ_{rel} , to correlate efficiencies of a given process with similar work from other laboratories in the active area of Heterogeneous Photocatalysis. The procedure is simple and requires no sophisticated instrumentation. These efficiencies can ultimately be converted to ***quantum yields*** for the photocatalyzed oxidation of a given substrate since the corresponding quantum yield for the photooxidative degradation of phenol was determined using an integrating sphere method [42,43] to determine the extent of light absorbed by the photocatalyst Degussa P-25 TiO_2 taken as the standard.

The quantum yield can be calculated from photonic efficiencies using $\Phi = \xi_{rel}$ Φ_{phenol}. The procedure of limiting photonic efficiencies for high loadings of photocatalyst TiO_2 may provide an alternative method to assess quantum yields in heterogeneous photocatalysis, *albeit limited* to heterogeneous dispersions and one which does carry some uncertainty (see above). The latter procedure is precluded, for example, when the photocatalyst TiO_2 is immobilized on a support since no limiting photonic efficiency can be determined under these conditions.

Examination of the quantum yields and relative photonic efficiencies for different photocatalyst materials (Table 2) shows a nine-fold variation between the lowest value

(Hombikat UV-100 TiO_2) and the highest (Fluka) as expected from the lower extent of light absorbed by the former (see ref. [53]). Such variations may also be due to several other non-photonic factors: (1) differences in the crystalline phase of the titania (anatase versus rutile - the latter is known to be relatively inactive in photodegradations); (2) differences in the size and shapes of the particles, thereby affecting the extent of light scattered; (3) differences in the density of OH^- groups on the particle surface and in the number of water molecules hydrating the surface, particularly for particles for which the hydrophilic/hydrophobic properties vary; (4) differences in the number and nature of trap sites both in the lattice and at the surface; and finally (5) the adsorption/desorption characteristics of each surface that may vary according to the nature of the photocatalyst material but also on the nature of the organic substrate. Such adsorption/desorption variations may also affect the efficiency of the photocathodic reduction of molecular oxygen which is thought to control the efficiency of the photoanodic process, not to mention the possibility, as suggested by Fox [54], that active sites switch identity with inactive sites during the photocatalytic sequence. Taking all these factors into consideration precludes a definition [33] for a *heterogeneous quantum yield* {defined as a function of a heterogeneous rate in terms of amount (mol) of species converted per unit time per surface area of the catalyst (mol min^{-1} cm^{-2}) divided by the amount (einstein) of photons absorbed per unit time and unit volume of suspension (einstein min^{-1} cm^{-3})}. The treatment of quantum yields presented herein has assumed a pseudo-homogeneous treatment.

Finally, the congruence between the quantum yield of photooxidation of phenol by

illuminated Degussa P-25 TiO_2 of 0.14 (Table 1) with the value of 0.11 reported by Augugliaro and coworkers [55] for the photooxidation of phenol using "home prepared" polycrystalline TiO_2 specimens in the size range 44 to 250 μm and using an entirely different approach is indeed noteworthy. It would be of interest to confirm this alternative approach by assessing the quantum yield of some other substrate(s).

9. REFERENCES

[1]. D.P. Colombo Jr., K.A. Russel, J. Saeh, D.E. Skinner and R.M. Bowman, *Chem. Phys. Lett.*, **232**, 207 (1995).

[2]. D.E. Skinner, D.P. Colombo Jr., J.A. Cavaleri and R.M. Bowman, *J.Phys.Chem.*, **99**, 7853 (1995).

[3]. N. Serpone, D. Lawless, R. Khairutdinov, and E. Pelizzetti, *J.Phys.Chem.*, **99**, 16655 (1995).

[4]. (a) See e.g., M.A. Fox and M.T. Dulay, *Chem.Rev.*, 93 (1993) 341.
(b) Y. Li and L. Wang, in *Semiconductor Nanoclusters*, P.V. Kamat and D. Meisel, Eds., Studies in Surface Science and Catalysis, vol 103, 1997, Elsevier Science B.V., Amsterdam, pp.391-415.

[5]. R. Terzian, N. Serpone, and M. A. Fox, *J.Photochem.Photobiol.A:Chem.*, **90** , 125 (1995) .

[6]. N. Serpone, D. Lawless, and R. Khairutdinov, *J.Phys.Chem.*, **99**, 16646 (1995).

[7]. C. Kutal, in "*Photosensitive Metal-Organic Systems - mechanistic principles and applications*", C. Kutal and N. Serpone, Eds., *Adv.Chem.Series*, **238** , 1 (1993).

[8]. N. Serpone, E. Pelizzetti and H. Hidaka, in "*Photochemical and Photoelectrochemical Conversion and Storage of Solar Energy*", Z.W. Tian and Y. Cao, Eds., International Academic Publishers, Beijing, China, 1993, pp. 33-73.

[9]. J.W. Verhoeven, *Pure & Appl.Chem.*, **68**, 2223 (1996).

[10]. F. Chanon and M. Chanon, in *Photocatalysis - Fundamental and Applications*, N. Serpone and E. Pelizzetti, Eds., Wiley-Interscience, 1989, Ch. 15.

[11]. H. Kisch, in *Photocatalysis - Fundamental and Applications*, N. Serpone and E. Pelizzetti, Eds., Wiley-Interscience, 1989, Ch. 1.

[12]. R.G. Salomon, *Tetrahedron*, **39**, 485 (1983).

[13]. C. Kutal, *Coord.Chem.Rev.*, **64**, 191 (1985).

[14]. H. Hennig, D. Rehorek, and R.D. Archer, *Coord.Chem.Rev.*, **61**, 1 (1981).

[15]. M.J. Mirbach, *EPA Newslett.*, **20**, 16 (1984).

[16]. L. Moggi, A. Juris, D. Sandrini, M.F. Manfrin, *Rev.Chem.Intermed.*, **5**, 107 (1981).

[17]. G.G. Wubbels, *Acc.Chem.Res.*, **16**, 285 (1983).

[18]. L.P. Childs and D.F. Ollis, *J.Catal.*, **66**, 383 (1980).

[19]. A. Salinaro, A.V. Emeline, V.K. Ryabchuk, N. Serpone, *J.Photochem.Photobiol. A: Chem.*, submitted April 1999.

[20]. J.R. Bolton, K.G. Bircher, W. Tumas and C.A. Tolman, *J.Adv.Oxid.Technol.*, **1**, 3 (1996).

[21]. A.M. Braun, personal communication to N. Serpone.

[22]. A.M. Braun, personal communication to J.R. Bolton (1993). See also A.M. Braun et al., *Adv.Photochem.*, **18**, 235 (1993).

[23]. L. Jakob, T.M. Hashem, M.M. Kantor, and A.M. Braun, *Proc.Symp.Aquatic & Surface Photochemistry*, ACS Meeting, San Francisco, CA, 1992, pp.108-111.

[24]. E. Pelizzetti, C. Minero, L. Tinucci and N. Serpone, *Langmuir*, **9**, 2995 (1993).

[25]. (a) J.G. Calvert and J.N. Pitts, Jr., *Photochemistry*, Wiley, New York, 1966, p. 780.

(b) S.L. Murov *et al.*, Handbook of Photochemistry, 2nd edn., Marcel Dekker, New York 1993.

[26]. A.M. Braun, M.-T. Maurette, and E. Oliveros, *Photochemical Technology*, Wiley, New York, 1991, ch.2.

[27]. H.G. Heller and J.R. Langman, *J.Chem.Soc.Perkin II*, 341 (1981); see also information bulletin from Aberchromics Ltd., The University of Wales, College of Cardiff, Cardiff CF1-3TB, UK.

[28]. D.W. Bahnemann, D. Bockelmann and R. Goslich, *Sol. Energy Mater.*, **24**, 564 (1991).

[29]. P. Pichat, in "*Photochemistry, Photocatalysis and Photoreactors*", M. Schiavello, Ed., Reidel, Dordrecht, The Netherlands, 1985, pp. 425-455.

[30]. M. Schiavello, V. Augugliaro, and L. Palmisano, *J.Catal.* **127**, 332 (1991).

[31]. V. Augugliaro, L. Palmisano and M. Schiavello, *AICh.J.*, **37**. 1096 (1991).

[32]. L. Palmisano, V. Augugliaro, R. Campostrini, and M. Schiavello, *J.Catal.*, **143**, 149 (1993).

[33]. M.I. Cabrera, O.M. Alfano and A.E. Cassano, *Ind.Eng.Chem.Res.*, **33,** 3031 (1994).

[34]. N. Serpone, G. Sauve, R. Koch, H. Tahiri, P. Pichat, P. Piccinini, and E. Pelizzetti, and H. Hidaka, *J.Photochem.Photobiol.A:Chem.*, **94,** 191 (1996).

[35]. M. Boudart and G. Djega-Mariadassou, *Kinetics of Heterogeneous Catalytic Reactions*, Princeton University Press, 1984, pp.6-8.

[36]. G. Lepore, B.C. Pant and C.H. Langford, *Can.J.Chem.*, **71**, 2051 (1993).

[37]. G. Lepore, C.H. Langford, J. Vichova and A. Vlcek Jr., *J.Photochem.Photobiol. A: Chem.*, **75,** 67 (1993).

[38]. G. Lepore, A. Vlcek Jr. and C.H. Langford, in "*Photocatalytic Purification and Treatment of Water and Air*", D.F. Ollis and H. Al-Ekabi, Eds., Elsevier Science Publishers, Amsterdam, 1993, pp. 95-109.

[39]. See e.g., D.H. Everett, "*Basic Principles of Colloid Science*", Royal Society of Chemistry, London, 1988.

[40]. I. Rosenberg, J.R. Brock and A. Heller, *J.Phys.Chem.*, **96,** 3423 (1992).

[41]. *Handbook of Chemistry & Physics*, vol.51, CRC Press, Cleveland, Ohio, 1970-1971.

[42]. L. Sun and J.R. Bolton, *J.Phys.Chem.*, **100**, 4127 (1995).

[43]. A. Salinaro, A.V. Emeline, J. Zhao, H. Hidaka, V.K. Ryabchuk, N. Serpone, *Pure & Appl. Chem.*, **71**, 321 (1999).

[44]. N. Serpone, R. Terzian, D. Lawless, P. Kennepohl and G. Sauve, *J. Photochem. Photobiol. A: Chem.*, **73**, 11 (1993).

[45]. A. Emeline, A.V. Rudakova, V. Ryabchuk, N. Serpone, *J.Phys.Chem.B*, **102**, 10906 (1998).

[46]. N. Serpone, G. Sauve, P. Pichat, and E. Pelizzetti, *Proc. IPS-10 Conference*, Interlaken, Switzerland, 1994.

[47]. H. Tahiri , N. Serpone, and R. Le van Mao, *J.Photochem.Photobiol.A:Chem.*, **93,** 19 (1996).

[48]. R. Terzian, Ph.D. Thesis, Concordia University, Montreal, Canada, 1993.

[49]. R.W. Matthews and S.R. McEvoy, *J.Photochem.Photobiol.A:Chem.*, **64**, 93 (1992).

[50]. D.W. Bahnemann, A. Henglein and L. Spanhel, *Faraday Discuss.Chem.Soc.*, **78,** 151 (1984).

[51]. M. Anpo, T. Shima, S. Kodana and Y. Kubokawa, *J.Phys.Chem.*, **91,** 4305 (1987).

[52]. J.E. Valladares and J.R. Bolton, in "*Photocatalytic Purification and Treatment of Water and Air*", D.F. Ollis and H. Al-Ekabi, Eds., Elsevier Science Publishers. Amsterdam, 1993, pp. 111 -120.

[53]. M.I. Cabrera, O.M. Alfano and A.E. Cassano, *J.Phys.Chem.*, **100**, 20043 (1996).

[54]. M.A. Fox, personal communication to N. Serpone, July 1995.

[55]. V. Augugliaro, V. Loddo, L. Palmisano and M. Schiavello, *Sol.Energy Mater. Sol.Cells*, **38**, 411 (1995).

10. APPENDIX

GLOSSARY OF PROPOSED TERMS IN HETEROGENEOUS PHOTOCATALYSIS

Photocatalysis: A label that refers simply to a reaction or process that is **photon-driven** and that is **catalytic** as established by assessing the *turnover number* of the reaction or process.

Φ_λ Quantum yield of a process at wavelength λ defined as:
(1) number of events which occur per photon ***absorbed*** by the system at wavelength λ.
(2) amount (mol) reactant consumed or product formed per amount (einstein) of photons ***absorbed*** at wavelength λ.
(3) initial rate of reactant consumed or product formed ($R^{initial}$) per photon flow ($R_{o,\lambda}$) ***absorbed*** at wavelength λ.

$R^{initial}$ ***Initial rate*** of reactant consumed or product formed. {mol min^{-1}}.

$R_{o,\lambda}$ ***Incident*** photon flow of the irradiation source at a given wavelength λ {einstein min^{-1}}.

$R_{o,\lambda 1-\lambda 2}$ Integrated ***incident*** photon flow of the irradiation source in the wavelength range λ_1 to λ_2 {einstein min^{-1}}.

$R_{Ac,\lambda}$ Rate at which photons are ***absorbed*** by the actinometric substance Ac at the wavelength λ. {einstein min^{-1}}.

η Photo-efficiency of a process, defined as: amount (mol) of reactant consumed or product formed in the bulk phase per amount (einstein) of photons ***absorbed*** under polychromatic radiation over the spectral range λ_1 to λ_2 used during the reaction period and where the action spectrum of the light harvester or photocatalyst is unknown.

Φ_{poly} Quantum yield of a process under polychromatic radiation in the wavelength range λ_1 to λ_2 if the action spectrum of the light harvester or photocatalyst over this wavelength range is known.

n Amount (mol) of reactant consumed or product formed in the bulk phase.

n_{ph} Amount (einstein) of incident photons from the radiation source.

E_o Irradiance of the light source. {W m^{-2} or mW cm^{-2}}

E_{sc} Irradiance of the light scattered by a molecule or a particle. {W m^{-2} or mW cm^{-2}}

ξ Photonic efficency of a process defined as: amount (mol) of reactant consumed or product formed per amount (einstein) of ***incident*** photons on the reaction system either at a given wavelength or under broadband irradiation. {**Usage is Not Recommended**}.
(Values of photonic efficiencies are *apparent* quantum yields or *lower limits* of the quantum yield).

ξ_{rel} Relative photonic efficiency of a process given by the initial rate of reactant substrate consumed (or CO_2 product formed from substrate) divided by the initial rate of phenol consumed (or CO_2 product formed from phenol). {both reactions of the substrate and phenol are carried out under exact identical conditions}.

ξ_{lim} Limiting photonic efficiency of a process at high loading of the light harvester or photocatalyst.

V Volume of particle or molecule.

r Distance between the particle or molecule and the detector in light scattering experiments.

n_1 Refractive index of the solvent medium.

n_o Refractive index of the TiO_2 particles.

E_g	Bandgap energy between the valence and conduction bands of a semiconductor, in this case TiO_2.
N_p	Number of particles in light scattering for a solid/liquid system.

CHAPTER 3

TERMINOLOGY, RELATIVE PHOTONIC EFFICIENCY, AND QUANTUM YIELDS IN HETEROGENEOUS PHOTOCATALYSIS

PART II:

EXPERIMENTAL DETERMINATION OF QUANTUM YIELDS

Summary

In the preceding Chapter 2 we examined two principal features of heterogeneous photocatalysis that demanded scrutiny: (i) description of *photocatalysis* and (ii) description of process efficiencies. For the latter we proposed a protocol to assess the *relative photonic efficiency* which could subsequently be converted to quantum yields. A difficulty in expressing a quantum yield in heterogeneous photochemistry is the very nature of the system, either solid/liquid or solid/gas, which places severe restrictions on measurement of the photon flow absorbed by the light harvesting component, herein the photocatalyst TiO_2, owing to non-negligible scattering by the particulates. It was imperative therefore to examine the extent of this problem. Extinction and absorption spectra of TiO_2 dispersions were determined at low titania loadings by normal absorption spectroscopy and by

an integrated sphere method, respectively, to assess the extent of light scattering. The method is compared to the one reported by Grela *et al.* {*J.Phys.Chem.*, **100**, 16940 (1996)} who used a polynomial extrapolation of the light scattered in the visible region into the UV region where TiO_2 absorbs significantly. This extrapolation underestimates the scattering component present in the extinction spectra, and will no doubt affect the accuracy of the quantum yield data. Further, we report additional details in assessing limiting photonic efficiencies and quantum yields in heterogeneous photocatalysis.

1. INTRODUCTION

Heterogeneous photocatalysis has had its usefulness explored as a viable alternative technology to classical "best" technologies in both environmental detoxification [1-9] and in energy conversion devices [10]. This technology has witnessed significant advances during the last decade, and is actively being exploited towards the photooxidative mineralization of harmful environmental organic substrates (e.g., pesticides, herbicides, and others) by the utilization of illuminated semiconductor photocatalysts, amongst which anatase TiO_2 predominates.

Acting as pools of electrons and holes, photoexcited TiO_2 particulates can be capitalized in redox reactions. The scheme below summarizes but a fraction of the several events/processes that can ensue following illumination of this semiconductor at the bandgap energy E_g = 3.2 eV or higher (wavelengths below ~385 nm), where subsequent to their

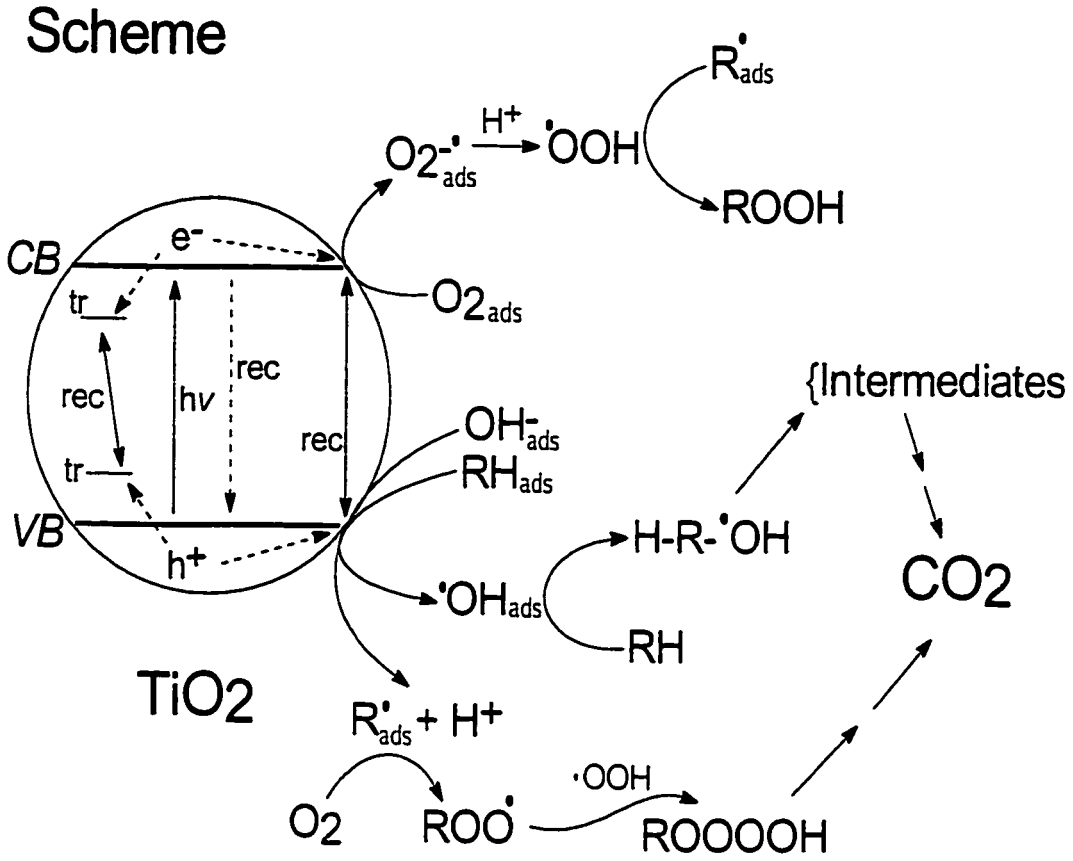

formation conduction band electrons and valence band holes are trapped by lattice defects or as Ti^{3+} (trapped electron) and as $Ti^{IV}-O^{-\bullet}-Ti^{IV}$ (trapped hole), recombine in the bulk and/or migrate to the surface in short time (few ps) where they may also be trapped by surface defects or trapped by adsorbed species such as O_2 for the electron to give the super-oxide radical anion, $O_2^{-\bullet}$, and by surface OH^- (or H_2O) for the hole to yield a surface-bound •OH radical, ≡Ti-•OH [11]. Ultimately, these surface trapped carriers react with organic substrates RH to give photooxidized intermediates and ultimately carbon dioxide; reducible species such as metal ions form metal deposits. Additional steps/processes can be envisaged

some of which have been corroborated, e.g. formation of organic peroxides [12], or inferred, e.g. formation of tetraoxides ROOOOH [4]. Conference proceedings [7], monographs [8] and review articles [1-6,9,13] have been published that summarize much of the recent knowledge of this exciting novel technology: heterogeneous photocatalysis.

An issue of significant debate in this area has been the expression of process efficiency for the light-driven conversion of an organic substrate RH to its ultimate mineralization. The goal is to assess process quantum yield, Φ_λ, as described in homogeneous photochemistry {see Part I of this series [14], Chapter 2}. Unfortunately, the presence of a heterogeneous (e.g. solid/liquid) phase has limited our ability to determine the exact number (or photon flow, $R_{o,\lambda}$) of photons absorbed by the solid phase, since the extent of light scattered by the metal-oxide (e.g. TiO_2) photocatalyst is not insignificant. According to a recent report, the extent of scattering can vary from 13% to 76%, depending on conditions of the total incident photon flow; variation in pH of the suspension also appears to influence the extent of scattering [15]. As well, Cabrera *et al.* [16] noted that only ca. 15% (Aldrich TiO_2) of the radiation measured by homogeneous actinometry inside a reactor was effectively absorbed. Possible solutions to assess the fraction of light absorbed in a heterogeneous photocatalytic process have been proposed [15-20]. A simple protocol to assess process efficiencies was proposed in Part I [14] (Chapter 2), and referred to as *relative photonic efficiency*, ξ_{rel}. Subsequently, values of ξ_{rel} can be converted to quantum yields.

The efficiencies ξ_{rel} reported elsewhere [17] and reproduced earlier (cf. Tables I and

2 of Part I [14]) referred specifically to substrate disappearance and demonstrated the general applicability of the proposed protocol. Although the ξ_{rel} are those for substituted phenols, the concept of relative photonic efficiency is not restricted to these species; it can also be applied to other aromatic substances with phenol as the standard substrate against which all ξ_{rel} are reported. The effects of variations in light irradiance, reactor geometry, pH, temperature, concentration of organic substrate, and loading of photocatalyst material TiO_2 on the ξ_{rel} data have also been examined [17] for 2-methylphenol, 2,4-dimethylphenol, and 4-chlorophenol (see Figure 1) as well as for other organic substrates.

The effects of the nature and the source of various TiO_2 specimens on ξ_{rel} were also explored [17]. The Tioxide, Sargent-Welch and Fluka titania specimens were twice more efficient than the Degussa P-25 TiO_2 specimen, at least for the initial photooxidation of phenol. Spin-trap EPR studies have demonstrated that production of •OH radicals on Degussa P-25 TiO_2 (ca. 80% anatase, 20% rutile) relative to those generated on an Aldrich (100% anatase) sample differed by a factor of ~1.9 [21] inferring the Degussa P-25 TiO_2 to be more efficient towards photooxidations by such radicals.

In assessing the quantum yield of a photochemical, photophysical, or photocatalytic process there is the requirement that the actual number of photons, n_{ph}, or photon flow, $R_{o,\lambda}$, from the radiation source absorbed by the substrate or photocatalyst in a heterogeneous system be known. To evaluate the fraction of light absorbed necessitates that the absorption spectrum of the light harvester or photocatalyst also be known. In a heterogeneous system

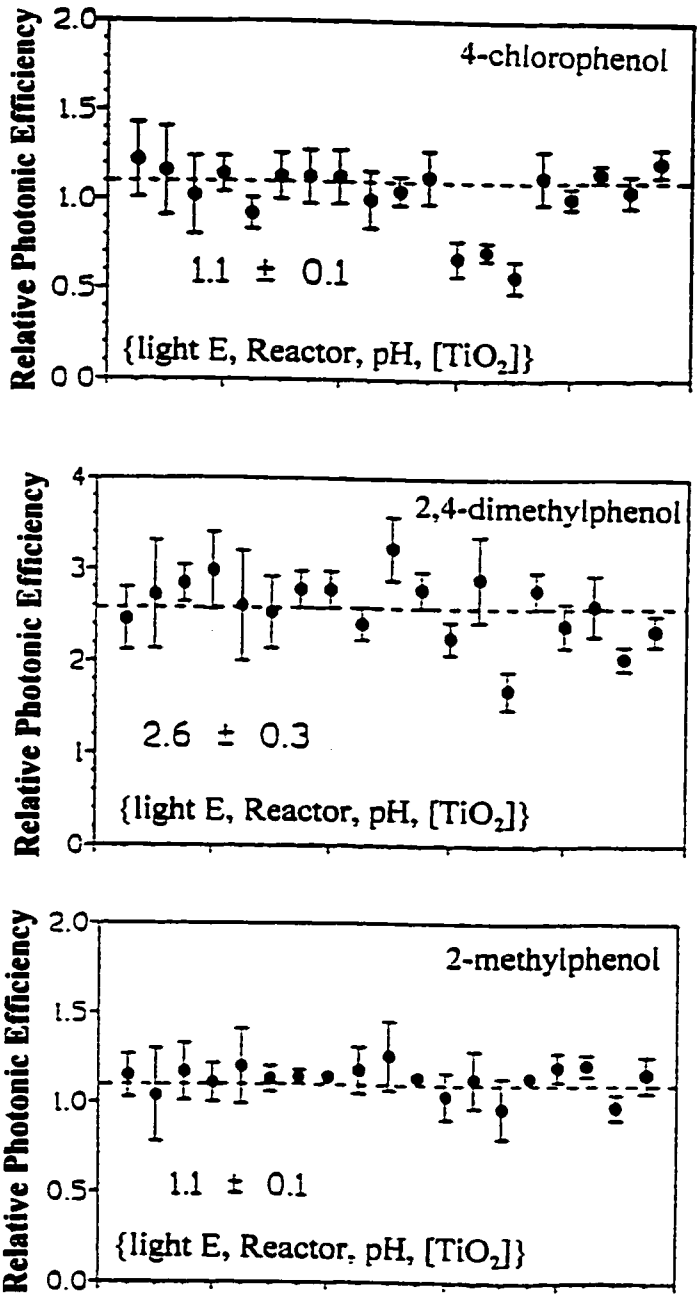

Figure 1. - Relative photonic efficiencies for 4-chlorophenol, 2,4-dimethylphenol and 2-methylphenol showing the values used to calculate averages; it includes only the effects of light intensity, reactor geometry, pH and concentration of titania; $[substrate]_i \sim 20$ mg L^{-1}. From ref. [17].

such as solid/liquid, scattering effects impinge strongly on the absorption spectrum; what is typically measured in such a system is the extinction spectrum. Brief consideration suggests that determination of the true absorption spectrum of polydispersed titania particles suspended in an aqueous medium is best carried out by a spectrophotometric integrating sphere technique which will account for the photons scattered, transmitted and absorbed. This method has recently been applied successfully [18,19].

Grela and coworkers [20] reported an empirical simple method to estimate the extent of scattering at 295 nm in a thin slab of polydispersed illuminated TiO_2 sol to assess the ***approximate*** *quantum yield* for the initial formation of the DMPO-•OH spin adduct. The baseline at wavelengths between 400 and 550 nm in the extinction spectrum of the sol was extrapolated to 250 nm by a quadratic extrapolation method, rather than by the theoretical λ^{-4} dependence that typically describes light scattering by particles. No reasons were given for the choice of a quadratic extrapolation method. The absorbance of the TiO_2 colloidal sol examined and corrected for residual scattering at 295 nm was ~70% of the extinction spectrum determined by normal absorption spectroscopy [20].The discrepancy between this study and the methods used by others [15,16], together with the rather empirical and simplistic approach of ref. [20], especially since the conditions of the suspensions can affect the proportion of light scattered, led us to examine the degree to which titania particles scatter incident light radiation.

During the course of our work [19] to systematize a protocol and methodology to determine quantum yields in heterogeneous photochemistry, we measured the absorbance

of Degussa P-25 TiO_2 (the same as used by Grela *et al.* [20]) and of a sample of the Hombikat UV-100 TiO_2 by the integrating sphere method employing the procedures reported elsewhere [18,19]. We compare the integrating sphere method with the empirical method used by others [20] to test the validity of the latter. We find that the empirical method significantly underestimates the extent of scattering below ca. 380 nm. The scattering tends to plateau below ca. 340 nm in the region where the Degussa P-25 TiO_2 absorbs significantly. We also report some experimental details in the protocol used to estimate relative photonic efficiencies and quantum yields.

2. EXPERIMENTAL

2.1 Materials

The Degussa P-25 TiO_2 specimen was a gift from Degussa Canada Ltd. and the Hombikat UV-100 titania sample was obtained from Sachtleben Chemie GmbH (Duisburg, Germany). The phenol and the 4-chlorophenol were available from earlier studies.

Degussa P-25 TiO_2 consists of two crystalline phases ~80% anatase and ~ 20% rutile and contains traces of SiO_2, Al_2O_3, HCl and Fe; it is a non-porous solid with a BET specific surface area of ~55 $m^2\ g^{-1}$ and its crystallites range between 25 and 35 nm [22].These crystallites aggregate in a regular dispersion; sizes vary between 50 nm and 200 nm [23,24]. The Hombikat UV-100 TiO_2 is 100% anatase with particle size less than 10 nm and with a BET specific surface area of ca. 186 $m^2\ g^{-1}$ [25].

The polydispersed titania sols were obtained by sonication/centrifugation procedures

reported elsewhere [18-20]. To prepare the colloidal sols, a 250-mL acidifed (0.01 M HCl) aqueous suspension of 2 g L^{-1} in Degussa P-25 TiO_2 was sonicated with an ultrasonic 250-watt cell disrupter (Sonics & Materials) at a power of ~50 watts for 15 min; the milky dispersion was then centrifuged (2,000 rpm) in 50-mL portions until a transparent colloidal sol was obtained. This sol was extracted and left to evaporate slowly at ambient temperature. Approximately 250 mg of the TiO_2 was recovered and later used to prepare a stock colloidal sol with a loading of 1 g L^{-1} in titania in 0.01 M HCl aqueous media.

2.2. *Extinction and absorption spectra, and determination of the fraction of photon flow absorbed by TiO_2*

The extinction and absorption spectra at various titania loadings at pH ~ 2 were recorded using a 0.2 mm quartz cell and a Shimadzu UV-265 spectrophotometer equipped with an integrating sphere (Figure 2) with an internal diameter of 60 mmϕ and a R-446U photomultiplier at the base (incidence angle to reflecting sample: 8° ; beam size ca. 3 mm width and 5.5 mm height. The standard white reflecting plates contained $BaSO_4$ (Eastman Kodak White Reference Standard; reflectance, 98.23% at 365 nm). The modified method used to assess the fraction of the photon flow, f_λ , absorbed by the titania sols (loading range:10 mg L^{-1} to 150 mg L^{-1}) is identical to that reported earlier [18,19].

The method of calculating the absorption spectra with the integrating sphere followed the method of Sun and Bolton who used an identical instrument [18,19]. With the 0.20-mm cell and the geometry of the integrating sphere, unaccountable light scattered was negligible. Under our conditions, the instrument response A_t for a solution with no titania particles is

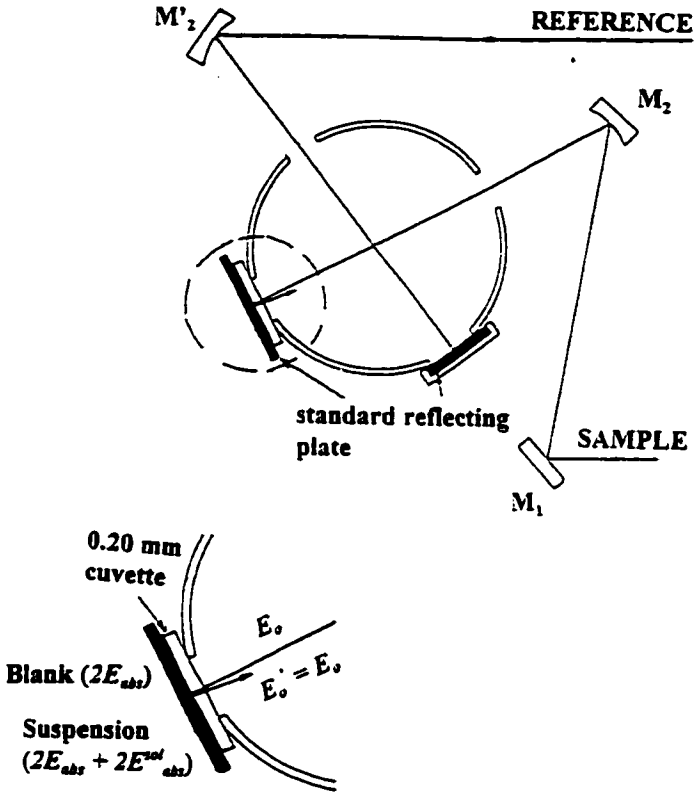

Figure 2.- Modified integrating sphere assembly method to determine the fraction of absorbed light by titania colloidal sols.

given by,

$$A_1 = \frac{-\log(E_o - 2E_a)}{E_o} \qquad (1)$$

whereas

$$A_2 = \frac{-\log(E_o - 2E_a - 2E_a^{sol})}{E_o} \qquad (2)$$

is the response for the titania colloidal sol from which the fraction f_l was evaluated; E_o is the light irradiance from the light source and E_a is the irradiance of the light absorbed.

$$f_\lambda = \frac{10^{-A_1} - 10^{-A_2}}{2} \tag{3}$$

The absorbance spectrum of the titania particles in the sol was calculated from

$$A = -\log(1 - f_\lambda) \tag{4}$$

The incident photon flow $R_{o,\lambda}$ at 365 ± 10 nm was determined by Aberchrome 540 actinometry [26].

Figure 3 summarizes the fraction of photon flow f_λ absorbed at 365 nm for the Degussa P-25 TiO_2 and the Hombikat UV-100 TiO_2 sol specimens in the concentration range 0.010 to 0.150 g L^{-1}. The fraction of light absorbed at loadings of 0.300 and 0.500 g L^{-1} were estimated assuming Beer's law behavior (see Table 1).

2.3. Determination of quantum yields

In the photocatalyzed oxidations of phenol and 4-chlorophenol by illuminated titania particulates, as indicated in Part I [14], the titania/phenol aqueous dispersion was stirred in the dark for about 30 to 60 minutes to bring the system to an adsorption/desorption

equilibrium stage prior to irradiation.

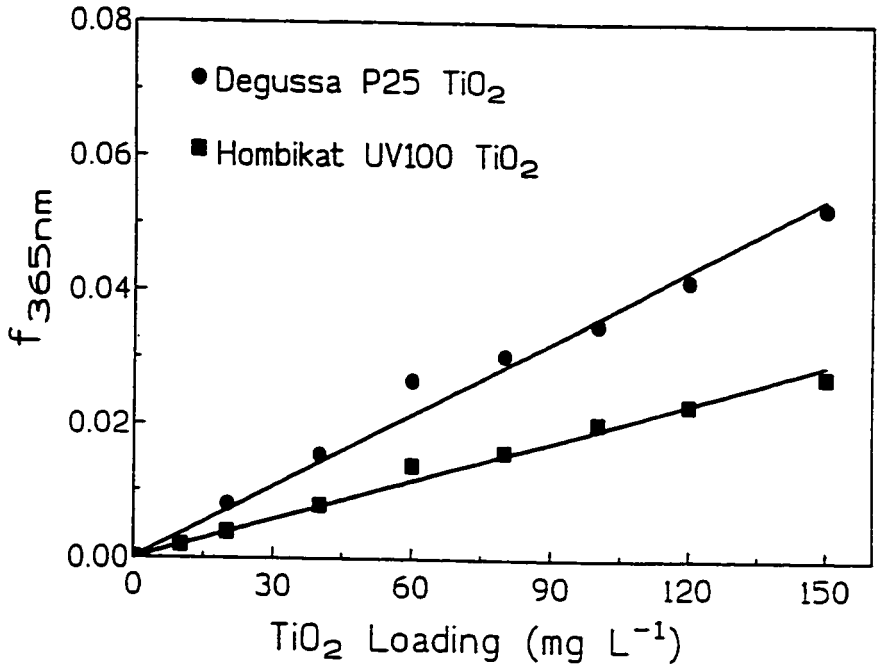

Figure 3. - Fraction of photon flow absorbed at 365 nm versus titania sol concentration for the Degussa P-25 TiO_2 and the Hombikat UV-100 TiO_2 specimens.

The initial rates of the photocatalyzed oxidation of phenol {Aldrich, 99%+ redistilled; pH was 2.7} were obtained by monitoring the temporal variations of the concentration of phenol by HPLC chromatography {Waters 501 HPLC pump; Waters 441 HPLC detector; HP 3396A integrator; Waters Bondapak C-18 reverse phase column} after 365 ± 10 nm irradiation (selected with Bausch & Lomb 0.25-meter monochromator) of the aqueous TiO_2 /phenol dispersion in a quartz reactor employing an Oriel 1000-watt Hg/Xe lamp as the

radiation source. Samples were collected at various time intervals and filtered through a 0.20-μm Teflon filter prior to HPLC analysis to remove suspended particulates. Initial rate data are given in Table 1 and illustrated in Figure 4.

Table 1.- Initial rates, R^{in}, photon flow, $R_{o,\lambda}$, fraction of light absorbed at 365 nm, f_{365}, quantum yields for the initial photocatalyzed oxidative transformation of phenol, $\Phi_{dis\,(PhOH)}$, and photonic efficiencies, ξ, at ambient temperature and for air-equilibrated sols.

TiO_2 Loading (g L^{-1})	$10^8 R^{in}$ (mol min^{-1})	$10^6 R_{o,365}$ [a] (einstein min^{-1})	f_{365} [b]	Φ_{dis} (PhOH)	$10^3 \xi_{365}$ [d]
0.060	0.54 ± 0.21	2.13	0.0216	0.118	2.5 ± 1.0
0.10	1.31 ± 0.65	2.60	0.0359	0.140	5.0 ± 2.5
0.15	1.91 ± 0.61	2.13	0.0539	0.167	9.0 ± 2.9
0.30	3.14 ± 1.02	2.13	(0.108) [c]	0.137	14.7 ± 4.8
0.50	5.00 ± 0.26	2.13	(0.180) [c]	0.131	23.5 ± 1.2
1.0	4.49 ±0.51	1.86	-------	-------	24.1 ± 2.4
1.0	5.13 ±0.45	2.05	-------	-------	25.0 ± 2.1
2.0	6.08 ±0.72	1.69	-------	-------	35.9 ± 3.4
3.0	6.27 ±0.79	1.69	-------	-------	37.0 ± 3.7
4.0	6.33 ±0.75	1.69	------	------	37.5 ± 3.5

Average $\Phi_{dis\,(PhOH)} = 0.14 \pm 0.02$

[a] The incident photon flow was measured by Aberchrome actinometry using a procedure supplied by Aberchromics Ltd. of the University of Wales College of Cardiff, Cardiff CF1-3TB, UK.

[b] Corrected (see Figure 3).

[c] Estimated from the experimentally obtained fraction of light absorbed for TiO_2 loadings from 10 mg L^{-1} to 150 mg L^{-1}. (See Figure 3).

[d] Calculated from equation $\xi_{365} = R^{in} / R_{o,365}$

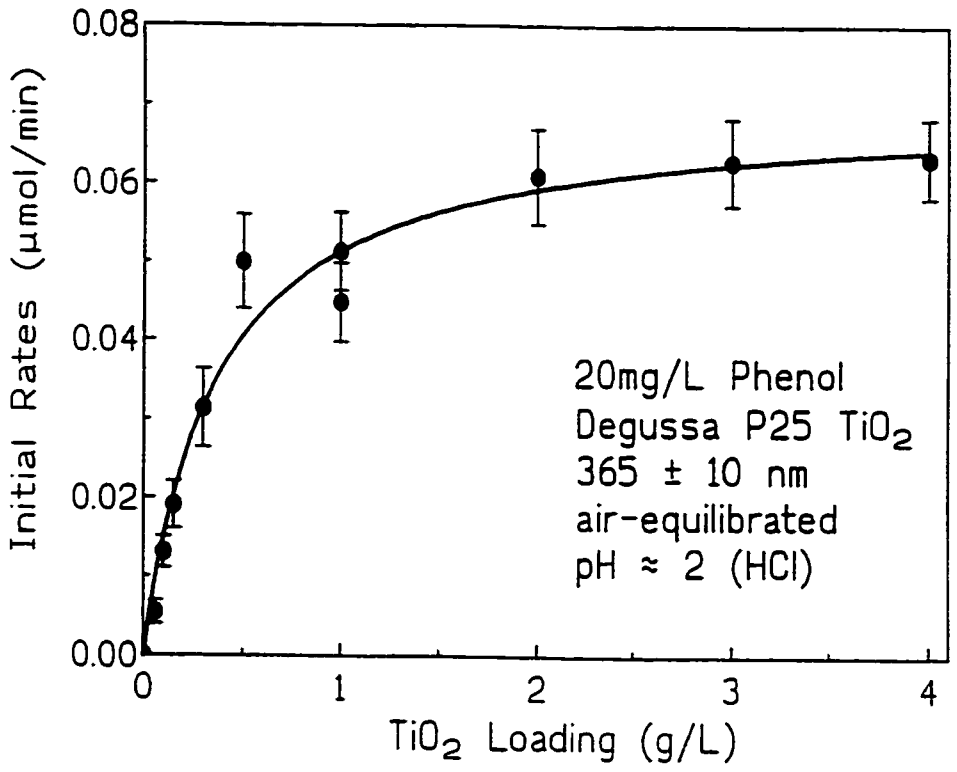

Figure 4.- Initial rates for the photooxidative degradation of phenol versus TiO_2 loading for the Degussa P-25 TiO_2 specimen.

3. RESULTS AND DISCUSSION

In the previous Chapter 2, Part I [14], we observed that when a photon hits a photocatalyst particle such as TiO_2 in condensed phase, the fraction of light scattered (E_{sc}/E_o) depends on several factors: (i) on the number of particles (N_p), (ii) on the square of the particle volume (V^2) - hence on the sixth power of the particle radius, (iii) on a geometric factor $\{P(\theta)\}$ that accounts for scattering from different parts of the particle, (iv) on the

reciprocal of the fourth power of the wavelength of irradiation (λ^{-4}), and (v) on the square of the distance of the observer (detector), r^2, from the particle. A more crucial factor that affects E_{sc}/E_o is the fourth power of the ratio of the refractive indices $\{(n_l/n_o)^4\}$ of the photocatalyst particle (n_l) and of the surrounding medium (n_o).

For the particular case examined here, two variables are most critical to the fractional light scattering: (a) an increase in the TiO_2 loading $\{N_p\}$ increases scattering, and (b) increasing the size (radius, R) of either the particles (~30-nm crystallites) or of the ubiquitous particle aggregates, usually omnipresent in such suspensions, augments scattering significantly since E_{sc}/E_o scales with R^6.

3.1. Extinction and Absorption Spectra

Extinction (i.e. absorption and scattering/reflection of light by a substrate) and absorption spectra of TiO_2 dispersions were recorded at low titania loadings by normal absorption spectroscopy and by an integrated sphere method, respectively, to explore the extent of light scattered by the photocatalyst nanoparticles. This method contrasts the one proposed recently by Grela *et al* [20]. Determination of the degree of scattering in titania dispersions is especially critical since TiO_2 has even been suggested as an actinometer for UV radiation [27].

Figure 5 illustrates the extinction spectra of the Degussa P-25 TiO_2 and the Hombikat UV-100 TiO_2 in aqueous phase. Also shown are the scattering curves extrapolated to the

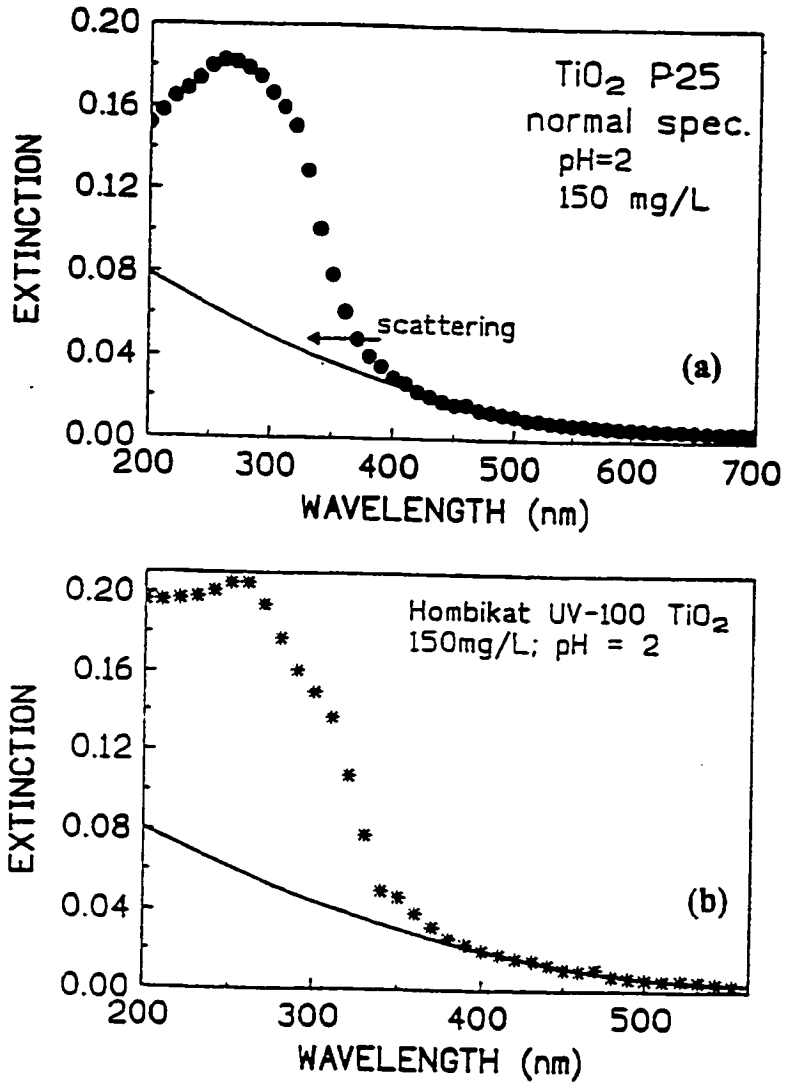

Figure 5.- Extinction spectra (solid circles and asterisks) of polydispersed TiO_2 sols in aqueous media at pH ~ 2: loading, 150 mg L^{-1}. (a) Degussa P-25 TiO_2; (b) Hombikat UV-100 TiO_2. The solid line that extrapolates the baseline from the visible region reflects the scattering of light; the extrapolation was carried out by a quadratic polynomial (see text).

ultraviolet range from the experimental baseline in the visible region using the quadratic polynomial expression (eqn 5) to probe the extent of light scattered in the UV region [20],

$$E_{sc} = a + b\lambda + c\lambda^2 \qquad (5)$$

where TiO_2 absorbs significantly (a , b, and c are coefficients).

The extinction spectra of titania sols at 40 mg L^{-1} and 150 mg L^{-1} loadings are compared with the calculated (integrating sphere) absorbance spectra (Figure 6) by the method reported earlier [18,19]. The differences between the extinction spectra and the absorbance spectra are also illustrated; they reflect the wavelength-dependent scattering component in the extinction spectra. In the comparison, the values were set to zero at 400 nm where anatase titania does not absorb. (Note that the absorption threshold of titania anatase used is at ca. 385 nm). The scattering component increases monotonically up to ca. 350 nm and then levels off to 200 nm for the Degussa P-25 TiO_2 (~80% anatase). For the Hombikat UV-100 TiO_2 anatase specimen [25], the scattering component increases continually from 400 nm to 200 nm. Evidently, scattering is greatly attenuated as titania absorption increases in the uv region, as expected. Indeed, relative scattering drops from ~80% at 390 nm to about 30-40% at 300 nm for the 150 mg L^{-1} Degussa P-25 TiO_2 and to ca. 40-50% at 320 nm for the corresponding Hombikat UV-100 titania sample. However, to the extent that the degree of light absorption can be as low as ~15% [15,16], the (apparent) quantum yields determined by the extrapolation method [20] could be discrepant by as much as a factor of 2 to 5.

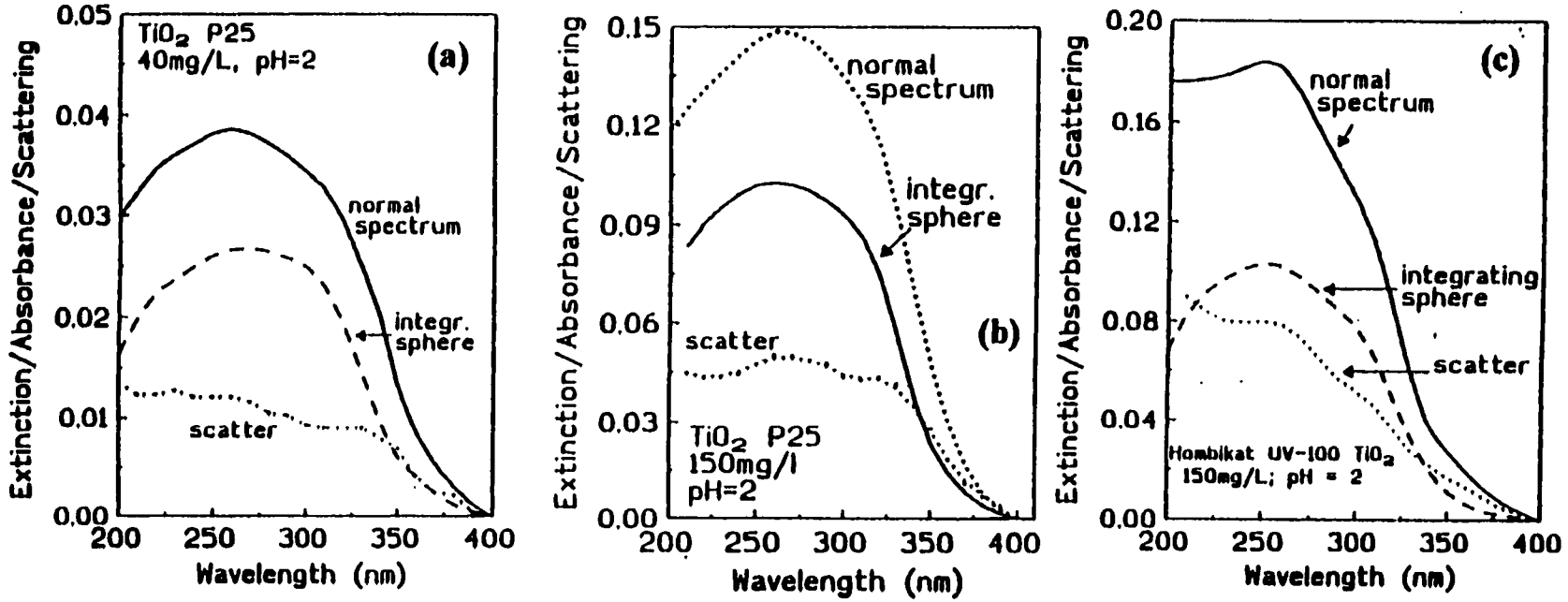

Figure 6.- Plots illustrating the extinction (normal spectrum), absorbance (integrating sphere method) and scattering (obtained by subtracting the absorbance from the extinction spectra) of polydispersed titania sols: (a) 40 mg L^{-1} Degussa P-25 TiO_2; (b) 150 mg L^{-1} Degussa P-25 TiO_2; (c) 150 mg L^{-1} Hombikat UV-100 TiO_2. All spectra were corrected for the extent of scattering in the visible region and thus placed at zero at 400 nm..

More revealing are the comparisons between the experimental (at wavelengths > 400 nm) and the quadratic and cubic polynomial extrapolations (to wavelengths < 400 nm) of the light scattering components illustrated in Figures 7a and7b for the 40 mg L^{-1} and 150 mg L^{-1} Degussa P-25 TiO_2 loading, respectively, and for the Hombikat UV-100 TiO_2 sample (also 150 mg L^{-1}; Figure 7c). The scattering components in Figure 6 were added to the corresponding experimental scattering (data points) in Figure 7. It is clear that the quadratic extrapolation method (curves b in Figure 7) [20] significantly underestimates the experimental scattering component (curves a) between 380 nm and 220 nm in two cases presented (Figures 7a and 7b), whereas for the Hombikat UV-100 TiO_2 specimen (Figure 7c) this extrapolation totally underestimates the scattering component at all wavelengths below 380 nm. The cubic extrapolation (curves c in Figures 7a,7b, and 7c; here the term $d\lambda^3$ was added to eqn 5) is an improvement but still underestimates the scattering behavior of the titania solutions.

The scattering component does indeed follow the expected λ^{-4} dependence as demonstrated in Figure 8a for the Degussa P-25 TiO_2 for all wavelengths down to 350 nm, and in Figure 8b for the Hombikat UV-100 TiO_2 system down to 250 nm. At shorter wavelengths, the scattering levels off in both instances (see caption in Figure 8).

It is clear that the empirical method used [20] to assess the degree of scattering consistently underestimates the extent of scattering below 380 nm. Scattering tends to plateau for the Degussa P-25 TiO_2 sols (not for the Hombikat UV-100 TiO_2 specimen) below ~340 nm in the region where they absorb significantly.

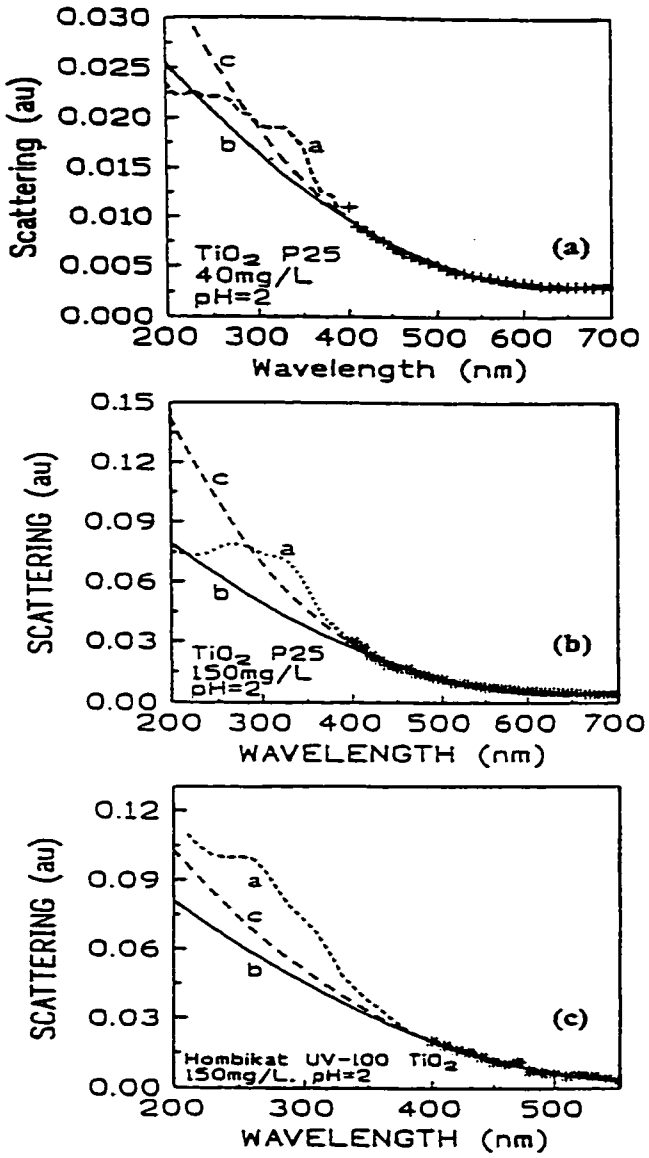

Figure 7.- Plots showing the experimental baseline at wavelengths above 400 nm (scattering) for the three titania samples at different loadings (see Figure 6). The curve **a** in each graph denotes the scattering component in the 200-400 nm region (see Figure 6) added to the visible component. Curve **b** refers to the scattering expected from the extrapolation using the quadratic polynomial method, whereas curve **c** is the scattering component expected if we use a cubic polynomial method (see text).

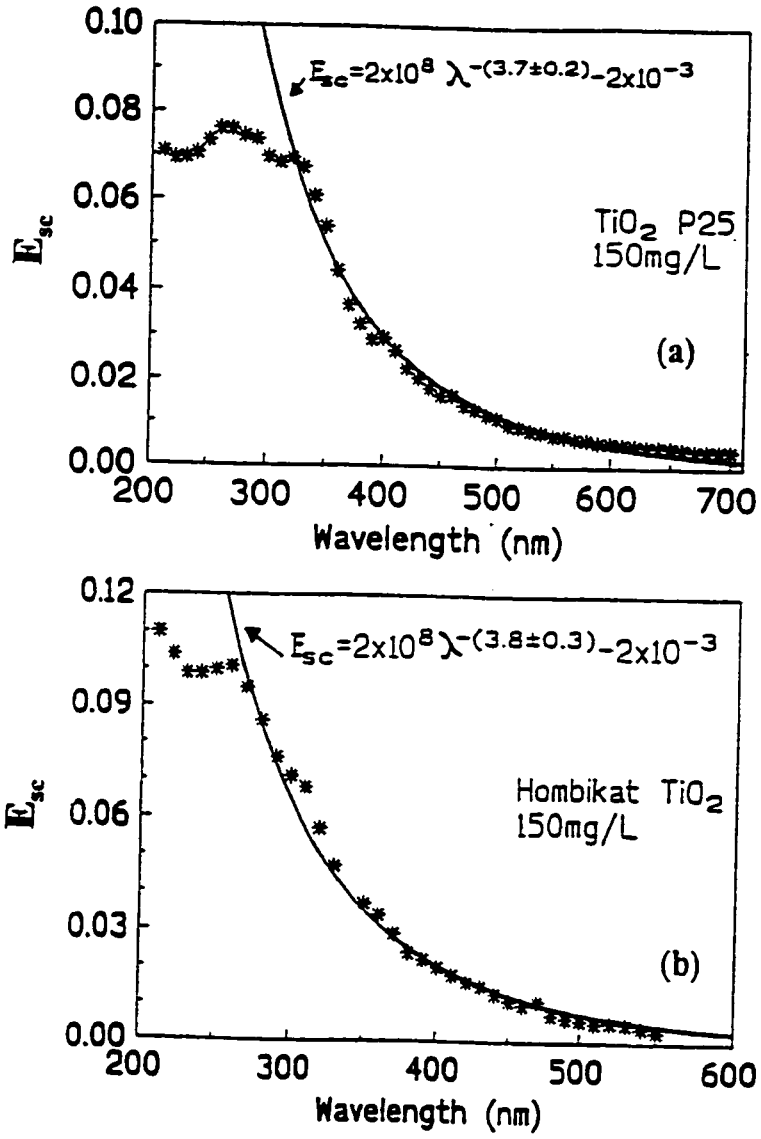

Figure 8.- Scattering for the Degussa P-25 TiO_2 (a) and the Hombikat UV-100 TiO_2 (b) at 150 mg L^{-1} loadings. The solid curve in both graphs was drawn using the equation indicated, namely scattering follows the λ^{-1} law down to ca. 340 nm for Degussa P-25 TiO_2 and to ca. 260 nm for the Hombikat UV-100 TiO_2 specimen. The apparent levelling off at the shorter wavelengths is due to the considerable attenuation of the scattering by the increased absorption in this region of the UV.

The spectral features of Figure 6 are qualitatively similar to the features reported recently by Cabrera and coworkers [28] for TiO_2 specimens from various sources (Degussa P-25 TiO_2, Hombikat UV-100 TiO_2, Fluka, Fisher, Aldrich and Merck). These authors also assessed the specific extinction (Figure 9A), scattering (Figure 9B), and absorption (Figure 9C) coefficients in the UV region (270-400 nm) illustrated here only for the Degussa P-25 TiO_2 and Hombikat UV-100 TiO_2 systems. Figure 9D illustrates the scattering versus absorption ratio at various wavelengths; note the relatively rapid rise in scattering towards the visible wavelengths. Except for the Degussa P-25 TiO_2 and the Hombikat UV-100 TiO_2 specimens. the specific absorption coefficients for all other samples are fairly similar and constant. At 360-370 nm the specific absorption coefficients for the Degussa P-25 and Hombikat UV-100 TiO_2 are less than that for the other titania specimens. The specific scattering coefficients follow the trend: Fisher/Fluka < Hombikat UV-100 < Merck < Aldrich << Degussa P-25. Scattering influences the extinction spectra which follow a similar trend. On the basis of specific surface area alone, the authors [28] inferred that the catalytic properties should follow the trend: Hombikat UV-100 >>> Degussa P-25 >> Aldrich/Merck/ Fluka/Fisher. However, taking into account the photonic properties of these specimens. the expected process photonic efficiencies should be: Degussa P-25 >>> Aldrich/Merck/ Fluka/Fisher > Hombikat UV-100 [28]. This trend is consistent with the photonic efficiencies we observed earlier [17,25] between the Degussa P-25 and the Hombikat UV-100 TiO_2 specimens.

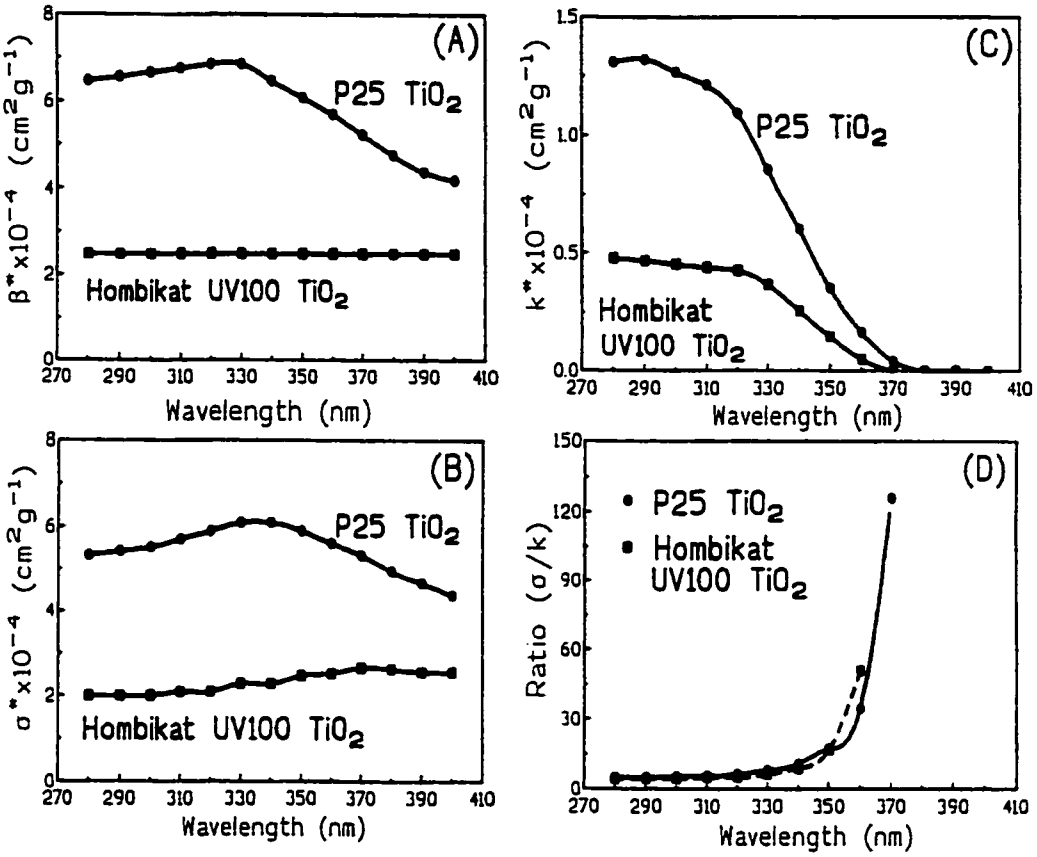

Figure 9. (A) Extinction coefficients versus wavelength for Degussa P-25 TiO_2 and for Hombikat UV-100 TiO_2 particles; (B) scattering coefficients of the Degussa P-25 TiO_2 and the Hombikat UV-100 TiO_2 particles; (C) absorption coefficients of the Degussa P-25 TiO_2 and Hombikat UV-100 TiO_2 particles; (D) scattering to absorption coefficients ratio of the Degussa P-25 TiO_2 and Hombikat UV-100 TiO_2 particles. Data adapted from ref. [28].

We deduce from our spectroscopic data that any determination of *absolute* quantum yields in heterogeneous photochemistry necessitates an experimental approach to assess the number (or photon flow) of absorbed photons. The integrating sphere method is one such

approach since the transmitted, scattered and absorbed photons can be accounted for. Quadratic or cubic polynomial extrapolations of the spectral baseline in the visible region remain simply approximations that if used will still only provide an *apparent* quantum yield [20] for the process being examined.

3.2. *Determination of quantum yields*

Perusal of the initial rates of photodegradation of phenol (Table1) by illuminated Degussa P-25 TiO_2 together with the corresponding graphical representation of R^{in} as a function of increasing TiO_2 loading (Figure 4) shows that the rates increase linearly from 0 to about 0.50 g L^{-1} loading and then level off to 4.0 g L^{-1} loading. This is understandable since, as the titania loading increases, the suspension becomes more opaque to light such that only photons absorbed by titania particles onto which a phenol molecule is pre-adsorbed may be effective in carrying out the redox chemistry. Other incident photons, absorbed or otherwise, are wasted. In essence the titania particles themselves act as an inner filter (see Figure 10) despite good stirring of the dispersion during irradiation, a problem also encountered in homogeneous photochemistry.

Given the fraction of light absorbed at 365 nm, f_{365} in Table 1, together with the initial rates of photooxidation of phenol, R^{in}, under 365 nm irradiation and with the rate of incident photons, $R_{o,\lambda}$, at TiO_2 loadings from 0.060 to 0.500 g L^{-1} collected in Table 1 we

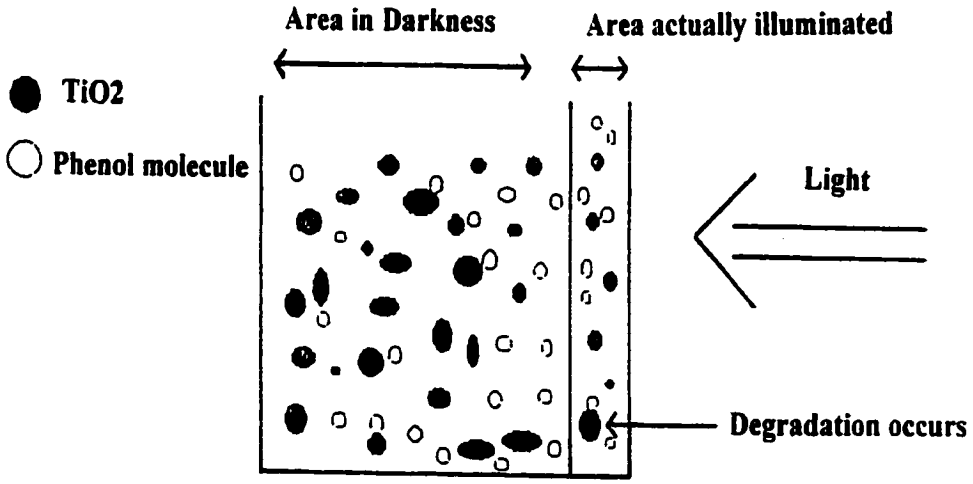

Figure 10.-Typical reactor cell used in the photocatalyzed oxidative degradation of phenol in determining initial rates of disappearance of phenol and subsequently the preliminary quantum yield data.

calculated the quantum yield by equation 6:

$$\Phi_{phenol} = \frac{R^{initial}}{R_{o.365}\, f_{365}} \qquad (6)$$

The resulting quantum yields are summarized in Table I for five titania loadings for which initial rates are nearly linear with loading. The average Φ_{phenol} (365 nm) for the initial photodegradation of phenol is 0.14 ± 0.02. The photonic efficiency dependence on the TiO_2 loading reported in Table I and shown graphically in Figure 2 of Part I [14] (Chapter 2) follow the expected Langmuirian type trend. The intercept from the linear transform gave a limiting photonic efficiency of $\xi_{lim} \sim 0.12$, in good agreement with the estimated quantum

yield (Table 1).

In an independent set of experiments, we determined the photonic efficiencies (as $\xi = R^{in} / R_{o.300-400}$) for the photooxidation of 20 mg L^{-1} phenol with irradiated Degussa P-25 TiO_2 (0.050 to 4.0 g L^{-1} loading) under broadband radiation (ca. 300-400 nm) at pH ~2 in a pyrex reactor (Figure 11). The insert in Figure 11 illustrates the corresponding linear

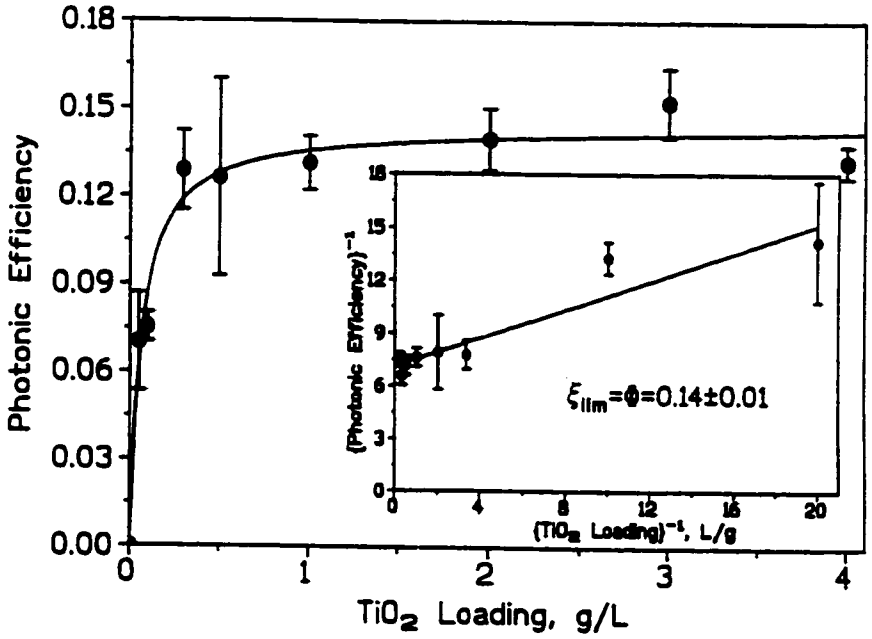

Figure 11. - Photonic efficiencies versus TiO_2 loading (Degussa P-25) for the photodegradation of phenol (20 mg L^{-1}) in air-equilibrated suspensions at pH ~ 2 (HCl); wavelength range of irradiation: 300-400 nm. The Degussa P-25 TiO_2 was used without any prior treatment.

transform of the data. The limiting photonic efficiency, ξ_{lim}, at high titania loading is surprisingly also 0.14 ± 0.01. In this instance, the Degussa P-25 TiO_2 specimen received no

prior treatment, except for allowance made to stir the dispersion to establish the adsorption/desorption equilibrium.

The quantum yields for the photooxidation of other organic substrates and of phenol using other photocatalyst materials (Tables 1 and 2 of ref. [14]; see also Chapter 2), experiments done under otherwise identical conditions, were reported earlier. The validity of the procedure advocated herein was further assessed by determining first the photonic efficiencies and subsequently from the limiting photonic efficiency the quantum yield for the photooxidation of 4-chlorophenol: $\xi_{lim} = \Phi = 0.19 \pm 0.02$, in good agreement with the estimated value of 0.17 ± 0.02 [14]. Likewise, we assessed the limiting photonic efficiency for the photooxidation of phenol using the Hombikat UV-100 TiO_2 under conditions otherwise similar to those employed for the Degussa P-25 TiO_2 system (loading 0.10 to 5.0 g L^{-1}, pyrex reactor, pH ~2, broadband radiation from 300 nm to 400 nm). The ξ_{lim} was 0.052 ± 0.009, a value consistent with the estimated quantum yield of 0.035 ± 0.003 (Table 2 of ref. [14]).

4. CONCLUDING REMARKS

In the previous Chapter 2, Part I, we presented a useful protocol, *Relative Photonic Efficiency*, ξ_{rel}, to correlate efficiencies of a given process in a heterogeneous (solid/gas or solid/liquid) photocatalytic experiment with similar work from other laboratories. The procedure is simple and required no sophisticated instrumentation. ξ_{rel} is convertible to

quantum yields for the photocatalyzed oxidation of a given substrate since the quantum yield for the photooxidative degradation of phenol, Φ_{phenol}, was assessed by first determining the fraction of the incident photon flow from the radiation source absorbed by the photocatalyst material Degussa P-25 TiO_2 taken as a standard using a spectrophotometric integrating sphere method. Quantum yields so calculated from relative photonic efficiencies satisfied the photochemical definition of Φ of homogeneous photochemistry. In this Part II Chapter 3 we have presented some of the issues regarding the non-insignificant extent of light scattered by the heterogeneous phase and have also dealt with a potentially useful experimental method to determine the process quantum yield by assessing the limiting relative photonic efficiency ξ_{lim} that is equivalent to Φ when complete absorption of light takes place at high photocatalyst loadings.

From the few cases so far examined, the method of limiting photonic efficiencies to ascertain an estimate of the true quantum yield is worth pursuing, with due care for the precision in the experimental data as this extrapolation method (see insert to Figure 11) carries substantial uncertainty. The factors that affect the quantum yields of photochemical processes on the surface of nano/micro-particulates of wide bandgap metal oxides in solid/gas and solid/liquid heterogeneous systems were examined theoretically by Emeline and coworkers [29] by solving the continuity equation for a one-dimensional plate, and by considering also the spatial non-uniformity of photogeneration of charge carriers in the bulk of the solids and their limited probability of diffusion toward the particle surface.

5. REFERENCES

[1]. N. Serpone, in "*Kirk-Othmer Encyclopedia of Chemical Technology*", Wiley-Interscience, NewYork, vol. 18, 1996, pp. 820-837.

[2]. M.A. Fox, M.T. Dulay, *Chem.Rev.*, **93**, 341 (1993).

[3]. P.V. Kamat, *Chem.Rev.*, **93**, 267 (1993).

[4]. A. Heller, *Acc.Chem.Res.*, **28**, 503 (1995).

[5]. M.R. Hoffmann, S.T. Martin, W. Choi, D.F. Bahnemann, *Chem.Rev.*, **95**, 69 (1995).

[6]. D.F. Bahnemann, J. Cunningham, M.A. Fox, E. Pelizzetti, P. Pichat, N. Serpone, in "*Aquatic and Surface Photochemistry*", D. Crosby, G. Helz, R. Zepp. R. Eds.; Lewis Publishers, Boca Raton, FL., 1994, pp. 261-316.

[7]. D.F. Ollis, H. Al-Ekabi, eds. "*Photocatalytic Purification and Treatment of Water and Air*", Elsevier Science, Amsterdam, 1993.

[8]. N. Serpone, E. Pelizzetti, "*Photocatalysis - Fundamentals and Applications*", Wiley-Interscience, New York, 1989.

[9]. N. Serpone, *Res.Chem.Interm.*, **20**, 953 (1994).

[10]. M.K. Nazeeruddin, K. Kay, I. Rodicio, R. Humphry-Baker, E. Mueller, N. Vlachopoulos, M. Gratzel, *J.Am.Chem.Soc.*, **115**, 6382 (1993).

[11]. (a) N. Serpone, D. Lawless, R.F. Khairutdinov, E. Pelizzetti, *J.Phys.Chem.*, **99**, 16655 (1995).

(b) N. Serpone, D. Lawless, R.F. Khairutdinov, *J.Phys.Chem.*, **99**, 16646 (1995).

[12]. (a) J. Zhao, H. Hidaka, A. Takamura, E. Pelizzetti, N. Serpone, *Langmuir*, **9**, 1646 (1993).

(b) H. Hidaka, Y. Suzuki, K. Nohara, S, Horikoshi, Y. Hisamatsu, E. Pelizzetti, N. Serpone, *J.Polym.Sci.A:Polym.Chem.*, **34**, 1311 (1996).

[13]. N. Serpone, E. Pelizzetti and H. Hidaka, in "*Photochemical and Photoelectrochemical Conversion and Storage of Solar Energy*", Z.W. Tian and Y. Cao, Eds., International Academic Publishers, Beijing, China, 1993, pp. 33-73.

[14]. N. Serpone, A. Salinaro, *Pure & Appl.Chem.*, **71**, 303 (1999).

[15]. V. Augugliaro, V. Loddo, L. Palmisano, M. Schiavello, *Sol.Energy Mater.Sol.Cells*, **38,** 411 (1995).

[16]. M.I. Cabrera, O.M. Alfano, A.E. Cassano, *Ind.Eng.Chem.Res.*, **33,** 3031 (1994).

[17]. N. Serpone, G. Sauve, R. Koch, H. Tahiri, P. Pichat, P. Piccinini, E. Pelizzetti, H. Hidaka, *J.Photochem.Photobiol.A:Chem.*, **94**, 191 (1996).

[18]. L. Sun, J.R. Bolton, *J.Phys.Chem.*, **99**, 4127 (1995).

[19]. N. Serpone, *J.Photochem.Photobiol. A:Chem.*, **104**, 1 (1997).

[20]. M.A. Grela, M.E.J. Coronel, A.J. Colussi, *J.Phys.Chem.*, **100**, 16940 (1996).

[21]. G. Riegel, J.R. Bolton, *J.Phys.Chem.*, **99,** 4215 (1995).

[22]. K. Tanaka, M.F.V. Capule, T. Hisanaga, *Chem.Phys.Lett.*, **187**, 73 (1991).

[23]. P. Ruterana, P.-A. Buffat, K.R. Thampi, M. Gratzel. *Mater.Res.Soc.Symp.Proc.*, **139**. 327 (1989).

[24]. P. Ruterana, P.-A. Buffat, K.R. Thampi, M. Gratzel, *Ultramicroscopy*, **34**, 66 (1990).

[25]. H. Tahiri, N. Serpone, R. Le van Mao, *J.Photochem.Photobiol.A:Chem.*, **93,** 199 (1996).

[26]. H.G. Heller, J.R. Langman. *J.Chem.Soc.Perkin II* (1981) 341; see also information bulletin from Aberchromics Ltd., The University of Wales, College of Cardiff, Cardiff CF1-3TB, UK.

[27]. C. Huang *et al.*, *Anal.Chim.Acta*, **311**, 115 (1995)

[28]. M.I. Cabrera, O.M. Alfano, A.E. Cassano, *J.Phys.Chem.*, **100,** 20043 (1996).

[29]. A.V. Emeline, V.K. Ryabchuk, N. Serpone, *J.Phys.Chem.B*, 103, 1316 (1999).

CHAPTER 4

TURNOVERS AND PHOTOCATALYSIS
A MATHEMATICAL DESCRIPTION

Summary

In previous articles during the past decade, Serpone and coworkers {*J.Photochem. Photobiol. A:Chem.*, **94**, 191 (1996); *ibid.*, **104,** 1 (1997); *ibid.*, **73,** 11 (1993)} dwelled on the usage of relative photonic efficiencies and quantum yields Φ as they pertain to assess process efficiency in heterogeneous photocatalysis. In Chapters 2 and 3 we provided an experimental protocol to measure Φ in heterogeneous media {see also, *Pure & Appl. Chem.*, **71,** 303 (1999)} to infer which of several photocatalyzed processes might be the more significant and efficient processes. In this Chapter we consider additional fundamentals of photocatalysis and mathematically describe (photo)catalytic activity and how (photo)catalytic activities of various materials may be compared. Specifically, we address the usage and provide a kinetic description of the three turnover quantities: turnover number (TON), turnover rate (TOR) and turnover frequency (TOF) as they bear on the (photo)catalytic activity of a given material in heterogeneous solid/liquid or solid/gas (photo)catalysis. Contrary to earlier

assertions, we herein argue that these turnover quantities are conceptually distinct. Unlike the requirement to determine TOF, the quantities TON and TOR require knowledge of the number of active sites on the (photo)catalyst's surface. Most significant, these turnovers depend on the nature of the active state of the catalyst, and hence on how the active centers are described. This recalls attention to some of the differences in the nature of photocatalysis and photoinduced catalysis.

1. INTRODUCTION

Heterogeneous photocatalysis has come to describe the field of study and the technology in which irradiated semiconductor particles generate charge carriers (e^- and h^+) that are ultimately poised at the particle surface. These carriers undergo various processes, the most important of which are photoreductions (e.g. metal ions of Au, Pt, Ag, Rh, Hg, Pb, and others) and photooxidations of a large variety of organic substances (e.g. surfactants, pesticides, herbicides and others) to their complete mineralization. Our recent research efforts in this area have focussed on assessing the factors that underlie the temporal evolution of redox reactions taking place predominantly on metal oxide materials [1-5].

Understanding heterogeneous photocatalysis necessitates a suitable description of (i) what (photo)catalysis is, (ii) what turnover quantities are (numbers, TON; rates, TOR; frequencies, TOF) and (iii) how quantum yields Φ can be established. For the latter, a protocol for determining Φ in heterogeneous photocatyalysis has been proposed [6] and experimental details given [7] (see Chapter 3). Relative photonic efficiencies, ξ_{rel} ,provide

a method by which the work from many laboratories in environmental photochemistry can be calibrated when the more auspicious parameter Φ cannot be assessed because of certain experimental limitations [7]. The terminology "photocatalysis" has been characterized by the continued use of labels to describe a variety of mechanistic possibilities for a given process. The turnover quantities, while being relatively understood in homogeneous (photo)catalysis, require further reflection in heterogeneous (photo)catalysis as they require knowledge of the number of (photo)catalytically active sites for TON and TOR. These turnovers depend on how the (photo)catalytic process is viewed. It is relevant therefore to revisit the description of photocatalysis briefly as it impacts on the major focus of this Chapter.

1.1 Photocatalysis

We should first recall that catalysis refers to a process in which a substance (the catalyst, Cat) accelerates an otherwise thermodynamically favored but kinetically slow reaction, with the catalyst fully regenerated at the conclusion of the catalytic cycle. When photons are also involved, the expression photocatalysis is used to describe, without the implication of any specific mechanism, the acceleration of a photoreaction by the presence of a catalyst. The catalyst may accelerate the photoreaction by interacting with the substrate either in its ground state or in its excited state and/or with the primary product, depending on the mechanism of the photoreaction [8]. Note that the latter makes no mention of whether photons also interact with the catalyst. Such a description also embraces photosensitization

[9] and yet such a process, defined officially [10] as a process whereby a photochemical change occurs in one molecular entity as a result of initial photon absorption by a another molecular species known as the photosensitizer, is not necessarily catalytic without assessing a turnover quantity and/or the quantum yield. The issue rests entirely on the role of the photons. Chanon and Chanon [11] suggested that the non-descriptive term photocatalysis be taken simply as a general label to indicate that light and a substance (the catalyst or initiator) are necessary entities to influence a reaction [12]. Such a broad description indicates the required reagents without undue constraints as to the (often unknown) mechanistic details of the chemical process (eqn1).

$$\text{Substrate} + \text{light} + \text{Catalyst} \rightarrow \text{Products} + \text{Catalyst} \qquad (1)$$

Teichner and Formenti [13] described heterogeneous photocatalysis as an increase in the rate of a thermodynamically allowed ($\Delta G < 0$) reaction in the presence of an irradiated solid with the increase originating from the creation of some new reaction pathways involving photocreated species and a decrease of the activation energy. In this sense, one might argue that many of the reactions involving irradiated semiconductors belong to the class of photogenerated catalysis (see below). Yet reaction 2 was labelled [13] a photocatalytic oxidation.

$$CH_3CHOHCH_3 + \tfrac{1}{2}\,O_2 \xrightarrow[TiO_2]{h\nu} CH_3COCH_3 + H_2O \qquad (2)$$

It was also suggested that if $\Phi > 1$ (as in reactions involving radical species) the process is catalytic in photons, but if $\Phi \leq 1$ then the process is non-catalytic in photons. The latter suggestion is somewhat artificial to the extent that if Φ is greater than 1, then either the process is a photoinduced catalysis (see below) or the process is a photoinitiated chain reaction which is not necessarily catalytic. Typically, the quantum yield of a primary reaction step is less than 1.

Salomon [14] proposed that the broad description of photocatalysis can be subdivided into two main classes: (i) photogenerated catalysis which is catalytic in photons, and (ii) catalyzed photolysis which is non-catalytic in photons (Table 1). In the former, ground

Table 1. - Salomon's classification of photocatalysis and summary of various mechanism-specific labels [14].

Catalytic in Photons	Non-Catalytic in Photons
Photogenerated catalysis [14]	**Catalyzed photolysis** [14]
photoinduced catalytic reactions [16]	catalyzed photochemistry [15]
(Stoeichiometric photogenerated catalysis [14])	catalyzed photoreactions [15,18]
	sensitized photoreactions [15,16]
	photosensitized reactions [19]
	photo-assisted catalysis [16,20]
	(stoichiometric photogenerated\ catalysis [14])
	substance-assisted photo-reactions [21]
	substance-catalyzed photo-reactions [21]

states of the catalyst and the substrate are involved in the thermodynamically spontaneous (exoergic) catalytic step, whereas in the latter either the nominal catalyst T (Figure 1) or the substrate, or both, are in an excited state during the catalytic step (note: C is the catalytic

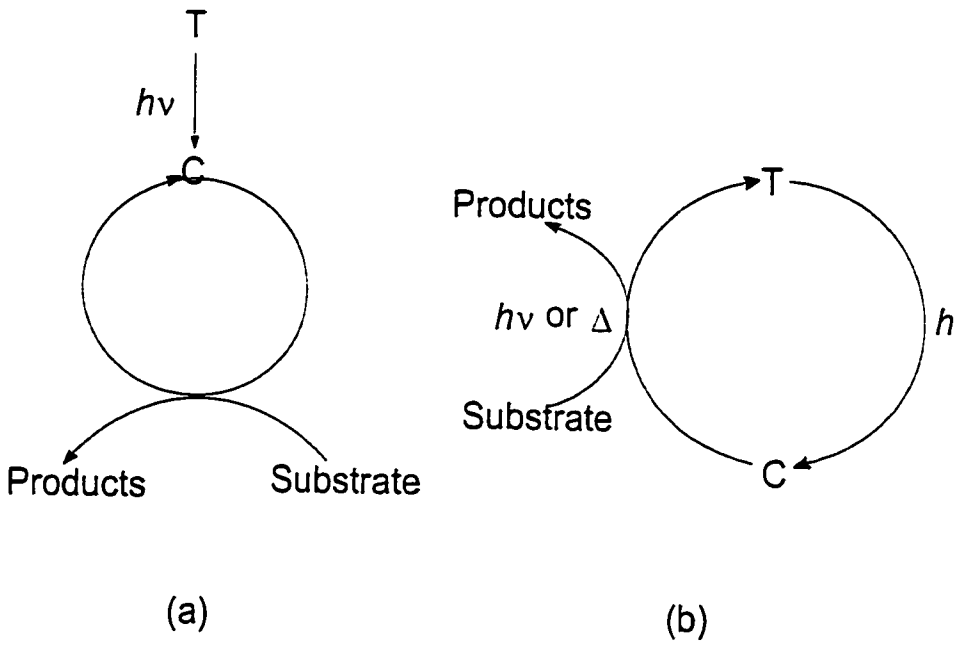

Figure 1. - Proposed scheme of an example of photogenerated catalysis (a) which is catalytic in photons, and of catalyzed photolysis (b) which is non-catalytic in photons. Note that T refers to a nominal catalyst and C denotes the catalytic entity. (Adapted after refs. 8 and 11).

entity). Kutal [8,15] clarified Salomon's formal schemes and Hennig *et al.* [16] proposed consistent labels that applied to experimental observations. A quagmire of mechanism-specific labels appeared (see Chanon and Chanon [11] for an elaborate account of this topic). This calls attention to usage of the more broad description of photocatalysis suggested by

Chanon and Chanon [11] and later emphasized by Serpone and coworkers [6,7,17] (see above). Figure 1a illustrates a simple scheme of photogenerated catalysis, whereas Figure 1b depicts an example of catalyzed photolysis.

The distinction between an assisted photoreaction (TON < 1) and a catalyzed photoreaction (TON >> 1) generally poses no difficulty in homogeneous (photo)catalysis since turnover numbers can be described. This is not the case in heterogeneous (photo)catalysis where a solid catalyst semiconductor, for example TiO_2, fulfills the dual role of light harvester and catalytic entity. An example is provided of the photocatalyzed reduction of water by the bifunctional catalyst TiO_2/Pt in the presence of some electron donor D (Scheme I). Several photoreactions that take place in the presence of semiconductor particles and that have been claimed to be photocatalytic may be described more appropriately as semiconductor-assisted photoreactions [21].

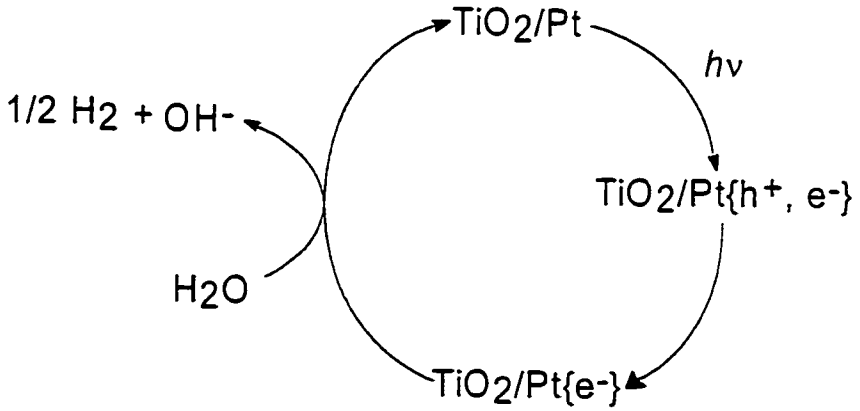

Scheme I

1.2 Turnover Quantities

The quantitative measure of (photo)catalytic activity of a solid (photo)catalyst is an essential quantity in heterogeneous (photo)catalytic gas/solid or solution/solid chemistry, particularly in industrial processes where catalytic activities bear on process economics and thus on acceptance of a given process. Such measures are characteristically derived from process kinetics to express a rate referenced to the number of (photo)catalytic sites to infer how many times a catalytic cycle turnsover. Traditionally, this parameter is the turnover number. Two other related parameters are sometimes used and described [22–24]: (a) turnover rate which designates the number of reagent molecules consumed or product molecules formed per surface active site per unit time, and (b) turnover frequency which denotes the number of reactant molecules consumed, or product molecules formed, per active site per unit time (note the similarity with turnover rate). Laidler [22] noted that because turnover numbers (and by extension, turnover rates and turnover frequencies) vary with temperature, concentration and other experimental conditions, they are not a useful quantity in kinetic work.

The expression sought to signify activity should serve two basic functions: (i) establish whether a given process is **catalytic** or **stoichiometric**, and (ii) provide a quantity to compare activities (unrelated to photons) of various catalysts for a given process under a set of conditions. An IUPAC article [25] pointed out that:

> "...the *turnover frequency*, N, (commonly called the *turnover number*) *defined*, as in enzyme catalysis, *as molecules reacting per active site in unit time*

> can be a useful concept if employed with care. In view of the problems in measuring the number of active sites discussed in..., it is important to specify exactly the means to express....in terms of active sites. A realistic measure of such sites may be the number of surface metal atoms on a supported catalyst but in other cases estimation on the basis of a BET surface area may be the only readily available method. Of course, *turnover numbers* (like rates) must be reported at specified conditions of temperature, initial concentration (or initial pressure) and extent of reaction...."

It is not surprising then that some workers (see e.g. [22–24,26]) have taken TON, TOR and TOF to refer to a singular description, *viz.*, that they describe the number of molecules reacted (or produced) per active site per unit time. Boudart [26,27] makes no distinction between *turnover rate* and *turnover frequency*.

Conceptually, we view the three quantities (1) *turnover number*, (2) *turnover rate* and (3) *turnover frequency* as being distinct from one another. The problem originates from common usage in which turnover rate and turnover frequency are often used interchangeably by catalycists just as photochemists often make no distinction between quantum yield and quantum efficiency and chemical kineticists often use the rate constant to mean the rate of a reaction.

Recently, Boudart [27] deplored usage of the quantity *turnover number* (TON) because it has become to be not a dimensionless number but a number expressed in units of $time^{-1}$, i.e. a number which expresses a frequency. Thus, the equivalence often made by many workers between turnover number and turnover frequency. For some {see e.g. [28]}, turnover number is understood to be a quantity that does not involve the element of time (see

below).

Only in a very specific case will the turnover rate and the turnover frequency be identical. Just as a unique quantum yield is described for a zero-order process. equivalence of TOR and TON may occur solely for zero-order processes and for small conversion of reactants (initial rates).

For a semiconductor-based heterogeneous photocatalytic process, a description of the number of photocatalytic active sites and thus of the measure of activity of a photocatalyst is rendered difficult as photons can easily generate new active sites on the semiconductor particle, not to mention the possible changes in the surface adsorption/desorption characteristics. Added to this, there is a likely possibility that active and inactive sites switch identities during a photocatalytic sequence and that activity during a photocatalytic process may then have a different meaning for different steps of the process [29]. For example, in a photocatalyzed oxidation of an organic substrate involving TiO_2 nanoparticles. oxidation may be mediated by an •OH radical at some surface site on the particle. Once oxidation has occurred, this particular surface site becomes extinct and is no longer active until such time as the site has been reconstructed and another •OH radical formed on that very same site.

Despite the above issues, it will nonetheless be useful to report a turnover quantity (to paraphrase from Boudart [27]) in heterogeneous solid/liquid or solid/gas (photo)catalysis (a) that can be reproduced in various laboratories, (b) that can disclose whether a given process is truly (photo)catalytic, (c) that can ascertain the absence of artifacts in rate measurements, (d) that can indicate the importance or the irrelevance of anisotropy in

crystalline (photo)catalysts, and (e) that can prove useful in assessing new materials as (photo)catalysts.

Although much has been written on catalysis (see refs in [27]), it is worthwhile to briefly revisit some of the major steps of the photocatalytic process in a heterogeneous phase.

Where the (photo)catalyst is a solid material, the following events typically take place [30]: (i) the molecule is adsorbed on the particle surface; (ii) the molecule undergoes chemical transformation while visiting several reaction surface sites by surface diffusion; and (iii) the intermediate or product molecule is subsequently desorbed to the gas phase or to the condensed phase.

A closer scrutiny of the adsorption step reveals that if the reactant molecule or any subsequent intermediate product is strongly chemisorbed, i.e., has formed strong chemical bonds with the surface atoms at the site, no (photo)catalysis will be possible. The process is stoichiometric because one molecule of product has formed per surface active site (TON = 1), signifying that the reaction has turned only once on that site. Moreover, if during the (photo)catalytic process the reactant molecule is strongly (chemically) bonded to surface atoms, the (photo)catalytic site becomes inactive and is said to be poisoned. By contrast, if (chemical) bonding interactions are too weak, the substrate is poorly adsorbed and there will be no opportunity for chemical bond rupture, an integral part of any catalytic process [30]. Thus, interactions between the reactant molecule and the (photo)catalyst's surface site must be such that bond breaking and bond making can take place within the residence time of the intermediate(s), and that desorption/adsorption can occur.

In heterogeneous (photo)catalysis a primary difficulty with describing the turnover number or the turnover rate is how to specify the *number of surface active sites.* It has become common practice to substitute this quantity by the total surface area (m^2) or by the specific surface area ($m^2\ g^{-1}$) of the catalyst particles, as determined by physical adsorption of nitrogen or argon at low temperatures. The use of the usual "Brunauer-Emmett-Teller" (BET) surface area *in lieu* of the number of active sites is tenuous, since the latter is seldom known in catalysis and much less known (if at all) in heterogeneous photocatalysis. In some cases, however, the number of active sites may be determined by kinetic measurements of gas photoadsorption (stoichiometric process) when the conditions of uniform irradiation of the catalyst surface and maximum surface coverage are satisfied. Such sites may be taken to reflect the concentration of surface centers. The number of active sites is known for electron and hole centers on ZnO, TiO_2, BeO, $MgAl_2O_4$ and SiO_2/TiO_2 (and some others); they range between 10^{10} and 10^{12} centers cm^{-2} [31]. It must be emphasized that the BET surface areas reflect the number of adsorption sites and *not necessarily the number of catalytically active sites*. On this point, it was noted [30] that about 10% ***or less*** of the surface sites may be active in any given catalytic reaction/process, and that the specific turnover number is only a conservative estimate of the real turnover. In other cases, the surface density of OH^- groups (10^{14} to 10^{15} cm^{-2} for TiO_2) has been used *in lieu* of the surface area to express catalytic activity [31,32]. However, this usage also does not address the real issue. The turnover number estimated in this manner also represents a lower limit.

Contrary to the other two turnover quantities, turnover frequency (TOF) requires no

knowledge of the surface area [30], nor the number of surface photocatalytically active sites, a number impossible to assess in heterogeneous photocatalysis. TOF increases with increasing active surface area and thus may be different from one batch of a catalyst to another and between various catalysts for the same reaction/process. Note that both TOR and TOF may be less than one. When the turnover quantity depends on the surface characteristics (e.g., number of active sites) it represents only a conservative estimate. It must be emphasized that an active site {or (photo)catalyst} will have a finite lifetime for various reasons, one being inactivation through poisoning by impurities.

We now consider these turnovers on a more quantitative basis to determine the parameters or factors that may influence the assessment of these quantities and thereby the extent of (photo)catalytic activity.

2. MATHEMATICAL FORMULATION OF TURNOVER QUANTITIES

2.1 Description of Photocatalysis

For a chemical reaction described by equation 3 there may be a corresponding catalytic process, equation 4:

$$A \rightleftharpoons B \tag{3}$$

$$A + Cat \rightleftharpoons B + Cat \tag{4}$$

The simplest description of a catalytic process is that catalysis occurs when addition of a

catalyst (Cat) changes the rate of establishing an equilibrium state in reaction 4, compared to the equilibrium state of reaction 3. After a single act of the reaction (or completion of reaction), the catalyst can be separated in the same original state as before the reaction. This description requires no prior knowledge of the mechanism of any particular catalytic process. A more complex and more precise description of catalysis would also add that the catalyst is intimately involved in the chemical steps (the reaction pathway in the catalytic process is different from that of reaction 3). After completion of the reaction cycle that yields products, the catalyst is regenerated into its original state. Note that there is no need to know the mechanistic details of the process except for the existence of interactions {e.g., adsorption in heterogeneous (photo)catalysis} between reagents and catalyst. This notion is valid for acid-basic catalysis, redox catalysis and biocatalysis (and other types). The reaction rate increases if the total activation energy in the catalytic process (eqn 4) is less than the corresponding energy in reaction 3. In thermal (catalytic) reactions, changes in the electronic configuration of the system occur following the regrouping of nuclei/fragments without transitions to electronic excited states.

As emphasized earlier, a definition of photocatalysis should also be general just as in the case of catalysis, and must not depend on any particular mechanism of the process.

Transformation of chemistry to photochemistry occurs when a chemical reaction is induced by absorption of photons by some reagent A, equation 5:

$$A + h\nu \rightarrow B \qquad (5)$$

and the corresponding photocatalytic process is:

$$A + h\nu + Cat \rightarrow B + Cat \qquad (6)$$

Unlike thermal reaction 3, photoreaction 5 occurs through an excited electronic state of the reagents followed by regrouping of the various nuclei/fragments. Typically, the photochemical reaction 5 is irreversible. If light is taken as a quasi-reagent in reaction 5 (as used in kinetic mechanisms), the back reaction must follow the pathway,

$$B \rightarrow A + h\nu$$

where $h\nu$ denotes photons of identical energy as those used in the forward reaction 5. Clearly, such back reaction is unlikely, and the process B ➜ A must proceed by a different pathway.

For discussion, we consider two different approaches to photocatalysis. The first approach sees the sequence 3 ➜ 4 ➜ 6, that is from chemistry (eqn 3) to catalysis (eqn 4) to photocatalysis (eqn 6). The second approach is 3 ➜ 5 ➜ 6 (chemistry ➜ photochemistry ➜ photocatalysis). From this point of view, the problem of defining photocatalysis is associated with our approach(es) to photocatalysis. Indeed, using the approach 3 ➜ 4 ➜ 6 we consider photocatalysis as **catalysis of a thermal reaction** (eqn 3) by an excited state of the catalyst produced as a result of light absorption by the catalyst. Thus, the role of light is to form the active (excited) state of the catalyst (for a molecule), or to produce more active sites on its surface (for a solid) during photoexcitation. An example of such a process is the

photoinduced isotope exchange of oxygen and hydrogen on photogenerated surface hole centers (O^-_S) on metal oxides. Oxidation of organic compounds over TiO_2 particles is another example if absorption of photons by TiO_2 generates the active (state) sites.

In the second approach (3 ➞ 5 ➞ 6), photocatalysis can be treated as **catalysis of a photoreaction**. Photoexcitation of molecules adsorbed on a photochemically inactive surface is an example of this approach if the adsorbed state of the molecule leads to a decrease of the total activation energy, and thus to an increase of the reaction rate. Note also that changes in the structure of adsorbed molecules compared to their original state as free molecules can increase the absorption probability, stabilize the excited state of such adsorbed molecules (decrease the rate of decay) and increase the reaction rate. In addition, the different structures of adsorbed molecules can lead to spectral (red) shifts of photoexcitation, in which case the photoreaction may be initiated by photons of lesser energy that otherwise would not be active for the original photoreaction (eqn 5). The latter can be taken as the analog of decreasing the total activation energy in thermal catalysis.

Subsequent to light absorption by the catalyst, surface photochemical processes may be treated as catalysis of a photoreaction if light is considered as one of the reagents. In this case, there is catalysis of photochemical reaction 5 with changes of the reaction pathway, in which the first step is interaction of the catalyst with the reagent (light) to form an intermediate species (e.g. an excited state of the catalyst), which subsequently reacts with another reagent (molecule A) to form the final reaction product (B).

Clearly, a definition of photocatalysis must be quite general to cover all particular

processes (considered above and others) when there is an acceleration of reactions equivalent to 4 with the participation of light, or of reactions analogous to 5. In the final reaction step. the photocatalyst is regenerated into its original state. In catalysis, the kinetic parameters {turnover rate, turnover frequency and turnover number} are used to determine whether a given surface reaction is catalytic. We consider below some particular but quite common processes to determine the corresponding kinetic parameters to demonstrate whether photocatalysis is catalytic.

2.2 Catalyzed Photolysis

We first consider a simple photochemical process. summarized by mechanism I that takes place on an inactive surface of a photocatalyst when light is absorbed by an adsorbed substrate.

Mechanism I

$$\{1\} \quad M + S \rightarrow M_{ads} \qquad (k_1)$$

$$\{2\} \quad M_{ads} \rightarrow M + S \qquad (k_2)$$

$$\{3\} \quad M_{ads} + h\nu \rightarrow M^*_{ads} \qquad (k_3)$$

$$\{4\} \quad M^*_{ads} \rightarrow M_{ads} \qquad (k_4)$$

$$\{5\} \quad M^*_{ads} \rightarrow S + \text{products} \qquad (k_5)$$

Stage {1} describes adsorption of reagent M on the surface site S of the catalyst. whereas stage {2} reflects the desorption of adsorbed molecules M_{ads}. Both processes lead to the establishment of an adsorption/desorption Langmuir equilibrium whose constant is K =

k_1/k_2. Stage {3} is photoexcitation of adsorbed molecules to form some appropriate excited state M^*_{ads} followed by the spontaneous decay of excitation (stage {4}) and chemical reaction (stage {5}) to regenerate the original state of the catalyst surface S, as required by the definition of catalysis (otherwise mechanism I would simply describe a surface stoichiometric photoreaction).

All the kinetic parameters defined by the turnover quantities TOR, TOF, and TON are determined under steady-state conditions for all the mechanisms considered I – III, i.e. when the concentrations [M] and [S], and photon flow ρ are constant. In the general case, the reaction rate is given by,

$$\frac{dC}{dt} = \frac{d[M]}{dt} = \frac{k_3 k_5 \rho [M][S_o]}{((K + \frac{k_3 \rho}{k_2})[M] + 1)(k_4 + k_5)} \qquad (7)$$

where C denotes a generic concentration of some species. According to the definitions given earlier, TOF is proportional to dC/dt and TOR is proportional to $\{dC/dt\}/[S_o]$, that is

$$TOF \propto \frac{dC}{dt} s \qquad (8)$$

where s is the total surface area of the catalyst participating in the process. By contrast,

$$TOR \propto \frac{k_3 k_5 \rho [M]}{((K + \frac{k_3 \rho}{k_2})[M] + 1)(k_4 + k_5)} \tag{9}$$

and TON is proportional to $\int (dC/dt)\, dt/[S_o]$, equation 10. (Note that dC/dt is a constant because of the steady-state conditions),

$$TON \propto t \frac{k_3 k_5 \rho [M]}{((K + \frac{k_3 \rho}{k_2})[M] + 1)(k_4 + k_5)} \tag{10}$$

where t is the time at which TON is determined. Clearly, if there are no side reactions to block the surface sites (ideal situation) one can always choose the time period t' when TON >> 1: in other words, the process is photocatalytic provided that the period $t' < \tau$. where τ is the lifetime of the catalytic site S (catalyst). Other additional steps such as energy transfer to any acceptor molecules or other decay pathways of the excited state of adsorbed molecules, have no effect on the general conclusions and can be included in the effective (apparent) constant k_4.

The turnover quantities TOF, TOR and TON depend on the concentration of reagent M (because of the dependence of the concentration of M_{ads} on M) and on photon flow ρ (since we deal with a photoprocess and ρt is taken as the concentration of another reagent. namely light). If the rate of achieving adsorption/desorption equilibrium is much greater than

the rate of photoexcitation (i.e. if $k_3 \rho << k_1$ or $k_3 \rho << k_2$) then,

$$\frac{dC}{dt} = \frac{k_3 k_5 \rho K[M][S_o]}{(K[M] + 1)(k_4 + k_5)} = \frac{k_3 k_5 \rho [M'_{ads}]}{(k_4 + k_5)} \tag{11}$$

where M'_{ads} is an equilibrium concentration of the adsorbed molecules in the dark.

$$TOF \propto \frac{dC}{dt} s \tag{8}$$

and

$$TOR \propto \frac{k_3 k_5 \rho \theta}{(k_4 + k_5)} \tag{12}$$

where θ is the equilibrium coverage of the surface by adsorbed molecules $\theta = [M'_{ads}] / [S_o]$ in the dark at concentration [M]. TON is then given by equation 13,

$$TON \propto t \frac{k_3 k_5 \rho \theta}{(k_4 + k_5)} \tag{13}$$

Introducing the photochemical parameter, Φ, i.e. the quantum yield of product formation we have

$$\Phi = \frac{k_5}{(k_4 + k_5)} \varphi \tag{14}$$

where φ is the quantum yield of absorption of light ($\varphi = 1$), and

$$TOF \propto \Phi\ k_3\ \rho\ [M_{ads}] \tag{15}$$

$$TOR \propto \Phi\ k_3\ \rho\ \theta \tag{16}$$

$$TON \propto \Phi\ t\ k_3\ \rho\ \theta \tag{17}$$

To the extent that TON yields information about "photocatalysis" being catalytic, the efficiency and activity of the photocatalytic process are better characterized by the quantum yield. The greater the quantum yield is, the greater are the three turnovers. Note that the same expression for the quantum yield is obtained for the photochemical reaction if in stages {3} – {5} we substitute M_{ads} with M and M^*_{ads} with M*. The rate of such a photochemical process at the same concentration [M] is given by:

$$\frac{dC}{dt} = \frac{k'_3 k'_5 \rho [M]}{(k'_4 + k'_5)} \tag{18}$$

(The primed parameters are for a homogeneous process). Thus, acceleration of the photoreaction in a heterogeneous system (over a homogeneous one) is observed provided that

changes in the structure of the adsorbed molecule cause an increase in photon absorption cross-sections (i.e. $k_3 > k'_3$), stabilization of the excited state of the molecule (i.e. $k_4 < k'_4$), and a decrease of the reaction activation energy leading to $k_5 > k'_5$ (see above). Of course, the rate depends on the concentration of adsorption sites on the surface of the catalyst. The overall condition to observe an acceleration of the reaction is given by:

$$\left(\frac{k_3 k_5}{k'_3 k'_5}\right)\left(\frac{k'_4 + k'_5}{k_4 + k_5}\right)\left(\frac{[M_{ads}]}{K[M]}\right) > 1 \qquad (19)$$

that is,

$$\frac{k_3\ \Phi}{k'_3\ \Phi'}\ \left(\frac{[M_{ads}]}{K[M]}\right) > 1 \qquad (20)$$

Consequently, if the absorption spectra of adsorbed and free molecules are similar (i.e. if $k_3 \sim k'_3$), then in order to observe photocatalytic acceleration the quantum yield of the heterogeneous photoreaction must be greater than the corresponding quantum yield of the homogeneous process, that is $\Phi > \Phi'$ (see eqn 20).

2.3 Langmuir-Hinshelwood Photocatalytic Process

We now consider the case of a Langmuir-Hinshelwood photocatalytic reaction that occurs at a photochemically active surface when light is absorbed by the catalyst leading to

the generation of surface electrons (e^-) and surface holes, (h^+), as described in mechanism II:

Mechanism II

$$\{6\} \quad M + S \rightarrow M_{ads} \qquad (k_6)$$

$$\{7\} \quad M_{ads} \rightarrow M + S \qquad (k_7)$$

$$\{8\} \quad Cat + h\nu \rightarrow e^- + h^+ \qquad (k_8)$$

$$\{9\} \quad M_{ads} + h^+ \rightarrow M_{ads}^+ \qquad (k_9)$$

$$\{10\} \quad M_{ads}^- + e^- \rightarrow M_{ads} \qquad (k_{10})$$

$$\{11\} \quad M_{ads}^+ \rightarrow \text{product} + S \qquad (k_{11})$$

Stages {6} and {7} are identical to {1} and {2} above, and both processes lead to the establishment of an adsorption/desorption Langmuir equilibrium with constant $K = k_6 / k_7$. Stage {8} reflects the photoexcitation of the catalyst producing electrons and holes. Stage {9} describes carrier (hole) trapping by the adsorbed molecule to form a reactive radical state, whose decay occurs through recombination with an electron described by stage {10}. Stage {11} is the chemical reaction that yields products and regenerates the original state of the catalyst surface, S. The surface concentrations of holes and electrons in the kinetic approach are given by:

$$[h^+] = \alpha_h \rho \tau_h \qquad (21)$$

and

$$[e^-] = \alpha_e \rho \tau_e \tag{22}$$

where α_h and α_e are the absorption coefficients of holes and electrons absorption bands (note that in the intrinsic absorption region $\alpha_h = \alpha_e$), and τ_h and τ_e are the lifetimes of holes and electrons, respectively. The disadvantage of the kinetic approach is that it considers a spatially uniform carrier generation in the bulk of the catalyst (i.e. $\alpha \rho$ = const) and there is no diffusion limitation for carrier motion. For a more detailed description one should use the expression for the concentration of surface carriers reported earlier by Emeline and coworkers [4].

The rate of the (photo)catalytic reaction at steady-state is given by equation 23:

$$\frac{dC}{dt} = \frac{k_6 k_9 k_{11}[S_o][h^+][M]}{(k_{10}[e^-] + k_{11})(K[M] + \frac{k_9[h^-]}{k_7} + 1)} \tag{23}$$

If establishment of the adsorption/desorption equilibrium is faster than the rate of hole trapping, that is if $k_9 [h^-] << k_7$ or if $k_9 [h^-] << k_6 [M]$, then

$$\frac{dC}{dt} = \frac{k_6 k_9 k_{11}[S_o][h^+][M]}{(k_{10}[e^-] + k_{11})(K[M] + 1)} \tag{24}$$

or

$$\frac{dC}{dt} = \frac{k_6 k_9 k_{11}[h^+][M_{ads}]}{(k_{10}[e^-] + k_{11})} \tag{25}$$

and

$$TOF \propto \frac{dC}{dt}\, s \tag{8}$$

$$TOR \propto \frac{\frac{dC}{dt}}{[S_o]} = \frac{k_6 k_9 k_{11}[h^+]\theta}{(k_{10}[e^-] + k_{11})} \tag{26}$$

$$TON \propto t\, \frac{\frac{dC}{dt}}{[S_o]} = t\, \frac{k_6 k_9 k_{11}[h^+]\theta}{(k_{10}[e^-] + k_{11})} \tag{27}$$

As in the previous case, all the parameters depend on concentration and photon flow. In the present instance, the time period t can also be chosen to obtain turnover numbers (TON) greater than unity.

The similarity of equations 8, 24–27 with equations 8, 11–13 (for mechanism I) is evident. In fact, the process described by mechanism II can be treated as a photochemical reaction on the surface of a solid whose role is to absorb light. Subsequent charge carrier transfer to the adsorbed molecule produces an ionized state of the adsorbed molecule as might also occur by direct interaction between the adsorbed molecule and light (not shown in mechanism II). The excitation rate in mechanism II, is analogous to the rate $k_3\,\rho$ in

mechanism I.

$$k_9 [h^+] = k_9 \alpha_h \rho \tau_h$$

In mechanism II, the photocatalyst also takes part in the deactivation process such that k_{10} $[e^-]$ (or k_{10} for thermal ionization of the adsorbed molecule) corresponds to k_4 in mechanism I. The "inert" catalyst in mechanism I also plays a role in the decay step (stage {4}) changing the probability of deactivation.

If $\alpha_h = \alpha_e = \alpha$, the rate of photon absorption is given by $\int_v \alpha \rho \, dV$, where V is the volume of the catalyst, and in the case of spatially uniform photoexcitation this rate is $\alpha\rho V$. The quantum yield of the photocatalytic process is then given by:

$$\Phi = \frac{TOF}{\alpha\rho V} = \frac{s}{V} \frac{k_6 k_9 k_{11} \tau_h [M_{ads}]}{(k_{10}[e^-] + k_{11})} = \frac{s}{V} \frac{k_6 k_9 k_{11} \tau_h [M_{ads}]}{(k_{10}\alpha\rho\tau_e + k_{11})} \tag{28}$$

Consequently,

$$TOF = V \alpha \rho \Phi \tag{29}$$

$$TOR = \frac{\alpha \rho \Phi}{[S_o]} \frac{V}{s} \tag{30}$$

$$TON = t \frac{\alpha \rho \Phi}{[S_o]} \frac{V}{s} \tag{31}$$

Hence, just as in mechanism I, all the turnover quantities are associated with the quantum yield of the photoprocess. Once again the activity and efficiency of the (photo)catalyst are determined by Φ.

In a previous consideration, we assumed that the surface adsorption centers S are the active centers of (photo)catalysis, so that photoelectrons and photoholes are the intermediates produced from the interaction between the catalyst with one of the reagents, light. In the electronic theory of catalysis, however, Volkenstein [34] proposed that the free surface electrons and holes are the reactive centers. In such instance, TOR and TON are given by,

$$TOR \propto \frac{k_6 k_9 k_{11}[M_{ads}]}{(k_{10}[e^-] + k_{11})} = \left(\frac{V}{s}\,\tau_h\right)\Phi \tag{32}$$

$$TON \propto t\left(\frac{V}{s}\,\tau_h\right)\Phi \tag{33}$$

In this case, catalysis occurs from the excited state of the catalyst and neither TOR nor TON depend on light intensity (photon flow), unless the decay of the ionized state of the adsorbed molecule is caused by recombination or photoionization, and $k_{10}\,[e^-] \approx k_{11}$.

2.4 Catalytic Activity

According to the electronic theory of catalysis [34], the activity of the catalyst is related to the concentrations of electrons and holes on the surface, which in turn are

determined by the position of the Fermi level (or by the electrochemical potential of the electron) in the catalyst. The concentration of free carriers is given by,

$$[e^-] = \int_E N_C(E) f(E, T)\, dE \tag{34}$$

and

$$[h^+] = \int_E N_V(E) \{1 - f(E, T)\}\, dE \tag{35}$$

where

$$f(E,T) = \frac{1}{1 + e^{\left(\frac{E - F}{\kappa T}\right)}} \tag{36}$$

E refers to an energy scale and F is the Fermi level: $N_c(E)$ and $N_v(E)$ are the density of states in the conduction and valence bands, respectively. If the catalyst is not a degenerate semiconductor (typical of photocatalysts), then

$$[e^-] = N_C\, e^{\left(\frac{F - E_c}{\kappa T}\right)} \tag{37}$$

and

$$[h^+] = N_V\, e^{\left(\frac{E_v - F}{\kappa T}\right)} \tag{38}$$

where E_c is the lowest energy level in the conduction band and E_v is the highest energy level in the valence band. On the one hand, the number of reaction centers (electrons and holes) depends on the position of the Fermi level. On the other hand, the different positions of the

Fermi level correspond to different states of the catalyst, i.e. to different catalysts. Indeed, for different concentrations of reactive centers (e.g. metal ions doped on the surface) we can distinguish different types of catalysts with corresponding positions of the Fermi level. Under irradiation, the Fermi level of the catalyst splits into two quasi-Fermi levels: one for electrons and the other for holes, provided that the relaxation time of momentum and energy is much less than the lifetime of the carriers in the corresponding bands.

In the dark, the next expression is true (E_G is the band gap energy):

$$[e^-][h^+] = N_C N_V \cdot e^{-(\frac{E_G}{\kappa T})} \qquad (39)$$

Under irradiation, expression 39 can be written as

$$[e^-][h^+] = N_C N_V \cdot e^{-(\frac{E_G - \Delta F}{\kappa T})} \qquad (40)$$

where $\Delta F = F_e - F_h$

Thus, a catalyst under irradiation behaves differently with an apparent band gap given by $E_G - \Delta F$. The energy difference between the two quasi-Fermi levels, ΔF, depends on the intensity of irradiation. Consequently, we have different states which behave as different catalysts at different light intensities. In fact, at the higher light intensities we have higher concentrations of electrons and holes, i.e. of the reactive centers.

2.5 Eley-Rideal Photocatalytic Process

Another family of heterogeneous photochemical processes is observed when the catalysts are photoexcited. Below we consider some common cases for such processes from the kinetics point of view.

Mechanism III

{8}	$Cat + hv \rightarrow e^- + h^+$	(k_8)
{12}	$S + h^+ \rightarrow S^+$	(k_{12})
{13}	$S^+ + e^- \rightarrow S$	(k_{13})
	{13a} $S^+ \rightarrow S + h^+$	(k_{13a})
	{13b} $S^+ + h\nu \rightarrow S + h^+$	(k_{13b})
{14}	$S^+ + M \rightarrow (S—M)^+$	(k_{14})
{15}	$(S—M)^+ \rightarrow S$ + products	(k_{15})
	{15a} $(S—M)^+ \rightarrow S^+$ + product	(k_{15a})

As in the previous mechanism II, stage {8} corresponds to the photogeneration of free carriers. Stage {12} describes the trapping of carriers (in this particular case, holes) by the surface defects (i.e. "potential" surface active centers) S to produce surface active centers S^+. Stage {13} represents the "physical" decay pathway of surface active centers through recombination with charge carriers of opposite sign , *viz.*, electrons; it may also be a first-order thermal deactivation process (stage {13a}), or a second-order photoionization process (stage {13b}). Stage {14} is a chemical reaction (chemisorption) which yields the intermediate species $(S—M)^+$ followed by secondary reactions to produce the photoreaction

products (stage {15}). Note the difference between stages {15} and {15a}. In stage {15} the original (ground) state S of the photocatalyst is restored (the quantum yield $\Phi < 1$, the so-called process non-catalytic in photons), whereas in stage {15a} the ionized state S^+ remains at the end of the reaction cycle (the quantum yield Φ may be greater than 1, the so-called process catalytic in photons). Parmon [35] refers to the latter process as **photoinduced (photoinitiated) catalysis**, whereas the former is denoted **photocatalysis**. It is instructive to compare the kinetic parameters for both of these types of catalysis.

2.5.1 Photocatalysis

For the photocatalytic process with stage {15} the steady-state reaction rate is given by

$$\frac{dC}{dt} = \frac{k_{12}k_{14}k_{15}[S_o][h^+][M]}{k_{15}(k_{13}[e^-] + k_{14}[M]) + k_{12}[h^+](k_{15} + k_{14}[M])} \qquad (41)$$

and with stage {15a} the rate will be given by,

$$\frac{dC}{dt} = \frac{k_{12}k_{14}k_{15}[S_o][h^+][M]}{k_{15}k_{13}[e^-] + k_{12}[h^+](k_{15} + k_{14}[M])} \qquad (42)$$

where $[h^+] = \alpha_h \rho \tau_h$ and $[e^-] = \alpha_e \rho \tau_e$ are the (surface) concentrations of holes and electrons, respectively. These equations reflect the fact that, in the process described by stage {15a}, the only pathway for deactivation of the excited state of the catalyst is the "physical"

decay path (recombination $k_{13}[e^-]$), whereas in the catalytic process with stage {15} deactivation occurs by both the "physical" decay pathway and through the chemical reaction ($k_{13}[e^-] + k_{14}[M]$). In the latter case, the reaction rate is smaller provided that all the kinetic constants in both processes are identical. Note also, that both dependencies of the rates on concentration of reagent M resemble the Langmuir-Hinshelwood kinetics, although both are of the Eley-Rideal type. Maximal rates would be observed (eq. 41) when $k_{14}[M] >> k_{15}$ and $k_{14}[M] >> k_{13}[e^-]$. Then,

$$\frac{dC}{dt} = \frac{k_{12}k_{15}[S_o][h^+]}{k_{15} + k_{12}[h^+]} \tag{43}$$

which for $k_{12}[h^+] >> k_{15}$, yields

$$\frac{dC}{dt} = k_{15}[S_o] \tag{44}$$

that is, under the given conditions the rate of the process equals the rate of regeneration of the surface reaction centers S after completion of the reaction cycle, and for $k_{12}[h^+] << k_{15}$, yields

$$\frac{dC}{dt} = k_{12}[S_o][h^+] \tag{45}$$

that is, the reaction rate is determined by the production of excited (ionized) states of the surface reactive centers.

Since the rate of the photocatalytic reaction is known, the only problem remaining to determine the turnover quantities is to decide on the nature of the surface active centers in photocatalysis. The simplest way is to infer that the ionized states S^+ are such centers. In such case,

$$TOF \propto \frac{dC}{dt} s \tag{8}$$

$$TOR \propto \frac{\frac{dC}{dt}}{[S^+]} = k_{14}[M] \tag{46}$$

$$TON \propto t\, k_{14}\, [M] \tag{47}$$

As in the case of surface photochemical reactions (mechanisms I and II), TON is greater than unity if turnover is determined for time $t < \tau$, where τ is the lifetime of the catalytic site. Hence the process can be said to be catalytic. It should be emphasized that TOR and TON are independent of light intensity (photon flow). They depend solely on reagent concentration, whereas the reaction rate and TOF behave differently. The latter two depend on light intensity and (perhaps) on temperature for constant concentration of M. Indeed, as $k_{13}[e^-]$ (or k_{13}) $\rightarrow \infty$, then $dC/dt \rightarrow 0$ and TOF $\rightarrow 0$, whereas, according to equations 34 and

35, TOR and TON are constant. The physical sense of this behavior is that at high rate of "physical"decay, i.e. when $k_{13} \rightarrow \infty$, the concentration of the active centers $[S^{+}] \rightarrow 0$, and so do the reaction rate and TOF. However, to the extent that TOR and TON are determined relative to a single center, as soon as this center becomes available the reaction cycle occurs and TOR and TON remain constant. Thus, TOR and TON reflect the activity of a given active center (ionized state) S^{+} but say nothing about the efficiency and activity of the catalyst. Moreover, for an effective physical decay (e.g. at sufficiently high light intensity), the rates of both processes (photoinduced catalysis (stage {15a}) and photocatalysis (stage {15})) become equal since they are determined only by the rate of photogeneration and (photo)decay of the ionized state. Only one (or less) reaction cycle can occur during the lifetime of the active center.

In another approach, when we consider catalysis of a photochemical reaction and assume that light is one of the reagents, all the excited states of the catalyst (electrons, holes, and S^{*} states) may be taken as intermediates of the catalytic photoreaction. The latter takes place by a different reaction pathway in contrast to the original photochemical reaction. Hence, the original state of the catalyst is S which is restored at the end of the reaction and the number of active centers is given by S_o. This is analogous to thermal catalysis. For example, oxidation of molecule M can follow the path:

$$O_s + M \rightarrow MO\uparrow + V_{Os} \qquad (48)$$

$$V_{Os} + \tfrac{1}{2} O_2 \rightarrow O_s \qquad (49)$$

The reactive center in such a process is neither surface oxygen O_s nor the oxygen vacancy V_{Os}, but is some cluster corresponding to oxygen vacancies either with or without oxygen in the cluster. By analogy, in photocatalysis there are surface centers (defects) which can be in a state with trapped carriers (i.e. an intermediate, just like surface oxygen in the previous example) or without trapped carriers. These centers are then the centers of (photo)catalysis).

TOF is identical to that given by eq. 8, whereas TOR and TON are given by equations 50 and 51, respectively:

$$TOR \propto \frac{\frac{dC}{dt}}{[S_o]} = \frac{k_{12}k_{14}k_{15}[h^{\cdot}][M]}{k_{15}(k_{13}[e^{-}] + k_{14}[M]) + k_{12}[h^{\cdot}](k_{15} + k_{14}[M])} \qquad (50)$$

and

$$TON \propto t\,\frac{k_{12}k_{14}k_{15}[h^{\cdot}][M]}{k_{15}(k_{13}[e^{-}] + k_{14}[M]) + k_{12}[h^{\cdot}](k_{15} + k_{14}[M])} \qquad (51)$$

In this case TOR and TON depend on light intensity and on the concentration of reagent M. The rate of decay of the active state S^{-} (i.e. $k_{13}[e^{-}]$) affects both TOR and TON parameters which now characterize the activity of the (photo)catalyst.

Note that the quantum yield of the photocatalytic process in the kinetic approach used in this Chapter can be described by equation 52:

$$\Phi = \frac{(const)\ \frac{dC}{dt}\ s}{\alpha\rho V} = \frac{TOF}{\alpha\rho V} \qquad (52)$$

where s is the total surface area of the catalyst, V is the volume of the catalyst, α is the absorpion coefficient of the catalyst and ρ is the photon flow. Then, equations 29 – 31 can be used to describe the relationships between TOF, TOR and TON with the quantum yield of the photocatalytic process.

2.5.2 Photoinduced Catalysis

To complete the consideration of the previous examples, it is relevant to note that photoinduced catalysis (stage {15a}) does not require continuous irradiation since the excited state is reproducible. In this case, the excited state is created during pre-irradiation and there is no "physical" decay during the course of the reaction. Consequently, stages {12} and {13} must be excluded from this consideration and the rate of the photoinduced catalytic process is then given by,

$$\frac{dC}{dt} = \frac{k_{14}k_{15}[S_o^*][M]}{k_{15} + k_{14}[M]} \qquad (53)$$

so that

$$TOF \propto \frac{dC}{dt}\ s \qquad (8)$$

$$TOR \propto \frac{k_{14}k_{15}[M]}{k_{15} + k_{14}[M]} \tag{54}$$

and

$$TON \propto t\,\frac{k_{14}k_{15}[M]}{k_{15} + k_{14}[M]} \tag{55}$$

Thus, even though in both cases the active (excited) state of the catalyst is restored, the kinetic parameters of photoinduced catalysis (case 2.5.2) and photocatalysis (case 2.5.1) are different, since we deal with a different excited state of the catalyst, i.e. effectively we deal with different catalysts. Indeed, under irradiation the state of the catalyst may be characterized by the splitting of the Fermi level into two quasi-Fermi levels (see above), whereas in photoinduced catalysis (in the dark) the state of the catalyst is characterized by a unique Fermi level. This level may be shifted compared to the original state of the catalyst because of the possibility of having different excited states after pre-excitation of the catalyst.

3. FURTHER CONSIDERATIONS

It must be noted that there is nothing special about photocatalysis. It is simply another type of catalysis joining, as it were, redox catalysis, acid-base catalysis, enzyme catalysis, thermal catalysis, and others. Consequently, any description of photocatalysis must correspond to the general definition of catalysis. This said, we might then argue that ***photocatalysis*** simply describes ***catalysis of a photochemical reaction***. To ascertain this

proposition we consider the following.

If reaction 56 describes the catalyzed reaction between reagent A and reagent B,

$$A + B + Cat = products + Cat \qquad (56)$$

then in the absence of the catalyst (Cat) one is left with the chemical reaction:

$$A + B = products \qquad (57)$$

which is no longer catalyzed by Cat as in reaction 56.

If we carry this argument further to the photocatalyzed reaction 58.

$$A + h\nu + Cat \rightarrow products + Cat \qquad (58)$$

removal of the catalyst (Cat) leads to the photochemical reaction described by equation 59.

$$A + h\nu \rightarrow products \qquad (59)$$

By analogy, then, we deal with catalysis of a photochemical reaction by the catalyst (Cat) in its ground state. This notion is very important for determining the kinetic turnovers TOR and TON since their evaluation requires knowledge of which state of the catalyst (i.e. the state

of the surface reactive centers) must be considered.

Some additional points are worth noting:

1. The photochemical reaction 59 takes place through the excited electronic state of the reagent, A*, produced by the primary act of light absorption by reagent A, unlike the chemical reaction 57 which occurs through the ground states of the reagents A and B. In the photocatalytic process 58, the reaction also takes place after electronic photoexcitation of either the catalyst (Cat) or the adsorbed molecules (A_{ads}), unlike catalysis which involves only the ground electronic states (but thermally excited vibrational states).

2. The photocatalyzed reaction (eqn 58) and the photochemical reaction (eqn 59) are irreversible processes, unlike thermal catalysis (eqn 56) and the thermal chemical reaction 57.

Thus, photocatalysis is a photochemical process and the photocatalyst accelerates this process as any catalyst must do according to the definition of catalysis.

Photoexcitation of the catalyst can be considered as changing the photochemical reaction pathway that is typical of a catalytic process. It can also lead to possible changes in the spectral range of photoexcitation relative to the non-catalytic photochemical reaction (eq. 59) which, by analogy, can be considered as a change of the total activation energy because of the different reaction pathway in the catalytic process (eqn 56). Indeed, photoexcitation of the catalyst to form its excited state (eqn 60) in reaction 58 is analogous to the formation of the intermediate adsorption complex (eqn 61) in thermal catalysis (eqn 56), both of

$$Cat + h\nu \rightarrow Cat^* \quad (60)$$

$$B + Cat \rightarrow (Cat — B) \quad (61)$$

which are followed by secondary interaction steps with another reagent A.

Hence, just as in thermal catalysis (eqn 56) in which such an adsorption complex is not considered as the reactive center, the excited state of the (photo)catalyst in the photocatalytic process 58 is not a reactive center but an intermediate. Consequently, to determine TOR and TON in the proposed earlier mechanisms I – III (see above) we need to consider as reaction centers the corresponding surface centers **S** in the **original state** of the (photo)catalyst and not S^- nor M^*_{ads}. As an example, we note the photocatalytic oxidation of organic compounds over TiO_2 in aqueous media. In this case, the ground state of S centers corresponds to the surface OH^- groups. It is these OH^- groups that should be taken as the catalytic centers, whereas the •OH radicals formed by hole trapping represent intermediate species. Note also that the original **S** state of surface active centers is restored after reaction is completed. In the example of TiO_2, this restoration or reconstruction of the original state of the catalyst is achieved by dissociative adsorption of water on the particle surface. ***Thus, photocatalysis is catalysis of a photochemical reaction by the original ground state of the catalyst prior to photoexcitation.*** Catalyzed photolysis (mechanism I) is also a case of photocatalysis, unlike photoinduced catalysis which is not photocatalysis (i.e., it is not catalysis of a photochemical reaction).

In photoinduced catalysis, pre-irradiation of the original state of the catalyst is the

only means for the physical development of a new catalyst to create new centers; the corresponding catalytic process completely follows reaction 56. The similar changes to the state of the catalyst can be achieved by chemical doping, irradiation with ions or electrons, and additive coloration process, among others. Thus photoinduced catalysis is thermal catalysis by a catalyst produced by *pre*-irradiation (Figure 1a). The principal difference between photoinduced catalysis and photocatalysis can best be described as follows.

Any photochemical reaction (eqn 59) starts from light absorption by the reagent to form an excited state of the molecule A:

$$A + h\nu \rightarrow A^* \tag{62}$$

and there always exists a physical pathway (radiative and nonradiative) for relaxation of this state back to the ground state:

$$A^* \rightarrow A \tag{63}$$

Thus there is always a competition between chemical and physical pathways for decay of excited states. If the chemical pathway is inefficient, then the physical path will lead to relaxation of A* to its ground electronic state.

The same is true for photocatalysis. Indeed, since photocatalysis is catalysis of a photochemical reaction there is a physical pathway for decay of the system back to its ground

state. If the photocatalytic process occurs through photoexcitation of the catalyst, physical decay may occur through recombination, and/or through thermal and photo ionization of the excited state of the surface centers which ultimately lead to regeneration of the original state of the catalyst. Obviously, there is no such process in the case of photoinduced catalysis. In the latter case, the state of the catalyst does not have a physical decay pathway and is the same before and after reaction as in any thermal catalytic reaction. Note also that the catalytic process in photoinduced catalysis is reversible unlike in photocatalysis.

4. CONCLUDING REMARKS

One of the major conclusions of this Chapter is that determination of the turnover quantities TOR and TON in photocatalysis necessitates that the concentration of the surface centers (S) in the original state of the (photo)catalyst be taken into account and not the concentration of one of its excited states (e.g. S^*). This simplifies the experimental determination of turnover quantities. However, in most cases, assessment of the concentration of surface reactive centers remains a great challenge, except in some particular cases (see e.g. ref. [31]). Another problem connected with turnover parameters is that all are likely to depend on light irradiance (or photon flow), an effect yet to be determined and verified experimentally. Indeed, although light irradiance incident on the reactor can easily be measured by actinometry, scattering and absorption keep changing from particle to particle and are different at different points of the reactor, not least of which is the dependence on reactor geometry. This requires complex calculations of the light irradiance distribution in

a given reactor. Also, it is worth noting that the irradiated surface area is not necessarily equal to the total surface area of the catalyst, s. Thus, the practical determination of turnover quantities remains a very complex challenge.

On the basis of the above discussion then, we propose that the ***turnover rate*** be taken simply as the number of molecules reacted (or produced) per unit time per active site [36] (units: **molecules site^{-1} time^{-1}**); ***turnover frequency*** as the number of molecules reacted (or produced) per unit time (units: **molecules time^{-1}**); and, in accord with others [30], ***turnover number*** as a quantity that describes how many times a reaction or process turnsover at some active site (or at some catalyst molecule in homogeneous catalysis) integrated over time (units: **molecules site^{-1}**).

5. REFERENCES

[1]. A.V. Emeline, A.V. Rudakova, V.K. Ryabchuk and N. Serpone, *J. Phys. Chem. B.* **102,** 10906 (1998).

[2]. A.V. Emeline, G.V. Kataeva, A.S. Litke, A.V. Rudakova, V.K. Ryabchuk and N. Serpone, *Langmuir,* **14,** 5011 (1998).

[3]. A.V. Emeline, S.V. Petrova, V.K. Ryabchuk and N. Serpone, *Chem. Mater.*, **10,** 3484 (1998).

[4]. A.V. Emeline, V. K. Ryabchuck, and N. Serpone, *J. Phys. Chem. B*,**103,** 1316 (1999).

[5]. A.V. Emeline, E.V. Lobyntseva, V.K. Ryabchuck and N. Serpone, *J. Phys. Chem. B*, **103,** 1325 (1999).

[6]. N. Serpone and A. Salinaro, *Pure & Appl.Chem.*, **71,** 303 (1999).

[7]. A. Salinaro, N. Serpone, A. Emeline, V. Ryabchuk, and H. Hidaka, *Pure & Appl.Chem.*, **71,** 321 (1999).

[8]. C. Kutal, *Adv. Chem. Ser.*, **238,** 1 (1993).

[9]. H. Kisch, in "Photocatalysis – Fundamentals and Applications", N. Serpone and E. Pelizzetti, Eds., Wiley-Interscience, New York, 1989, chapter 1.

[10]. "Glossary of Terms in Photochemistry", *EPA Newsletter*, **25,** 13 (1985).

[11]. F. Chanon and M. Chanon, in "*Photocatalysis – Fundamentals and Applications*", N. Serpone and E. Pelizzetti, Eds., Wiley-Interscience, New York, 1989, chapter 15.

[12]. This cannot be a complete description of photocatalysis. An example of a photo-catalytic process of a different type is the photoexcitation of surface metal-oxo complexes on some inert support, e.g. $M^{2+}—O^{2-}$. For example,

$$M^{2+}—O^{2-} + h\nu \rightarrow M^{+}—O^{-}$$

$$M^{+}—O^{-} + (A)(D) \rightarrow M^{-}(A)—O^{-}(D)$$

where photoexcitation of the surface metal-oxo complex leads to photoinduced electron transfer from the oxide to the metal to form the reactive state $M^{+}—O^{-}$. This reacts with (acceptor)(donor) molecules (A)(D) with the electron localized on the

metal cation or on the hole-like state O^-. Note that there is no generation of free electrons and holes. This is local excitation. A similar process is described by mechanism I, which is also an example of local photoexcitation without photogeneration of free electrons and holes.

[13]. S.J. Teichner and M. Formenti, in "*Photoelectrochemistry, Photocatalysis and Photoreactors*", M. Schiavello, Ed., Reidel, Dordrecht, 1985, pp. 457-489.

[14]. R.G. Salomon, *Tetrahedron*, **39,** 485 (1983).

[15]. C. Kutal, *Coord. Chem. Rev.*, **64,** 191 (1985).

[16]. H. Hennig, D. Rehorek and R.D. Archer, *Coord. Chem. Rev.*, **61,** 1 (1985).

[17]. N. Serpone, E. Pelizzetti and H. Hidaka, in "*Photochemical and Photoelectrochemical Conversion and Storage of Solar Energy*", Z.W. Tian and Y. Cao, Eds., International Academic Publishers, Beijing, 1993, p. 33.

[18]. G.G. Wubbels, *Acc. Chem. Res.*, **16,** 285 (1983).

[19]. M.J. Mirbach, *EPA Newsletter*, **20,** 16 (1984).

[20]. L. Moggi, A. Juris, D. Sandrini and M.F. Manfrin, *Rev. Chem. Intermed.*, **5,** 107 (1981).

[21]. L.P. Childs and D.F. Ollis, *J. Catal.*, **66,** 383 (1980).

[22]. K.J. Laidler, "*Chemical Kinetics*", 3rd. edn., Harper-Collins Publishers, New York, 1987, ch.10.

[23]. J.B. Butt and E.E. Petersen, "*Activation, Deactivation and Poisoning of Catalysts*", Academic Press, San Diego, CA, 1988, ch. 4.

[24]. B.C. Gates, "*Catalytic Chemistry*", Wiley, New York, 1992, ch. 3 and 6.

[25]. "*Manual of Symbols and Terminology for Physicochemical Quantities and Units* (Part II: heterogeneous catalysis)", *Adv. Catal.*, **26,** 351 and 372 (1977).

[26]. M. Boudart and G. Djega-Mariadassou, *Kinetics of Heterogeneous Catalytic Reactions*, Princeton University Press, 1984, pp.6-8.

[27]. M. Boudart, *Chem. Rev.*, **95,** 661 (1995).

[28]. N.A. Mohd-Zabidi, D. Tapp, and T.F. Thomas, *J. Phys. Chem.*, **99,** 14733 (1995).

[29]. M.A. Fox, personal communication to N. Serpone, July 1995.

[30]. G. Somorjai, in "*Photocatalysis - Fundamentals and Applications*", N. Serpone and E. Pelizzetti, Eds., Wiley-Interscience, New York, 1989, chapter 9.

[31]. (a) L.L. Basov,.G.N. Kuzmin,.I.M. Prudnikov, and Yu.P. Solonitzyn, *Uspekhi Photoniki.*, Th.I. Vilesov, Ed., LGU (Leningrad State University), **6,** 82 (1977).

(b) A.V. Emeline and V.K. Ryabchuk, *Russ. J. Phys. Chem.*, **71,** 2085 (1997).

(c) S.V. Kurganov, andYu.M. Artem'ev, *Vestnik LGU*, Iss.4: Physics, Chemistry, **4,** 9 (1988)

[32]. M. Schiavello, V. Augugliaro, and L. Palmisano, *J. Catal.*, **127,** 332 (1991).

[33]. L. Palmisano, V. Augugliaro. R. Campostrini and M. Schiavello, *J.Catal.*, **143,** 149 (1993).

[34]. Th. Th. Volkenstein. "*Electronic Processes on the Surface of Semiconductors during Chemisorption*", "Nauka", Moscow, 1987.

[35]. V. Parmon, *Catalysis Today*, **39,** 137 (1997).

[36]. Somorjai [30] referred to this as a "specific turnover rate".

Chapter 5

SPECTRAL DEPENDENCE AND WAVELENGTH SELECTIVITY IN HETEROGENEOUS PHOTOCATALYSIS. *EXPERIMENTAL EVIDENCE FROM THE PHOTOCATALYZED TRANSFORMATION OF PHENOLS*

Summary

The photocatalyzed transformation of phenol (PhOH) and 4-chlorophenol (ClPhOH) in air-equilibrated TiO_2 dispersions has been used to examine the spectral behavior of the quantum yields Φ (and photonic efficiencies, hereafter in this Chapter is given the symbol η) of loss of these two substrates at various wavelengths. Contrary to the band model of semiconductors and conventional wisdom, which predict rapid thermalization of photogenerated charge carriers to the lowest energy levels in their respective conduction and valence band states, and consequently to spectrally independent quantum yields, experimental results demonstrate that in fact the quantum yields of loss of PhOH and ClPhOH are spectrally dependent displaying well resolved band structures at 3.13, 3.21, 3.32, 3.60, 3.81, 4.28 and 4.57 eV for phenol and at 3.16, 3.25, 3.41, 3.59, 3.70 and 4.15 eV for 4-chlorophenol. These energies correlate with absorption and emission band energies of direct and indirect band-to-band transitions reported earlier by Serpone et al {*J.Phys.Chem.*, **99**, 16655 (1995)} and with theoretical

estimates by Daude and coworkers {*Phys.Rev.B*, **15**, 3229 (1977)} for TiO_2 crystals. Both the spectral dependence of Φ and η, and the wavelength selectivity of TiO_2 (S_e and S_h) are discussed in terms of theoretical predictions based on the solution to the continuity equation. The implicit emphasis of this Chapter is the need to rethink the predictions based on the conventional band model of semiconductors. Thermalization of hot carriers may not (in some cases) be as rapid as once envisaged.

1. INTRODUCTION

The last three decades have witnessed much attention on studies of photostimulated processes in heterogeneous (solid/gas, solid/liquid) systems by the photochemical community [1-10]. The extensive studies carried out in numerous laboratories have produced a massive array of experimental data on the photochemical behavior of different heterogeneous systems, and in most cases have established the major mechanistic features of photochemical and photophysical processes taking place at solid/gas and solid/solution interfaces. Nonetheless, the quantitative description and characterization of the photostimulated processes in such heterogeneous systems is still a matter of current interest [11-13]. In particular, a major issue has been the lack of an appropriate protocol to compare the activities of different photocatalysts in different heterogeneous systems.

A few parameters have been suggested for the characterization of photocatalytic activities in heterogeneous systems. One is the photonic efficiency (η, eqn 1) which has been defined as the ratio between the number of molecules formed or degraded in the system

$$\eta = \frac{\frac{dN_r}{dt}}{\frac{dN_{hv(inc)}}{dt}} \qquad (1)$$

per unit time, dN_r/dt (molecules s^{-1}), and the number of photons acting on the system per unit time, $dN_{hv}(inc)/dt$ (photons s^{-1}), at a given wavelength (some workers have referred to this, albeit incorrectly, as a quantum yield). In other words, photonic efficiency is a reaction rate normalized to the photon flow from the light source, and that describes how many molecules are transformed per photon incident on the system.

Another parameter used to characterize the photochemical activity of heterogeneous systems is the more fundamental quantum yield (Φ) of the photoreaction given by equation 2, and defined as the ratio between the number of molecules formed (or degraded) in the

$$\Phi = \frac{\frac{dN_r}{dt}}{A\left(\frac{dN_{hv(inc)}}{dt}\right)} = \frac{\frac{dN_r}{dt}}{\frac{dN_{hv(abs)}}{dt}} \qquad (2)$$

system per unit time, dN_r/dt (molecules s^{-1}), and the number of photons ***absorbed*** by the system per unit time, $dN_{hv}(abs)/dt$ (photons s^{-1}), at a given wavelength; A represents the fraction of the photon flow absorbed by the heterogeneous system. Thus, the quantum yield

represents how many molecules are transformed per photon actually absorbed. The essential difference between photonic efficiency η and quantum yield Φ is that not every incident photon will necessarily act upon the heterogeneous system and initiate the chemical transformation. Only those photons absorbed will do so. Consequently, and especially for weak absorption of light, although the photonic efficiency may be close to 0, the quantum yield may nevertheless reach high values. Appropriate determination of the fraction of absorbed light in heterogeneous systems has made the measurements of quantum yields a complex issue. This problem was solved in solid/gas heterogeneous systems by using either diffuse reflectance spectroscopy with a standard reference sample, or a black body-like reactor [14-17]. A protocol for determining the fraction of absorbed light in solid/liquid heterogeneous systems has been suggested recently (see Chapters 2 and 3) using an integrating sphere assembly [18,19]. With this method, the quantum yield of photobleaching methylene blue and the photodegradation of phenol were determined to be $\Phi = 0.040 \pm 0.003$ in the spectral range 300 –400 nm [18] and $\Phi = 0.14 \pm 0.02$ at $\lambda = 365$ nm, respectively[19].

To establish both the photonic efficiency and the quantum yield of a photostimulated reaction in heterogeneous systems, two important conditions must be satisfied [20,21]: (i) the reaction rate must be linearly dependent on photon flow, and (ii) the reaction rate must be independent of the concentration of reagent. Otherwise, if both photonic efficiency and quantum yield depended on photon flow and reagent concentration, photocatalytic activities as might be described by η or Φ from different heterogeneous systems and different laboratories could not be compared.

In earlier studies [12,19] a simple parameter, the relative photonic efficiency (in this Chapter defined by the symbol η_{rel}), was introduced so as to compare photochemical activities of different heterogeneous systems (eqn 3).

$$\eta_{rel} = \frac{\eta'}{\eta_{st}} \tag{3}$$

It was described as the ratio between the photonic efficiency of a given reaction (η') to the photonic efficiency η_{st} of a standard reaction (i.e. the photodegradation of phenol over TiO_2 "Degussa P-25" chosen as a standard photocatalyst [12,19]). In turn, this equals the ratio of the corresponding reaction rates under otherwise identical irradiation conditions (eqn 4).

$$\eta_{rel} = \frac{\dfrac{dN'_r}{dt}}{\dfrac{dN_{r,st}}{dt}} \tag{4}$$

To compare photocatalytic activities for the same photocatalyst but for reactions of different reagents under identical irradiation and light absorption conditions, the relative photonic efficiency may also be defined as the ratio of the appropriate quantum yields of the corresponding processes (eqn 5).

$$\eta_{rel} = \frac{\Phi'}{\Phi_{st}} \tag{5}$$

Using this approach and the value of the quantum yield of phenol photodegradation over TiO_2 P-25 as the standard reaction and photocatalyst, respectively, has led to the estimation of the quantum yields of photodegradation of different aromatic compounds [22].

In many cases, however, both the photonic efficiencies and the so-called quantum yields were determined using broadband radiation rather than under monochromatic irradiation conditions, as required by the definitions of both parameters [23]. This problem would not be an issue if both parameters were spectrally independent. However, for all the solid/gas heterogeneous systems examined earlier [14-17,24-27] both photonic efficiencies and quantum yields were seen to be spectrally dependent. The spectral dependence of η and Φ may be a rather general phenomenon, and one may therefore expect to observe such dependencies even for solid/liquid heterogeneous systems.

To interpret the spectral dependency of the quantum yield, Emeline and coworkers [28] recently proposed a model based on the one-dimensional solution to the continuity equation considering the spacial non-uniform photogeneration of charge carriers (electrons and holes) and the diffusion limitation for carriers generated in the bulk of the solid to reach the surface in order to take part in surface chemical reactions. The model predicted that the quantum yield increases with an increase of the absorption coefficient, and that Φ becomes spectrally independent under strong absorption conditions. Another consequence of the solution to the continuity equation was a demonstration that photocatalysts may be spectrally selective; that is, the photocatalyst's selectivity changes on varying the wavelength of the incident light [28]. This phenomenon was first observed experimentally in solid/gas

heterogeneous systems by Kuzmin et al [29] and by Ryabchuk and coworkers [30].

In the present Chapter we examine two cases, namely the photodegradation of phenol and 4-chlorophenol in aqueous TiO_2 dispersions to assess whether the expected quantum yields for the photodegradation of these two substrates are spectrally dependent, and whether the photocatalyzed reactions display wavelength selectivity.

2. EXPERIMENTAL

2.1 Materials

The photocatalyst was P25 TiO_2 kindly provided by Degussa Canada Ltd. The phenol and 4-chlorophenol were Aldrich reagents and were used as received. Solvents for liquid chromatography were Omnisolv HPLC grade, and the water was doubly distilled.

2.2 Procedures

Photonic efficiencies and quantum yields were determined using recently reported protocols [11,12] (see Chapters 2 and 3). The photon flow (ρ) from the irradiation source was established using Aberchrome 540 and ferrioxalate actinometry using well established standard procedures {see e.g. ref. [23]}.

All experiments were carried out at pH ~ 3 (HCl). Typically, irradiation of a phenol solution in an air-equilibrated dispersion with a TiO_2 loading of 0.3 g L^{-1} was carried out in a sphere-like pyrex reactor using an Oriel 1000-Watt Hg/Xe lamp as the light source whose radiation was filtered through a water filter to remove IR radiation. Appropriate

wavelengths of illumination were selected using a monochromator (spectral resolution ca. ± 5 nm). Neutral density "gray" metal supported pyrex filters were used to attenuate the photon flow, where needed. Rates of the photocatalyzed degradation of phenol and 4-chlorophenol were determined by monitoring the time evolutions of the concentrations of the aromatic compounds during irradiation utilizing liquid chromatographic methods with a Waters HPLC chromatograph (501 pump and either a Waters μBondapak C18 column or a Whatman Partisil 10 ODS-3 column) interfaced to a Shimadzu flow cell for absorption recording. The Shimadzu UV-265 spectrophotometer was also interfaced to an IBM PC computer for data acquisition and handling. For the determination of the quantum yields the initial concentrations used were 0.23 mM for phenol and 0.20 mM for 4-chlorophenol chosen subsequent to experiments as displayed in Figure 1. The fraction of light scattered and absorbed by theTiO_2 catalyst was assessed with the UV-265 spectrophotometer equipped with an integrating sphere using a method developed earlier [12,19]. Recording parameter settings, data collection, and data processing were carried out using the Spectroscopy Interface Software, Version 3 (Shimadzu Scientific Instruments, Inc.).

3. RESULTS

Two essential conditions must be satisfied to determine photonic efficiencies and *unique* quantum yields of surface photochemical reactions in heterogeneous media [31]: (i) reaction rates must be independent of the concentration of reagents, that is quantum yields must be determined under conditions of zero-order kinetics; and (ii) the rates must scale

linearly with the intensity (photon flow) of the incident *actinic* light. To verify whether these conditions were satisfied in the present cases, we carried out a set of control experiments to measure reaction rate dependencies on the concentration of phenol and on the photon flow at three different wavelengths (380 nm, 365 nm, 334 nm). The results showed that under the chosen experimental conditions the initial reaction rates for the degradation of the two test substrates reached saturation with respect to concentration and were linearly dependent on light intensity (see e.g. Figure 1). Consequently, the photonic efficiencies and the quantum yields measured under these conditions are uniquely defined, are maximal, and depend only on the intrinsic properties of the photocatalyst, so that wavelength dependencies of the photonic efficiencies and quantum yields reflect the features of photoexcitation and of transfer of the charge carriers from the catalyst particle bulk to the surface and then to the reagent molecules, features that are appropriate to the TiO_2 specimen used.

The experimental spectral dependencies of the photonic efficiency for the photocatalyzed degradation of phenol and chlorophenol are presented in Figure 2 and summarized in Table 1. The estimated positions of the maxima (and shoulders) of the spectral dependencies are summarized in Table 2.

We have noted earlier that the quantum yield differs from the photonic efficiency because the former takes into account the number of photons actually absorbed by the system per unit time, rather than the number of photons incident on such a system. Quantum yields were estimated with the aid of the spectral distribution of the fraction of light absorbed obtained for the TiO_2 (Degussa P25) loading employed in a previous study [12]

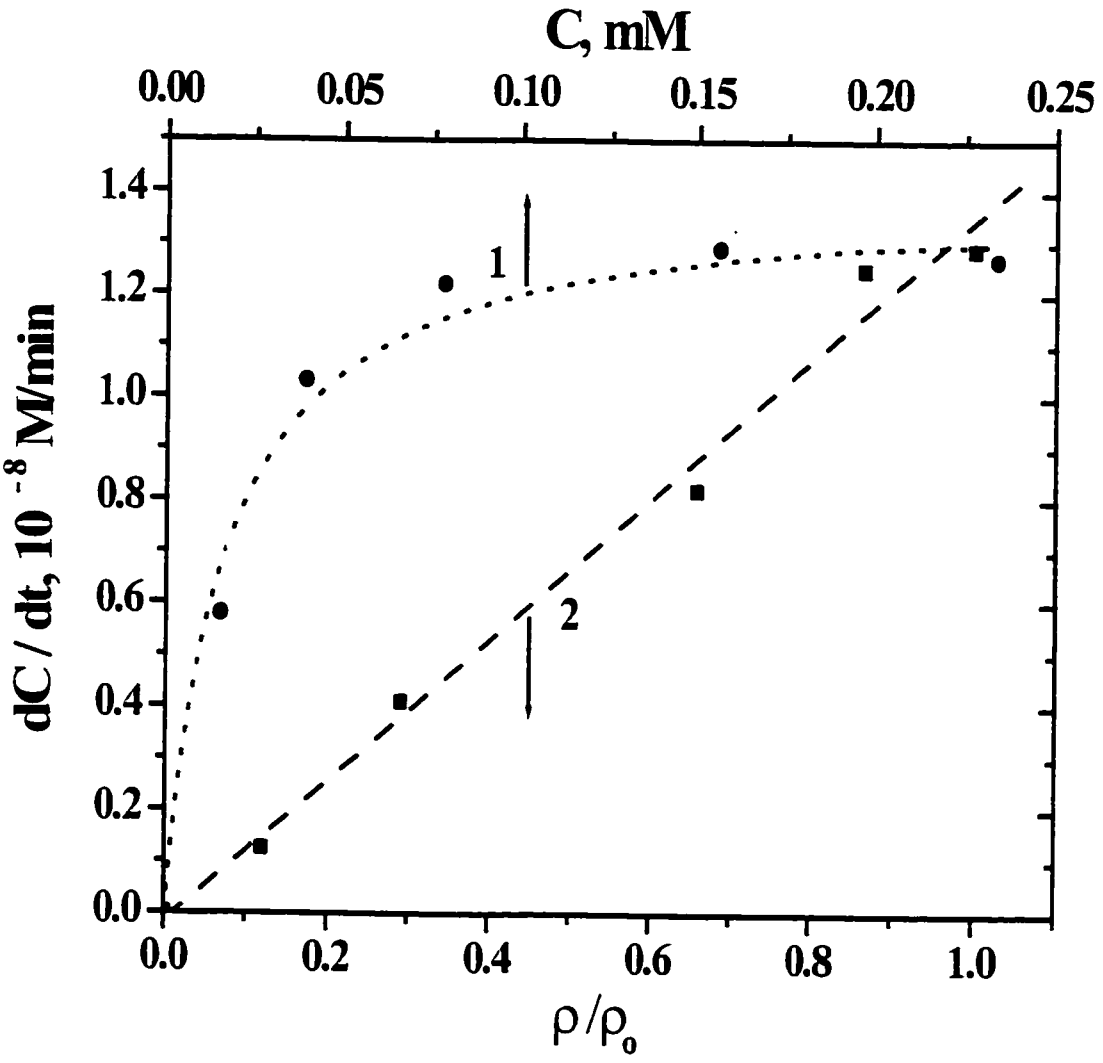

Figure 1. - Dependencies of the rate of photodegradation of phenol over TiO_2 on (1) the phenol concentration, and on (2) photon flow at photoexcitation with light at hν = 3.38 eV (365 nm).

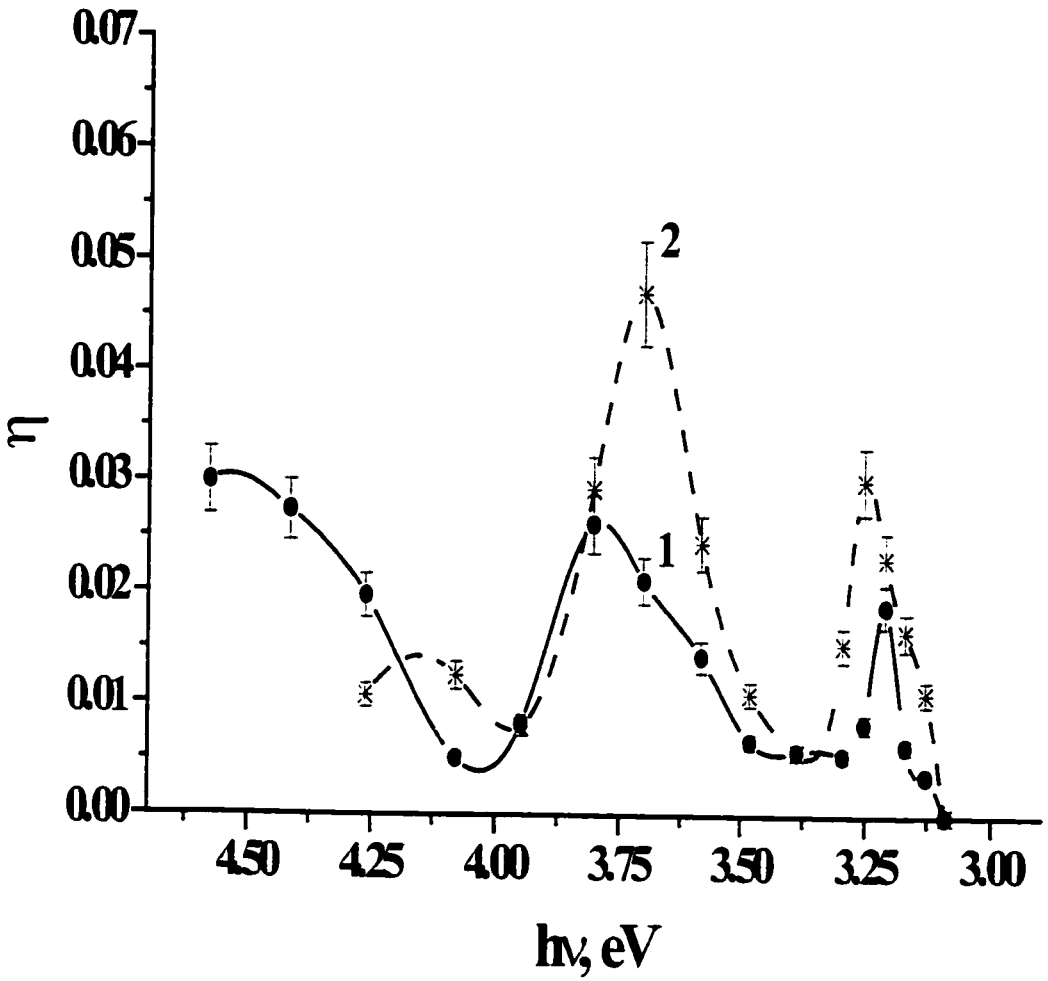

Figure 2. - Spectral dependencies of the photonic efficiencies of the photodegradation of (1) phenol and (2) 4-chlorophenol.

(See also Chapters 2 and 3). Figure 3 illustrates the spectral dependencies of the quantum yield of the photocatalyzed degradation of phenol and chlorophenol over TiO_2. The experimental quantum yields at various excitation energies are collected in Table 1. The dependencies display well-resolved band structures with two principal band maxima at ca.

Table 1. - Experimental quantum yields, photonic efficiencies, and relative photonic efficiencies for the photodegradation of phenol (C_o = 0.23 mM) and 4-chlorophenol (C_o = 0.20 mM) over TiO_2 (Degussa P25) aqueous dispersions illuminated at various wavelengths.

$\lambda_{excit.}$, nm	$h\nu_{excit.}$ eV	η_{PhOH} [a]	Φ_{PhOH} [a]	η_{ClPhOH} [a]	Φ_{ClPhOH} [a]	η_{rel}
270	4.58	0.030	0.062	-	-	-
280	4.41	0.027	0.054	-	-	-
290	4.26	0.020	0.04	0.011	0.021	0.54
303	4.07	0.0051	0.011	0.012	0.026	2.48
313	3.95	0.0082	0.019	0.0079	0.018	0.97
325	3.80	0.026	0.073	0.029	0.082	1.1
334	3.70	0.021	0.075	0.047	0.17	2.2
345	3.58	0.014	0.076	0.024	0.13	1.7
355	3.48	0.0066	0.048	0.011	0.078	1.6
365	3.39	0.0057	0.053	0.0057	0.052	0.99
375	3.30	0.0054	0.061	0.015	0.17	2.8
380	3.25	0.0082	0.11	0.030	0.40	3.7
385	3.21	0.019	0.26	0.023	0.32	1.2
390	3.17	0.0063	0.097	0.016	0.26	2.6
395	3.13	0.0036	0.057	0.011	0.18	3.1
400	3.09	0	0	0	0	-

[a] Estimated error ca. ±10%.

Table 2. - Estimated energy maxima for the photonic efficiencies and quantum yields of the photodegradation of phenol and 4-chlorophenol, and comparison with theoretical estimates and experimental energies (from absorption and photoluminescence) of indirect and direct electronic transitions.

hν (theoret.) [a] eV	hν (Abs/Lum) [b] eV	band maxima eV	Φ_{PhOH} (calc.) [c]	band maxima eV	Φ_{ClPhOH} (calc.) [c]
3.05	2.97	3.13	0.05	3.16	0.23
3.19	3.21	3.21	0.23	3.25	0.39
3.45	3.61 - 3.68	3.32	0.06	3.42	0.051
3.59	3.61 - 3.68	3.6	0.072	3.62	0.096
4.05	4.03 - 4.04	3.8	0.065	3.72	0.093
4.3	---	4.28	0.023	4.14	0.029
---	---	4.57	0.059	---	---

[a] From theoretical calculations by Daude and coworkers [31].

[b] From absorption and photoluminescence experiments [35].

[c] Obtained following a deconvolution of the spectral envelopes of Figures 2 and 3 using the PeakFit software Version 4.

3.2 eV and 3.7 eV, together with some additional finer details (see Table 2). These correspond to the energies of indirect and direct band-to-band transitions in the anatase polymorph (see below and Table 2).

The spectral dependence of the ratio of the quantum yields of 4-chlorophenol photodegradation to the quantum yield of phenol photodegradation (i.e. the relative photonic efficiency for the photodegradation of chlorophenol, see Introduction) is presented in Figure 4.

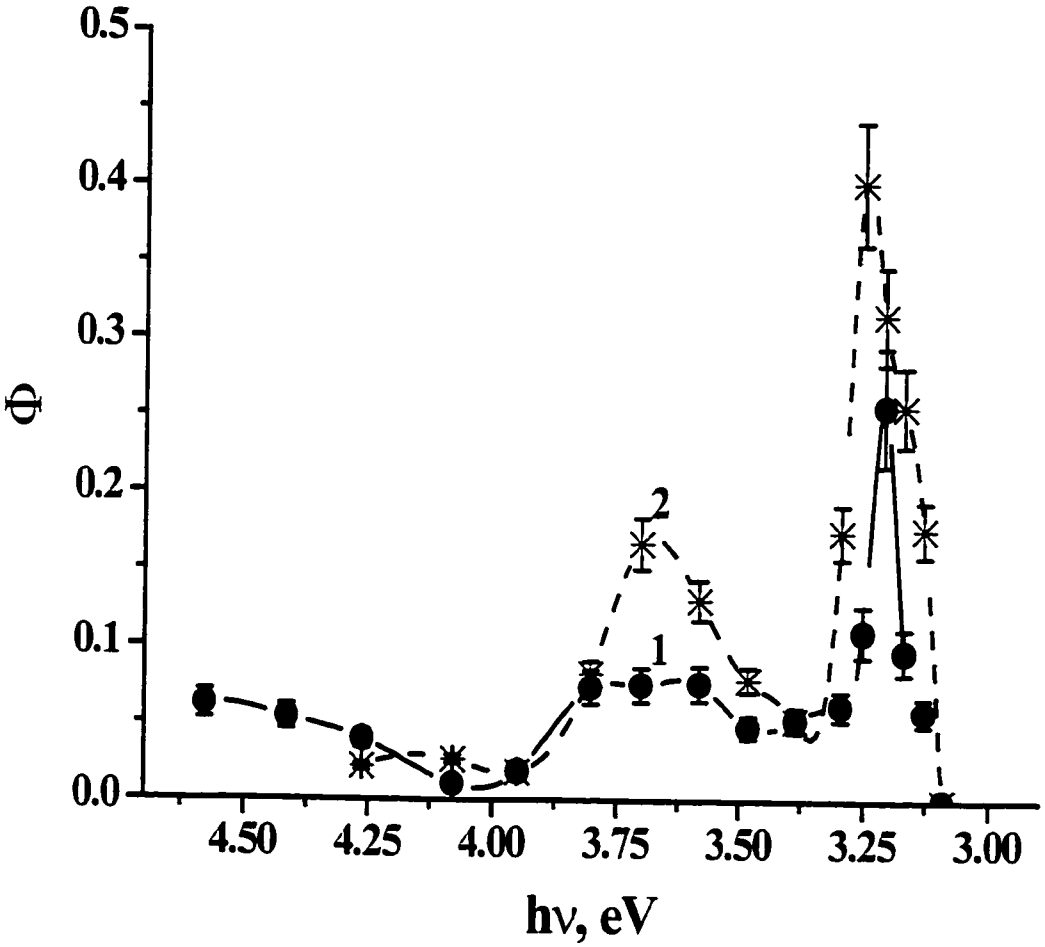

Figure 3. - Spectral dependencies of the quantum yields of the photodegradation of (1) phenol and (2) 4-chlorophenol.

All three parameters (namely, quantum yield, Φ, photonic efficiency, η, and relative photonic efficiency, η_{rel}) described earlier, which can be used to characterize the photoactivity of the TiO_2 photocatalyst with regard to phenol and chlorophenol photodegradation, show spectrally dependent behavior. Spectral maxima and shoulders of

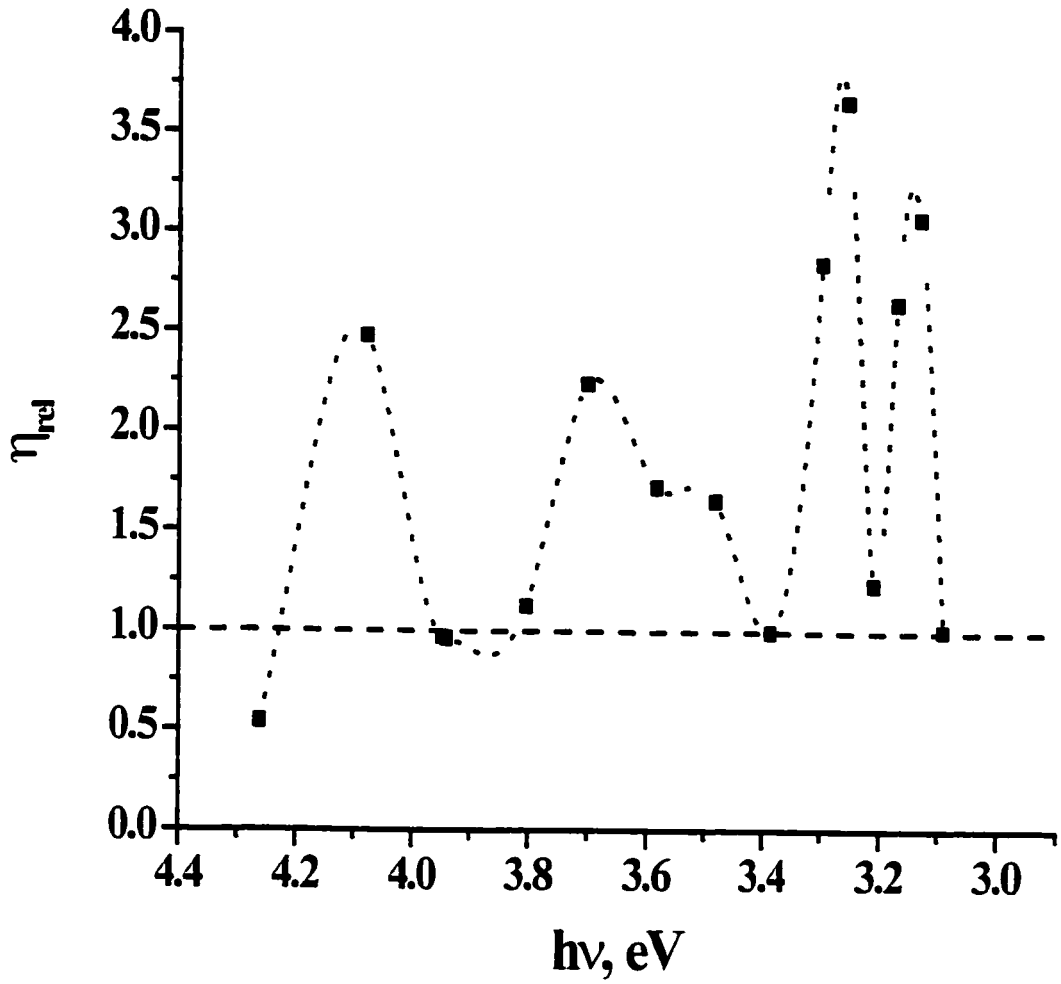

Figure 4. - Spectral dependence of the relative photonic efficiency (η_{rel}) of the photodegradation of 4-chlorophenol with respect to the photodegradation of phenol.

all parameters are also summarized in Table 2.

The kinetics of formation of benzoquinone (one of the principal intermediates) were determined on photoexcitation of 4-chlorophenol at several wavelengths of the incident light. Note the striking differences in the kinetic behavior in the formation of benzoquinone at the

four wavelengths illustrated (Figure 5). Relevant quantum yields for the initial formation of this intermediate are summarized in Table 3.

Table 3. - Experimental initial quantum yields and selectivities in the formation of benzoquinone during the photodegradation of 4-chlorophenol (C_o = 0.20 mM) over TiO_2 (Degussa P25; loading 0.3 g L^{-1}) in aqueous dispersions illuminated at various wavelengths.

Experimental Run[a]	hv, eV (λ, nm)	ρ (photons s^{-1})	Φ_{BQ} [b]	S_{BQ} [b]
1	3.21 (385)	2.08 x 10^{15}	0.0024	0.008
2	3.38 (365)	2.26 x 10^{16}	0.03	0.58
3	3.53 (350)	4.4 x 10^{15}	0.086	0.78
4	3.70 (334)	3.9 x 10^{15}	0.001	0.006

[a] Numbers correspond to the curves in Figure 5. [b] Estimated error ca. ±15%.

4. DISCUSSION

4.1 Spectral Dependence of Quantum Yields

For a titania/phenol aqueous heterogeneous system and within the spectral range 280–400 nm, light absorption concerns mostly TiO_2 since the two organic substrates examined do not absorb in this wavelength range under the conditions used. A result of this primary photoexcitation of the photocatalyst is generation of electron/hole pairs (eqn 6).

$$TiO_2 + hv \rightarrow e^- + h^+ \qquad (6)$$

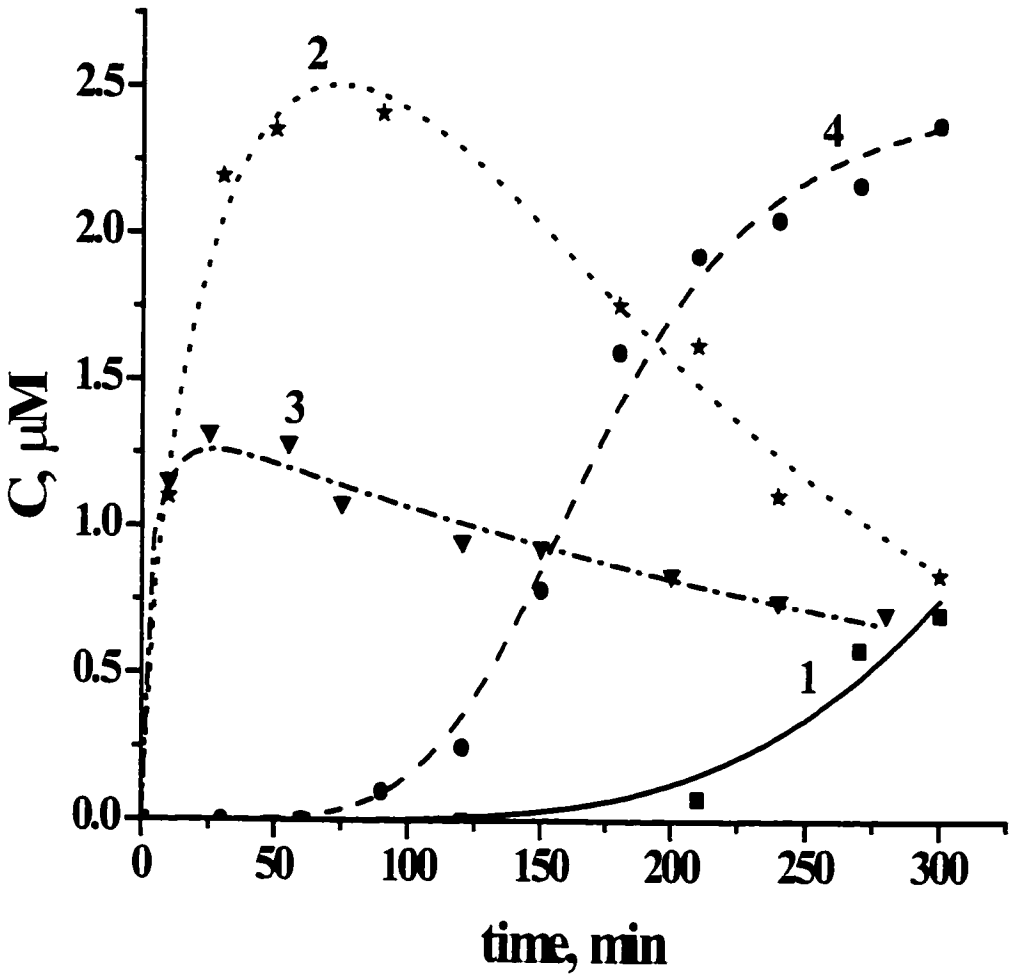

Figure 5. - Kinetics of formation of benzoquinone during the photocatalyzed transformation of 4-chlorophenol (C_o = 0.20 mM) at photoexcitation with light at (1) hν = 3.21 eV (385 nm); ρ = 2.08 x 10^{15} photons s^{-1}; (2) hν = 3.38 eV (365 nm) ρ = 2.26 x 10^{16} photons s^{-1} ; (3) hν = 3.53 eV (350 nm) ρ = 4.4 x 10^{15} photons s^{-1} ; and (4) hν = 3.70 eV (334 nm) ρ = 3.9 x 10^{15} photons s^{-1}.

Those charge carriers that reach the photocatalyst surface are poised to participate in surface chemical processes. Thus, regardless of the mechanism of the photocatalytic process, its rate will depend on the surface concentration of the corresponding charge carriers, n_s. In the steady state approximation, the latter is determined (a) by the rate of photostimulated carrier generation in the bulk of the photocatalyst, (b) by the rate of carrier diffusion flow from the bulk to the surface and (c) by their decay through surface recombination and reaction pathways. For the one-dimensional model the surface concentration of the carriers is expressed by equation 7 [28]:

$$n_s = \frac{2(1 - e^{-\alpha d})\,\chi\,\rho\,\alpha\,L^2}{D\,(\tanh(\frac{d}{2L}) + \xi)\,(1 - \alpha^2 L^2)}\,[\tanh(\frac{d}{2L})\coth(\frac{\alpha d}{2}) - \alpha L] \qquad (7)$$

where D is the diffusion coefficient of the carriers, χ is the quantum yield of internal photoeffects (generation of carriers and other internal events), ρ is the photon flow of the incident light, α is the absorption coefficient of the photocatalyst at a given wavelength, $L = (D\tau)^{1/2}$ is the diffusion length of the carriers (τ is the lifetime of carriers in the bulk), and $\xi = s\,L/D$ is taken as the ratio of surface recombination (here described by the symbol s) to bulk recombination rates. Then, for the simplified primary step (eqn 8) involving

$$M + h^+(e^-) \rightarrow M^+(M^-) \qquad (k_r) \qquad (8)$$

reagent molecules M interacting with surface carriers of the proper sign, the photonic efficiency η of the disappearance of M molecules is given by equation 9,

$$\eta = \frac{k_r M 2(1 - e^{-\alpha d}) \chi \alpha L^2}{D (\tanh(\frac{d}{2L}) + \xi) (1 - \alpha^2 L^2)} [\tanh(\frac{d}{2L})\coth(\frac{\alpha d}{2}) - \alpha L] \quad (9)$$

and the quantum yield Φ of the primary reaction (eqn. 8) is described by equation 10.

$$\Phi = \frac{k_r M \chi \alpha L^2}{D (\tanh(\frac{d}{2L}) + \xi) (1 - \alpha^2 L^2)} [\tanh(\frac{d}{2L})\coth(\frac{\alpha d}{2}) - \alpha L] \quad (10)$$

As soon as free charge carriers are photogenerated in a few femtoseconds (that is, 10^{-15} s), two possibilities may arise. The first is that if there exists rapid communication between the different sub-band states in the valence and conduction bands, in a few picoseconds (~ 10^{-10} s) the photocarriers will occupy the lowest states in their corresponding bands (i.e. they become thermalized). At moderate excitation energies, their distributions obey (quasi)-Boltzmann statistics with the carrier temperature equal to ambient temperature, and the carriers will have similar average mobilities and lifetimes and become indistinguishable regardless of the initial state occupied immediately upon photoexcitation. In terms of time scale, this means that the time of energy relaxation of the carriers τ_{rlxn} is much shorter then their lifetimes $\tau_{e,h}$; that is, $\tau_{rlxn} << \tau_{e,h}$. In such instance, the diffusion

coefficient D and diffusion length L, as well as the recombination parameters in eqns. 8–10, are constant and all the spectral variations of either the photonic efficiency η or the quantum yield Φ would have their origins simply from variations in the absorption coefficient α in the product αL and αd (eqn. 10). For example, the quantum yield of the surface photoreaction (eqn 8) within a single absorption band increases with an increase of α and becomes spectrally independent when $\alpha L >> 1$, provided that the diffusion length L of the carriers is much less than the crystal size, i.e. for $L << d$ [28]. Thus, one may expect to observe a spectral dependence of the quantum yield and photonic efficiency just at the edge of the intrinsic absorption where the absorption coefficient rises from ~ 10^2 cm^{-1} to about 10^4 –10^6 cm^{-1}. Where the absorption coefficient is of the same order of magnitude as the diffusion length, weak spectral fluctuations of the quantum yield (and photonic efficiency) may be expected.

A second possibility appears when the energy relaxation time is longer than the lifetime of the free carriers; i.e. when $\tau_{rlxn} >> \tau_{e,h}$. This possibility arises when elastic collisions dominate the inelastic collisions as a major pathway for electron/phonon interactions in the solid. This pathway leads to a fast momentum relaxation and to the establishment of equilibrium in the momentum in the electronic subsystem during a time when energy relaxation is not yet completed. In particular, this may lead to a higher population of the valleys of the sub-bands of higher energy compared to the thermally equilibrated state (Figure 6) [32], and thus to a higher temperature of electron gas because

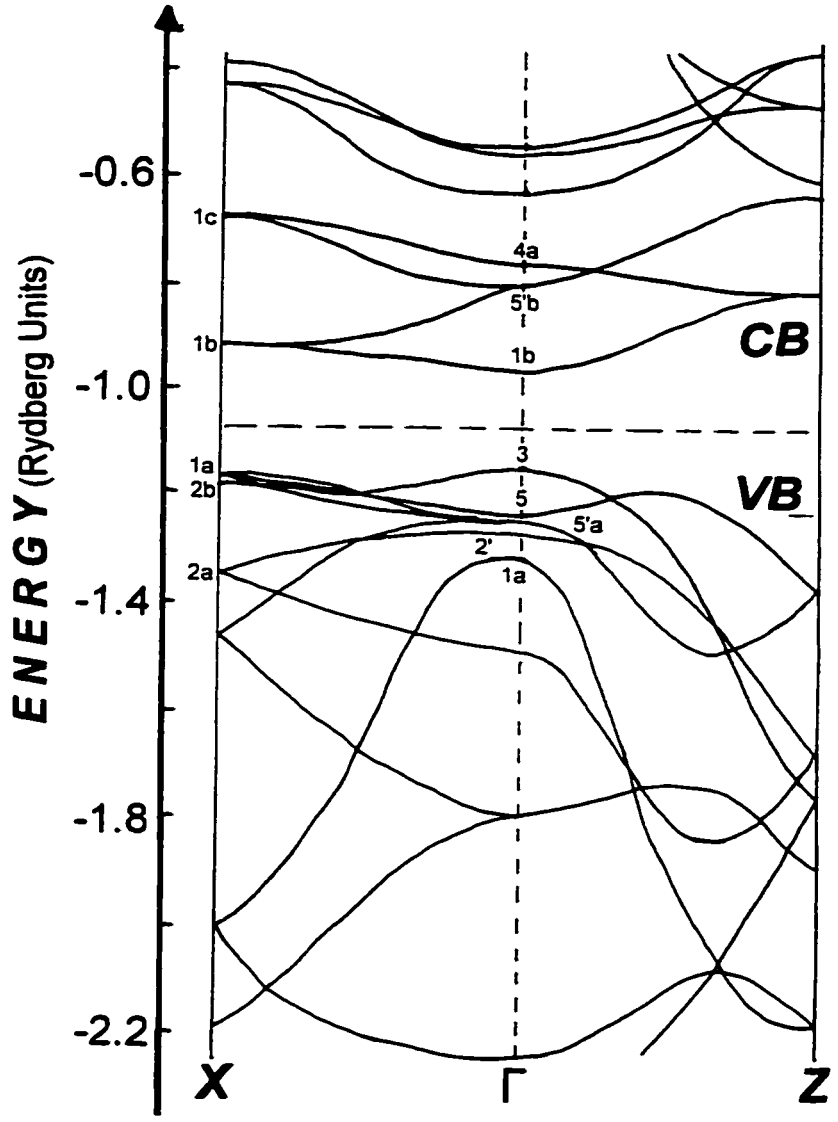

Figure 6. - Graph illustrating some relevant valence and conduction band levels in the Brillouin Zone for a TiO_2 crystal in the ***X*** and ***Z*** edges and in the center Γ. Adapted from reference [31].

of the presence of hot carriers [33,34].

An additional cause for the longer energy relaxation times arises if communication between the different states in the respective conduction and valence bands in nanoparticles is much less effective than in bulk solid crystals, or if there exists no communication between such states. The reason for weak (or non-existent) communication between such states in nanoparticles, unlike bulk crystals, could be that the translation symmetry in spatially confined nanoparticles is valid only for the short-length crystal units, and that the number of atomic states forming the band states is very limited compared to the number of atomic states in bulk crystals. In the simplest of cases, the number of states (Q) scales with the ratio of the crystal volume (V) to the volume of the elementary unit (V_o); that is,

$$Q \cong \frac{V}{V_o} \tag{11}$$

Consequently, if the number of states for the bulk crystal is very large because of a larger number of elementary units that form the crystal, the number of such states in nanosized particles is likely to be somewhat limited. A similar effect arises as a quantization in the depletion layer at the surface of bulk semiconductors when a thinner layer (with respect to the effective mass of carriers) causes formation of localized weakly or non-communicating electronic states in the spatially confined depletion layer (note, that nanoparticles are also spatially confined systems) [35-38].

Taking the average size of the particle as ca. 30 nm (typical of Degussa P25 TiO_2), the volume of the particle $V \approx 2.7 \times 10^{-27}$ m^3, and the volume of the elementary unit of anatase $V_o \approx 10^{-30}$ m^3. The number of electronic states in the bands is then ca. 10^6, whereas in the bulk crystal $Q >> 10^6$. Accordingly, energy relaxation in nanoparticles may be more difficult. In turn, the carriers occupying the different valleys of the different states in the conduction and valence bands (Figure 6) will be characterized by different lifetimes and different mobilities (and diffusion coefficients), and consequently different diffusion lengths. Hence, the lifetimes, the mobilities and the diffusion lengths in eqns 8–10 become spectrally dependent since the population of the given electronic states depends on the energy of the photons. Consequently, the surface concentration of carriers becomes spectrally dependent because of the spectral variation of carrier mobilities.

An appropriate description of the spectral dependence necessitates that we take into account (a) the size of the TiO_2 particles which for the Degussa P25 specimen is ca. 20–40 nm [39], (b) the spectral variation of the absorption coefficient ($\alpha \approx 10^2$ to 10^6 cm^{-1}), and (c) the diffusion length for electrons ($L_e \approx 10^{-6}$ cm). The diffusion coefficient for Degussa P25 titania is taken to be $D = 5 \times 10^{-3}$ cm^2 s^{-1} [40,41] and the lifetime of free electrons τ_e is a few tens of picoseconds [42,43]. The diffusion length of free holes (L_h) is taken to be longer than the diffusion length of electrons (i.e. $L_e << L_h$) since the lifetime of electrons and holes are of about the same magnitude, but hole mobility appears to be faster than for electrons in TiO_2 [40]. This inference is in keeping with the rather broad valence band of

TiO_2 [32,44]. Note that a precise estimate of the diffusion length of free holes is difficult because of the lack of appropriate experimental data. The rate of surface recombination (s) for a highly defective surface of nanoparticles is likely to be around 10^5 cm s^{-1}. Then the variation of α from 10^2 cm^{-1} to ca. 10^5 cm^{-1} at the fundamental absorption edge, which is associated with indirect transitions, corresponds to the theoretical case of ***weak*** light absorption when αL and αd are much less than unity. Also note that even a maximal absorption coefficient of $10^6 cm^{-1}$ at the higher photon excitation energies, corresponding to direct band-to-band transitions, will not satisfy the conditions of ***strong*** light absorption considered previously because they would require that $\alpha L >> 1$ and that $\alpha d >> 1$ [28].

Earlier theoretical considerations and experimental evidence from various studies [15,17,28] have inferred for the case of ***weak*** light absorption (i) that the quantum yield Φ is spectrally independent {i.e. $\Phi = fn\ (\alpha)$, eqn 12}, (ii) that the photonic efficiency η follows the absorption spectrum {i.e. $\eta = fn\ (\alpha)$; eqn 13} either within a single absorption band, or in a complex absorption band if the carriers are formed as a result of light absorption in the band and occupy the same states (corresponding to a thermally equilibrated system)

$$\Phi = \frac{2\ k_{tr}\ S_o\ \chi\ L^2}{D\ d}\ \left[\frac{\tanh(\frac{d}{2L})}{\tanh(\frac{d}{2L}) + \xi}\right] \qquad (12)$$

$$\eta = \frac{2\, k_{tr}\, S_o\, \chi\, L^2\, \alpha}{D} \left[\frac{\tanh(\frac{d}{2L})}{\tanh(\frac{d}{2L}) + \xi}\right] \qquad (13)$$

in their respective conduction and valence bands, and (iii) that the quantum yield of carrier formation χ is spectrally independent.

By contrast, in the case of the photocatalyzed degradation of phenol and 4-chlorophenol over TiO_2 particles, the spectral distributions of the corresponding photonic efficiencies (Figure 2) and the quantum yields (Figure 3) demonstrate a well-resolved band structure. In previous studies, Emeline and coworkers [15,28] described the reasons for observing band-like spectral dependencies of quantum yields of surface photochemical processes for the case of weak *extrinsic* light absorption by lattice defects. They concluded that the band-like spectral dependence of Φ is caused by an overlap of different absorption bands corresponding to different types of defects that do not communicate with each other, and that differ by the quantum yield of internal photoeffects. In particular, the spectral dependence was observed where active and inactive absorption bands overlapped [15,28].

The fundamental absorption spectrum of TiO_2 particles is formed by several direct and indirect electronic band-to-band transitions [32]. A review of experimental [45-47] and theoretical [32,44,48] data indicates that the edge of *intrinsic* absorption by TiO_2 is formed by indirect transitions from the edge to the center of the Brillouin Zone (BZ), for example

$X_{1a} \rightarrow \Gamma_{1b}$ and $X_{2b} \rightarrow \Gamma_{1b}$, as well as by indirect transitions from the center to the edge, i.e. $\Gamma_3 \rightarrow X_{1b}$ (Figure 7). The lowest energy direct transition $\Gamma_3 \rightarrow \Gamma_5$ is forbidden [32]. The first allowed direct transitions occur at the X edge of the Brillouin Zone: namely, $X_{1a} \rightarrow X_{1b}$ (3.45 eV) and $X_{2b} \rightarrow X_{1b}$ (3.59 eV), and the next allowed lowest energy transitions are $\Gamma_{5',b} \rightarrow \Gamma_{1b}$ (4.05 eV) and $\Gamma_{2'} \rightarrow \Gamma_{1b}$ (4.3 eV). Thus, as a result of band-to-band electronic transitions during photoexcitation with different photon energies, electrons initially occupy different conduction band states, whereas holes of various energies occupy different valence band states.

Despite the notion that the fundamental absorption band of TiO_2 is formed by an overlap of different electronic transitions (see above), the concept of inactive absorption or absorption with different quantum yields of internal photoeffects cannot be applied to the case of *intrinsic* light absorption because each absorbed photon causes generation of electron-hole pairs with a quantum yield of 1, and no inactive background absorption exists. Thus, the only reason for observing a spectral dependence at the edge of the *intrinsic* absorption band is that the photogenerated carriers in the different states have different recombination constants (i.e. different recombination cross-sections), and consequently different lifetimes, different mobilities, and different rate constants for the surface reactions [28]. Because of weak communication between the different states, the carriers do not thermalize rapidly and maintain the corresponding parameters attributed to the given state during their lifetime in that state. This means that in equations 8–10 and equations 12 and 13 either that the parameters D, L and ξ are spectrally dependent, or that the concept of

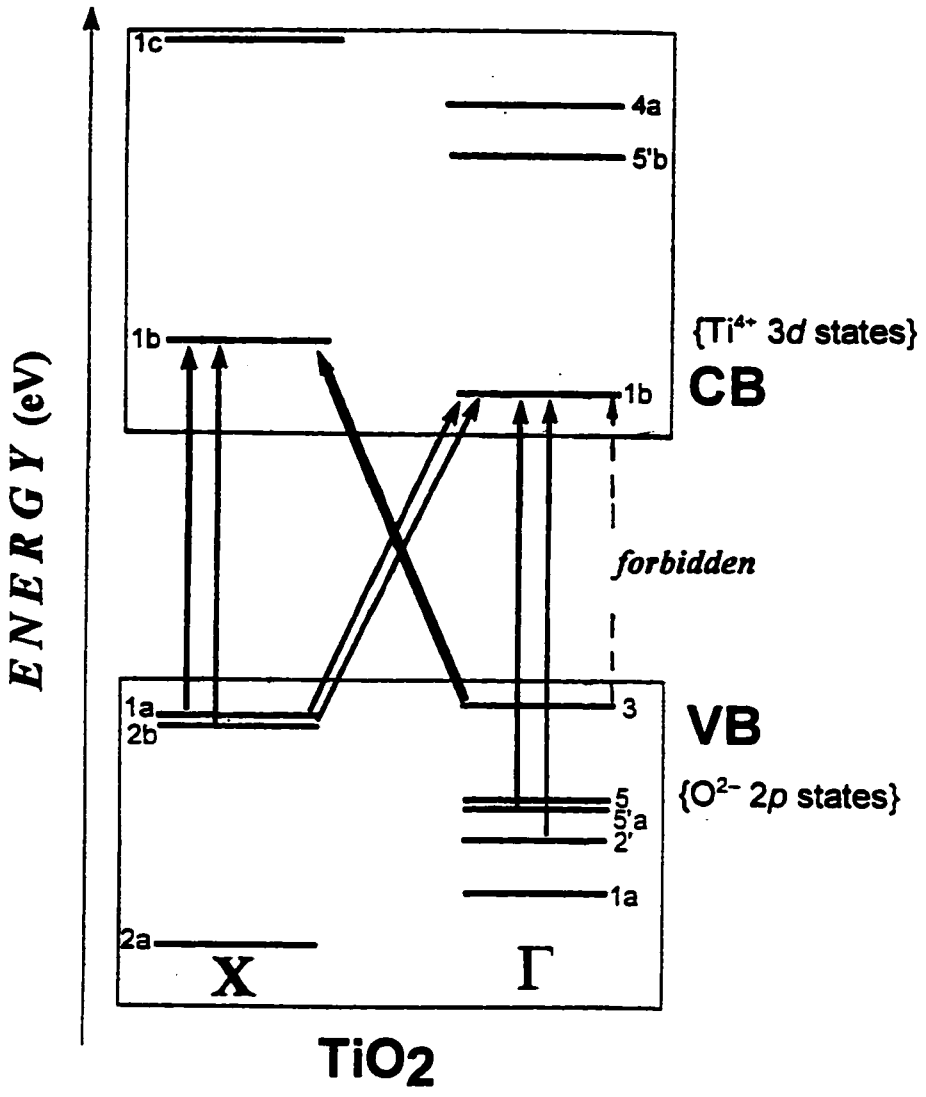

Figure 7. - Energy level diagram summarizing the relevant allowed direct and allowed but phonon-assisted indirect electronic transitions between valence and conduction band states in TiO_2. Adapted from reference [32]. (The numbers refer to the labels of the states as in Figure 6).

overlapping different absorption bands is applicable which correspond to different band-to-band transitions, and which lead to different energy distributions of carriers in the bands and to different efficiencies of photoprocesses for each transition. In this case, however, it is the different lifetimes of carriers and their mobilities, as well as their different ability to be localized at the surface and their reactivity that are responsible for the different efficiencies of photoexcitation of the solid in the fundamental absorption band, instead of differences in the quantum yields of internal photoeffects for weak *extrinsic* light absorption. Hence, the spectral dependence of the quantum yield and of the photonic efficiency can be estimated from equations 12 and 13, respectively, by applying the spectral variation of the average diffusion length and carrier lifetimes, or by considering both of these two parameters as being constant within each of the single absorption band corresponding to a given band-to-band transition.

Experimentally, the total quantum yield is obtained from equation 14.

$$\Phi_{total} = \frac{\Sigma_i A_i \Phi_i}{\Sigma_i A_i} \tag{14}$$

and the photonic efficiency from equation 15,

$$\eta_{total} = \Sigma_i \eta_i \tag{15}$$

where A_i is the fraction of photons absorbed for a given transition, Φ_i is the quantum yield

within a single absorption band for a given transition (eqns. 10 and 12), and η_i is the photonic efficiency also within a single absorption band corresponding to a given transition (eqns. 9 and 13).

The first step in the photocatalyzed degradation of phenol (see Scheme I) is interaction of phenol molecules with surface trapped holes , more precisely with surface-trapped •OH radicals formed by trapping of holes by surface OH^-_{surf} groups (eqn 16).

$$h^+ + OH^-_{surf} \rightarrow \bullet OH_{surf} \qquad (16)$$

At the fundamental absorption edge, holes are formed in the X_1, X_2 and in Γ_3 states due to indirect transitions (2.91 eV, 3.05 eV and 3.19 eV, respectively) which of necessity are phonon-assisted. Consequently, holes at the edge of the BZ zone are heavier than those generated at the center of BZ, and communication between these states during the carrier lifetimes may be somewhat difficult. To the extent that hole mobilities in different states are (expectedly) different causes the band-like spectral dependencies of photonic efficiencies and quantum yields to be observed in the photodegradation of phenol at the edge of the fundamental absorption.

The diffusion length of photogenerated holes should be comparable to the particle size of the photocatalyst, since the quantum yield achieves a rather significant value (Φ = 0.25). At higher photoexcitation energies, direct electronic transitions at the X-edge of BZ

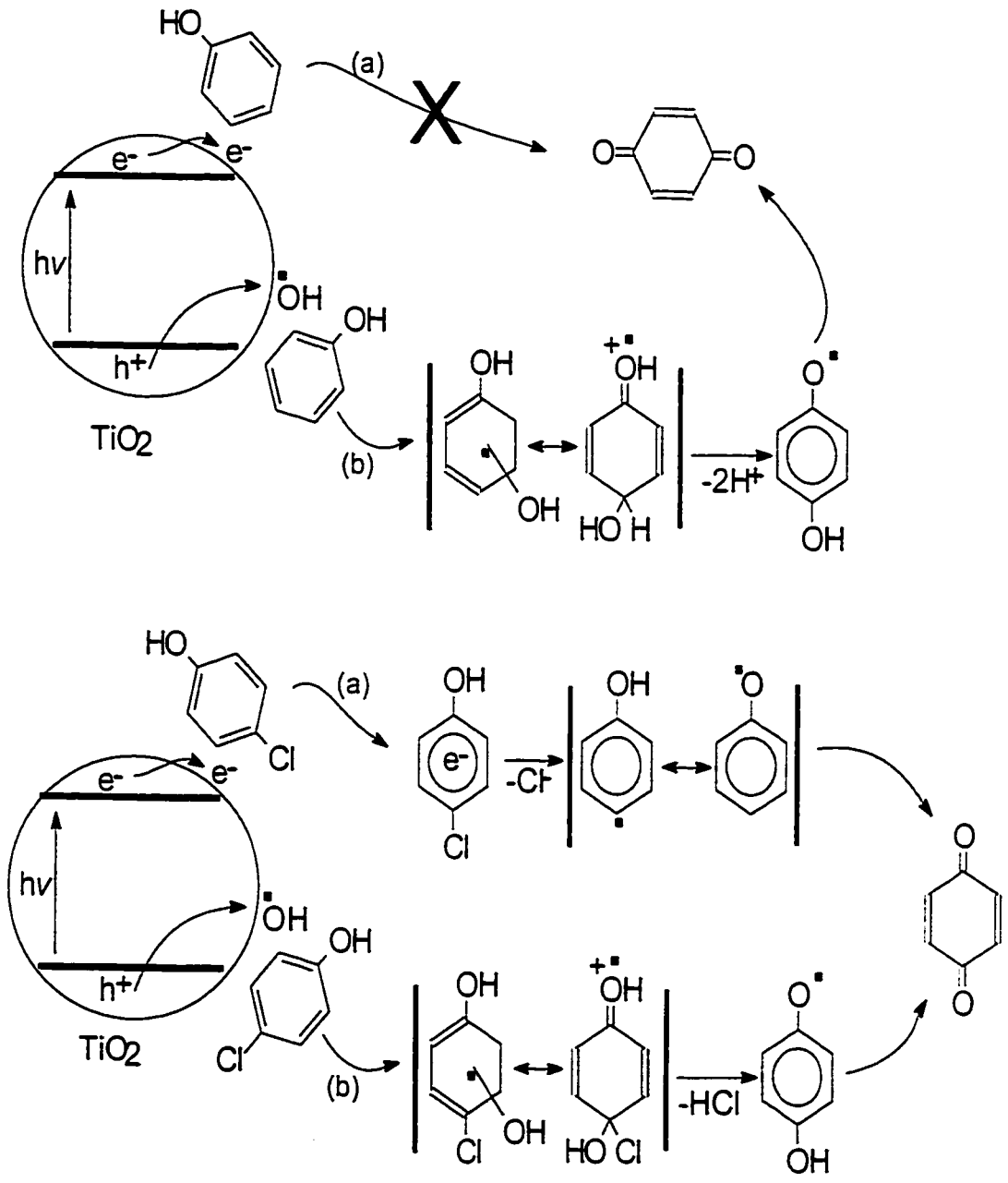
HO
(a)
e-
e-
hν
•OH
h+
TiO2
OH
(b)
OH
OH
+•OH
HO H
-2H+
O•
OH
O
O
HO
Cl
(a)
e-
e-
hν
•OH
h+
TiO2
OH
Cl
(b)
OH
e-
-Cl-
Cl
OH
•O
O
O
OH
+•OH
Cl
OH
HO Cl
-HCl
O•
OH

Scheme I

take place leading to the generation of holes in the X_1 and X_2 states, the same statesinvolved in the indirect transitions at the fundamental absorption edge. In this case, however, the absorption coefficient becomes comparable to the diffusion length and to the crystalline size, and thus the spectral variation of αd and αL in equations 8–10 also contribute to the observed spectral dependence of the quantum yields. This contribution demonstrates itself within the photon energy range 3.48 eV to 3.95 eV as an increase of the quantum yield until it reaches a nearly constant value between 3.58 eV and 3.80 eV followed by its decrease beyond this range. An example of such a behaviour was previously considered by Emeline and coworkers [28] who assumed that the increase of the absorption coefficient in the relation αL within the absorption band causes the increase in the quantum yield until $\alpha L >> 1$, at which point Φ becomes spectrally independent.

The spectral dependencies of the photonic efficiency (Figure 2) and the quantum yield (Figure 3) of the photodegradation of 4-chlorophenol is qualitatively similar to those for phenol photodegradation. We infer from this that the spectral dependencies are caused by the same electronic band-to-band transitions that generate free electrons and holes. However, unlike phenol, the mechanism of photodegradation of 4-chlorophenol may involve interaction of the phenol with both electrons and holes (see Scheme I) [49], so that the total quantum yield of 4-chlorophenol disappearance is the sum of quantum yields of degradation caused by electrons Φ_e and holes Φ_h:

$$\Phi_{ClPhOH} = \Phi_e + \Phi_h \qquad (17)$$

and the total photonic efficiency is the sum of the corresponding photonic efficiencies of photodegradation caused by both electrons η_e and holes η_h, respectively:

$$\eta_{ClPhOH} = \eta_e + \eta_h \tag{18}$$

If we further assume that both the quantum yields and photonic efficiencies of 4-chlorophenol photodegradation caused by surface-bound holes are similar to the photonic efficiencies and quantum yields of phenol disappearance also caused by holes {this is true if the kinetics of attack of phenol and 4-chlorophenol by •OH radicals in the heterogeneous media are nearly identical, which is the case in homogeneous media : k_{OH} = 9.6 x 10^9 M^{-1} s^{-1} for phenol and k_{OH} = 9.3 x 10^9 M^{-1} s^{-1} for 4-chlorophenol [50,51]}, then the relative photonic efficiency η_{rel} will be given by,

$$\eta_{rel} = \frac{\eta_{ClPhOH}}{\eta_{PhOH}} = \frac{\Phi_{ClPhOH}}{\Phi_{PhOH}} \tag{19a}$$

and

$$\eta_{rel} = 1 + \frac{\eta_e}{\eta_h} = 1 + \frac{\Phi_e}{\Phi_h} = 1 + \frac{R_e}{R_h} \tag{19b}$$

where R_e and R_h are the rates of the primary steps in the 4-chlorophenol photodegradation caused by electrons and holes, respectively. Thus, η_{rel} = ca. 1 (horizontal line in Figure 4)

if at a given wavelength of photoexcitation the degradation of 4-chlorophenol caused by electrons is negligible relative to oxidation by holes (indeed observed at hv = 3.2 eV, 3.4 eV, 3.8–3.95 eV, and 4.25 eV), and if the spectral variation in η_{rel} is caused by the spectral variation of the ratio of the corresponding rates R_e and R_h (quantum yields, photonic efficiencies), which in turn depend on the spectral changes of the ratio between the surface concentrations of electrons $[e_s]$ and holes $[h_s]$ and the spectral variation of rate constants k_{re} and k_{rh} (eqn 20).

$$\eta_{rel} = 1 + \frac{k_{re}[e_s]}{k_{rh}[h_s]} \tag{20}$$

Substituting the corresponding values of the quantum yields or the photonic efficiencies using equations 12 and 13, respectively, with the corresponding parameters for electrons and holes, we obtain

$$\eta_{rel} = 1 + \frac{k_{re}\,\tau_e}{k_{rh}\,\tau_h}\left(\frac{\tanh(\frac{d}{2L_e})\,[\tanh(\frac{d}{2L_h}) + \xi_h]}{\tanh(\frac{d}{2L_h})\,[\tanh(\frac{d}{2L_e}) + \xi_e]}\right) \tag{21}$$

Hence, the spectral variation of the relative photonic efficiency depends on the spectral variations of diffusion lengths and lifetimes of carriers owing to different populations of the different valence band states and conduction band states. Note that for small nanosized

particles the lifetime of carriers in the bulk, τ, may reflect the time of escape of the carriers from the bulk to the surface (eqn 22):

$$\tau = \frac{d^2}{D} = \frac{d^2[e]}{\mu\kappa T} \tag{22}$$

The condition expressed by equation 22 corresponds strictly to the case where $L >> d$, but formally it is taken to reflect the transformation to the conventional kinetic behavior of carriers. However, for very small particles another behavioral feature caused by spatial confinement may appear and a stochastic approach should then be contemplated [52,53]. The spectral dependence of reaction efficiencies for such small sized particles (i.e. when $d << L$) could then be caused by different reactivities of the surface carriers on photoexcitation by photons of different energies, i.e. by a spectral variation of k_{re} and k_{rh}, and by a spectral variation of the recombination constants (either bulk or surface recombination).

4.2 Wavelength Selectivity of Photodegradation

The relative photonic efficiency η_{rel}, as defined by equation 20, represents the inverse of the selectivity of the photocatalyst (eqn 23), provided that only the two reaction pathways considered in Scheme I take place. The selectivity of the photocatalyst with respect to oxidation by holes (S_h) and reduction by electrons (S_e), respectively, is described by equations 23 and 24.

$$S_h = \frac{R_h}{R_h + R_e} = \frac{k_{rh}[h_s]}{k_{rh}[h_s] + k_{re}[e_s]} = \frac{\frac{k_{rh}[h_s]}{k_{re}[e_s]}}{\frac{k_{rh}[h_s]}{k_{re}[e_s]} + 1} \quad (23)$$

and

$$S_e = \frac{R_e}{R_h + R_e} = \frac{k_{re}[e_s]}{k_{rh}[h_s] + k_{re}[e_s]} = \frac{\frac{k_{re}[e_s]}{k_{rh}[h_s]}}{\frac{k_{re}[e_s]}{k_{rh}[h_s]} + 1} \quad (24)$$

Clearly, alteration of the $[e_s]/[h_s]$ ratio will change the principal reaction pathway and favor the formation of one or more reaction products and intermediates [28]. Assuming that the rate constants of 4-chlorophenol interaction with surface electrons and •OH radicals are nearly identical {in homogeneous phase, $k_e = 1.5 \times 10^9$ M^{-1} s^{-1} and $k_{OH} = 9.3 \times 10^9$ $M^{-1}s^{-1}$ [49,51]} and considering that on average a single photon acts on the particle about every 10^{-5} s under our experimental conditions, we infer that the limiting steps of the photoreactions are the photogeneration and diffusion of carriers to the surface, and subsequently the surface trapping of carriers to form •OH radicals or electron centers (such as Ti^{3+}). Thus, the selectivity of a photocatalyst will depend on the spectral variation of the mobilities of carriers which alter the ratio of the surface concentration of carriers and/or active surface centers.

Benzoquinone is one of the intermediates formed in the photodegradation of 4-chlorophenol regardless of the reaction pathway (see Scheme I). However, in the case where

the surface concentration of electrons [e_s] is greater than that of holes [h_s] in eqn. 23, the kinetic behavior will reflect more the sequence (a) than (b), whereas if [e_s] is smaller than [h_s] the major pathway will be oxidation by holes (sequence (b)) and the kinetics should then reflect the concentration evolution of the appropriate intermediate.

The result of these expectations is observation of different kinetic behaviors for the formation of benzoquinone. At those wavelengths where the relative photonic efficiency is about 1 (see horizontal line in Figure 4), and thus the selectivity for oxidation by holes ($OH^{\bullet}$-radicals) also approaches 1 (compare eqns 23 and 24), the kinetics of formation of benzoquinone correspond to the kinetic behavior often observed for consecutive reactions (eqn 25) [54], where for one case the intermediate B forms rapidly followed by its slow decay, that is $k_B >>> k_C$.

$$A \xrightarrow{k_B} B \xrightarrow{k_C} C \rightarrow\rightarrow \text{Products} \qquad (25)$$

The •OH-radical initiated reaction sequence goes through a fast radical process(es) to form benzoquinone, a behavior that seems typical for excitation at hv = 3.38 eV and 3.53 eV. Note also, that the selectivity of formation of benzoquinone is close to unity at these energies (see Table 3). By contrast, for excitation at hv = 3.25 eV and 3.70 eV, where the contribution of electrons into the total reaction may be significant, the selectivity of the photocatalyst (eqns. 23 and 24) turns toward an electron initiated reaction pathway {sequence (a) of Scheme I}

and the behavior of benzoquinone formation kinetics become different and follow the typical behavior of formation of intermediate C in reaction 25; the selectivity of formation of benzoquinone is close to 0 at these excitation energies (Table 3). The electron initiated reaction pathway presumably goes through some relatively stable intermediate(s) before production of benzoquinone. Also noteworthy is the difference between the quantum yields of benzoquinone formation at photon energies hν = 3.38 eV and 3.53 eV when the reaction with trapped holes is the dominating process, and for excitation at hν = 3.25 eV and 3.70 eV when the reductive pathway becomes more significant (Table 3). Thus, the different kinetic behavior of benzoquinone formation can be rationalized in terms of the spectral selectivity of photocatalysts [28].

This behavior also accords with the spectral variations of the quantum yields of phenol and 4-chlorophenol photodegradation and with the relative photonic efficiency of 4-chlorophenol destruction. These infer that the spectral variation of carrier mobilities (hence, diffusion length) is connected to the different population of the separate electronic states in the valence and conduction bands. The population changes parallel the changes in the surface concentration of carriers and in their ratio $[e_s]/[h_s]$ to alter both the activity and selectivity of the photocatalyst. Note, that the spectral difference in population of the electronic states of a photocatalyst can also lead to the spectral variation of the corresponding reaction rate constants, and hence also affect the selectivity of the photocatalyst.

5. CONCLUDING REMARKS

The photocatalyzed degradation of phenol and 4-chlorophenol was re-examined to assess the spectral dependence of process photonic efficiencies and quantum yields. These were determined using a protocol reported in Chapters 2 and 3, and earlier [11,12]. In both cases, the reactions displayed a well-defined spectral dependence with some fine structure. The results contrast with expectations based on the classical band model of semiconductors (and on conventional wisdom) which would predict that the photogenerated charge carriers would thermalize very rapidly and any reaction would simply result from these thermalized carriers; that is, there should be no spectral dependence. By contrast, a model based on the solution to the continuity equation for a one-dimensional crystal proposed previously by Emeline and coworkers [28] predicted not only a spectral dependence for the quantum yields but also suggested a selectivity for the photocatalyst. The experimental results clearly point to the need for a reconsideration of the band model to take into account the existence of conduction band states and valence band states that may not communicate effectively with each other within their respective bands. Lack of this communication bears on the various factors that affect the properties of charge carriers , and consequently on the photocatalytic process. One important conclusion from this Chapter is that thermalization of carriers may not be as fast as conventional wisdom might dictate. For the 4-chlorophenol, we have also inferred that at certain wavelengths of excitation a non-insignificant electron initiated reduction takes place which also contributes to the overall quantum yield of the degradation of this chlorinated phenol.

6. REFERENCES

[1]. N. Serpone and E. Pelizzetti, Eds. *Photocatalysis - Fundamentals and Applications*; John Wiley & Sons, Inc.; New York; 1989.

[2]. M.A. Fox and M.T. Dulay, *Chem. Rev.*, **93**, 341 (1993).

[3]. K.I. Zamaraev and V.N. Parmon, Eds., *Photocatalytic Transformation of Solar Energy. Heterogeneous, Homogeneous and Organized Molecular Structures*, Nauka, Novosibirsk, Soviet Union, 1991.

[4]. V.G. Baru and Th.Th. Volkenstein, *The effect of irradiation on surface properties of semiconductors*, Nauka, Moscow, Russia, 1978.

[5]. E. Pelizzetti and M. Schiavello, Eds.*"Photochemical Conversion and Storage of Solar Energy"*, Kluwer Academic Publisher, Dordrecht, 1991.

[6]. M. Schiavello, Ed., *Photocatalysis and Environment. Trends and Applications*, Kluwer Academic Publisher, Dordrecht, 1987.

[7]. T.L. Rose, B.E. Conway, O.J. Murphy, and E.J. Rudd, Eds., *Water Purification by Photocatalytic,Photoelectrochemical, and Electrochemical Processes*., The Electrochemical Society, Pennington, N.J., 1994.

[8]. P.V. Kamat, *Chem.Rev.*, **93**, 267 (1993).

[9]. F.F. Ollis and H. Al-Ekabi, Eds., "*Photocatalytic and Purification and Treatment of Water and Air*", Elsevier Science, Amsterdam, 1993.

[10]. Ph.I. Vilesov Ed., *Uspekhi Photoniki.*, Iss.6., LGU (Leningrad State University), **1977**.

[11]. N. Serpone and A. Salinaro, *Pure & Appl.Chem.*, **71**, 303 (1999).

[12]. A. Salinaro, N. Serpone, A. Emeline, V. Ryabchuk, and H. Hidaka, *Pure & Appl. Chem.*, **71**, 321 (1999).

[13]. N. Serpone, A. Salinaro, A.V. Emeline, V.K. Ryabchuk, *J. Photochem. Photobiol. A: Chem.*, **130**, 83 (2000).

[14]. L.L. Basov, G.N. Kuzmin, I.M. Prudnikov, and Yu.P. Solonitsin, *Uspekhi Photoniki.*, Iss.6., Th.I. Vilesov, Ed., LGU (Leningrad State University), **1977**, pp. 82 - 120.

[15]. A.V. Emeline, G.N. Kuzmin, D. Purevdorj, V.K. Ryabchuk, and N. Serpone, *J.Phys. Chem.B*, **104**, 2989 (2000).

[16]. V.N. Kuznetsov and A.A. Lisachenko, *Sov. J. Phys. Chem.*, **65**. 1568 (1991).

[17]. A.V. Emeline, E.V. Lobyntseva, V.K. Ryabchuk, and N. Serpone, *J.Phys.Chem. B.*, **103**, 1325 (1999).

[18]. L. Sun and J.R. Bolton, *J.Phys.Chem.*, **99**, 4127 (1995).

[19]. N. Serpone, *J.Photochem.Photobiol. A:Chem.*, **104**, 1 (1997).

[20]. A.V. Emeline, A.V. Rudakova, V.K. Ryabchuk, and N. Serpone, *J. Phys. Chem.*, **102**, 10906 (1998).

[21]. A.V. Emeline, V.K. Ryabchuk, and N. Serpone, *J.Photochem.Photobiol. A:Chem.*, **133**, 89 (2000).

[22]. N. Serpone, G. Sauve, R. Koch, H. Tahiri, P. Pichat, P. Piccinini.E. Pelizzetti, and H. Hidaka , *J.Photochem.Photobiol.A:Chem.*, **94**, 191 (1996).

[23]. A.M. Braun, M.-T. Maurette, and E. Oliveros, "*Photochemical Technology*", translated by D.F. Ollis and N. Serpone, John Wiley & Sons; Chichester, England, Chapter 2, 1991.

[24]. Yu.P. Solonitsin, G.N. Kuzmin, F.L. Shurigin, and V.M. Yurkin, *Sov. J. Kinet. Catal.*, **17**, 1267 (1976).

[25]. V.S. Zakharenko and A.E. Cherkashin, *React. Kinet. Catal. Letters*, 131 (1983).

[26]. G.N. Kuzmin, D. Purevdorj, and I.G. Shenderovich, *Russian J. Kinet.Catal.*, *36*, 790 (1995).

[27]. A.V. Emeline, G.N. Kuzmin, D. Purevdorj,and I.G. Shenderovich, *Russian J. Kinet.Catal.*, **38**, 446 (1997).

[28]. A.V. Emeline, V.K. Ryabchuck, and N. Serpone, *J.Phys.Chem. B*, **103**, 1316 (1999).

[29]. G.N. Kuzmin, M.V. Knatko, and S.V. Kurganov, *React. Kinet. Catal. Letters*, **23**, 313 (1983).

[30]. V.K. Ryabchuk, L.L. Basov, and Yu.P. Solonitsin, *Sov. J.Chem.Phys.*, **8**, 1475 (1989).

[31]. In homogeneous photochemistry, it is well known that a unique quantum yield of a given photochemical process can only be defined under conditions where the rate of that process in independent of substrate concentration, i.e., for a zero-order process. Experimentally this is done for only a few percent conversion of the substrate (typically for less than 5 to 10%), conditions that also ensure that any intermediates formed do not affect the quantum yield measurement.

[32]. N. Daude, C. Gout, and C. Jouanin, *Phys.Rev. B*, **15**, 3229 (1977).

[33]. V.L. Bonch-Bruevich and S.G. Kalashnikov, *Physics of Semiconductors*, "Nauka". Moscow, Russia, 1990.

[34]. R.T. Ross and A.J. Nozik, *J. Appl. Phys.*, **53**, 3813 (1982).

[35]. D.S. Boudreaux, F. Williams, and A.J. Nozik, *J. Appl. Phys.*, **51**, 2158 (1980).

[36]. G. Cooper, J.A. Turner, B.A. Parkinson, and A.J. Nozik, *J. Appl. Phys.*, **54**, 2158 (1983).

[37]. C.A. Koval and P.R. Segar, *J. Am. Chem. Soc.*, **111**, 2004 (1989).

[38]. C.A. Koval and R. Torres, *J. Am. Chem. Soc.*, **115**, 8368 (1993).

[39]. H. Hidaka, S. Horikoshi, N. Serpone,and J. Knowland, *J.Photochem.Photobiol. A: Chem.*, **111**, 205 (1997).

[40]. J.M. Warman, M.P. de Haas, P. Pichat, and N. Serpone, *J.Phys.Chem.*, **95**, 8858 (1991).

[41]. B. Enright and D. Fitzmaurice, *J.Phys.Chem.*, **100**, 1027 (1996).

[42]. N. Serpone, D. Lawless, R. Khairutdinov, and E. Pelizzetti, *J.Phys.Chem.*, **99**, 16655 (1995).

[43]. D.P.Jr. Colombo and R.M. Bowman, *J.Phys.Chem.*, **100**, 18445 (1996), and references therein.

[44]. K.M. Glassford and J.R. Chelikowsky, *Phys.Rev. B*, **45**, 3874 (1992).

[45]. N. Serpone, D. Lawless, and R. Khairutdinov, *J.Phys.Chem.*, **99**, 16646 (1995).

[46]. F. Arntz and Y. Yacoby, *Phys.Rev.Lett.*, *17*, 857 (1966).

[47]. A. Frova, P.J. Body, and Y.S. Chen, *Phys.Rev.*, **157**, 157 (1967).

[48]. R.V. Kasowski and R.H. Tait, *Phys.Rev. B*, **20**, 5168 (1979).

[49]. M. Ye, Ph.D. Thesis, University of Notre Dame, Notre Dame, IN, 1989.

[50]. R.W. Mattews and D.F. Sangster, *J.Phys.Chem.*, **69**, 1938 (1965).

[51]. U. Stafford, K.A. Gray, and P.V. Kamat, *J.Phys.Chem.*, **98**, 6343 (1994).

[52]. R.F. Khairutdinov, L.Ya. Burshtein, and N. Serpone, *J.Photochem.Photobiol.A: Chem.*, **98**, 1 (1996).

[53]. R.F. Khairutdinov and N. Serpone, *Progr.React.Kinet.*, **21**, 1 (1996).

[54]. K.J. Laidler, "*Chemical Kinetics*", 3rd. Edn., Harper & Row Publishers, New York, pp. 278-281, 1987.

CHAPTER 6

UVA AND UVB PHYSICAL AND CHEMICAL FILTERS IN SUNSCREEN LOTIONS

GENERAL INTRODUCTION

"We must be careful not to confuse the consumer about what a sunscreen can and cannot do until these latter effects* (other than sunburns) *are understood. Perhaps we should be referring to the SunBurn protection Factor (SBS) and not the Sun Protection Factor (SPF)."

F.P. Gasparro, in "*Sunscreen Photobiology. Molecular, Cellular and Physiological Aspects*", F.P. Gasparro, Ed., Springer-Verlag, New York, 1997, Chapter 10, p. 177.

Summary

Sunscreen lotions are widely used to prevent some immediate effects of overexposure of skin to sunlight and presumably to prevent skin cancers, though the latter remains controversial. Despite massive education efforts and the availability of various sunscreen lotions, the incident of skin cancers continues to rise worldwide. UVB (290 to 320 nm) sunlight causes sunburn (erythema) and leads to skin damage. Topical sunscreens are meant to provide a protective layer of exogeneous UV chromophores on the skin to

block UV radiation before it penetrates the epidermis and affects DNA, so that photochemistry and subsequent photobiology are reduced. Sunscreens that penetrate the epidermis and the cells, if irradiated, yield photoadducts and/or generate reactive oxyradicals that can cause DNA lesions, the effects of which are felt several years later as prematurely aged skin and as skin cancer. UVA sunlight (320 to 400 nm) also contributes to actinic premature skin ageing and skin cancer. Sunscreens that predominantly block UVB radiation may therefore accentuate skin damage. Consequently, manufacturers have turned to inorganic (e.g. TiO_2, titania) rather than organic compounds as suitable and effective *physical* sunscreens. Titania is an UV protecting agent opaque to both UVA and UVB radiation. Although used to mineralize many undesirable organic pollutants, the active sunscreen agent, TiO_2, has been considered to be a safe *physical* sunscreen agent because presumably it reflects and scatters both UVB and UVA sunlight. However, TiO_2 also absorbs substantial UV radiation which, in aqueous media, yields hydroxyl radical (•OH) species, which can cause substantial damage to DNA {*J. Photochem. Photobiol. A:Chem.*, **111**, 205 (1997)}.

1. INTRODUCTION

1.1 Solar Radiation

Solar radiation reaching the Earth's surface consists mostly of ultraviolet, visible and infrared radiation (see Figure 1). Ultraviolet radiation is conventionally divided into three main wavelength regions: UVC(100-290 nm), UVB (290-320 nm), and UVA (320-400 nm) radiation. UV-C is not a component of sunlight reaching the Earth's surface, since the ozone layer absorbs all UV wavelengths below 290 nm. Approximately 70 to 90 % of the

UVB component of sunlight is also absorbed by ozone. The total solar radiation reaching the Earth's surface consists of ca. 15% of UV radiation , 60% of visible light and the remaining 25% is infrared radiation. Even though UV radiation is the smallest fraction of terrestrial solar radiation, it is nonetheless the most energetic and can induce some biological damage to living systems. The overall wavelength distribution of sunlight at the Earth's surface and

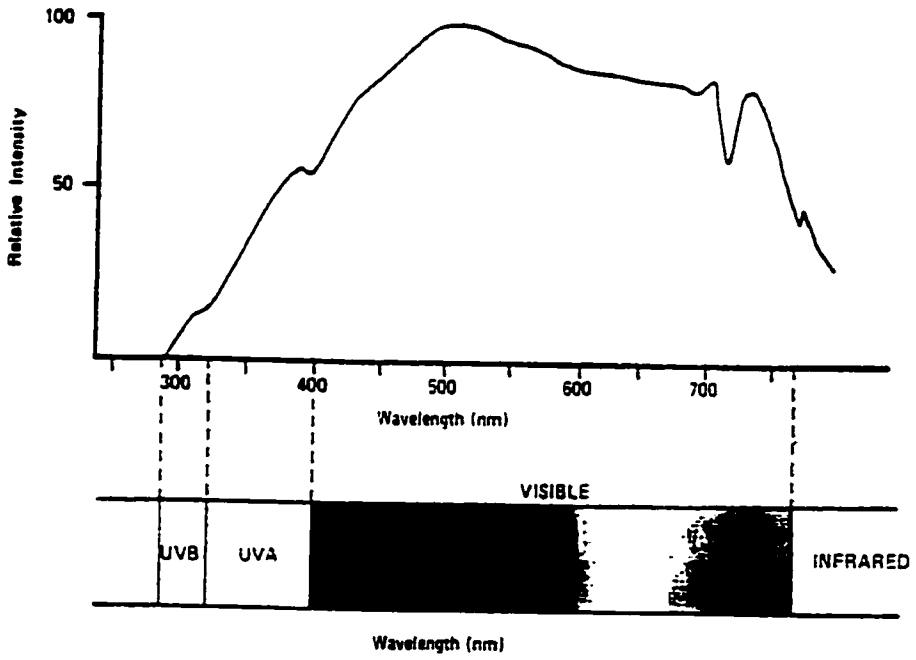

Figure 1. - Sunlight spectrum reaching the Earth's surface. From W. Frain-Bell, *Cutaneous Photobiology*, Oxford University Press, 1985.

the relative intensities of UVA and UVB present are illustrated in Figure 1. The visible range begins at 400 nm and ends at ca. 760 nm, beyond which exists the near-infrared radiation (wavelengths greater than 760 nm).

Figure 2 depicts the extent to which various wavelengths of sunlight penetrate the

skin. Not shown is the near-infrared radiation which is completely transmitted through the various layers of the skin (recall shining a flashlight through your hand as a child). The relevance of Figure 2 is that the longer wavelengths penetrate deeper into the subcutis. The UVA and UVB wavelengths tend to penetrate less into the skin so that much of the Sun's UVA damage occurs in the dermis and epidermis and UVB damage in the epidermis layers.

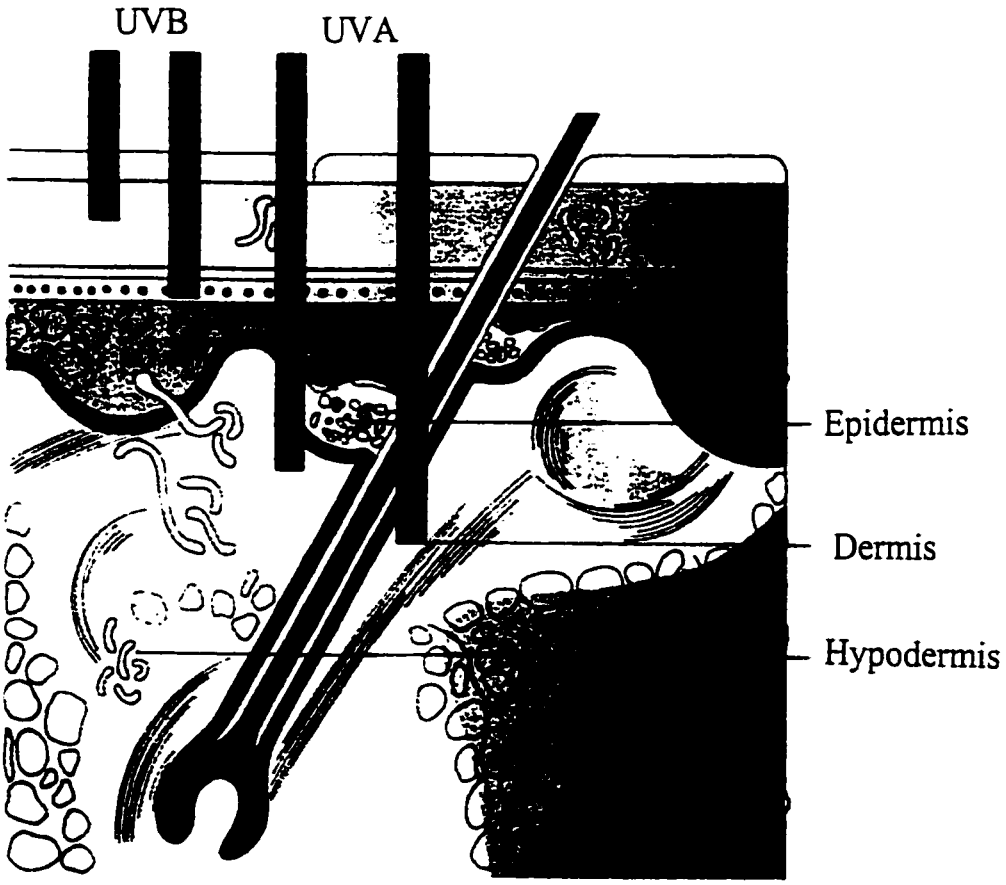

Figure 2. - Cartoon illustrating the penetration depth of various wavelengths. From R. Selleri, C. Botre and G. Orzalesi, *Chimica e Tecnologia dei Prodotti Cosmetici*, Proserpio, 1988.

As noted above, UVB (290 to 320 nm) radiation is the principal component of

sunlight that causes *erythema* of the skin. It can cause structural and cellular skin damage (e.g. elastosis, actinic keratosis, telangiectasis and skin cancers) [1]. Various sunscreen lotions have been formulated and commercialized to protect human skin from such damage. Topical sunscreens are intended to provide a protective layer of exogeneous UV chromophores on the skin surface to absorb or block UV radiation before it can penetrate the epidermis and affect endogenous UV chromophores such as DNA (deoxyribonucleic acid). In doing so, sunscreens should substantially reduce endogenous photochemistry and subsequent photobiology [2].

UVA sunlight contributes significantly to actinic premature skin ageing, dryness, and exfoliation, and to dermatological photosensitivity and skin cancer [3,4]. Repeated and chronic UV exposure leads to *photoaging* of the skin and initiation of skin cancers some of which are incurable (e.g., malignant melanoma). Photoaging is typically manifested as a leathery, thick and wrinkled appearance of the skin resulting from free radical oxidation of cell membrane lipids caused by the photogenerated reactive oxygen species (ROS).

Not surprisingly consumers seek protection from the harmful effects of UVA/UVB radiation by applying a thin film of sunscreen lotion, an emulsion (oil-in water or water-in-oil) invariably composed of *physical* filters (e.g. TiO_2 and ZnO) in combination with (organic) *chemical* filters (see below).

To the extent that sunlight affects human skin when the latter is exposed to it, it is instructive to describe briefly some of the properties of human skin.

1.2 Properties of Human Skin

Human skin consists of various types of cells that form the layer in the epidermis (Figure 3). The upper portion (i.e. the stratum corneum) is composed of dead stratified keratinising squamous cells. The basal layer between the dermis and the stratum corneum is made up of actively proliferating cells; it contains melanocytes which produce melanin. These are transferred in melanosomes to overlying keratinocytes. Cells produced in the proliferating basal layer move to the surface of the epidermis where they become flattened to form, ultimately, the dense protective keratin matrix of the stratum corneum. The dermis

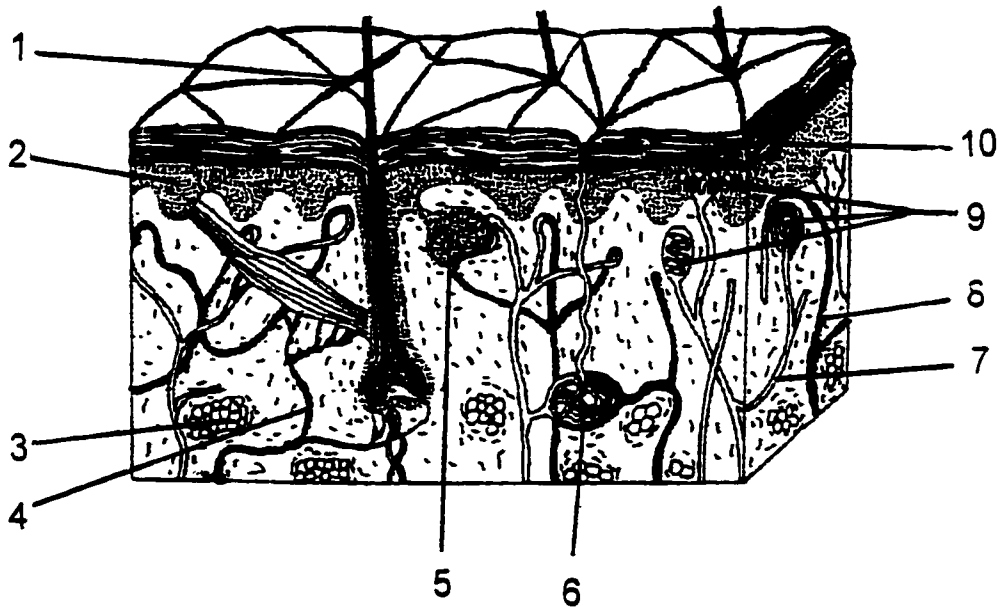

Figure 3. - Diagram of the layers and cell types present in normal skin. The melanocytes give rise to malignant melanomas. Basal and squamous cells are located in the fibroblast region of the dermis. They produce basal cell carcinomas (BCC) and squamous cell carcinomas (SCC), respectively. (1) hair, (2) germinative layer, (3) fat layer, (4) nerve, (5) sebacea gland, (6) sweat gland, (7) nerve, (8) blood vessel, (9) sensitive receptors, (10) corneum layer. From R. Selleri, C. Botre and G. Orzalesi, *Chimica e Tecnologia dei Prodotti Cosmetici*, Proserpio, 1988.

consists of irregularly arranged fibrous tissues containing a network of collagen and elastic fibers, together with an extensive capillary blood supply.

Skin has been classified into six categories depending on its appearance and properties [5].

- **Skin type I** is very fair, freckles easily, burns readily, never tans and most often belongs to people with red hair and blue eyes.
- **Skin type II** is also quite fair, burns readily but may tan slightly.
- **Skin type III** is more resistant to sunburns and often tans relatively soon after exposure to sunlight.
- **Skin type IV** is light brown all year round and is associated with people with dark hair (e.g. people of Mediterranean origin) who burn minimally and always tan.
- **Skin type V** is minimally sensitive, rarely sunburns, always tans profusely and appears brown.
- **Skin type VI** never sunburns and faces a very low risk of skin cancer; it belongs to highly pigmented dark brown people.

1.3 Effects of Skin Exposure to UV Radiation

Under "The Sun Wise School Program", the US Environmental Protection Agency has identified some health effects from overexposure to the Sun [6]:

- Skin cancers (melanoma, basal-cell carcinoma, and squamous-cell carcinoma).
- Premature aging of the skin and other skin problems (e.g., actinic keratoses).

- Cataracts and other eye damage (e.g., pterygium, skin cancer around the eyes and degeneration of the macula).
- Suppression of the immune system and the skin's natural defenses (e.g., impaired response to immunizations; increased sensitivity to sunlight; and reactions to certain medications), and this regardless of skin color

Ultraviolet wavelengths penetrate the skin with UVA more deeply than UVB (Figure 2). UV radiation is absorbed by different molecular species, e.g. proteins, DNA and lipids, at various wavelength-dependent depths. This is very important since specific tumor types are associated with different cell types. Such tumors may be initiated or promoted by different wavelengths in the sunlight [7].

The overall photochemical interactions resulting from light absorption, together with secondary interactions (e.g. generation of reactive species) are responsible for UV-induced damage displayed in a wide variety of harmful clinical effects [8]. Although effects of sunlight may be detrimental, exposure to sunlight is also beneficial for at least one reason: it is essential for vitamin D production, albeit only a relatively small amount of sunlight is required to keep healthy levels of this vitamin [9].

1.3.1 Sunburns

An immediate response promoted by skin exposure to UV radiation is the visible effect of sunburn (i.e. *erythema*) or reddening due to vasodilation, as well as edema (i.e. swelling) and cytolysis. Sunburned cells show defective and premature keratinisation with

lymphocyte nuclei present in basal and suprabasal locations as early as one hour after exposure [10]. Sunlight impinging on the skin is typically quantified in terms of the amount required to produce *erythema*. One minimal erythemal dose (i.e. MED) is the dose of light required to produce a slightly perceptible reddening of the skin. The effect varies depending on the skin type. For example, the MED for **type I skin** ranges between 150 and 300 J/m^2 of effective UVR (= UVA + UVB radiation), whereas the MED for **type VI skin** typically lies between 1000 and 2000 $J\ m^{-2}$ of effective UVR [11]. The yield of pyrimidine dimers [10] correlates with the susceptibility of skin to sun-induced *erythema*. Wavelengths that are most efficient at producing *erythema* are also the most efficient at producing pyrimidine dimers. The threshold of UV damage needed to develop *erythema* is then used as a marker of UV damage. *Erythema* is currently used as an indicator to measure sunscreen safety and efficacy, and to estimate the so-called Sun Protection Factor (SPF) numbers. Sunburn and *erythema* are independent risk factors for both melanoma and non-melanoma skin cancers.

1.3.2 Tanning

Tanning is caused by melanogenesis, i.e. to an increase of melanocytes in the skin. Their activity starts about 3 days after exposure to UVR. To absorb the radiation and protect the skin, the number and activity of melanocytes increase to release cytokines, and endothelins (or growth factors). These signals communicate to cells in non-exposed skin which shows the same response but to a lesser extent. Melanogenesis for **skin types III-VI** can be initiated by sub-erythemal doses of sunlight.

1.3.3 Photoaging

Repeated and chronic UV exposure leads to *photoaging* of the skin and initiation of skin cancers. The light-induced formation of reactive oxygen species (ROS) causes free radical oxidation of cell membrane lipids. The resulting lipid peroxides decompose to form lower aldehydes, which in turn cause crosslinking of normal proteins (mainly) to elastin and collagen proteins. Photoaging results in a leathery, wrinkled appearance of the skin often seen in people over 60 years of age. In extreme cases, however, it can also be seen in people as young as 20 years old. The exposed skin damage includes degeneration of collagen and accumulation of elastotic material into the upper and middle parts of the dermis resulting in skin thickening, especially in the highly exposed area of the skin. Skin blood vessels may look clinically abnormal and prominent; as well, there is an increase in the activity of fibroblasts, inflammatory cells and mast cells, in contrast to normally aged skin [12].

1.3.4 Immunomodulation

Immunomodulation is another effect of UV radiation on the skin. It is a reduction in immune responses to antigens following UV exposure [13].

1.3.5 Skin Cancer

There are three main types of *skin cancer*: (a) non-melanoma skin cancers (NMSC) that fall into two categories, namely basal cell carcinoma (BCC) and squamous cell carcinoma (SCC); and (b) malignant melanoma. In humans, BCCs appear most often on the face and

neck, change gradually over a period of months or even years, and cause substantial local damage. SCCs also appear in sun-exposed areas of the face and scalp as persistent red crusted lesions. SCCs metastasise more often than BCCs. Malignant melanomas, initiated in melanosomes, often occur in areas rarely exposed to the sun, e.g. on the trunk in men and lower leg in women.

Early studies on UV radiation provide evidence that cumulative UV exposure, especially in the UVB region, is responsible for inducing formation of SCCs. Studies employing UVA sources indicate that exposure to UVA is not safe and is sufficient to induce SCCs [14].

The world-wide incidence of NMSCs [15] and malignant melanomas [16] has increased significantly in recent years [17]. This has been attributed to alterations in population behavior, e.g. an increasing exposure to sunlight related to an increased desire for a tan. Additional evidence suggests that NMSCs, particularly SCCs, are related to cumulative regular sun exposure [18]. Risk of melanoma clearly increases with sun exposure, but the risk is also dependent on exposure pattern. This supports the idea that intermittent exposure may be more risky than regular exposure [19], although hereditary factors also play a role. In addition, exposure to sunlight during childhood and adolescence represents critical periods for melanoma initiation [20]. It must also be remembered that sunlight is not only an initiator of cancer, but is also a promoter [20a].

Two decades ago, high SPF sunscreens were widely recommended for the prevention of skin cancer, including melanoma [21]. However, a more recent report suggested that use

of sunscreens may in fact be associated with an increased risk of melanoma [22]. This was ascribed either to a smaller amount of sunscreen applied than the recommended 2 mg cm^{-2} to determine the SPF numbers, or to an increase in sunlight exposure when using a sunscreen because of the consumer's belief of long term protection. Only a detailed investigation of the effects of sunlight exposure in the presence and absence of sunscreens at the molecular level will shed light on this problem.

1.4 Absorption of Solar UV Radiation and DNA damage

DNA is the most important target of UV-induced skin damage through direct or indirect absorption of UV radiation [23]. Figure 4 shows that DNA bases (see Figure 5) absorb light directly in the UVB region and strongly in the UVC region (maximum absorption at 260 nm) yielding various oxygen-independent reactions and photoproducts. UV radiation can also be absorbed by the DNA bases through energy transfer from sensitizers yielding oxygen-dependent reactions and formation of reactive oxygen species. Pyrimidine bases appear to be more sensitive to UV damage than purine bases [24, 25].

Direct absorption of UV radiation causes pyrimidine bases to produce cyclobutanedimers and pyrimidine (6-4) pyrimidone photoproduct from adjacent pyrimidines. They are the major forms of direct UV-induced DNA damage that leads to mutations if DNA is improperly repaired. Longer wavelengths in the UVB region cause 6-4 photoproducts to isomerise to the Dewar isomer [24,25] (an important lesion to be considered in solar mutagenesis) to produce a different range of mutations from 6-4 photoproducts. Purine bases

produce a minor amount of photoproducts and less significant UV-induced damage than pyrimidine bases.

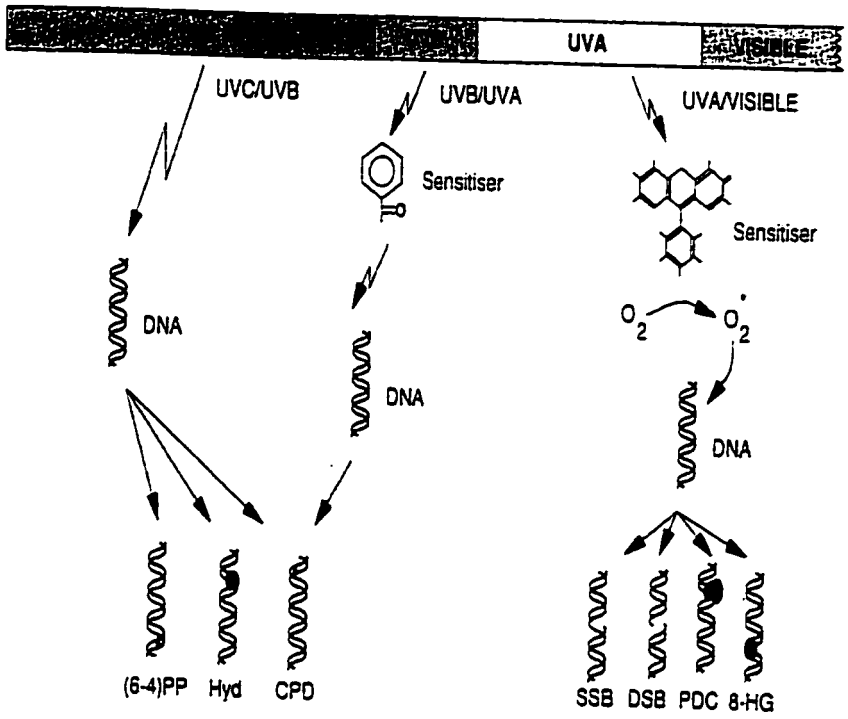

Figure 4. - Summary of principal pathways of UVR-induced DNA damage. Only those pathways producing the most common photoproducts at each wavelength range are shown: (6-4)PP, pyrimidone photoproduct; Hyd, pyrimidine hydrates; CPD, cyclobutane pyrimidine dimers; SSB, single strand breaks; DSB, double strand breaks; PDC, protein-DNA crosslinks; 8-HG, 8-hydroxyguanine. From ref. [23].

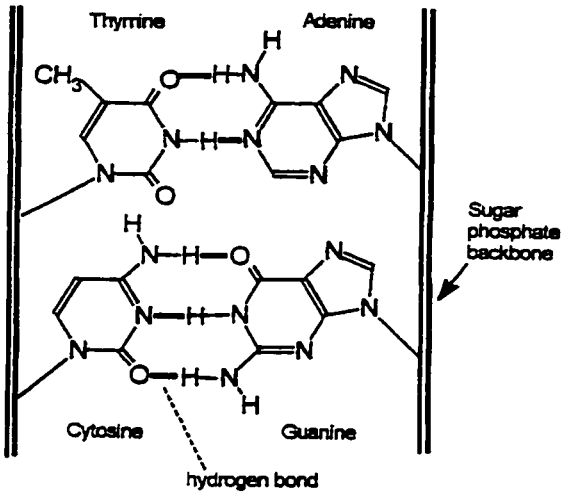

Figure 5 - Simplified DNA structure illustrating the pyrimidine and purine bases and the sugar phosphate backbone.

2. SUNSCREEN ACTIVE INGREDIENTS

Sunscreens have been typically classified as (a) organic *chemical* sunscreen filters which absorb UV radiation and (b) *physical* sunscreen filters whose principal feature is to block the UV light through reflection and scattering (however see below and ref. [26]). They must have three important properties if they are to prevent sunburns and protect people from more serious skin damage (see above):

(1) They must block UVB and UVA radiation effectively from reaching DNA in cell nuclei.

(2) They must be photostable (ideally 100%) and must dissipate the absorbed energy efficiently through photophysical and photochemical pathways that preclude formation of singlet oxygen, other ROS species and/or other deleterious intermediates.

(3) Sunscreens must not be transported into the cells

When excited, the active suncream ingredients likely undergo photochemical changes and energy and/or electron transfer. Such processes as photofragmentation and photo-isomerization are typical. Photoisomerization may yield isomers that are less light absorbing than the parent species, and thus less useful as sunscreen agents. As well, reactive intermediates or photoproducts produced could potentially be toxic to DNA [27].

Lists of sunscreen filters approved in various countries may be found elsewhere [28]. Chemical filters can be classified into seven groups and subdivided into either UVA (benzophenone, anthranilates and dibenzoylmethanes) or UVB (PABA derivatives, salicylates, cinnamates and camphor derivatives) filters depending upon which type of radiation they absorb (Figure 6).

A wide variety of organic chemicals are permitted in sunscreens, at least in Europe and elsewhere where they are considered cosmetic products, but not in North America. Table1 lists those active sunscreen agents recognized as over-the-counter (OTC) drugs and approved by the U.S. Food and Drug Administration for use in sunscreen lotions. They all work by absorbing UVB and UVA sunlight energy. This of course raises the question of what happens to that UV energy. In the case of Padimate-O, some of the UV radiation generates excited state species that can attack and damage DNA [29].

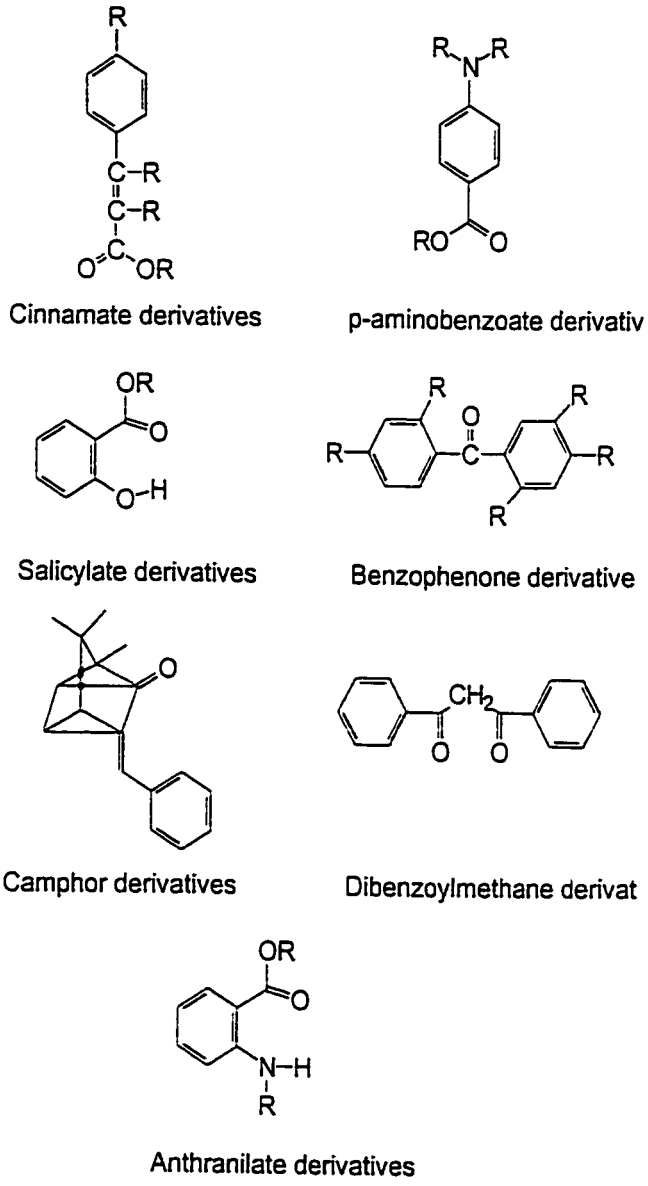

Figure 6. - The seven major groups of chemical sunscreen filters currently used in the suncare industry.

Table 1 - List of sunscreen active agents allowed under the U.S. Federal Register (May 21, 2000) [5].

PABA (≤15%)	Homosalate (≤ 15%)	Octyl Salicylate (≤ 5%)	Sulisobenzone (≤ 10%)
Avobenzone (≤ 3%)	Menthyl Anthranilate (≤ 5%)	Oxybenzone (≤ 6%)	**Titanium Dioxide** (≤ 25%)
Cinoxate (≤ 3%)	Octocrylene (≤ 10%)	**Padimate-O** (≤ 8%)	Trolamine Salicylate (≤ 12%)
Dioxybenzone (≤ 3%)	Octyl Methoxycinna-mate (OMC; ≤ 7.5%)	Phenylbenzimidazole Sulfonic acid (≤ 4%)	Zinc Oxide (≤ 25%)

Commercial formulations typically employ a combination of *physical* filters (e.g. TiO_2 and ZnO) for protection over the UVA and UVB regions with *chemical* filters [30-32]. Table 2 summarizes some of the active ingredients in three well known commercial sunscreen lotions (purposely not identified). Currently, a widely used organic sunscreen active agent seems to be octylmethoxycinnamate (OMC) [2]. Presumably the metal oxides TiO_2 and ZnO, which are both inert and nontoxic in the dark, attenuate light in these regions [26]. As we discuss in some detail in Chapter 7, ultrafine TiO_2 irradiated with (simulated) sunlight is harmful to supercoiled plasmid DNA [33]. Specifically, irradiated TiO_2 causes single- and double-strand breaks in DNA, and photoexcited TiO_2 specimens extracted from commercial sunscreens show similar DNA damage and similar strand breaks in nuclei of whole human skin cells. TiO_2 is genotoxic to human skin.

Table 2. - Typical active ingredients in three commercially popular sunscreen lotions.

Sunscreen 1	Sunscreen 2	Sunscreen 3
4-Methylbenzylidine camphor; 6% Parsol 1789; 1% Meroxyl SX; 1%	4-Methylbenzylidine camphor; 6% Parsol 1789; 2% Meroxyl SX; 2%	Ethylhexyl-p-methoxy-cinnamate; 7.5% Oxybenzone; 5% 2-Phenylbenzimidazole-5-sulfonic acid triethanolamine salt; 2.3%
Titanium dioxide; 3.2%	**Titanium dioxide; 5%**	**Titanium dioxide; 4.5%**
Pure melanin Vegetable extracts		

Parsol 1789 = butylmethoxydibenzoylmethane; Meroxyl SX = terephthalidine dicamphor sulfonic acid.

The marketing strategy used by manufacturers is worth a brief note. In 1996, the focus of this strategy popularized the *micronized* TiO_2 particles [34]:

> "*...protegge la pelle da scottature ed effetti dannosi provocati dal sole perche il suo sistema di protezione anti-UVA+UVB resistente all'acqua contiene Microriflettori*^{TM} *che agiscono come minuscoli specchi per proteggere la pelle dai raggi solari dannosi*".

> That is, *micronized* titania "... protects the skin against sunburns and harmful effects induced by the sun because its water-resistant anti-UVA+UVB protective system contains Microreflectors^{TM} which act as small reflectors to protect the skin from the sun's harmful rays".

A year later, publicity of sunscreen lotions was based on their containing Meroxyl as one of

the active sunblocks, whereas in 1998 marketing focused on the photostability of suncreams. In the year 2000, the marketing emphasis focused on Parsol-1789 as the active sunblock [34].

2.1 Spectroscopy of Sunscreens

Preliminary studies on several active ingredients show loss of absorption in a solar light simulator. Five sunscreen lotions that were examined displayed significant absorption spectral changes during irradiation in a solar simulator. Figure 7 shows the spectral behavior of the sunscreen p-aminobenzoic acid (PABA) in aqueous air-equilibrated solution at pH 5.5 (pH of the skin) and at a concentration of 20 mg L^{-1}. Note the loss of absorption at 280 nm. Irradiation for 3 hrs leads to significant loss in absorption. It is clear from the example above that sunscreen agents are not photostable, which we take up later in more detail (see Chapter 10), and consequently will lead to a photochemistry that can produce products and intermediates that may be deleterious to DNA and other organic matter making up human skin. Consequently, a brief background is relevant to understand the potential consequences on DNA.

Figure 8 illustrates the temporal dependent spectra of PABA under various conditions. Figure 8A and 8B show the spectra of PABA in aqueous and in hexane media, respectively. In a non-polar solvent such as hexane, the onset of absorption of the long wavelength band is considerably shifted toward the blue (from 325 nm in water to ca. 305 nm in hexane) to an extent that it no longer absorbs significant UVB radiation. Consequently one must question the usefulness of such a *chemical* UV filter in suncreams commercialized for over two

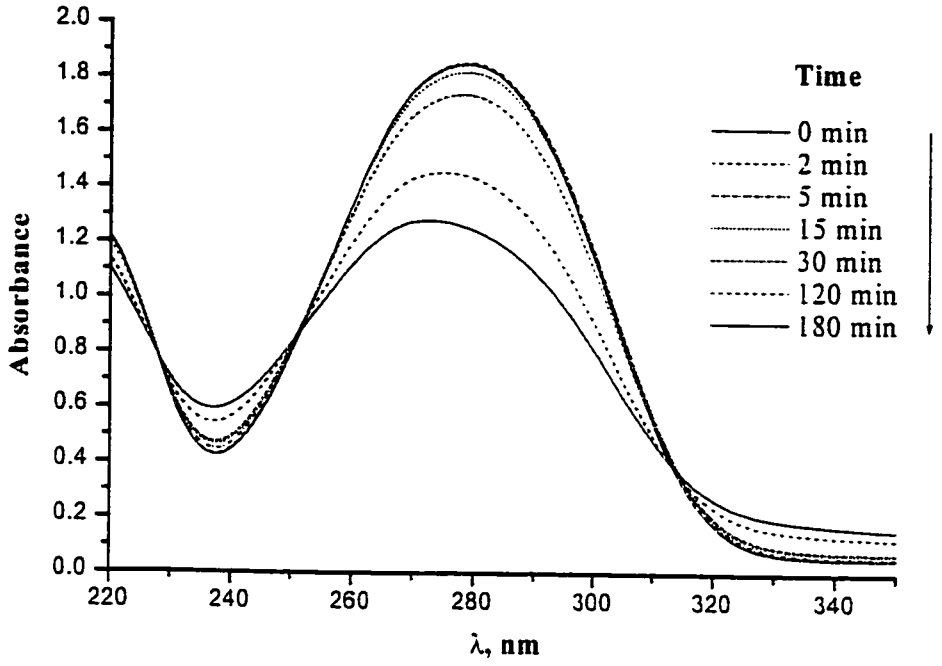

Figure 7. - Temporal changes in the absorption spectrum of PABA under irradiation in a solar light simulator.

decades. Figures 8C and 8D depict the effect of air oxygen when an aqueous PABA solution is illuminated with UVB radiation. Under aerobic conditions PABA degrades faster (Figure 8D) than in the absence of molecular oxygen (Figure 8C). This calls attention to the possibility of a reaction between the appropriate excited state(s) of PABA and molecular oxygen to yield, for example such species as singlet oxygen (see below). As well, on conversion of PABA to other substances the absorption band blue-shifts thereby decreasing considerably the extent of absorption of UVB. Nonetheless, whatever intermediate or photo-product is formed some UVA radiation is absorbed by the photoproducts.

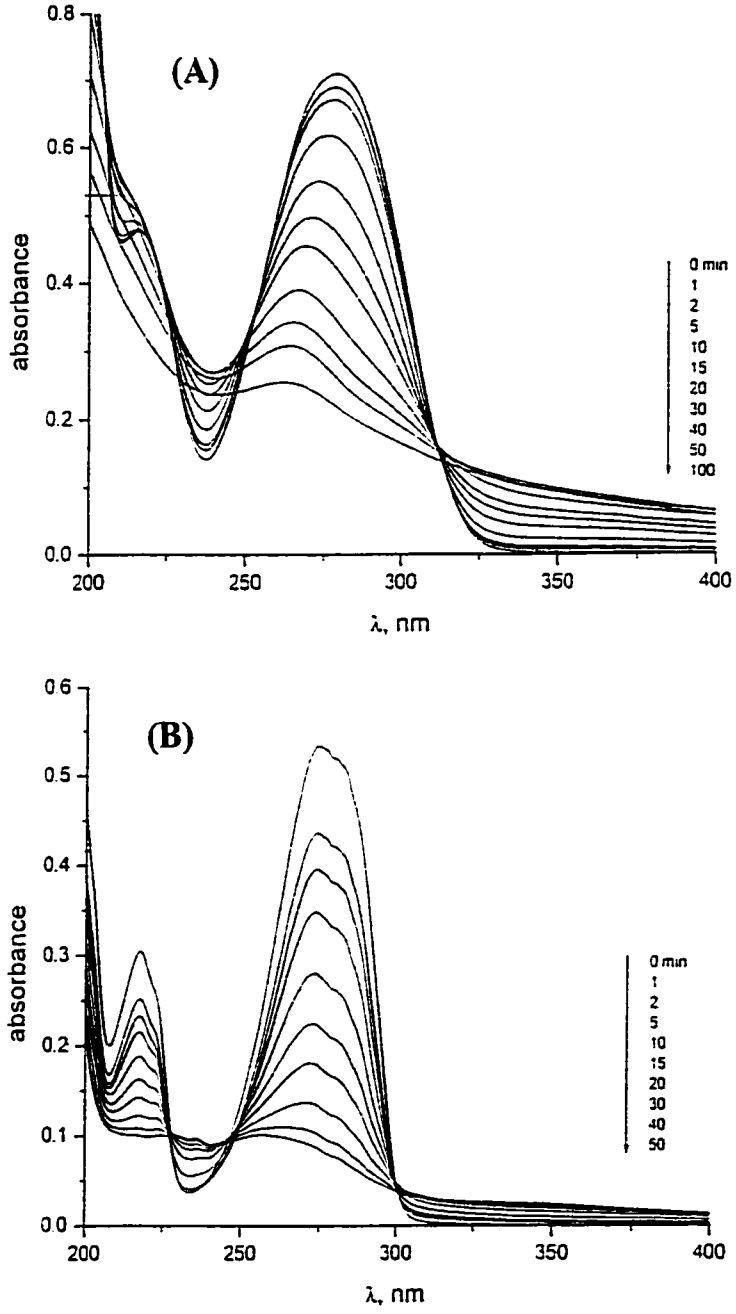

Figure 8AB. - Time-dependent spectra of PABA (8 mg L^{-1}) as absorbance *versus* wavelength under various conditions: (A) PABA in aqueous, air-equilibrated media; (B) PABA in air-equilibrated hexane solutions.

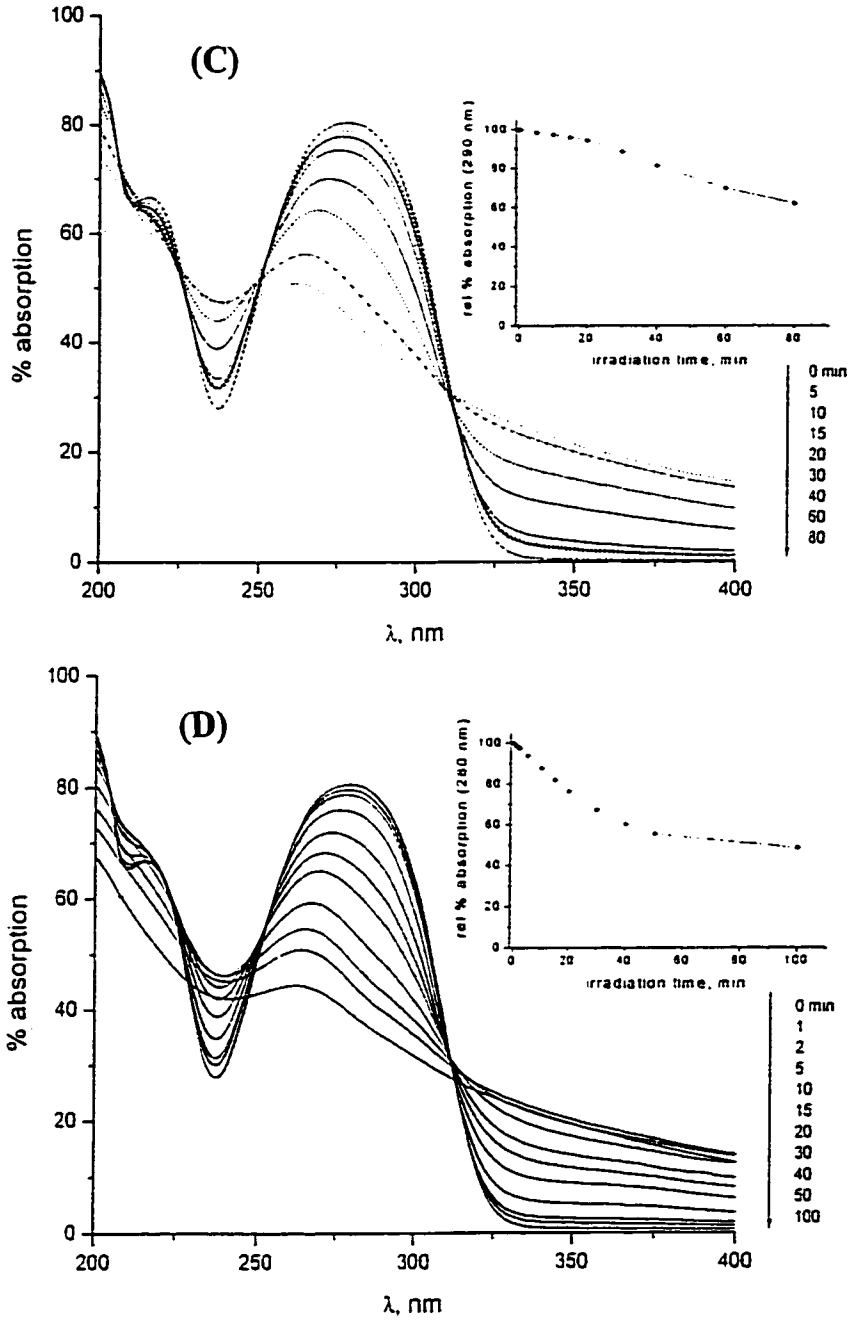

Figure 8CD. - Time-dependent spectra of PABA (8 mg L^{-1}) as percent absorption *versus* wavelength under various conditions: (C) PABA in aqueous *anaerobic* media; (D) PABA in aqueous *aerobic* media.

2.2 *Organic Sunscreen Active Agents*

Until recently, most commercial sunscreens depended entirely on organic UV-absorbing chemicals. One of the first commercially and widely used was *p*-aminobenzoic acid (PABA) which absorbs UV-B. Although not an ideal sunscreen, because of its crystalline

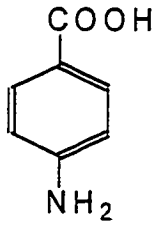

PABA = para-aminobenzoic acid

nature and thus not easily incorporated into lotions, and also because it is soluble in water, PABA was thought to be quite effective at preventing sunburns. Potentially harmful side-effects of PABA were also known. In the late 1970's, Hodges et al [35] showed that when bacteria were illuminated at 313 nm they were killed much more rapidly when PABA was present in the medium. Illumination at longer wavelengths reduced the effect. They attributed their results to increased formation of thymine dimers. When DNA absorbs UV-B radiation, thymine dimers form by reaction between two adjacent thymine residues on the same DNA strand. Unless repaired, thymine dimers lead to mutation when the cell divides. The work of Hodges and coworkers was later extended to human skin cells. Illumination in the presence of PABA produces thymine dimers and the cells exhibit abnormal growth characteristics [36,37].

Among the PABA derivatives that were later introduced into sunscreens was the

related ester 2-ethylhexyl-4-dimethylaminobenzoate (patented in 1968), known under various aliases as octyldimethyl-PABA, OD-PABA, O-PABA; Escalol 507, and Padimate-O (Figure 9). It was an attractive sunscreen component because it is virtually insoluble in water and is a colorless oily liquid easily incorporated into sunscreen lotions; it clings well to the skin. Figure 9 summarizes some of the structures of popular chemical active agents in sunscreens [29]. Note the structural similarities between Padimate-O, Padimate-A and PABA, between benzophenone and Michler's ketone (a known carcinogen), and between Parsol 1789 and dibenzoylmethane (also a well known toxic product).

Chemically, Padimate-O is identical to the corresponding ethyl ester (ethyl-4-dimethylamino-benzoate), an industrial photo-initiator of polymerisation reactions. This ethyl ester generates carbon-centered radicals under illumination [38]. It is likely that Padimate-O behaves in a very similar fashion. In the presence of air and water, carbon-centered radicals generate peroxy radicals (•OOH) and hydroxyl radicals (•OH), both of which are very reactive and therefore expected to attack a wide variety of biologically important molecules, including DNA. It is not surprising that Padimate-O damages DNA as evidenced from studies of model systems. It kills dividing yeast cells, especially if they are incapable of repairing certain lesions; it also induces mutations [29]. Though the precise nature of the attacking species of Padimate-O remains elusive, it breaks single DNA strands and inflicts other damage as well, notably at GC (guanine-cytosine; see Figure 5) base pairs [39]. Unlike PABA, however, Padimate-O does not sensitise formation of thymine dimers. Potentially, this has a very important consequence. Sunscreens like Padimate-O that absorb

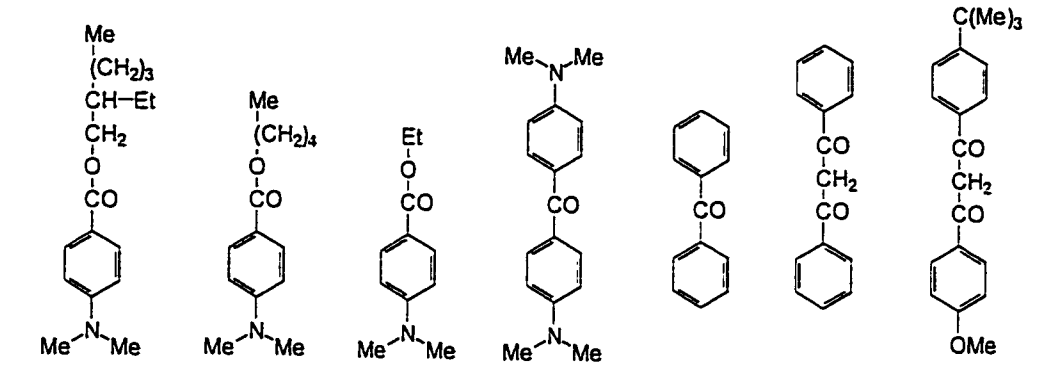

Commercial names			
Padimate-O	Padimate-A	Michler's ketone	Parsol 1789
Octyl Dimethyl PABA			Parsol A
O-PABA Escalol 507	Escalol 506		

Figure 9. - Chemical structures of some of the organic *chemical* sunscreen active agents and their commercial names. From ref. [29].

UV-B light may actually reduce formation of direct photoproducts such as thymine dimers, while simultaneously sensitising other forms of damage that thus far have escaped scrutiny.

Though Padimate-O has been a successful sunscreen component, the related Padimate-A has been rather less so. Reports of photo-allergy and other skin problems associated with the use of sunscreens containing Padimate-A have led to its withdrawal from the European market in 1989 [40]. Manufacturers gradually became wary of the effects of sunscreens that contain any compounds related to PABA. Not surprisingly, many sunscreens are typically marketed as PABA-free. Strictly speaking, however, PABA refers to *p-aminobenzoic acid*,

so that although a PABA-free sunscreen may not contain *p*-aminobenzoic acid, it might still contain either or both Padimate-O and Padimate-A. In some instances, the term PABA-free comprises the absence of all three compounds, so that in practice a PABA-free sunscreen may contain none of the three related systems. Nonetheless, the consumer would be wise to read the labels (i.e., the fine print).

Many of the sunscreen active ingredients, with PABA being the most efficient, are good triplet state sensitizers with the potential to convert harmless triplet oxygen, $^3O_2$, into singlet oxygen, $^1O_2$, a well-known cytotoxic species [41]. Some irradiated chemical sun-filters either increase the rate of formation of potentially carcinogenic DNA photoproducts (e.g. the cyclobutane-type pyrimidine dimers [42]) or undergo photochemical changes that result in a loss of UVB blocking ability [43].

There is of course no reason to believe that all organic *chemical* sunscreens behave in a like manner, but concern about their possible effects has to some extent fueled the search for inert alternatives. A UV protecting agent that is opaque to both UVA and UVB radiation, and that would be biologically inert, chemically inert, cosmetically acceptable, and compatible with conventional components of sunscreen formulations was therefore desirable. Manufacturers have increasingly turned to inorganic materials rather than to organic compounds [30-32]. The most popular and widely used inorganic material is *micronized* titanium dioxide, TiO_2, particles. In so doing, it is interesting to note that several commercial sunscreen lotions are marketed by the claim that they contain ***no chemical filters***.

2.3 *Inorganic Sunscreen Active Agents*

The maximal opacity of titanium dioxide particles to visible light occurs for sizes in the 180–220 nm (dia.) range. Light in this wavelength region is presumably attenuated mostly, but not completely, by reflection and scattering. Smaller particles transmit light. *Micronized* metal oxides are transparent to visible radiation and are the ones most currently used in cosmetic products. For these smaller particles, the mechanism of light attenuation is primarily due to Rayleigh scattering, with the intensity following the power law $I_{sc} \sim \lambda^{-4}$. Consequently, small particles scatter the UVB and UVA wavelengths more than the longer visible light wavelengths. However, TiO_2 also absorbs UVB and UVA light significantly [44], a point not fully appreciated by the authors of ref. [26]. For ZnO with particle size between 20 nm and 100 nm, UV radiation is scattered and absorbed by the particles. Recent work [45,46] (see also Chapter 3) has shown that the percent relative scattering (*versus* extent of absorption) at wavelengths below 400 nm decreases dramatically from about 80% at 390 nm to about 20% at 290 nm, i.e. in the wavelength region where UV sunlight is most damaging to human skin. Since sunscreen preparations are exposed to sunlight, the photocatalytic behavior of these *physical* UV blockers is indeed relevant.

The more common polymorphs of titanium dioxide are the two crystalline forms *anatase* and *rutile*. In the 400-700 nm region, titania particles only reflect and scatter light resulting in the expected $1/\lambda^4$ dependence, where λ is the wavelength, (see ref. [45] and Chapter 3), thereby making TiO_2 an excellent physical screen against certain photo-dermatoses (e.g. porphyria) that occur at the visible wavelengths [47]. However, titania nano-

and micro-crystallites absorb light significantly and, to a lesser extent, scatter UVA and UVB radiation [45], i.e. they absorb at wavelengths below 385 nm (absorption threshold: 3.20 eV; bandgap energy) for anatase and below ca. 405 nm (3.02 eV) for rutile. The anatase polymorph is a very photoactive UV semiconductor which has been used extensively as a photocatalyst to mineralize a variety of environmental organic pollutants [48,49]. The rutile TiO_2 polymorph is also a reasonably good photocatalyst under certain conditions [50].

Absorption of radiation of suitable energy (Figure 10) by TiO_2 nano- and micro-crystallites leads to a low-energy non-vertical, indirect electronic transition from the valence

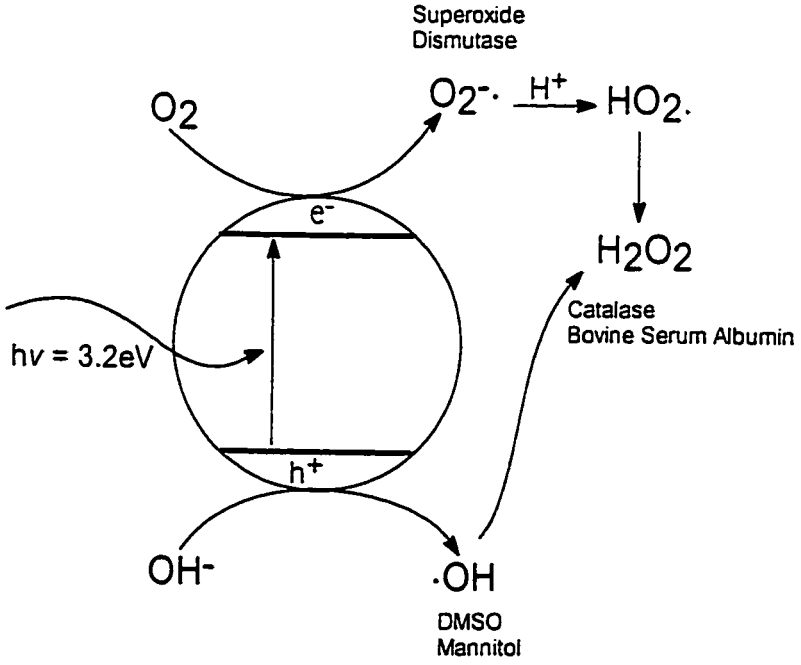

Figure 10. - Scheme illustrating the various events on illumination of a TiO_2 particle by UVB/UVA radiation together with formation of the superoxide radical anion, •OH radicals, and hydrogen peroxide. Also shown are the compounds that react with these reactive oxygen species.

band to the conduction band (indirect bandgap of anatase, 3.20 eV) and to direct, vertical transitions at higher energies (wavelengths < 385 nm) [51]. These transitions form bound excitons (bound electron-hole pairs, eqn 1b), which subsequent to their separation and migration (eqn 1b) towards the crystallite surface, while spanning various lattice and surface defects, ultimately yield surface-trapped electrons (e_{tr}^-) and holes (h_{tr}^+) in very short time (< 10^{-11} s [52]). These charge carriers are then poised to initiate photoreductions and photooxidations at the particle surface. The trapped holes (eqn 2) are identified with surface-bound •OH radicals which can combine to yield H_2O_2 (eqn 3) [53,54].

$$\{Ti^{IV}–O^{2-}–Ti^{IV} \equiv\}–OH + h\nu \rightarrow \{Ti^{III}–O^{-\bullet}–Ti^{IV} \equiv\}–{}^{\bullet}OH \quad (1a)$$

that is,

$$TiO_2 + h\nu \rightarrow (e^-/h^+) \rightarrow e_{cb}^- + h_{vb}^+ \quad (1b)$$

$$e_{cb}^- \rightarrow e_{tr}^- \{\text{as } Ti^{III}\} \quad (1c)$$

$$h_{vb}^+ \rightarrow h_{tr}^+ \{\text{as } {}^{\bullet}OH_{surf}\} \quad (1d)$$

$$\{Ti^{III}–O^{-\bullet}–Ti^{IV} \equiv\}–OH \rightarrow \{Ti^{III}–O^{2-}–Ti^{IV} \equiv\}–{}^{\bullet}OH \quad (2)$$

$$2\,\{Ti^{III}–O^{2-}–Ti^{IV} \equiv\}–{}^{\bullet}OH \rightarrow H_2O_2 \quad (3)$$

The •OH radical causes cellular damage *in vivo* [55] and although it does not diffuse from the surface of TiO_2 particles, its dimeric product H_2O_2 can diffuse to considerable distances and effect serious damage [56]. Some recent reports have even inferred formation of singlet oxygen when TiO_2 is UV-irradiated [57,58].

To test for the formation of •OH radicals produced on irradiation of TiO_2 extracted

from sunscreens and to verify their activity as initiators of harmful reactions inducing DNA damage, we examined the oxidation of organics by •OH radicals produced on illuminated TiO_2 (see ref. [33] and Chapter 7). Photodecomposition of a large variety of other organic compounds by irradiated TiO_2 has been reported extensively [59].

It is noteworthy that photoexcited titania particles are cytotoxic (*in vitro*) to HeLa cells and suppress their growth when implanted in nude mice; T-24 human cancer cells are destroyed *in vitro* and *in vivo* by illuminated titania [60]. Of greater import TiO_2 particles are located both on the surface of the cells and inside the cells [61]. This observation has important consequences.

Confirming the work of Fujishima and coworkers [60,61]. *in vitro* studies by McHugh and Knowland [39] using human cells in culture and simulated sunlight irradiated TiO_2 suggested that DNA is damaged. Also. Wamer [62] found that UVA excited TiO_2 is photocytotoxic to skin fibroplasts and is accompanied by photooxidative damage to cellular RNA (ribonucleic acid). Such damage to endogenous chromophores appears to occur by a process involving radical species.

To the extent that such reactive oxygen species as •OH and HOO• radicals, together with singlet oxygen and H_2O_2 are produced when TiO_2 particles are illuminated with UVA and/or UVB light and that TiO_2 particles have been seen in the interior and exterior of cell membrane walls [61], the question about the *safe* utilization of this inorganic material used as a UV sunblock in sunscreen lotions requires closer examination (see Chapter 7).

3. REFERENCES

[1]. M.W. Brown and E. Galley, *Cosmetics & Toiletries*, **105**, 69 (1990).

[2]. N.A. Shaath, "*Photochemistry and Photostability of Sunscreen Components, Mixtures, and Products*", Discussion of the Photochemistry and Photobiology of Sunscreens: Public Meeting and Reopening of the Administrative Record, U.S. Food and Drug Administration, Rockville, MD, September 19 & 20, (1996).

[3]. L.H. Kligman, *J.Invest.Dermatol.*, **84,** 274 (1985).

[4]. L.H. Kligman,., *Dermatol.Clin.*, **4**, 517 (1986).

[5]. See "Sunscreen Drug Products for Over-the-Counter Human Use; Final Monograph", U.S. Food & Drug Administration, Federal Register 64 27666, May 21, 2000, Final Rule. See website: http://vm.cfsan.fda.gov/~lrd/fr990521.html

[6]. "Sun Wise School Program: Health Effects of UV Radiation", U.S. Environmental Protection Agency, July 26, 2000. See website: http://www.epa.gov/sunwise/uvandhealth.html

[7]. F. P. Gasparro, M. Mitchnick, and J. F. Nash, *Photochem. and Photobiol.* **68**, 243 (1998).

[8]. M. F. Naylor and K. C. Farmer, *Arch Dermatol.*, **133**, 1146 (1997).

[9]. R. B. Sollitto, K. H. Kraemer. and J. J DiGiovanna.. *J. Am. Acad. Dermatol.* **37,** 942 (1997).

[10]. P. H. Andersen, K. Abrams, P. Bjerring, and H. Maibach, *Photodermatol Photoimmunol. Photomed.*, **8**, 123 (1991).

[11]. J. P Césarini, in *"Human Exposure to Ultraviolet radiation: Risks and regulations"*, W. F. Paschier and B. F. M. Bosnjaleovic, Eds., Elsevier, Amsterdam, 1987, pp. 33-44.

[12]. A. Oikarinen, *Photodermatol. Photoimmunol. Photomed.*, **7,** 3 (1990).

[13]. F. P. Noonan and E. C. De Fabo, in *"Environmental UV Photobiology"*, A. R. Young, L. O. Björn,, J. Moan, and W. Nultch, Eds., New York, Plenum Press, 1993, pp. 113-148.

[14]. H. J. C. M. Sterenborg, and J. C. van der Leun, *Photochem. Photobiol.*, **51**, 325 (1990).

[15]. D. S. Preston and R. S. Stern, *New. Engl. J. Med.*, **327**, 1649 (1992).

[16]. P. Boyle, P. Maisonneuve, and J. F. Dore, *Br. Med. Bull.*, **51**, 523 (1995).

[17]. (a) R. Marks, *Cancer*,, **75**, 607 (1995).

(b) A. Katsambas and E. Nicolaidou, *Arch.Dermatol.*, **132**, 444 (1996).

(c) D.L. Miller and M.A. Weinstock, *J. Am.Acad. Dermatol.*, **30**, 774 (1994).

[18]. C. D. Holman,, C. D. Mulroney, and B. K. Armstrong, *Int. J. Cancer*, **25**, 317 (1980).

[19]. M. Elwood and J. Jopson, *Int. J. Cancer*, **73**, 198 (1997).

[20]. P. Autier,, P. Boyle, and J. F. Dore, *The Lancet*, **352**, 738 (1998).

[20a]. M.L. Kripke and P. Wolf, *J. Natl. Cancer Inst.*, **86**, 798 (1996).

[21]. L. H. Kligman, F. J. Akin, and A. M. Kligman, *J. Am. Acad. Dermatol.*, **3**, 30 (1980).

[22]. C. F. Garland, F. C. Garland, and E. D. Gorham, *Am.J.Public Health*, **82**, 615 (1992).

[23]. N.A. Cridland and R.D. Saunders, *"Cellular and Molecular Effects of UVA and UVB"*, NAPB-R269, HMSO, London, 1994.

[24]. B. S. Rosenstein and D. L. Mitchell, *Photochem. Photobiol.*, **45**, 775 (1987).

[25]. E. C. Friedberg,, G. C. Walker, and W. Siede, *"DNA Repair and Mutagenesis"*, ASM Press. Washington, D. C., 1995.

[26]. U.S. Federal Register, Report 64 FR 27666, May 21, 2000. See ref. [5].

[27]. (a) B. Epe, *Chem. Biol. Interact.*, **80**, 239 (1991);

(b) J.M. Allen, C.J. Gossett, and S.K. Allen, *Chem.Res.Toxicol.*, **9**, 605 (1996).

[28]. (a) K. Klein "Encyclopedia of UV absorbers for sunscreen products". *Cosmetics and Toiletries*, **107**, 45 (1992).

(b) N.J. Lowe and N.A. Shaath *Cosmetic Sci. Technol. Series*, **10**, 65 (1995).

[29]. J. Knowland, E.A. McKenzie, P.J. McHugh, and N.A. Cridland, *FEBS Letters*, **324**, 309 (1993).

[30]. B. Catlow, *Seifen Oele Fette Wachse J.*, **119**, 497 (1993).

[31]. P. Alexander, *Manufacturing Chemist*, **62**, 21 (1991).

[32]. "Formulators Fine-Tune TiO_2-Based Screens", *Manufacturing Chemist*, **64**, 26 (1993).

[33]. R. Dunford, A. Salinaro, L. Cai, N. Serpone, S. Horikoshi, H. Hidaka, and J. Knowland, *FEBS Letts.*, **418**, 87 (1997).

[34]. N. Serpone, personal communication (1997).

[35]. N.D.M. Hodges, S.H. Moss, and D.J.G. Davies, *Photochem. Photobiol.* **26**, 493 (1977).

[36]. B.M. Sutherland, *Photochem. Photobiol.* **36**, 95 (1982).

[37]. J.C. Sutherland and K.P. Griffin, *Photochem. Photobiol.* **40**, 391 (1984).

[38]. M. Forster and R.E. Hester, *J. Chem. Soc. Faraday Trans. 2*, **77**, 1521 (1981).

[39]. P.J. McHugh and J. Knowland, *Photochem. Photobiol.* **66**, 276 (1997).

[40]. Official Journal of the European Communities. March 8, 1989, No L64, pp. 10-12.

[41]. J.M. Allen, C.J. Gossett, and S.K. Allen, "*Photochemical Formation of Singlet Molecular Oxygen ($^1O_2$) in Aqueous Solutions of Several Sunscreen Active Ingredients*", Discussion of the Photochemistry and Photobiology of Sunscreens: Public Meeting and Reopening of the Administrative Record, U.S. Food and Drug Administration, Rockville, MD, September 19 & 20, 1996.

[42]. S.Y. Wang, Ed., "*Photochemistry and Photobiology of Nucleic Acids*", vol.I. Academic Press, New York, 1976.

[43]. B.S. Martincigh,, "*DNA Photodamage Induced by Sunscreen Absorbers*". Discussion of the Photochemistry and Photobiology of Sunscreens: Public Meeting and Reopening of the Administrative Record, U.S. FDA. Rockville, MD, September 19 & 20, 1996.

[44]. N. Serpone, A. Salinaro, H. Hidaka, S. Horikoshi, J. Knowland, and R. Dunford, "Beneficial and Deleterious Effects of Solar Radiation", in *Solar Engineering 1998.*, J.M. Morehouse & R.E. Hogan, Eds., ASME, New York, 1998, pp. 287-298.

[45]. N. Serpone and A. Salinaro, *Pure Appl.Chem.*, **71**, 303 (1999).

[46]. A. Salinaro, A.V. Emeline, J. Zhao, H. Hidaka, V.K. Ryabchuk, and N. Serpone, *Pure Appl.Chem.*,, **71**, 321 (1999).

[47]. T.M. Macleod and W. Fran-Bell, *British J.Dermatol.*, **92**, 149 (1975).

[48]. D.W. Bahnemann, J. Cunningham, M.A. Fox, E. Pelizzetti, P. Pichat, and N. Serpone, in "*Aquatic and Surface Photochemistry*", D. Crosby, G, Helz, and R.G. Zepp, Eds., Lewis Publishers, Boca Raton, FL., 1994, pp. 261-316.

[49]. N. Serpone, , in "*The Kirk-Othmer Encyclopedia of Chemical Technology*", Wiley-Interscience, New York, vol.**18**, 1996, pp. 820-837.

[50]. A. Sclafani and J.-M. Herrmann,, *J.Phys.Chem.*, **100**, 13655 (1996).

[51]. N. Serpone, D. Lawless, and R.F. Khairutdinov, *J.Phys.Chem.*, **99**, 16646 (1995) .

[52]. N. Serpone, D. Lawless, E. Pelizzetti, and R.F. Khairutdinov, *J.Phys.Chem.*, **99**,16655 (1995) .

[53]. D. Lawless, N. Serpone, and D. Meisel, *J.Phys.Chem.*, **95**, 5166 (1991).

[54]. J.H. Arbour, J. Tromp, and M.L. Hair,, *Can.J.Chem.*, **63**, 204 (1985).

[55]. J. Russell, J. Ness, M. Chopra, J. McMurray, and W.E. Smith, *J. Pharmaceut. Biomed. Anal.*, **12**, 863 (1994).

[56]. H.M. Swartz, "*The Significance of Free Radicals in the Pathophysiology of the Skin*", Discussion of the Photochemistry and Photobiology of Sunscreens: Public Meeting and Reopening of the Administrative Record, U.S. FDA, Rockville, MD, September 19 & 20, 1996.

[57]. (a) W.C. Dunlap, Y. Yamamoto, M. Inoue, M. Kashiba-Iwatsuki, M. Yamaguchi, and K. Tomita, *Int.J.Cosmetic Sci.*, **20**, 1(1998).

(b) R. Konaka, E. Kasahara, W.C. Dunlap, Y. Yamamoto, K.C. Chien, and M. Inoue, *Free Radic.Biol.Med.*, **27**, 294 (1999).

[58]. Y. Yamamoto, N. Imai, R. Mashima, R. Konaka, M. Inoue, and W.C. Dunlap, *Methods Enymol.*, **319**, 29 (2000).

[59]. N. Serpone and E. Pelizzetti, "Solar Photochemical Remediation of Air and Water", in "*Photochemical and Photoelectrochemical Approaches to Solar Energy Conversion*", M.D. Archer and A.J. Nozik, Eds., Imperial College Press, London, 2001, vol. **III**, chapter 16.

[60]. R. Cai, Y. Kubota, T. Shuin, H. Sakai, K. Hashimoto, and A. Fujishima, *Cancer Res.*, **52**, 2346 (1992).

[61]. Y. Kubota, T. Shuin, C. Kawasaki, M. Hosaka, H. Kitamura, R.Cai, H.Sakai, K. Hashimoto, and A. Fujishima, *British J. Cancer*, **70**, 1107 (1994).

[62]. W. Wamer, "*Oxidative Damage to Nucleic Acids Photosensitized by Titanium Dioxide*", Discussion of the Photochemistry and Photobiology of Sunscreens: Public Meeting and Reopening of the Administrative Record, U.S. FDA, Rockville, MD. September 19 & 20, 1996.

Chapter 7

CATALYZED OXIDATION AND DNA DAMAGE *IN VITRO* AND IN HUMAN CELLS BY SUNLIGHT-ILLUMINATED INORGANIC SUNSCREEN AGENTS

"The cost of a bronzed body is growing steeper, as a sometimes-fatal skin cancer becomes alarmingly prevalent".

C.A. Sweet, *FDA Consumer*, June 1989.

Summary

In this Chapter we briefly examine the usage of such metal oxides as TiO_2 (and ZnO) in sunscreen lotions (suncreams) widely used as UVA/UVB blockers and intended to prevent sunburns and "protect" human skin from skin cancers (carcinomas and melanoma). As a physical sunscreen agent, titanium dioxide (TiO_2) was noted by an OTC Panel{U.S. Federal Register, 43FR38206, August 25,1978} to be a safe, opaque and effective product that provides a barrier to sun-sensitive individuals against sunburns, because it reflects and scatters UVA and UVB radiation (290-400 nm) rather than absorbing the rays. The more recent Federal Register 64FR27666 of May 21, 2000, changed little, if anything, in the earlier OTC Panel recommendation regarding the spectral characteristics of titania despite the vast body of literature to the contrary. In sunscreens TiO_2 is widely used as *micronised*

particles (microreflectors). However, not only does TiO_2 absorb a significant quantity (ca. 70%) of the incident UV radiation but also leads to the generation of hydroxyl radicals in aqueous environments and humid air. Using chemical methods, we show that all sunscreen TiO_2 samples tested catalyze the photooxidation of a representative organic substrate, viz., phenol. Most significantly, we also show that sunlight-illuminated TiO_2 catalyzes DNA damage, both *in vitro* and in human cells; another inorganic sunscreen, zinc oxide (ZnO), behaves similarly. We conclude that the photocatalytically active nature of these oxides necessitates some changes since even the TiO_2 presently used in suncreams causes significant DNA strand breaks.

1. INTRODUCTION

1.1 Development of Skin Cancers

"One in five Americans will develop skin cancer in their lifetime, and one American dies every hour from this devastating disease."

About 1.3 million Americans likely developed skin cancer in the year 2000 alone as predicted by the American Cancer Society [1]. The most serious form of skin cancer, melanoma, is one of the fastest growing types of cancer in the United States. Though not substantiated by hard evidence, dermatologists have linked this growth of melanoma, which appears late in life, to childhood sunburns. Non-melanoma skin cancers (i.e. basal-cell carcinomas and squamous-cell carcinomas) pose less danger than melanomas. Nonetheless, if left untreated, these carcinomas can spread, they can cause disfigurement, and they can

lead to more serious health problems [1]. It was guesstimated that more than 1.2 million Americans would develop these milder forms of skin cancer in the year 2000, and that more than 1,900 would likely die of this disease. The basal-cell carcinomas are the most common type of non-melanoma skin cancers; they appear as small fleshy bumps (or nodules) on the head and neck; they grow slowly, and rarely spread on other parts of the body. By contrast, squamous-cell carcinomas appear as nodules or as red scaly patches; they can also develop into large masses, and they can spread to other parts of the body.

We noted in the previous Chapter that sunlight UVA radiation can contribute to both acute and chronic skin damage such as erythema, melanogenesis, carcinogenesis, drug-induced photosensitivity, and photoaging, among other health effect indicators. UVB radiation has been recognized as the leader in causing sunburns (erythema). However, because of the greater quantity of UVA radiation impinging on the surface of the Earth (see Figure 1), and because of the greater penetration of the UVA wavelengths into the dermis (see Figures 2 and 3 in Chapter 6; approximately 40-50% of UVA radiation is transmitted through Caucasian epidermis, compared to about 10-30% of UVB radiation [2]), consumers that employ sunscreens with high SPF values, which reflect the degree of UVB protection alone [2,3], tend to remain exposed to the Sun's UV radiation far longer without burning, thereby increasing substantially their input of damaging UVA wavelengths. Consequently, protection against UVA radiation is as important as protection against UVB radiation. To this effect, commercial formulators of sunscreen products currently employ organic *chemical* suncreen agents and inorganic *physical* UV filters to "protect" consumers against UVA radiation wavelengths. *Micronized* titanium dioxide, TiO_2, and zinc oxide, ZnO, are used

as the *physical* filters.

In its recent Final Monograph on sunscreen drug products [3], the United States Food ans Drug Administration (US FDA) concluded that TiO_2 causes no deleterious effects on the basis of studies that assessed acute animal toxicity, irritation, sensitization, photo-irritation, photosensitization, and human repeat insult patch and skin penetration. Moreover. based on data and information presented at a public meeting held September 19 and 20, 1996, in Rockville, MD, on the Photobiology and Photochemistry of Sunscreens, the FDA stated that it *"is not aware of any evidence at this time that demonstrates a safety concern from the use of micronized titanium dioxide in sunscreen products"* [3]. Such a statement is particularly worrisome and rather premature, in as much as more recent studies reported since late 1996 would seem to indicate otherwise.

1.2 Sunscreens and Skin Cancers

In a controlled study carried out over the period of one summer in Australia. reported by Thompson and coworkers [4] in 1993 and designed to determine the effectiveness of sunscreens, the authors used a broad-spectrum SPF 17 sunscreen on 431 Caucasian subjects. The results showed that the group that used the sunscreen had significantly fewer solar keratoses and more remissions than the control group. However, the number of solar keratoses reduction in this study was somewhat small and neither a clinical nor a biological significance of this reduction was established by the study [3]. Nonetheless. it would appear that most solar keratoses never become skin cancers and typically resolve spontaneously [5].

Because of the wide variation in the commercial formulations of sunscreen products

{e.g., the FDA estimates [3] there are approximately 2,800 over-the-counter (OTC) sunscreen drug products}, it is pertinent to emphasize that not all sunscreen products are therefore identical in their UV radiation absorption characteristics. Accordingly, the degree and type of UV radiation protection reported in a given study, that used a specific sunscreen, may not be relevant to other sunscreen products. In this regard, it is also important to note that results from tests specifically designed to measure only erythema (sunburns) cannot be extrapolated to make claims regarding protection against skin cancers and other health effect endpoints.

Although all sunscreen products may provide some level of protection against erythema and possibly other endpoints caused by UV rays, there are no products that will screen out 100% of all the UVA radiation wavelengths (320-400 nm) [6]. For example, even if no sunburn has occurred after using a sunscreen and after being exposed to sunlight UV radiation, one cannot assume that sun-induced skin damage that might contribute to the eventual development of skin cancer or signs of photoaging has not occurred [3]. As an aside, it is also important to note that, on a cloudy day, as much as ca. 80% of the UV radiation is transmitted through the clouds [7] with possible serious consequences to the uninformed consumer.

The effectiveness of sunscreen products to protect consumers from both erythema and skin cancers has been hotly debated, especially for the latter. This topic remains a controversial issue with promoters and detractors from both sides of the problem. At the February 1998 Philadelphia meeting of the American Association for the Advancement of Science, epidemiologist M. Berwick of New York's Memorial Sloan-Kettering Cancer

Center cast serious doubt on the ability of sunscreens to protect people against melanomas. It was also suggested that sunscreens may even contribute (directly or indirectly) to formation of skin cancers [8]. She pointed to 10 earlier epidemiological studies carried out between 1974 and 1993, which compared the appearance of melanomas among suncreen users and non-users. Two of these studies (one performed on women) found that the use of sunscreens reduced the risk of skin cancer from 30% to 80%, whereas three other studies found no correlation between the usage of suncreen filters and the appearance of melanomas. By contrast, the other five studies found an increased risk of skin cancers; in two of these studies, performed in the 1970s, the risk of skin cancers increased by a factor of 2 to 3. The more recent three other studies showed a 30% to 90% increased risk of skin cancers in users of sunscreen lotions. She concluded that "sunscreen alone does not prevent melanoma". A long time skeptic in the usage of sunscreens [9], epidemiologist Frank Garland of the University of California at San Diego concurred with Berwick's findings. He did add [10], however, that the results from the above studies may be due to the formulations of the sunscreens available in the 1970s, which contained only UVB filters. The more recently available broad-spectrum sunscreens filter out UVB and most of UVA sunlight radiation.

The American Academy of Dermatology (AAD), through its President Dr. Roger Ceilley, strongly opposed the Berwick report and fully endorsed the use of sunscreens as one component of sun protection. In a "communiqué" released March 19, 1998, the Academy even accused Berwick of jeopardizing its 20 years of efforts to educate beach goers and sun-bathers on sun safety [8,11]. In support of Berwick's report, a recent study involving 631 children (aged 6 and 7), and carried out by Doré and coworkers [12], found that the

appearance of "grains de beauté" (i.e., beauty spots) on the abdomen of these children increased with usage of sunscreams. An Israeli study uncovered similar findings [8]. Two earlier European epidemiological studies also concluded there may be be a link between sunscreen use and skin cancers [13,14].

It is worth noting that epidemiologist Berwick did not blame the increased risk of skin cancers on the chemistry of sunscreens [8] but questioned the behavior of sunscreen users who wrongly believe they are protected from UV radiation injury when using high SPF sunscreens (note that such claims have been made by manufacturers of sunscreen products) owing to the absence of acute signals such as sunburns [15], to an increased period of sun exposure longer than necessary, and to a genetic predisposition of some people to develop skin cancers more so than others; note that the latter may well be the most important factor [16]. With regard to the longer sun exposures and the notion that a sunscreen with SPF 10 allows people to stay exposed to UVA/UVB radiation 10 times longer before getting a sunburn, epidemiologist Jean-François Doré (Lyon, France) noted [12] that:

> "*Donner cette information, c'est participer à la notion qu'une crème permet de rester plus longtemps au soleil. Les gens utilisent une crème pour bronzer sans rougir et c'est en prolongeant l'exposition qu'ils reçoivent des doses d'ultraviolets qui déclenchent les effets biologiques néfastes*".

Doré further stated that

> "*quant aux crèmes, il s'agit d'un dispositif de sécurité qui est mal employé. Il faudrait les utiliser....(mais) à l'ombre*".

Contrasting the above, in an extensive article [17] in which they reviewed sunscreen safety

and efficacy, Gasparro,* Mitchnick,** and Nash*** concluded that sunscreen ingredients or products pose no human health concerns, and that the regular use of appropriate broad-spectrum sunscreen products could have a significant and favorable impact on public health, as part of an overall strategy to reduce UV radiation exposure. Yet the saga has not ended.

A most comprehensive and detailed five-year study on the safety and efficacy of sunscreens to protect consumers against the two forms of carcinomas, titled "Daily sunscreen application and betacarotene supplementation in prevention of basal-cell and squamous-cell carcinomas of the skin: a randomized controlled trial" was recently reported by Green and coworkers [18]. This study was a community-based (1621 residents of Nambour in southeast Queensland, Australia) randomized trial which used a 2 by 2 factorial design: individuals were assigned to 4 treatment groups, namely

(1) daily application of a sun protection factor SPF 15+ sunscreen {contained 8 wt.% octylmethoxycinnamate (OMC) and 2 wt.% Parsol 1789} to the head, neck, arms, and hands, and betacarotene supplementation (30 mg per day);

(2) sunscreen plus placebo tablets;

(3) betacarotene only; and

(4) placebo only.

The scheme below summarizes the partitioning of the participants.

---

* F.P. Gasparro, Department of Dermatology & Cutaneous Biology, Thomas Jefferson University, Philadelphia, PA.

** M. Mitchnick, SunSmart Inc., Wainscott, N.Y.

*** J.F. Nash, Procter & Gamble Co., Cincinnati, OH.

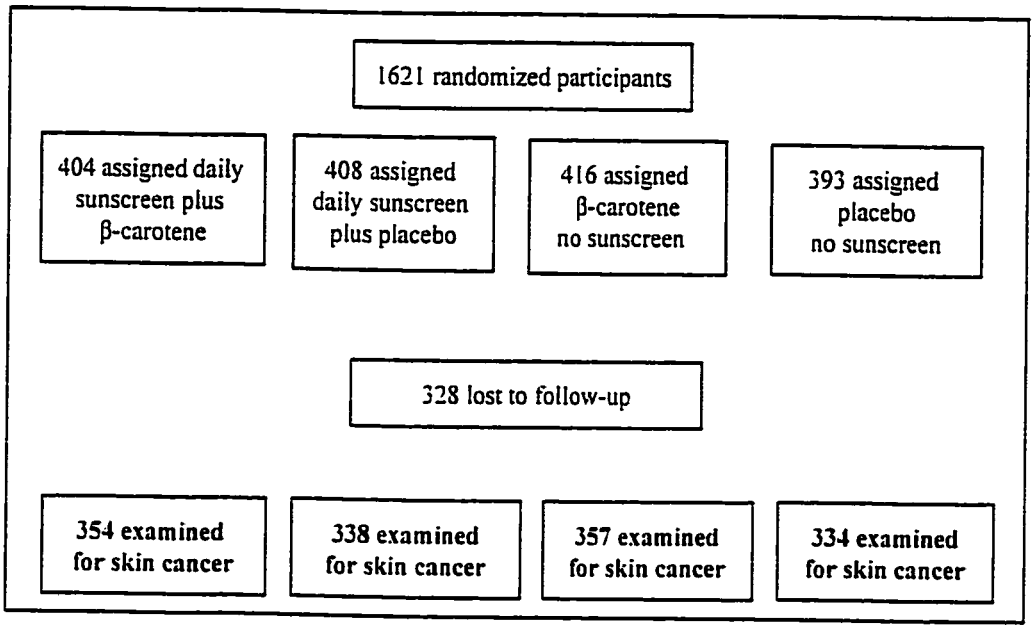

After 4.5 years of follow-up, the endpoints used to test the efficacy of the sunscreen were the incidences of basal-cell and squamous-cell carcinomas, both in terms of people treated for the newly diagnosed disease, and in terms of the numbers of tumors that developed. Analysis of the effect of the sunscreen was based only on skin cancers that resulted on sites of daily sunscreen application. Of the 1383 participants that underwent the dermatological follow-up, 256 individuals (or 18.5%) developed 789 new skin cancers during this period. Most noteworthy is that the rates of new skin cancers in this study were greater than the rates of basal-cell carcinomas (788 per 100,000) and squamous-cell carcinomas (321 per 100,000) reported for Australians overall despite the use of protective suncreams [19].

The study by Green et al [18] found no significant differences in the incidence of first new skin cancers between groups randomly assigned daily sunscreen and no daily

sunscreen (Table 1; basal-cell carcinoma: 2588 *versus* 2509 per 100,000; squamous-cell carcinoma: 876 *versus* 996 per 100,000). As well, the authors found no significant difference between the betacarotene and placebo groups in the incidence of either types of cancers (Table 2; basal-cell carcinoma: 3954 *versus* 3806 per 100,000; squamous-cell carcinoma:

Table 1. - Incidence of skin cancers in terms of people treated for skin cancer and tumors treated on the head, neck, arms, and hands by sunscreen treatment group [18].

Skin Cancer	Participants		Tumors	
	Sunscreen	No Sunscreen	Sunscreen	No Sunscreen
basal-cell carcinomas				
Number	65	63	153	146
Incidence per 100,000	2588	2509	6092	5814
squamous-cell carcinomas				
Number	22	25	28	46
Incidence per 100,000	876	996	1115	1832

Table 2. - Incidence of skin cancers on all sites by the betacarotene treatment group [18].

Skin Cancers	Participants		Tumors	
	betacarotene	placebo	betacarotene	placebo
basal-cell carcinomas				
Number	102	93	268	285
Incidence per 100,000	3954	3806	10390	11665
squamous-cell carcinomas				
Number	40	28	63	50
Incidence per 100,000	1508	1146	2442	2046

1508 *versus* 1146 per 100,000). In terms of the number ot tumors, application of sunscreen or betacarotene intake had no effect on the incidence of basal-cell carcinoma. However, in the case of squamous-cell carcinoma, the sunscreen group showed lower incidence than in the group that used no sunscreen (Table 1; 1115 *versus* 1832 per 100,000). In summary, cutaneous squamous-cell carcinomas, but ***not*** basal-cell carcinomas, appear to be amenable to some degree of prevention through routine use of sunscreens. By contrast, intake of an antioxidant such as betacarotene seems to have had neither harmful nor beneficial effects on the rates of either types of skin cancers.

1.3 Metal-Oxide Physical Filters

Such metal oxides as ZrO_2, TiO_2, ZnO, Sc_2O_3, and others are widely used in a variety of applications: for example, in protective coatings [20], mirrors [21], sensors [22] and as dielectrics in microelectronics [23]. They are also components in ferroelectric oxides, e.g. $Pb(Zr,Ti)O_3$ and $(Pb,La)(Zr,Ti)O_3$ which are potentially useful in infrared detectors [24] and in non-volatile computer memories [25]. Of particular interest is titanium dioxide (TiO_2) which is used, among others, in high permittivity gate dielectrics [26], in pollution abatement as a photocatalyst [27,28], and as a physical filter in sunscreen lotions to block UVA and UVB radiation [29]. The major focus of this Chapter concerns the latter two applications.

We begin by recalling that solar radiation reaching the Earth's surface consists of ~15% UV radiation (UVC, UVB and UVA), about 60% visible and the remaining ~25% is infrared radiation (Figure 1). Though UV radiation is a small fraction of terrestrial sunlight,

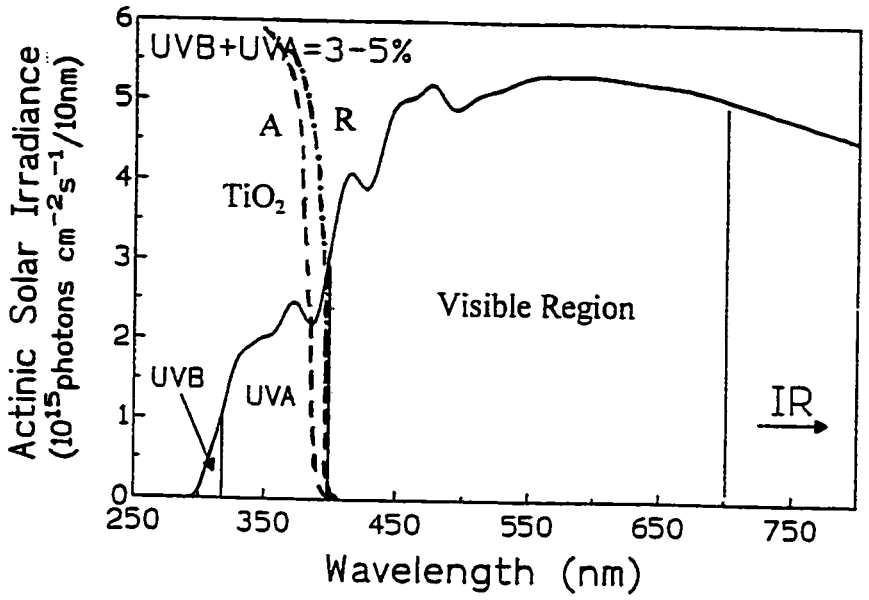

Figure 1 - Solar spectrum impinging on the Earth's surface and spectra of TiO_2 anatase (A) and rutile (R).

it can induce the most significant biological damage to living systems. The resulting overall photochemical interactions and the secondary reactions (e.g., generation of reactive species) are responsible for the UV-induced damage displayed in a wide variety of harmful clinical effects [30].

As we saw in earlier Chapters, titanium dioxide, TiO_2, absorbs UV light efficiently, catalyzing the formation of reactive oxygen species which can initiate oxidations [31]. These have been examined extensively in connection with the total oxidation of environmental pollutants [32], especially with the more active anatase form of TiO_2 [33]. Such photooxidations might help to explain the toxicity of illuminated TiO_2 [34,35]. To the extent that TiO_2 can enter human cells [36], it was imperative that its effects be examined in detail.

Damage to DNA could be particularly serious.

Although a recent evaluation of the safety aspects of TiO_2 [37] concluded that it is not mutagenic and thus could not damage DNA, that study did not examine, however, the effects of sunlight-illuminated TiO_2 nor the preparations used in sunscreens. These aspects are important, because although sunscreen particles are often coated with such compounds as alumina, silica, or zirconia that form hydrated oxides and which can capture or minimize formation of hydroxyl radicals and thus diminish photosensitivity [38], some TiO_2/Al_2O_3 and TiO_2/SiO_2 preparations have been shown to exhibit enhanced photo-activity [39]. Herein, we use chemical methods to examine photooxidations catalyzed by TiO_2 extracted from various sunscreens commercially available in Europe and North America. We also test the ability of TiO_2 and ZnO, another active sunscreen agent (a semiconductor with a bandgap of ca. 3.3 eV [40]) to attack DNA.

Since sunscreen preparations are exposed to sunlight, the photocatalytic behavior of these physical blockers is indeed relevant. The crystalline forms of TiO_2, anatase and rutile, are semiconductors with bandgap energies of 3.23 and 3.06 electron volts, respectively (ref. [38]), corresponding to 379 and 400 nm (1 eV corresponds to 8.06616×10^3 cm^{-1}). Light at or below these wavelengths contains enough energy to promote electrons from the valence band (VB) to the conduction band (CB), generating single electrons and positively charged spaces called holes (h^+). After their formation, electrons and holes either recombine or migrate rapidly (ca. 10^{-11} s) to the particle surface, where they react with adsorbed species. In aqueous environments, electrons react with oxygen, and holes with hydroxyl ions or

water, forming superoxide radical anions and hydroxyl radicals, respectively. Both species can initiate oxidation of the species adsorbed on the photocatalyst [41].

$$TiO_2 + h\nu \rightarrow TiO_2(e^-/h^+) \rightarrow e^-(cb) + h^+(vb)$$

$$e^- + O_2 \rightarrow O_2^{-}\bullet \rightarrow HOO\bullet$$

$$h^+ + OH^- \rightarrow \bullet OH$$

1.4 Catalyzed Oxidations by Commercial Sunscreen TiO_2

1.4.1 Catalyzed oxidation of phenol

Oxidation of organic materials by hydroxyl radicals from illuminated TiO_2 can be followed conveniently by examining the oxidation of a test molecule such as phenol [42]. Photodecomposition of a large variety of other organic compounds by irradiated TiO_2 has been reported extensively [41]. Table 3 compares the oxidative degradation of phenol by TiO_2 samples extracted from 10 different sunscreens (by washing away any organic chemical filter using either aqueous or nonaqueous solvents; e.g. water, acetonitrile, hexane) with those found for pure rutile and pure anatase. All the TiO_2 samples oxidize phenol. However, the activity does not appear to depend solely on the crystal type (anatase *versus* rutile). The most active sample, SN10, also contains ZnO. Note, however, that to the extent that the precise composition of the samples is unknown (in terms of particle size, surface area per unit weight, the presence and/or absence of coatings) disentanglement of the various factors that affect the photooxidations remains elusive. Evidently, other factors influence the

Table 3. - Relative rates of photodegradation of phenol by TiO_2 specimens and percent anatase and rutile forms present.

Specimen	Ratio anatase/rutile	Initial Rates (mmol h^{-1})	Relative rates
Pure anatase	100/0	31.6 ± 0.8	3803
Pure rutile	0/100	3.55 ± 0.12	427
SN1*	50/50	0.008 ± 0.016	1.0
SN2	0/100	0.023 ± 0.008	2.8
SN3	0/100	0.043 ± 0.010	5.2
SN4	54/46	0.043 ± 0.007	5.2
SN5	0/100	0.086 ± 0.015	10.4
SN6	100/0	0.146 ± 0.014	17.6
SN7*	0/100	0.189 ± 0.008	22.7
SN8	100/0	0.44 ± 0.11	53.3
SN9	63/37	1.11 ± 0.03	134
SN10**	0/100	31.6 ± 0.8	180

SN1 to SN10 are over-the-counter sunscreen lotions. * Also contains $Al(OH)_3$. ** Also contains 1.95% ZnO.

photodegradation, the most notable one being the very complex nature of the particle surface.

1.4.2 Catalyzed oxidation of DNA - nicking assays

Relaxation of DNA plasmids into its various forms (see Figure 2) caused by illuminated TiO_2 and ZnO, and suppression by dimethyl sulfoxide (DMSO) and mannitol is illustrated in Figure 3. In both panels, S, L and R show the migration of supercoiled, linear and relaxed plasmid. The top panel depicts the plasmid relaxation found after illumination with sunlight alone for 0, 20, 40 and 60 min (lanes 1-4) and in the presence of 1% (w/v)

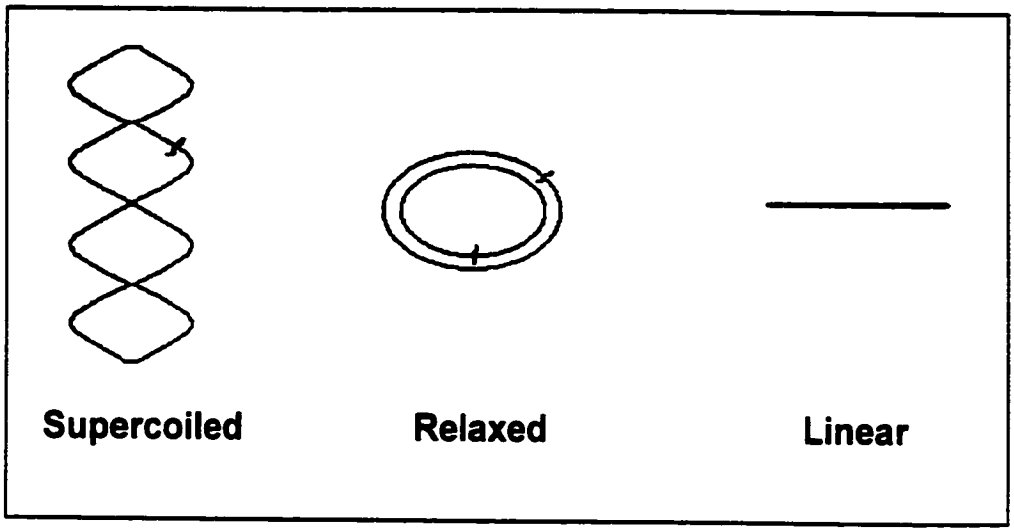

Figure 2. - Various forms of DNA after nicking: S, supercoiled form: R, relaxed form; L, linear form.

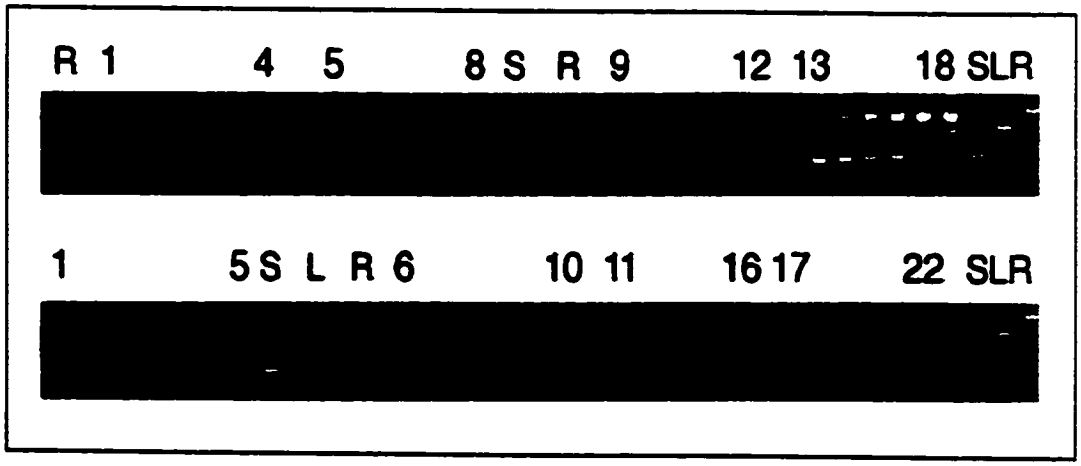

Figure 3. - Relaxation of plasmids caused by illuminated TiO_2 and ZnO, and suppression by dimethyl-sulfoxide and mannitol. From Dunford, Salinaro et al., *FEBS Letters*, **418**, 87 (1997).

anatase (lanes 5-8) or 1% (w/v) rutile (lanes 9-12) TiO_2 for the same times. Lanes 13-18

show illumination with TiO_2 from sunscreen SN8 for 0, 5, 10, 20, 40 and 60 min. the results are typical of those found with various samples. The bottom panel summarizes the results from illumination with 0.2% w/v ZnO for 0, 10, 20, 40 and 60 min before (lanes 1-5) or after (lanes 6-10) addition of DMSO, and with 0.0125% sunscreen TiO_2 for 0, 5, 10, 20, 40 and 60 min after addition of 200 mM DMSO (lanes 11-16) or 340 mM mannitol (lanes 17-22).

The authentic TiO_2 standards (Tioxide) were confirmed by X-ray diffraction to be 100% anatase or 100% rutile and were suspended in water at 2% w/v; ZnO (Aldrich, < 1 micron) at 0.4%. Twenty five microliters (25 µl) of each suspension were added to 25 µl of plasmid (2-3 µg of DNA) in 100 mM sodium phosphate (pH = 7.4) and illuminated as 50-µl droplets on siliconised microscope slides placed on a brass block embedded in ice. The solar simulator [43] consisted of a 250-Watt ozone-free lamp, a WG 320 filter and a quartz lens, resulting in an estimated fluence between 300 and 400 nm of 12 W m^{-2}. The plasmid used was the ***pBluescript II SK+*** (Stratagene) prepared and analyzed on agarose gels according to Maniatis [44]. Relaxed standards were made by depurinating plasmid in 25 mM sodium acetate (pH = 4.8) at 70°C for 20 min followed by cleaving with exonuclease III at 37°C [45] in 50 mM Tris-HCl, 5 mM $CaCl_2$ (the Ca^{2+} inhibits exonuclease but not cleavage at apurinic sites), 0.2 mM DTT, pH 8. Linear standards were obtained by cutting the supercoiled plasmid with EcoRI. A sunscreen containing only TiO_2 (7% w/v) was vortexed with water and centrifuged. The white pellet was washed three times with a mixture of chloroform and methanol (1:1), followed with methanol alone, and then dried. The powder

was suspended in water at 2%; however, most of it quickly settled out, leaving a cloudy supernatant with a TiO_2 content assayed at 0.025% w/v. This was mixed with an equal volume of plasmid DNA in buffer. We assayed TiO_2 concentrations according to Codell [46] using standards made from pure TiO_2 (Aldrich); a molar extinction coefficient for the complex assayed as 827 M^{-1} cm^{-1} at 404 nm.

Hydroxyl radicals inflict direct strand breaks on DNA. To test for such damage we illuminated supercoiled plasmids with simulated-sunlight alone and with TiO_2. Ultrafine titanium dioxide irradiated with simulated sunlight should be harmful to supercoiled plasmid DNA owing to photogenerated •OH radicals on TiO_2. Figure 3 shows that plasmids were converted first to the relaxed form R after one nick and ultimately to the linear form L after a second nick, demonstrating strand breakage. Sunlight alone had very little effect. The anatase form of TiO_2 appears more photo-active than rutile, consistent with observations from other photochemical comparative studies (Table 3 and ref. [33]). A TiO_2 sample extracted from a sunscreen was also photo-active, as was ZnO. The sunscreen illumination experiments contained much less TiO_2 than the pure anatase and rutile samples, suggesting that the sunscreen variety was especially active. DNA damage was suppressed by the quenchers [47] DMSO and mannitol, strongly confirming the notion that the damage to DNA was indeed caused by hydroxyl radicals.

Figure 4 depicts the effect of catalase on DNA damage inflicted by illuminated TiO_2 and also suggests the location of lesions in DNA. The top panel gives the results from a plasmid DNA illuminated (see Figure 3) with sunscreen TiO_2 alone for 0, 20, 40 and 60 min

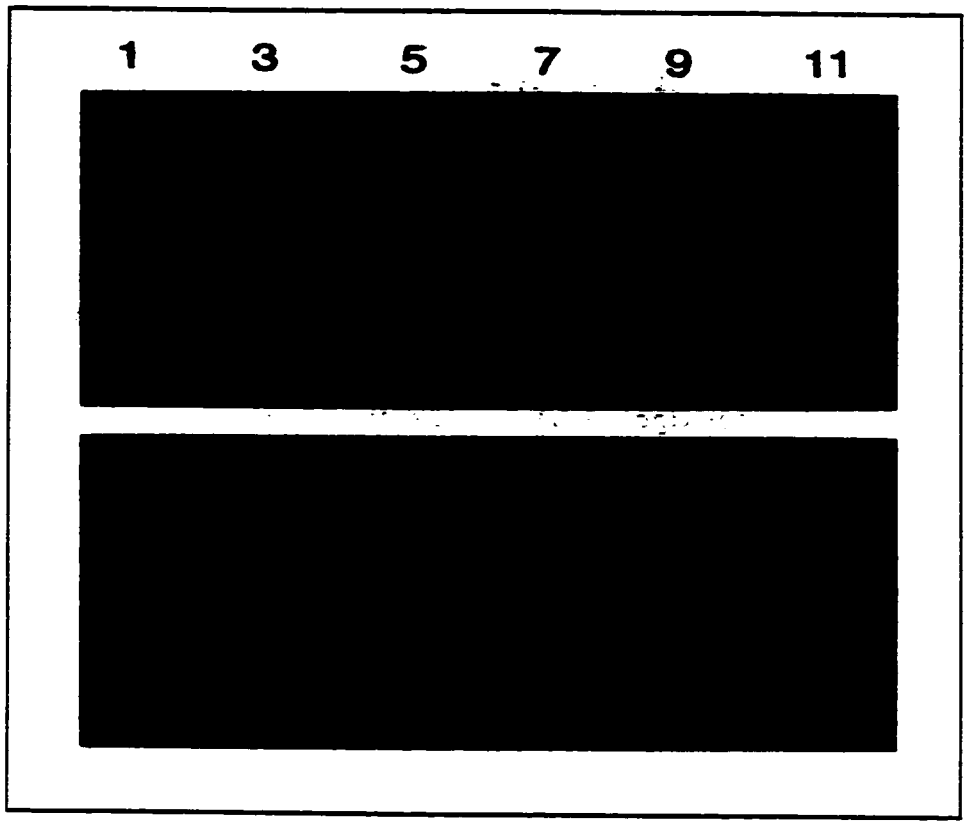

Figure 4. - Effect of catalase, boiled catalase, and bovine serum albumin on damage inflicted by illuminated TiO_2 and location of lesions in DNA.From Dunford, Salinaro et al., *FEBS Letters*, **418**, 87 (1997).

(lanes 1-4) and for the same times (lanes 8-11) after addition of 2.5 units ml^{-1} of catalase (0.1 mg ml^{-1} of protein). Lanes 5-7 show the supercoiled, linear and relaxed DNA plasmids.

The bottom panel reports illumination with sunscreen TiO_2 as above after addition of boiled catalase (lanes 1-4) or 0.1 mg/ml of bovine serum albumin (lanes 8-11). For the right panel, a 426 base-pair fragment of double-stranded DNA labelled at one 5'-end was illuminated in 0.0125% w/v sunscreen TiO_2. Samples were analyzed on a sequencing gel.

Lanes 1-4 refer to illumination for 0, 20, 40 and 60 min, whereas Lanes 5-8 show the results after illumination for the same times followed by treatment with N,N'-dimethyl-ethylenediamine for 30 min at 90°C before analysis. The latter reagent displaces many damaged residues from DNA and then cleaves the sugar-phosphate chain, leaving homogeneous, phosphorylated termini with consistent mobility, thus clarifying the spectrum of lesions generated [48]. Lanes 9-10 of the right panel depict the G and A dideoxy sequencing standards.

DNA damage caused by illuminated TiO_2 is only slightly suppressed by catalase (Figure 4); heat-inactivated catalase and bovine serum albumin show similar effects. Evidently, the limited quenching is caused by the surrounding protein and not by the catalase. In addition, superoxide dismutase did not suppress DNA damage. Consequently, we infer that any resulting DNA damage cannot be due to the superoxide radical anion, $O_2^{-\bullet}$, an intermediate active oxygen species formed by reaction between e^-(cb) and O_2, nor to the intermediate hydrogen peroxide, H_2O_2, formed by reaction between two •OH radicals. The cause of the observed strand breaks produced in the plasmid molecule must be caused by •OH radicals since the damage can be suppressed by such hydroxyl radical quenchers [47] as DMSO and mannitol (see above). Upon cleaving end-labelled DNA, other lesions (right panel) were uncovered principally at some, but not all, guanine residues. Evidently, DNA damage is not confined to strand breaks only.

1.4.3 Catalyzed oxidation of DNA - comet assays

Comet assays are ideal to confirm whether photoexcited TiO_2 causes strand breaks

in the nuclei of whole human skin cells. Such assays provide a basis for assessing the potential genotoxicity of ultrafine titanium dioxide on human skin. The assay is based on the effect that the introduction of strand breaks in DNA has on the supercoiling within the nucleus. Introducing a nick into supercoiled DNA causes relaxation and loss of supercoiling. If the nuclear membrane and most of the nuclear proteins are removed to create a nucleoid, the DNA strands that contain the nicks are released creating a so-called comet; otherwise the supercoil remains intact in undamaged nuclei and appears as a round whole circle.

Figure 5 demonstrates the damage inflicted on human cells revealed by Comet assays. After treatment, cells were embedded in low-melting agarose, lysed with 1% Triton X-100, subjected to alkaline gel electrophoresis and stained with ethidium bromide [49]. Row A shows the comets obtained using X-rays from a Gavitron RX30 source. The dose rate was 8.9 Grays/min and cells were exposed on ice for 0, 15, 30 and 60 sec, giving comets falling into the 5 main standard classes [49] shown: **1**, class 0; **2**, class I; **3**, class II; **4**, class III; and **5**, class IV. Rows B and C depict examples of comets obtained using simulated sunlight. The lens was omitted, giving an intensity similar to that found under the stratum corneum [43]. MRC-5 fibroblasts were illuminated on ice with or without sunscreen TiO_2 (0.0125% w/v). Samples were taken at increasing times, kept on ice, and subsequently all were processed at the same time. For each exposure, 100 cells were scored. The comets were classified by comparison with the standards (Row A). Row B illustrates the results from no treatment (1); sunlight alone for 20, 40 and 60 min (2-4), and the effect of TiO_2 in the dark for 60 min (5). Row C summarizes the comets obtained using sunlight with TiO_2

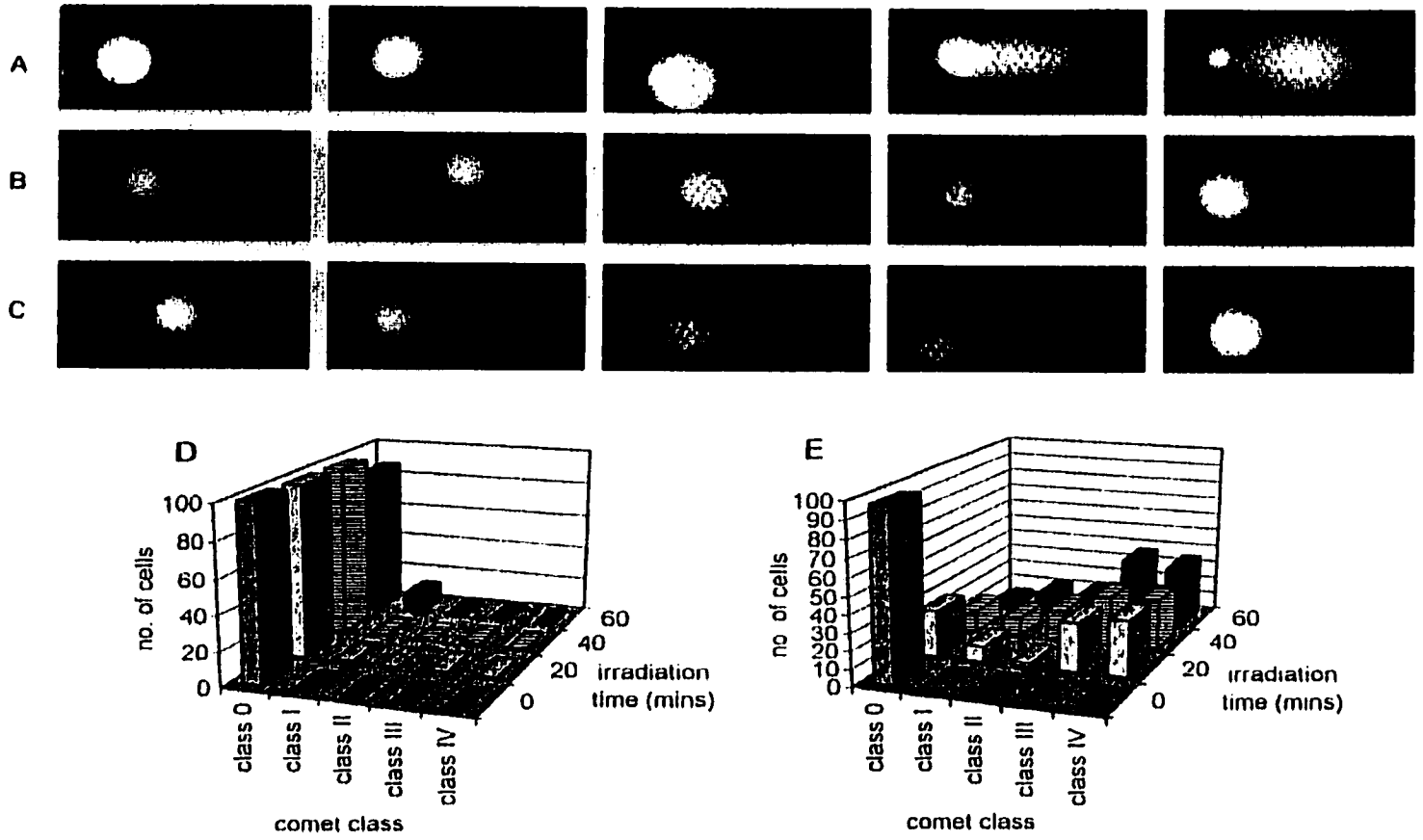

Figure 5. - Damage inflicted on human cells as revealed by Comet assays. The charts summarize the results from five independent experiments. Chart D shows that sunlight alone onflicts but a few strand breaks and/or alkali-labile sites, whereas chart E demonstrates that inclusion of TiO_2 catalyzes this damage. From reference [29].

present for 0, 20, 40 and 60 min (1-4) illumination, and for 60 min in the presence of TiO_2 and 200 mM DMSO (5). Results from five independent experiments were combined to generate the charts D and E. Chart D shows that sunlight alone inflicted only a few strand breaks and/or alkali-labile sites; chart E demonstrates that inclusion of TiO_2 catalyzes this damage to DNA.

The DNA damage data are typically assessed by classifying the comets produced into groups according to the length and area of the tail. The greater the area of the tail, the more damage has been caused. This was done visually using a fluorescence microscope. Figure 5 shows that light alone induced some breaks at 20,40 and 60 min of irradiation. Titania, TiO_2 (Degussa P-25), catalyzes this damage at identical irradiation times. Titanium dioxide samples present in commercially available sunscreens were also tested. The results confirmed that ultrafine TiO_2 does indeed inflict strand breaks in DNA.

Hidaka and coworkers [50,51] also showed that radicals formed on the surface of titanium dioxide particles during irradiation, which include surface-trapped electrons. peroxyl and hydroxyl radicals, can lead to substantial redox chemistry in the pyrimidine and purine bases, and also in the DNA and RNA nucleotides. Hydroxyl radicals appear to attack the sugar/phosphate backbone in these two nucleotides.

Whilst most researchers in heterogeneous photocatalysis have been attempting to fabricate the most ***photocatalytically <u>active</u>*** TiO_2 system to degrade the most stubborn of environmentally harmful pollutants, our efforts have been concentrated on producing the most ***photocatalytically <u>inactive</u>*** TiO_2 specimens for possible use in sunscreen lotions,

while retaining the spectroscopic features of TiO_2 (see Chapter 9) that make titania particles excellent UVA/UVB blockers. We have fabricated and/or examined some 20 specimens and present below brief relevant results of interest to the present discussion.

Figure 6 illustrates the kinetic behavior of these specimens before and after inactivation of the particle surface for the photooxidative degradation of phenol. It is clear that our methods have achieved some of the desired goals since the rate of photodegradation

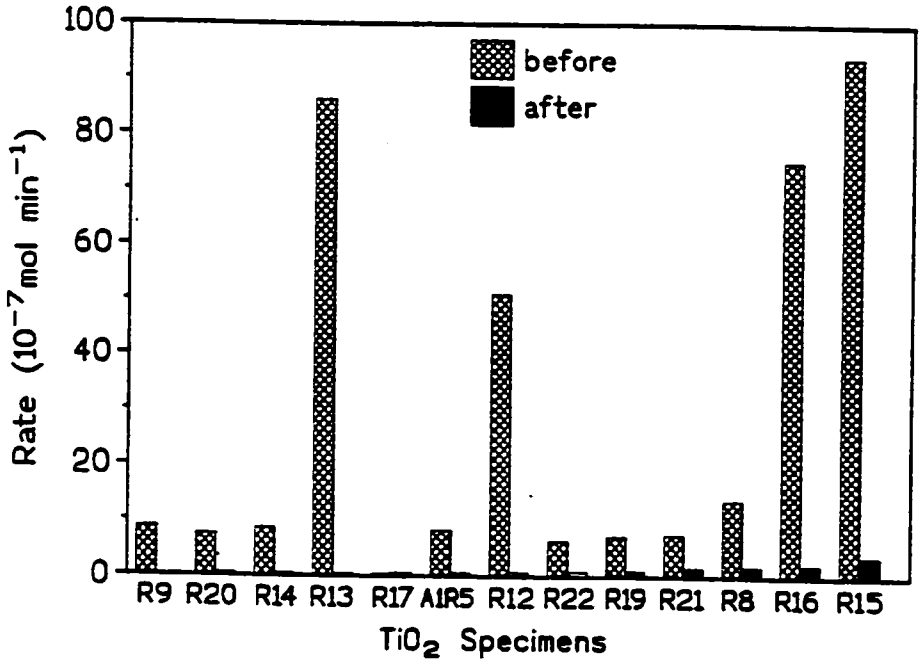

Figure 6. - Rates of photodegradation of phenol by several TiO_2 specimens before and after surface modification.

of phenol has been reduced dramatically for many of the specimens. Specimen R13 shows the largest drop in the rate of photooxidation of phenol, followed by R12, R16 and R15. Subsequently we examined the damaging effects of these samples on DNA plasmids.

Figure 7 displays some of the results in terms of the fraction of DNA plasmids remaining in the supercoiled state as a function of illumination time for a 1% w/v concentration of TiO_2. For pure anatase (Tioxide) and for the R12 and R19 specimens the data show that after modification, the irradiated R12A specimen has no influence on DNA relative to a DNA sample subjected to otherwise identical UVA/UVB illumination (calibrated solar simulator) and experimental conditions for a 30-min time period. Note that R12A (an R12 specimen after inactivation) displays the same spectral features as specimen R12B (specimen before inactivation; see Chapter 8 below). The Figure also demonstrates

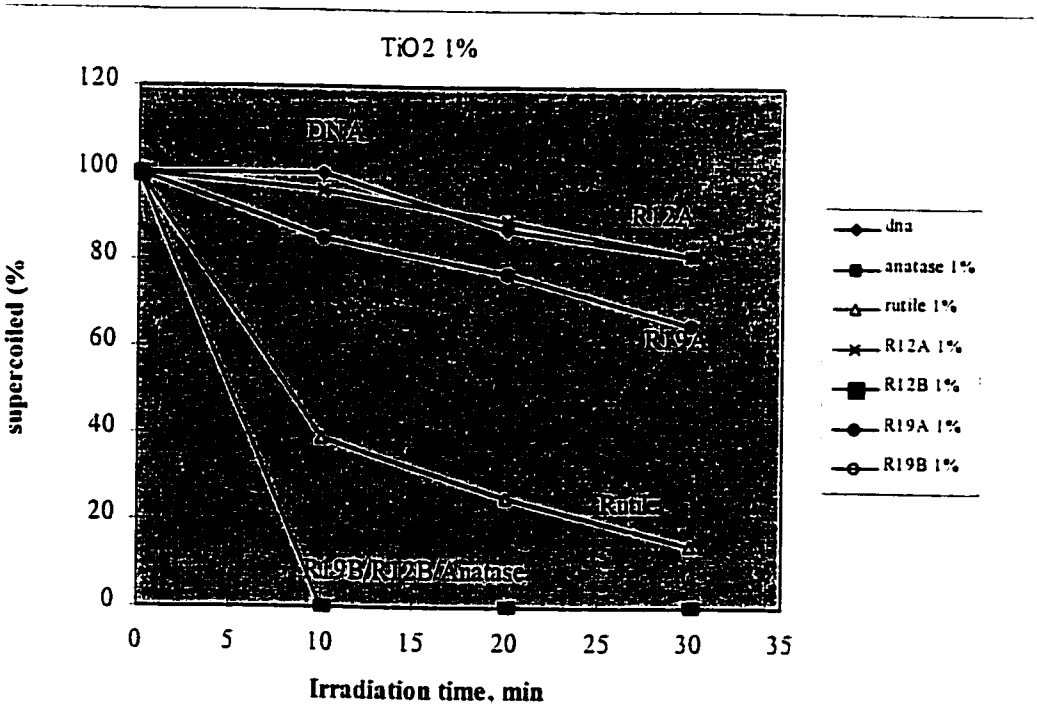

Figure 7. - Fraction of supercoiled DNA plasmids surviving the influence of various samples of irradiated TiO_2 (1 wt.%) for a 30-min period.

that the anatase R19B and R12B specimens have in fact destroyed nearly all the plasmids after only 10 min (or less) of irradiation. As well, the rutile form was less damaging than anatase (ca. 15% of the plasmids remained in the supercoiled state), as known from a multitude of studies on the photooxidation of environmental organic pollutants. Sample R19A was even better with only ca. 35% of the plasmids destroyed in the 30-min period. We present more details on this aspect in a later Chapter.

2. ADDITIONAL REMARKS

The results presented here demonstrate that sunscreen TiO_2 and ZnO can catalyze oxidative damage to DNA. The fate of these two metal-oxide materials applied onto the skin is uncertain. Autoradiographic studies with ^{65}ZnO have noted that it passes through rat [52] and rabbit [53] skin, probably through hair follicles. The chemical form of ^{65}Zn detected under the skin (and hence of the form that crosses the skin) is unknown. Some reports have raised the possibility that ZnO [54] and pigmentary TiO_2 [55,56] pass through human skin. A more recent study suggests that *micronised* TiO_2 in sunscreens also passes through human skin [57], although more systematic studies are evidently needed. Clearly then, it is important to characterize the fate and photochemical behavior of sunscreen agents, which not only serve to prevent sunburns, but have also been inferred to be effective in reducing skin cancers, a problem that has seen a rapid increased incidence in the last few years [58,59]. While they can reduce the formation of cyclobutane dimers in DNA [60], induced by direct absorption of UVB, the ability of TiO_2 and at least one organic sunscreen to produce free

radicals that can also inflict other forms of damage [43,61] is enough to point to the importance of investigating these forms too.

3. REFERENCES

[1]. "*The SunWise School Program*", United States Environmental Protection Agency, Washington, D.C., July 26, 2000.

[2]. Communication from D.E. Baker, Associate Commissioner for Regulatory Affairs, United States Food and Drug Adminsitration, to E.E. Kavanaugh, President of the Cosmetic, Toiletry, and Fragrance Association, October 1, 1999.

[3]. "*Sunscreen Drug Products for Over-The-Counter Human Use - Final Monograph*", U.S. Federal Register 64FR27666, United States Food and Drug Administration, Washington, D.C., May 21, 2000.

[4]. S.C. Thompson, J.D. Jolley, and R. Marks, *New England J.Med.*, **329**, 1147 (1993).

[5]. R. Marks and G. Rennie, *The Lancet*, 795 (1988).

[6]. "*Indoor Tanning*", United States Federal Trade Commission, Washington, D.C., August 1997. See http://www.ftc.gov/bcp/conline/pubs/health/indootan.html

[7]. P. Kurtzweil, "Seven Steps to Safer Sunning", *FDA Consumer*, June 1996 and February 1997.

[8]. T. Souccar, "Alerte aux Crèmes Solaires", *Sciences et Avenir*, August 1998.

[9]. F. Garland, et al., *Am. J. Public Health*, **124**, 614 (1991).

[10]. Quoted in various worldwide newspapers by: (a) D. Ahlstrom, *The Irish Times*, February 18, 1998; (b) R. Davis and T. Friend, *USA Today*, February 18, 1998; (c) M. McCullough, *The Philadelphia Inquirer*, February 18, 1998; (d) N. Hawkes, *The Times*, February 18, 1998; (e) A. Bazzi, *Corriere della Sera*, Milano, February 19, 1998; (f) A. Underwood, *Newsweek*, March 2, 1998.

[11]. L. Goldsmith, H.K. Koh, B. Bewerse, B. Reilley, S. Wyatt, W. Bergfeld, A.C. Geller, and P.F. Walters, *J. Am. Acad. Dermatol.*, **34**, 822 (1996).

[12]. Quoted in reference [8].

[13]. P. Autier, J.F. Doré, E. Schifflers, et al., *Int. J. Cancer*, **61**, 749 (1995).

[14]. J, Westerdahl, H. Ollson, A. Masback, et al., *Melanoma Res.*, **5**, 59 (1995).

[15]. C.F. Garland, F.C. Garland, and E.D. Gorham, *Ann. Epidemiol.*, **3**, 103 (1993).

[16]. Quoted in reference [10].

[17]. F.P. Gasparro, M. Mitchnick, and J.F. Nash, *Photochem.Photobiol.*, **68**, 243 (1998).

[18]. A. Green, G. Williams, R. Neale, V. Hart, D. Laslie, P. Parsons, G.C. Marks, P. Gaffney, D. Battistutta, C. Frost, C. Lang, and A. Russell, *The Lancet*, **354**, 723 (1999).

[19]. M. Staples, R. Marks, and G. Giles, *Int. J. Cancer*, **78**, 144 (1998).

[20]. R.D. Veltri and E.S. Galasso, *German Patent*, DE-3427911, 1986.

[21]. W.H. Lowdermilk, D. Milham, and F. Rainer, *Thin Solid Films*, **73**, 155 (1980).

[22]. V.K. Khanna and R.K. Nahar, *Appl.Surf.Sci.*, **28**, 247 (1987).

[23]. S.B. Desu, T. Shi, and C.K. Kwok, *Mater.Res.Soc.Symp.Proc.*, **168**, 349 (1990).

[24]. N.M. Shorrocks, S.G. Porter, R.F. Whatmore, A.D. Parsons, J.N. Gooding, and D.J. Pedder, *Proc. SPIE*, **1320**, 88 (1990).

[25]. (a) J.C. Crawford and F.L. English, *IEEE Trans.Electron.Devices*,, **ED-16**, 525 (1969).

(b) O. Auciello and R. Ramesh, *MRS Bull.*, **21**, 31 (1996).

[26]. S.A. Campbell, D.C. Gilmer, X.C. Wang, M-Ta Hsieh, H.-S. Kim, W.L. Gladfelter, and J. Yan, *IEEE Trans.Electron.Devices*, **44**, 104 (1997).

[27]. C.H. Peng and S.B. Desu, *J.Am.Ceram.Soc.*, **77**, 1799 (1994).

[28]. N. Serpone and A. Salinaro, *Pure Appl.Chem.*, **71**, 303 (1999).

[29]. R. Dunford, A. Salinaro, L. Cai, N. Serpone, S. Horikoshi, H. Hidaka, and J. Knowland, *FEBS Letts.*, **418**, 87 (1997).

[30]. R. B. Sollitto, K. H. Kraemer, and J. J. DiGiovanna, *J. Am. Acad. Dermatol.*, **37**, 942 (1997).

[31] N. Serpone, *Kirk-Othmer Encyclopedia of Chemical Technology*, Wiley-Interscience, New York, volume **18**, pp. 820-837, 1996.

[32]. D.F. Bahnemann, J. Cunningham, M.A. Fox, E. Pelizzetti, P. Pichat, and N. Serpone, in *Aquatic and Surface Photochemistry*, D. Crosby, G. Helz, and R. Zepp, Eds., Lewis Publishers, Boca Raton, Florida, pp 261-316 (1994).

[33]. A. Sclafani and J.-M. Herrmann, *J. Phys. Chem.*, **100**, 13655 (1996).

[34]. T. Saito, T. Iwase, J. Horie, and T. Morioka, *J. Photochem. Photobiol. B:Biol.*, **14** (1992).

[35]. Y. Kubota, T. Shuin, C. Kawasaki, M. Hosaka, H. Kitamura, R. Cai, H. Sakai, K. Hashimoto, and A. Fujishima, *Br. J. Cancer*, **70**, 1107 (1994).

[36]. R. Cai, K. Hashimoto, K. Itoh, Y. Kubota, and A. Fujishima, *Bull. Chem. Soc. Japan*, **64**, 1268 (1991).

[37]. Titanium dioxide. *IARC Monogr. Eval. Carcinog. Risks Humans*, **47**, 307 (1989).

[38]. V.S.P. Judin, *Chemistry in Britain*, pp. 503-505, June 1993.

[39]. C. Anderson and A.J. Bard, *J. Phys.Chem.*, **101**, 2611 (1997).

[40]. W.H. Strehlow and E.L. Cook, *J. Phys.Chem. Ref. Data*, **2**, 163 (1973).

[41]. N. Serpone and E. Pelizzetti, in "*Photochemical and Photoelectrochemical Approaches to Solar Energy Conversion*", M.D. Archer and A.J. Nozik, Eds., Imperial College Press, London, **2001**, volume III, Chapter 16.

[42]. A. Salinaro, A.V. Emeline, J. Zhao, H. Hidaka, V.K. Ryabchuk, and N. Serpone, *Pure Appl.Chem.*, **71**, 321 (1999).

[43]. J. Knowland, E.A. McKenzie, P.J. McHugh, and N.A. Cridland, *FEBS Lett.*, **324**, 309 (1993).

[44]. T. Maniatis, F.F. Fritsch, and J. Sambrook, *Molecular Cloning: A Laboratory Manual.* Cold Spring Harbor Laboratory, Cold Spring Harbor, New York (1982).

[45]. P.W. Doetsch and R.P. Cunningham, *Mutat. Res.* **13**, 3285 (1990).

[46]. M. Codell, *Analytical Chemistry of Titanium Metal and Compounds*, Interscience Publishers Inc, New York, 1959.

[47]. B. Halliwell and J.M.C. Gutteridge, *Free Radicals in Biology and Medicine.* Clarendon Press, Oxford, 1989.

[48]. P.J. McHugh and J. Knowland, *Nucleic Acids Res.*, **23**, 1664 (1995).

[49]. V.J. McKelvey-Martin, M.H. Green, P. Schmezer, B.L. Pool-Zobel, M.P. De-Meo, and A. Collins, *Mutat. Res.* **288**, 47 (1993).

[50]. H. Hidaka, S. Horikoshi, N. Serpone, and J. Knowland, *J. Photochem. Photobiol. A: Chem.*, **111**, 205 (1997).

[51]. S. Horikoshi, N. Serpone, S. Yoshizawa, J. Knowland, and H. Hidaka, *J.Photochem. Photobiol.A: Chem.*, **120**, 63 (1999).

[52]. G. Hallmans and S. Liden, *Acta. Derm. Venereol.* **59**, 105 (1979).

[53]. S.P. Kapur, B.R. Bhussry, S. Rao, and Y. Hormouth-Hoene. *Proc. Soc. Exp. Biol. Med.* **145**, 932 (1974).

[54]. M.S. Agren, *Dermatologica*, **180**, 36 (1990).

[55]. A. Dupre, P. Touron, J. Daste, J. Lassere, J.L. Bonafe, and R. Viraben, *Arch. Dermatol.*, **121**, 656 (1985).

[56]. C.A. Moran, F.G. Mullick, k.g. ishak, F.B. Johnson, and W.B. Hummer, *Hum. Pathol.*, **22**, 450 (1991).

[57]. M-H. Tan, C.A. Commens, L. Burnett, and P.J. Snitch, *Australas. J. Dermatol.*, **37**, 185 (1996).

[58]. D.S. Preston and R.S. Stern, *N. Engl. J. Med.*, **327**, 1651 (1992).

[59]. P. Boyle, P. Maisonneuve, and J.-F. Doré, *B. Med. Bull.*, **51**, 523 (1995).

[60]. H.N. Ananthaswamy, S.M. Loughlin, P. Cox, R.L. Evans, S.E. Ullrich, and M.L. Kripke, *Nature Med.*, **3**, 510 (1997).

[61]. P.J. McHugh and J. Knowland, *Photochem. Photobiol.*, **66**, 276 (1997).

Chapter 8

PREPARATION , MODIFICATION AND CHARACTERIZATION OF VARIOUS TiO_2 SPECIMENS

Summary

This chapter reports on the characterization of TiO_2 specimens extracted from sunscreen lotions and presents results of their physical properties that may affect their photocatralytic activity as expressed by the photooxidation of phenol, and by extrapolation plasmid DNA and human cells. Homemade colloids and several otherTiO_2 specimens obtained from various commercial sources were modified so as to passivate the particle surface to produce TiO_2 specimens of considerably reduced photoactivity. Deactivation of titania specimens has a profound impact on the kinetics of photooxidation of phenol, and thus is expected to have a significant effect on diminishing the damage caused to DNA plasmids, to human cells and to yeast cells by untreated titania systems (see Chapter 9). Some physical and spectral characteristics of these modified titania specimens are described.

1. INTRODUCTION

Inactive titanium dioxide specimens have been prepared in an ongoing effort to understand the processes involved in heterogeneous photocatalysis. Before describing the results, it is worth recalling briefly some of the prior results that have contributed to the overall knowledge of the photocatalytic activity of TiO_2 from our studies and from the many excellent reports in the literature.

Titanium dioxide exists in three different crystalline forms, namely rutile, anatase and brookite; an amorphous phase also exists for TiO_2. Only the rutile and anatase polymorphs have relevance in heterogeneous photocatalysis as well as in sunscreen lotions. Both these TiO_2 polymorphs possess the rock-salt tetragonal lattice, which consists of three somewhat distorted octahedra. Contrary to the normal rock-salt lattice, however, in which six octahedra share a common corner, only three do so in the titanium dioxide lattice. The principal difference between rutile and anatase is the divergence in photoactivity; anatase is the more photoactive form of titanium dioxide, whereas rutile is the more common form of titania even though anatase is more stable by about 8 to 12 kJ mol^{-1} [1]. The different crystalline forms found in TiO_2 rest with the different linkages of the TiO_6 octahedra. In anatase, each of the octahedra shares four edges with neighboring octahedra, whereas in rutile each octahedron shares opposite edges with neighboring octahedra leading to formation of chains; other chains are connected via corners common to three octahedra. Both lattices (see Figure 1) are highly symmetrical with respect to titanium atoms, but not about the 3-coordinate oxygen atoms in the OTi_3 units. Consequently, the basic distinction between anatase and

rutile forms rests with the symmetry about this oxygen and with differences in the polarization of the O^{2-} ions. These differing geometries of the Ti–O (Ti)–Ti units in anatase and rutile give rise to relatively high dielectric constants along the *c* axis: 173 and 48, respectively. The divergence in photoactivity between the two polymorphs is due to this difference in geometry and in symmetry, which ultimately is reflected in a variation of the surface structure.

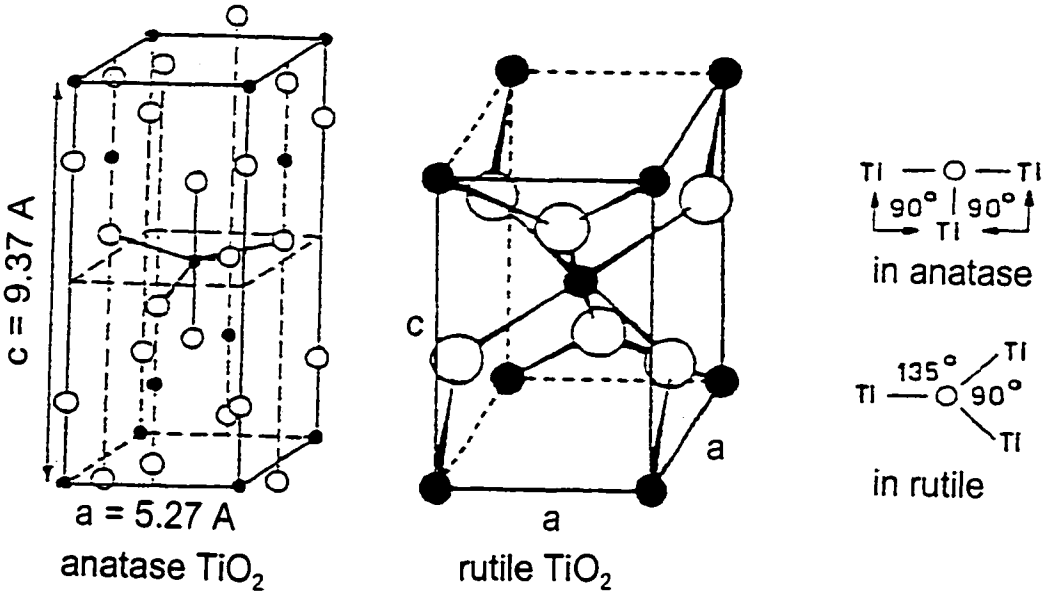

Figure 1. - Tetragonal lattices of anatase and rutile TiO_2 polymorphs. From references [1,2].

Titania is easily prepared by hydrolysis of a titanium (IV) precursor to give anatase and rutile, and some quantity of the amorphous phase. On contact with water (or water moisture) the surface of the nanocrystallites become highly hydroxylated. The surface

hydroxyl groups strongly influence photocatalyzed redox reactions that take place at the nanoparticle/solution or nanoparticle/gas interfaces. The titania surface has acid/base characteristics displaying two pKa's (reactions 1 and 2). The iso-electric point or point of zero zeta potential (pzc) of titania is described as the point at which the pH is the average of the pKa's, namely $[pKa_1 + pKa_2] / 2$.

$$\equiv Ti-O^- + H^+ \rightarrow \equiv Ti-O-H \qquad pKa_1 \qquad (1)$$

$$\equiv Ti-O-H + H^+ \rightarrow \equiv Ti-OH_2^+ \qquad pKa_2 \qquad (2)$$

At pHs below the pzc the surface is positively charged, and is neutral at the pzc. This change in the surface characteristic influences the adsorption/desorption of substrates coming in contact with titanium dioxide particles and thus will influence (somehow) the kinetics and mechanistic details of photocatalyzed reactions. The pzc for anatase titania is ca. 5.1 and for Degussa P-25 (75% anatase, 25% rutile) the pzc ranges between 5.5 and 6.0 [3].

Titanium(IV) dioxide is an indirect bandgap semiconductor. The lowest allowed electronic transition occurs from the highest level of the valence band to the lowest unoccupied level of the conduction band is an indirect transition; this transition involves a change in momentum. To conserve momentum, the transition necessitates, as required by the conservation rules, that a photon couple to a phonon (a lattice vibration) for the transition to occur. This causes the absorption probability for indirect transitions to be lower than for

allowed direct transitions.

A few years ago Serpone and coworkers [4] reported that the blue shifts seen in the absorption spectra of TiO_2 with decreasing size, and typically taken as a signature for size-quantization in several semiconductor nanoparticles, can be accounted for by the different electronic transitions that take place between the various energy levels of the valence and conductions bands in the nanoparticle. They concluded that nanoparticles of anatase with radius R_p greater than 1 nm display no size-quantization effects.

The photophysical events that occur after electron/hole pair formation are many and very complex. Following e/h formation and subsequent separation, the two charge carriers may migrate to the surface in competition with a multitude trapping and recombination events in the lattice bulk. At the surface, these carriers are poised to initiate redox chemistry with suitable pre-adsorbed acceptor and donor molecules in competition also with (not fully understood) recombination events to yield radiative and nonradiative emissions, and/or trapping of the charge carriers into shallow traps at lattice sites (e.g., oxygen vacancies, Ti^{4+}, and other defects). Recent studies by Emeline, Ryanchuck and Serpone on several metal oxides (e.g., ZrO_2, Sc_2O_3 and others) are beginning to unravel some of these otherwise complex photophysical events [5]. A complete picture of these events will ultimately increase our level of understanding of the photoactivity of titanium dioxide in contact with other chemical species or biological systems.

During the past decade, Serpone and coworkers [6,7] have contributed significantly to our present understanding and knowledge of photocatalysis. In this regard, the first part

of this thesis addresses some fundamental issues to increase our understanding of the photocatalytic process, knowledge that has proven crucial in our efforts to deactivate titanium dioxide for safe use in sunscreen lotions. In particular, Chapters 2 and 3 provide an experimental protocol to measure quantum yields Φ of processes in a heterogeneous medium to infer which of several photocatalyzed processes might be the more significant and efficient processes. Chapter 4 addresses the usage of and provides a kinetic description of the three turnover quantities: namely, turnover numbers (TON), turnover rates (TOR) and turnover frequencies (TOF). To the extent that they bear on the photocatalytic activity of a given material in heterogeneous solid/liquid or solid/gas systems, these parameters may prove useful in describing the photocatalytic activity of TiO_2 particulates.

Unlike the requirement needed to determine TOF, the quantities TON and TOR require knowledge of the number of active sites on the photocatalyst's surface. Most significantly, these turnovers appear to depend on the nature of the active state(s) of the catalyst, and hence on how the active centers are described. In heterogeneous photocatalysis a primary difficulty with describing the turnover rates and turnover numbers is the description of the number of surface active sites. It has become common practice to substitute this quantity by the specific surface area of the catalyst particle as obtained by the BET surface area procedure using the physical adsorption of nitrogen or argon at low temperatures. However, it must be emphasized that the BET surface area describes only the number of adsorption sites and not necessarily the number of catalytically active sites. Indeed, an active site will have a finite lifetime for various processes, and can be inactivated

through poisoning by impurities.

In as much as the key to change the activity of photocatalysts hinges on the number and type of surface active sites on metal oxide surfaces, we modified homemade TiO_2 colloids and several other titania specimens obtained from various commercial sources to produce photo-inactive TiO_2 systems. These modified specimens were characterized using different techniques. Their photo-activity was probed using the photooxidation of phenol, and damage caused to DNA plasmids, to human cells and to yeast cells (see e.g., Chapter 9).

Sunscreen TiO_2 specimens extracted from sunscreen were also characterized; they display some major surface physical changes.

2. MATERIALS AND METHODS

2.1. Characterization of Titanium Dioxide Extracted From Sunscreen Lotions

The titanium dioxide incorporated in a variety of sunscreen formulations available in North America and Europe was extracted using various organic solvents. Thus, 10 g of the suncream was added to 200 ml of the organic solvent (e.g., acetonitrile, acetone, and chloroform) to yield a slurry, which was then sonicated for about 5 min in a sonicator bath and centrifuged to remove the insoluble TiO_2 particulates. A fraction of the TiO_2 was recovered by centrifugation in pellet form; the rest was recovered by decantation from the supernatant after standing overnight. The pellet was dried at ambient conditions for a few days, typically yielding a fine white specimen; in a few cases the specimen had a yellowish

tinge to it.

The crystalline forms of the extracted specimens (anatase or rutile) were determined by X-ray diffraction using a Rigaku Denki Riny-1200 diffractometer at a lamp current of 40 mA and a scanning rate of 4.000°/min. The surface area was determined using the "Brunauer-Emmett-Teller" (BET) procedure utilizing a YASA IONICS Co Ltd instrument.

2.2. Homemade Specimens: Preparation of Titanium Dioxide Colloids

All chemicals were of reagent grade quality. The water was doubly distilled and deionized. Colloidal sols of titanium dioxide were prepared either by a low-temperature controlled hydrolysis of titanium (IV) chloride or by hydrolysis of titanium (IV) isopropoxide, according to the procedure reported by Lawless [8]. In a typical preparation by the hydrolysis titanium (IV) chloride, the $TiCl_4$ (Aldrich) was first doubly distilled to remove any extraneous impurities. Subsequently, 5.2 ml of the purified titanium tetrachloride was added dropwise to 200 ml of the doubly distilled water (**caution** !). To obtain colloids of different particle size, the water and the $TiCl_4$ were maintained at a certain temperature. Table 1 summarizes the temperature of both the $TiCl_4$ and water, together with the corresponding particle diameter of the resulting colloids. The resultant mixture was dialyzed {Viscase membrane, presoaked for 24 h in distilled water and then thoroughly rinsed prior to use} against doubly distilled water (replaced several times) overnight to remove the hydrochloric acid that is produced, leaving a suspension of ultra-fine titanium dioxide. Further drying of the suspension left an ultra-fine white powder.

Table 1. - Effect of temperature of $TiCl_4$ and water on the preparation of TiO_2 at different particle size.

Temperature of $TiCl_4$, (°C)	Temperature of Water, (°C)	Average particle diameter, (A°)	Sample Code
-20	0	23 ± 1	R20B
0	0	159 ± 21	R21B
24	24	281 ± 20	R22B

The smallest TiO_2 colloidal particles (dia. ~ 2.0 nm) were produced when the above procedure was used with $TiCl_4$ maintained at –20 °C and water at 0°C. Cooling was provided by a Model K4R Lauda constant temperature bath (50/50 mixture of ethylene glycol/water).

Titanium dioxide was also prepared by hydrolysis of titanium(IV) isopropoxide. A typical procedure [9] takes 125 ml of titanium (IV) isopropoxide (Aldrich) into a vigorously stirred 750 ml solution of doubly distilled water containing 5.25 ml of a nitric acid concentrate. The solution was then heated to ~ 80°C for 8 to 12 hrs under continued agitation, at which point the colloidal solution was nearly transparent. Removal of the solvent under vacuum at 100°C ultimately produced an ultra-fine powder of titanium dioxide; it was labeled RA1B.

2.3. Modification of Titanium Dioxide

Titanium dioxide specimens prepared either in our laboratory as described above or obtained from various commercial sources in North America and Europe were modified by a procedure suggested by Serpone [10]. Table 2 lists the names of the suppliers or the

manufacturers, and the corresponding code used to label the samples.

Table 2. - Coded modified and unmodified titanium dioxide specimens and source.

Sample Code*	Source	Sample Code*	Source
R8B, R8A	*Degussa P25*	R14B, R14A	*Baker & Adams*
R9B, R9A	*Hombikat*	R15B, R15A	*Aldrich, anatase*
R10B, R10A	*Bayer; rutile*	R16B, R16A	*Tioxide Canada*
R12B, R12A	*Sargent Welch*	R17B, R17A	*Puratronic*
R13B, R13A	*Fluka*	R19B, R16A	*Strem Chemicals*
Ra1B, Ra1A	$Ti[OCH(CH_3)_2]_4$	R21B, R21A	$TiCl_4$
R20B, R20A	$TiCl_4$	R22B, R22A	$TiCl_4$
R23B, R23A	*Aldrich, rutile*		

* B: before modification; A, after modification.

The characterization of modified specimens was carried out using different techniques; for example, by measurement of the BET specific surface area and by determining the changes in acidity of the titania samples in water. The temporal pH changes of both modified and unaltered specimens were measured by adding TiO_2 (loading of 2g L^{-1}) to doubly distilled water. Diffuse reflectance spectra were recorded on a Shimadzu UV-265 spectrophotometer fitted with a P/N 204-05857 integrating sphere reflectance unit.

2.4 Photocatalyzed Oxidation of Phenol

The ability of all these TiO_2 powders before and after modification to produce hydroxyl radicals was tested using phenol as an organic substrate to be catalytically oxidized

under exposure to UV light. Suspensions of each titania specimen were made up in distilled/ deionized water. The temporal course of the photodegradation of phenol by illuminated TiO_2 was monitored by high pressure liquid chromatography measuring the loss of phenol during irradiation.

Each TiO_2 specimen was illuminated at 0.05% w/v in 58 ml of phenol (200 μM in air-equilibrated aqueous media, pH = 5.5). The radiation source was either a solar simulator {Solarbox Milano; light flux between 310 and 400 nm ca. 48 mW cm^{-2}) or a 1000-Watt Hg/Xe lamp with a light flux between 310 and 400 nm of ca. 32 mW cm^{-2}. Appropriate aliquots (1 ml) of the irradiated dispersion were taken at various intervals and filtered trough a 0.1 μm membrane to remove the TiO_2 particles prior to analysis. The HPLC analyses were carried out employing isocratic procedures at ambient temperature on a Waters 501 liquid chromatograph equipped with a Waters 441 detector set at 214 nm and a HP 3396A recorder. The column was a Waters μBONDAPAK C-18 reverse phase and the mobile phase was a 50:50 mixture of methanol (BDH Omnisolv grade) and distilled/deionized water. The retention time of phenol in the HPLC chromatogram under the conditions used was 5 min.

3. RESULTS AND DISCUSSION

3.1. Titanium Dioxide in Sunscreen Lotions

Extraction of TiO_2 from sunscreen lotions with organic solvents removed all the soluble organic compounds leaving the pure TiO_2 powder and any other inorganic compound that may have been used as a coating or as co-physical sunscreen agent. Those sunscreen

lotions that contain aluminum hydroxide or zinc oxide are indicated in Table 3. The powders obtained after extraction from the sunscreen samples SN1, SN4, and SN9 had an off-white tinge to them; they were not the pure white expected of pure TiO_2 specimens. Iron oxides are sometimes used to improve the color-cosmetic acceptability in some lotions and suncare creams.

Titanium dioxide specimens extracted from several suncreens were characterized by their specific surface area, and anatase/rutile content as indicated in Table 3. X-ray diffraction patterns for samples SN2 (100% rutile) and SN4 are illustrated in Figure 2.

The data in Table 3 show that the specific surface area of these specimens ranges from a low of 1.49 $m^2 g^{-1}$ for the sample SN4 to a high of 70.40 $m^2 g^{-1}$ for the SN11 specimen. There is no clear correlation between the specific surface area and the photodegradation of phenol. Evidently, this photoactivity is not completely due to the surface area of the particles, but to other parameters as well, such as the anatase/rutile content, the presence of coatings on the TiO_2 particles, and the co-presence of other physical sunscreens. Since, the exact quantity of these extraneous compounds is unknown, their role in the photoactivity of titanium dioxide is unclear. For instance, specimen SN10 is somewhat efficient in the photodegradation of phenol relative to specimens SN1 to SN9, yet SN10 is predominantly rutile, its specific surface area is 35,1 $m^2 g^{-1}$, and contains ZnO another photoactive catalyst. However, comparison of the SN10 sample with the standard pristine rutile specimen, which has a smaller surface area of 6.62 $m^2 g^{-1}$, shows that the latter is more photocatalytically active toward phenol oxidation. Specimen SN1 shows the smallest

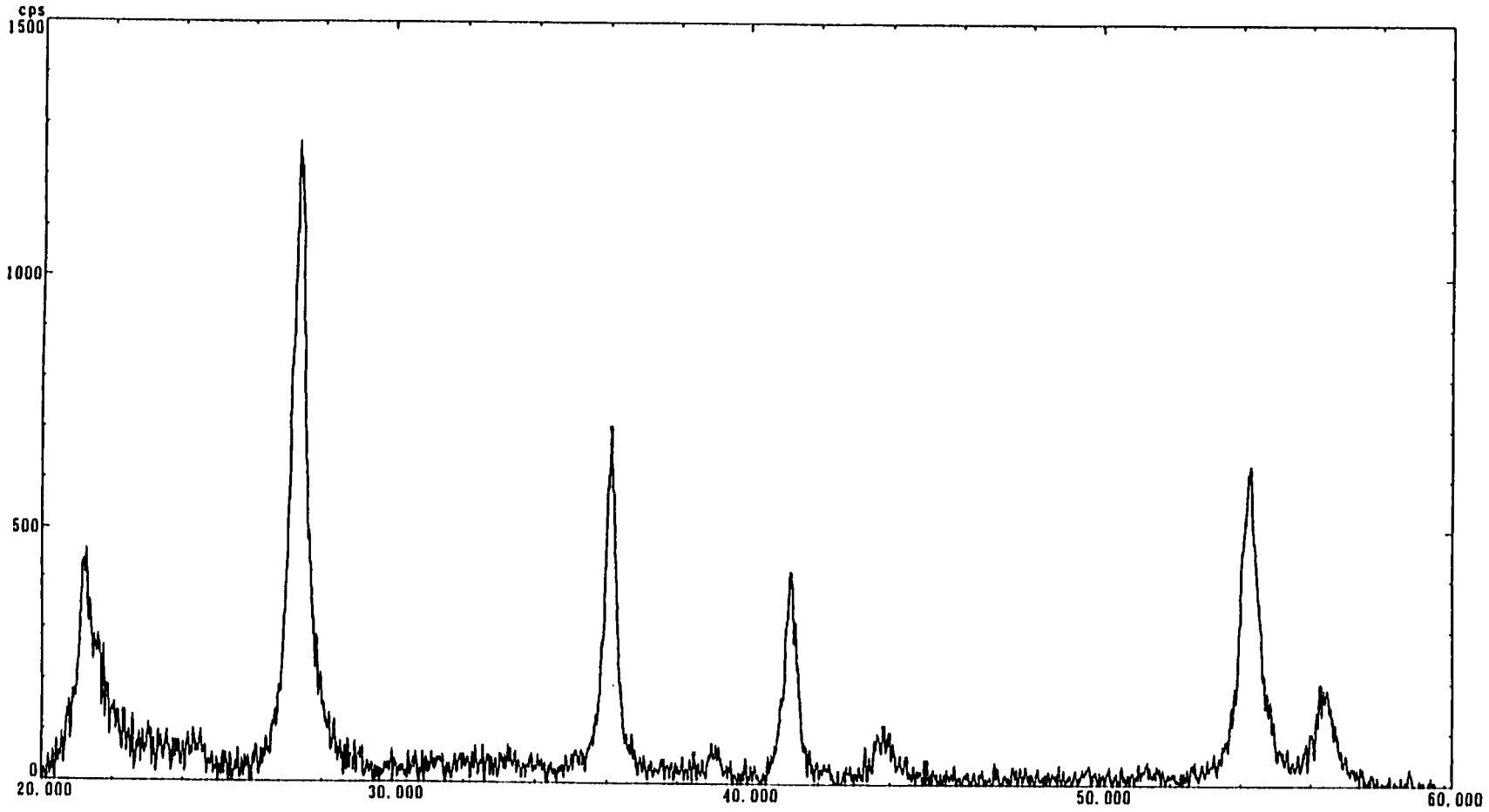

Figure 2A. - X-ray diffraction pattern for sunscreen titania specimen SN2 consisting of 100% rutile.

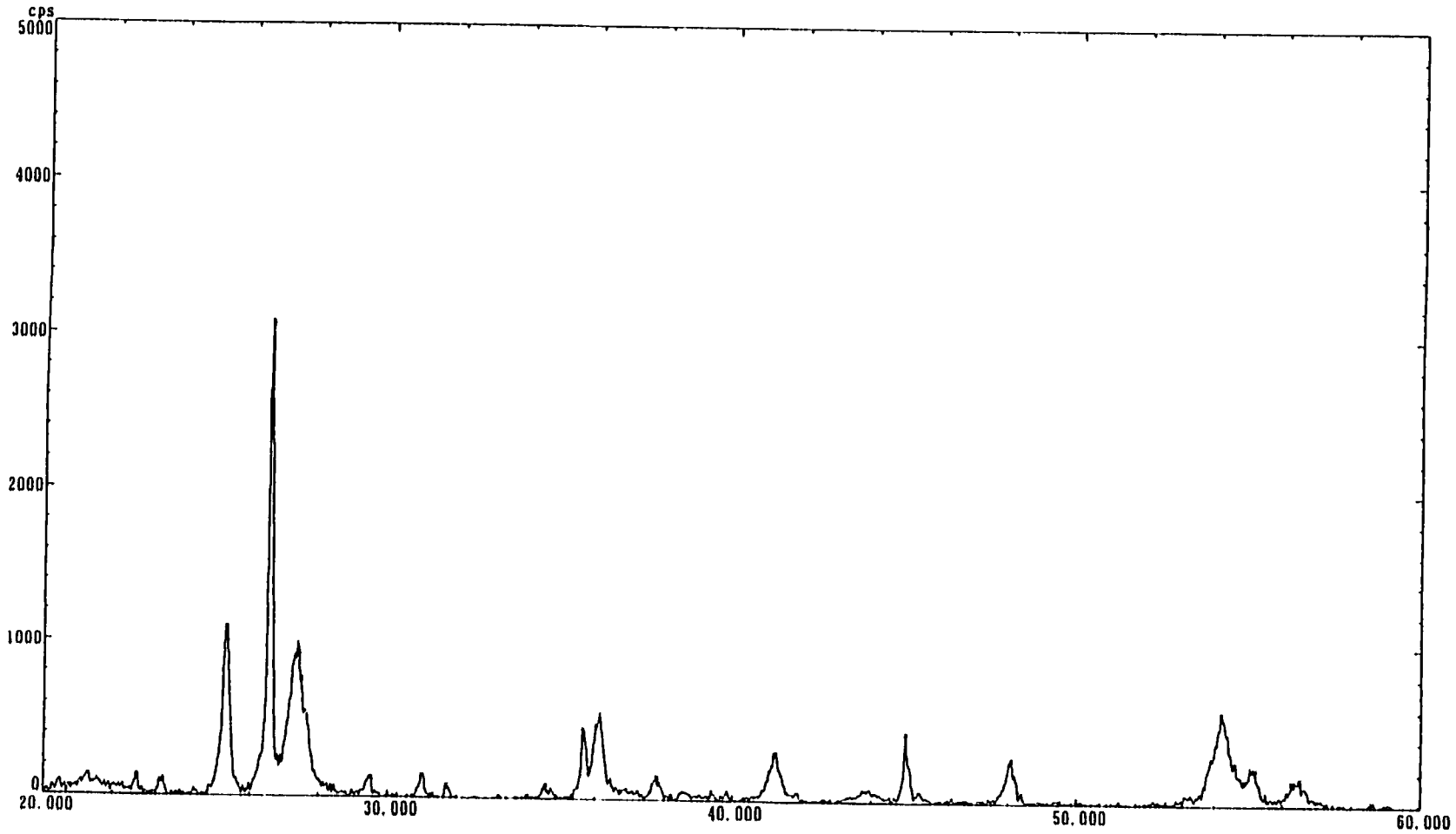

Figure 2B. - X-ray diffraction pattern for the sunscreen titania specimen SN4 consisting of 54% anatase and 46% rutile.

Table 3. - Summary of physical characterization of TiO_2 specimens extracted from sunscreen lotions and relative rates of phenol photodegradation.

Sunscreen Sample	SPF	Anatase/ rutile (%)	Surface area ($m^2 g^{-1}$)	Coating	Relative rates
SN1	19	50/50	3.14	$Al(OH)_3$	1.0
SN2	25	0/100			2.8
SN3	25	0/100			5.2
SN4	25	54/46	1.49		5.2
SN5	15+	0/100			10.4
SN6	20+	100/0			17.6
SN7	30	0/100		$Al(OH)_3$	22.7
SN8		100/0			53.3
SN9	15	50/50	25.3	ZnO	134
SN10	25	0/100	35.1	ZnO	180
SN11		0/100	70.4		
anatase rutile		100/0 0/100	7.76 6.62		3803 427
TiO_2 Degussa P25		75/25	55		

photoactivity for phenol photodegradation among the several sunscreen TiO_2 specimens examined; it consists of 50% rutile and 50% anatase, its specific surface area of 3.14 $m^2 g^{-1}$ is fairly small, and is coated with a layer of $Al(OH)_3$.

A water resistance test was performed on the original sunscreen lotions and on the TiO_2 extracted samples to examine the hydrophilic characteristics. Results showed that all specimens are highly hydrophilic.

3.2 Photoactivity of Modified Specimens Against Photooxidation of Phenol

This methodology to inactivate titanium dioxide can be applied to any metal-oxide specimen. Figure 3 illustrates the kinetic behavior of these specimens before and after inactivation of the particle surface for the photooxidative degradation of phenol. Sample R10 shows greater photoactivity before modification than after. The photooxidation of phenol was carried out using the solar simulator (Solarbox Milano) as the UV radiation source. The results indicate clearly that the modification method achieved the desired goals, since the rate of photodegradation of phenol has been reduced consistently and dramatically for many of the specimens.

Specimen R15B was the most photoactive of the specimens illustrated in Figure 3. Note the dramatic decrease in photoactivity after passivation of the particle surface. Specimen R13 displays the largest relative drop in the rate of photooxidation of phenol, followed by the R15, R16, and R12 systems.

3.3 Modified Titanium Dioxide Specimens

Modified titanium dioxide specimens showed a considerable decrease of photoactivity as evidenced by the photooxidation of phenol. These specimens also demonstrated a reduced photoactivity against DNA plasmids, human cells and yeast cells (see Chapter 9). This decrease in activity is the result of passivation of the catalyst surface subsequent to the procedure used. If these modified titania specimens are to serve as safe physical sunscreen to block both UVA and UVB radiation, it is important that the modified

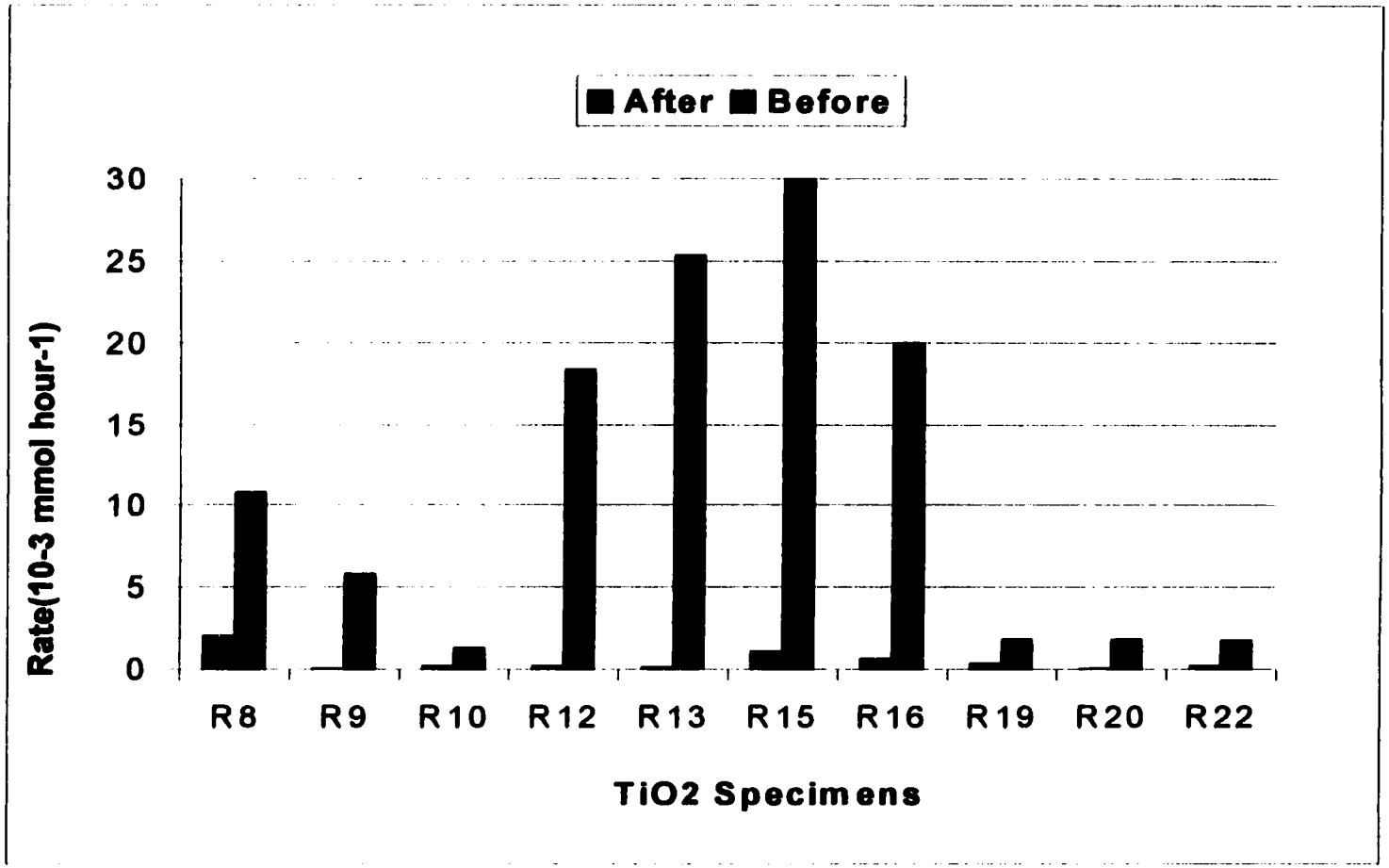

Figure 3. - Rates of photodegradation of phenol by several TiO_2 specimens before and after modification; radiation source was the solar simulator (solarbox)

specimens retain the spectral characteristics of the original sample.

Figure 4 illustrates the diffuse reflectance spectra of the R12 and R15 titania specimens before and after passivation of the particle surface. In both cases, the original R12B (Figure 4A) and R15B (Figure 4B) samples block UVA/UVB radiation efficiently at all wavelengths shorter than ca. 400 nm. After surface passivation, the onset of attenuation of the incident radiation is red-shifted to about 440 nm thus making the modified samples even better sunlight physical filters. The corresponding R23 specimen shows only a slight red-shift of the onset of attenuation after modification (Figure 5A). For this latter sample, originally 100% rutile, passivation of the particle surface brings about no change in the specific surface area of the specimen (ca. 6 $m^2 g^{-1}$). By contrast, the physicochemical passivation of the particle surface of the R8 titania specimen shows a reduction in the specific surface area from about 55 $m^2 g^{-1}$ to ca. 9.7 $m^2 g^{-1}$. Evidently, different specimens behave differently subsequent to the modification. Figure 5B illustrates the change-in-attenuation spectra (i.e. difference diffusion spectra) for R15 (red spectrum) and for the R23 sample. It is interesting to note that the difference spectrum is maximal at 3.2 eV for R15 which corresponds to the bandgap for an anatase titania system, whereas for the R23 specimen the maximum in the difference spectrum is seen at ca. 3.02 eV, which is the bandgap of rutile titanium dioxide.

The hydrophilic characteristics of the specimens are altered by the physicochemical surface passivation for many of the systems examined. This particular change is no doubt connected to surface changes that led to variations in either the number of or the type of

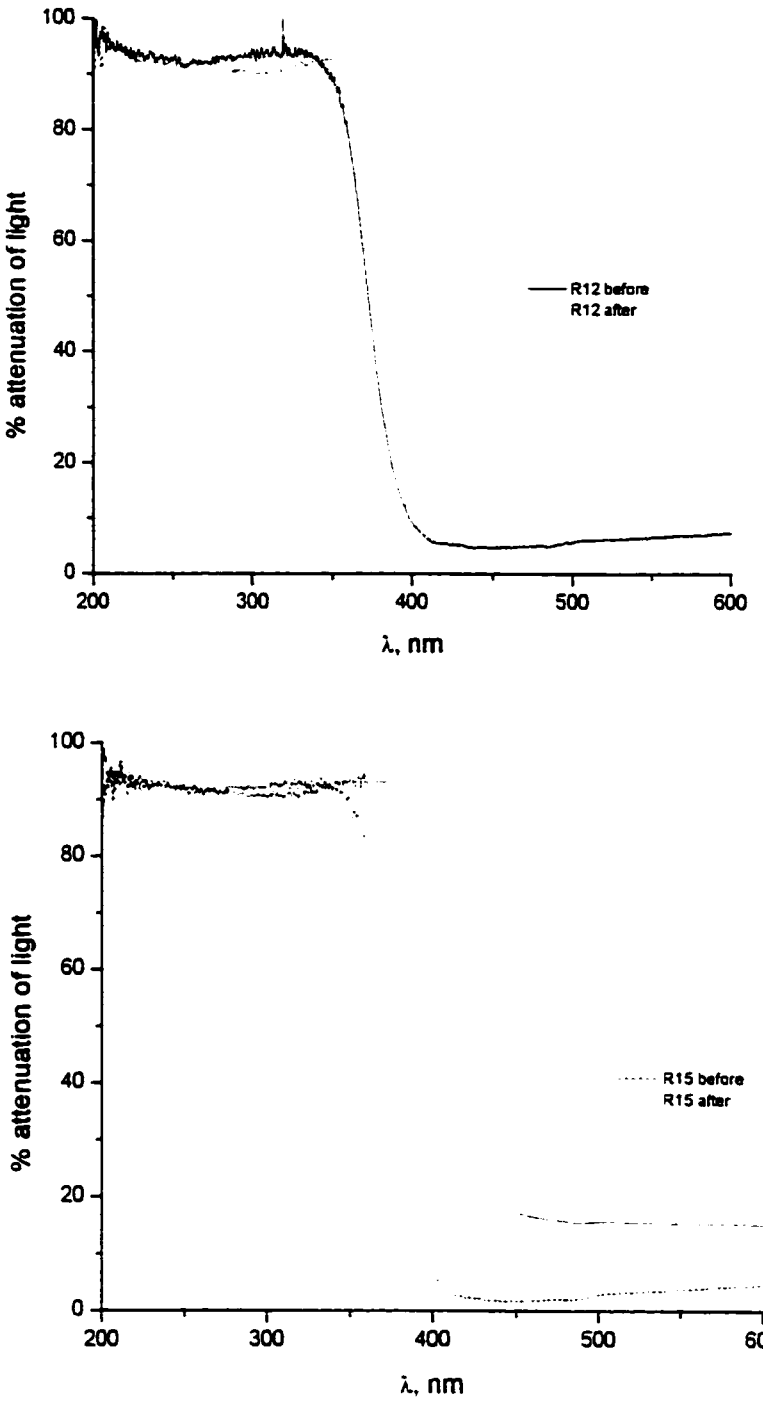

Figure 4. - Percent light attenuation by the (A) R12 and (B) R15 titania specimens before and after modification of the particles.

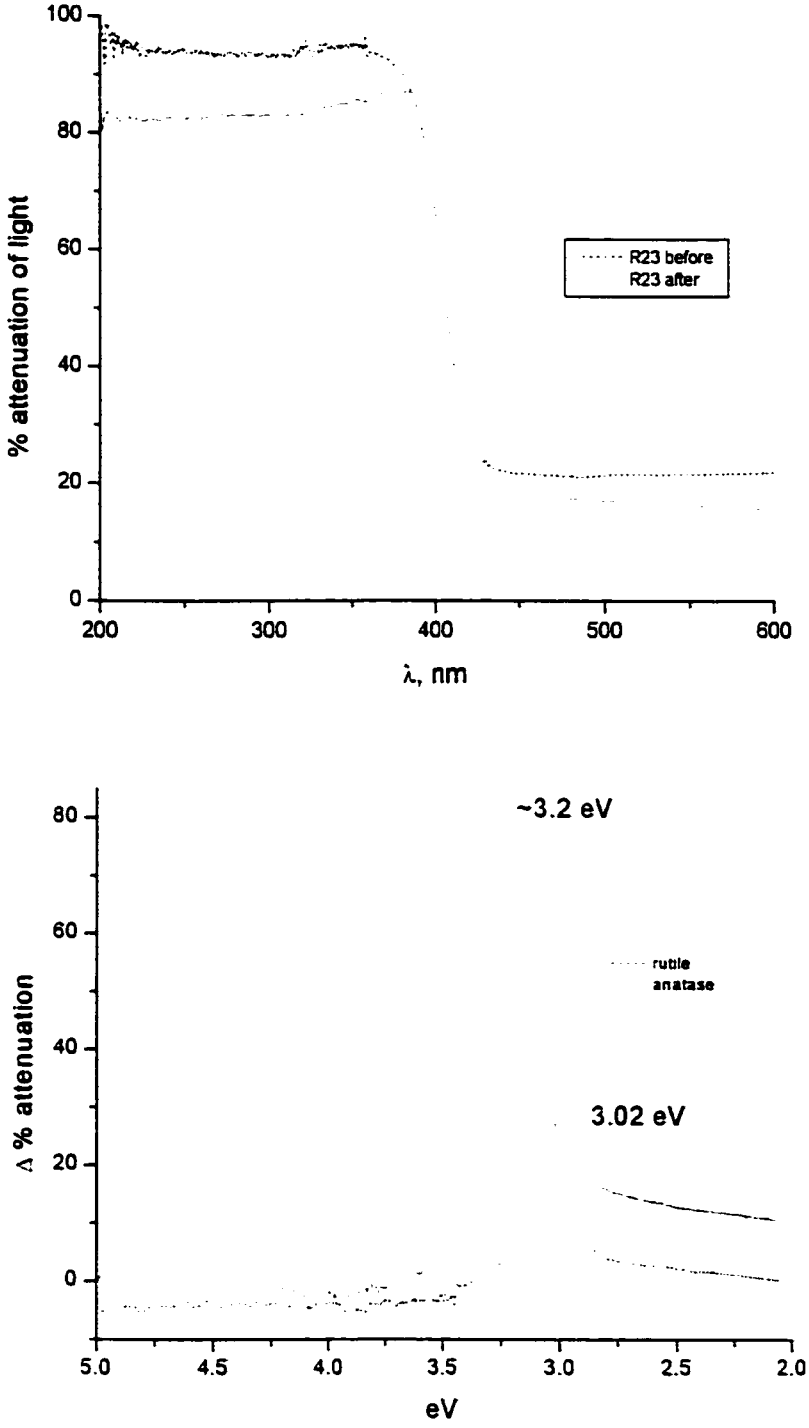

Figure 5. - (A) Percent light attenuation by the R23 titania specimen before and after modification. (B) Difference attenuation spectra for the R15 TiO_2 sample, and for the R23 titania specimen before and after treatment.

reactive centers present on the surface of the catalyst. Indeed, a change in hydrophilicity due to a change in the number of active centers present on the surface was confirmed by examining the change in surface acidity of the photocatalyst systems. The pH of a 2 g L^{-1} slurry of all TiO_2 specimens was altered with the modification.

Figure 6 shows that specimens R8A and R8B possess different surface characteristics as exemplified by the temporal variation in pH. On addition of the TiO_2 specimen to water, the pH varied significantly for R8B reaching a stable state after only a few minutes. This pH variation is probably the result of adsorption/desorption equilibria being established between the surface groups and the water molecules. Moreover, such changes in surface acidity may also be connected to variations in the nature of the active sites present at the particle surface.

Figure 7 depicts the pH changes for the R15B and R15A species. Addition of R15B to water rapidly leads to an increase in pH from ca. 5.6 to a maximal pH of about 7.0 after 25 s. This is followed by a decrease to 6.6 after 60 s, and finally reaches an equilibrium state after about 180 s. By contrast, the R15A specimen displays less dramatic pH changes increasing (as it were) from an initial pH of 5.6 (pH of water) to stabilize at about pH ca. 6.8 after 160 s. These pH changes confirm the complex nature of the particle surface, an issue well known those actively engaged in unraveling the mysterious nature of metal oxide surfaces.

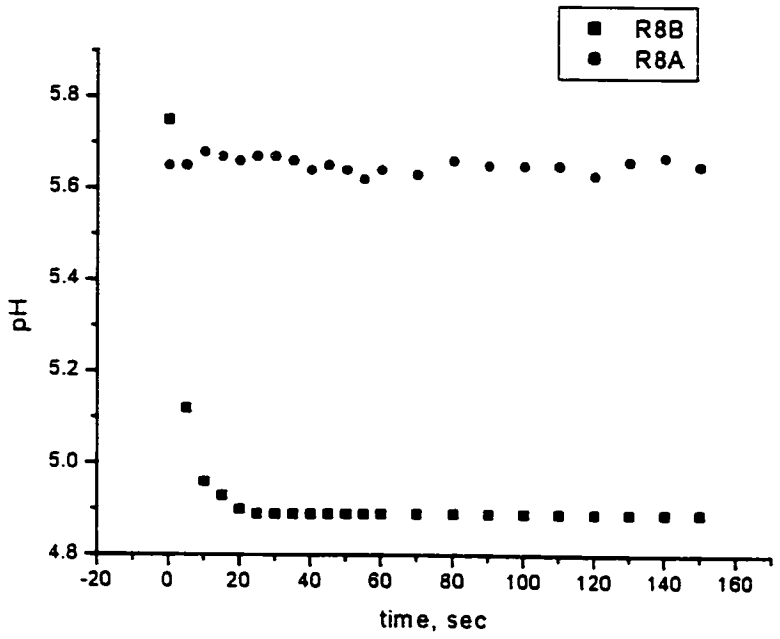

Figure 6. - Change in surface acidity of R8B and R8A specimens.

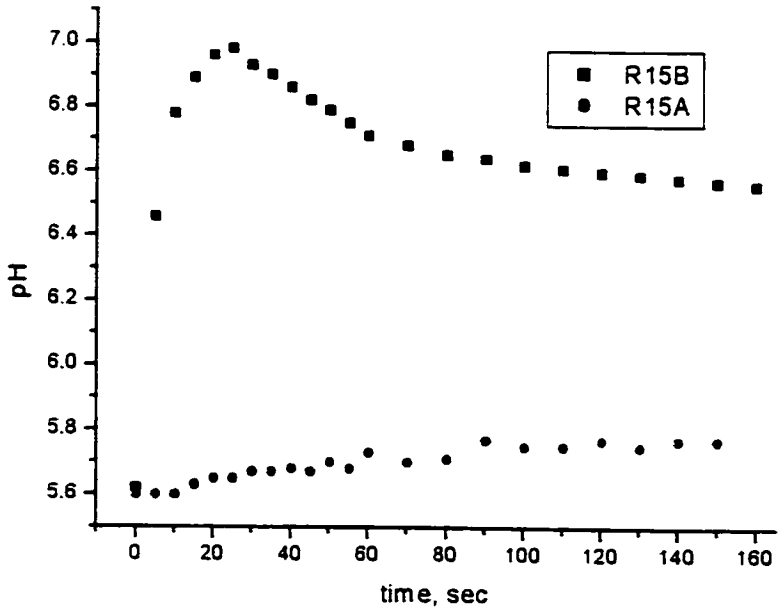

Figure 7. - Change in surface acidity of R15B and R15A specimens (2g L^{-1}).

4. CONCLUDING REMARKS

Titania specimens extracted from sunscreen lotions have been characterized by X-ray diffraction, by BET surface area measurements, and by assessing their photocatalytic activity against phenol photooxidation. The photoactivity of a given specimen is the result of several factors, not least of which are the crystalline forms of TiO_2 and the specific surface area, as well no doubt the number of OH^- groups on the particle surface which will have an effect on the adsorption/desorption properties of the particle surface.

Many other parameters play important roles in the photoactivity of sunscreen TiO_2, such as the presence and the amount of other catalysts (e.g. ZnO) and other inorganic coatings $Al(OH)_3$. Evidently, the coating does not inactivate TiO_2, but in certain samples the activity is increased. This is in keeping with the findings by Anderson and Bard [11], who reported an increase in photoactivity of titanium dioxide in the presence of silica SiO_2.

Specimens intended to be inactivated for potential use in sunscreen formulations were also characterized. As demonstrated in Chapter 9, the modified specimens reduced dramatically the damage inflicted to DNA by the harmful UV radiation and by the titania specimens currently used as physical filters in suncare products. Nonetheless, additional experiments need to be done to understand the changes that have been made to the particle surface. Two possible changes may have occurred after modification: (i) a change in the number of active centers, or in the type or nature of the active centers, and (ii) a change in the number of OH^- groups on the particle surface. Since adsorption/desorption events have been described as an important factor in heterogeneous photocatalysis, any change in the

surface properties that may affect adsorption/desorption characteristics of the specimens will influence the photoactivity of titanium dioxide, and by extrapolation any metal oxide.

5. REFERENCES

[1]. F.A. Cotton and G. Wilkinson, *Advanced Inorganic Chemistry*, 5th Edition, Wiley-Interscience, New York, 1988.

[2]. W. Huckel, *Structural Chemistry of Inorganic Compounds*, vol. II, Elsevier, Amesterdam, 1951, p. 678.

[3]. (a) E.A. Barringer and H.K. Bowen, *Langmuir*, 1, 420 (1985).

(b) J. Moser, *Ph.D. Thesis*, Ecole Polytechnique Federale de Lausanne, Lausanne, Switzerland, 1986.

[4]. N. Serpone, D. Lawless, and R.F. Khairutdinov, *J. Phys. Chem.*, **99**, 16646 (1995).

[5]. (a) A. Emeline and N. Serpone, *J. Phys. Chem.*, submitted February, 2001.

(b) A.V. Emeline, A. Salinaro and N. Serpone, *J.Phys.Chem.B*, **104**, 11202 (2000).

(c) N.S. Andreev, A.V. Emeline, V.A. Khudnev, S.A. Polikhova, V.K. Ryabchuk, and N. Serpone, *Chem.Phys.Letters*, **325**, 288 (2000).

(d) A.V. Emeline, V. K. Ryabchuk, and N. Serpone, *J.Photochem.Photobiol. A: Chem.*, **133**, 89 (2000).

(e) A.V. Emeline, G.N. Kuzmin, D. Purevdorj, V.K. Ryabchuk and N. Serpone, *J.Phys.Chem. B*, **104**, 2989 (2000).

(f) N. Serpone, A. Salinaro, A.V. Emeline and V. Ryabchuk, *J.Photochem.Photobiol. A:Chem.*, **130**, 83-94 (2000).

(g) A.V. Emeline, G.V. Kataeva, V.K. Ryabchuk, and N. Serpone, *J.Phys.Chem.*, **103**, 9190 (1999).

(h) A.V. Emeline, E.V. Lobyntseva, V.K. Ryabchuck, and N. Serpone, *J.Phys.Chem.*, **103**, 1325 (1999).

(i) A.V. Emeline, V.K. Ryabchuck, and N. Serpone, *J.Phys.Chem.*, **103**, 1316 (1999)

(j) A.V. Emeline, A.V. Rudakova, V.K. Ryabchuk, and N. Serpone, *J.Phys.Chem., B*, **103**, 10906 (1998).

(k) A.V. Emeline, S.V. Petrova, V.K. Ryabchuck, and N. Serpone, *Chem. Mater.*, **10**, 3484 (1998).

(l) A.V. Emeline, G.V. Kataeva, A.S. Litke, A.F. Rudakova, V.K. Ryabchuck, and N. Serpone, *Langmuir*, **14**, 5011 (1998).

[6]. (a) N. Serpone, "A Decade of Heterogeneous Photocatalysis in our Laboratory of Pure and Applied Studies in Energy Production and Environmental Detoxification", *Res. Chem. Intermed.*, **20**, 953 (1994).

(b) N. Serpone, in *Kirk-Othmer Encyclopedia of Technology*, Wiley-Interscience. New York, **18**, 820 (1996).

[7]. N. Serpone and E. Pelizzetti, in "*Photoconversion of Solar Energy - Photochemical and Photoelectrochemical Approaches*", M.D. Archer and A.J. Nozik, Eds., Imperial College Press, London, **2001**, volume III, Chapter **16.**

[8]. D. Lawless, *Ph.D. Thesis*, Concordia University, Montreal (Quebec), Canada, 1992.

[9]. C. Bignozzi, University of Ferrara, personal communication to N. Serpone, 1997.

[10]. N. Serpone, personal communication, 1997.

[11]. (a) C. Anderson and A.J. Bard, *J. Phys. Chem.*, **99**, 9882 (1995).

(b) C. Anderson and A.J. Bard, *J. Phys. Chem.*, **101**, 57 (1997).

Chapter 9

EFFECT OF UVA/UVB ILLUMINATED TiO_2 SPECIMENS ON PLASMID DNA , HUMAN CELLS, AND YEAST CELLS

Summary

Photoactive TiO_2 specimens present in sunscreen lotions cause damage to both DNA plasmids and to whole human skin cells. Considering that TiO_2 particles can reflect, scatter and absorb all the UV wavelengths, and have high SPF numbers and exceptional cosmetic acceptability, the present chapter examines various TiO_2 specimens untreated and treated by a modification procedure that makes them less photoactive toward the photooxidation of phenol (see e.g., Chapter 8). Untreated titania specimens significantly damage DNA plasmids, human cells, and yeast cells as demonstrated herein. By contrast, the damage is attenuated considerably by the modified titania samples, thereby making them safer for use in sunscreen lotions, as they also completely retain their UVB/UVA absorption characteristics.

1. INTRODUCTION

Mineral compounds have been used in such cosmetics as foundations, powders, eye-shadows and pencils. Titania, TiO_2, was reported as a sunscreen agent as far back as 1952 [1]. The ability of a mineral to be used as a physical filter in a sunscreen lotion is determined by two characteristics: the reflecting property of the inorganic filter and its cosmetic acceptability. The principal feature of physical filters is to block the UV light over the whole UV range through reflection and scattering, which in turn are determined by the intrinsic refractive index, the size of the particles, dispersion in the cream base, and by the film thickness. A physical sunscreen which functions well at reflecting light, however, is opaque and white on the skin and consequently is not acceptable for cosmetic use.

According to Fresnel's rules, the particle gives optimal reflection when its diameter d is half the wavelength of irradiation, $\lambda/2$, indicating that particle sizes for standard TiO_2 in the range 200–500 nm are best at reflecting visible light. Unfortunately, they have the disadvantage of being opaque on the skin. Efforts to improve cosmetic acceptability have included decreasing the particle size of TiO_2, and adding a brown tinge using iron oxide (Fe_2O_3) pigments to improve the suncream appearance. Smaller particles, or so-called *micronized* (20–50 nm) metal oxide particles, have been used in cosmetic products since 1989 [2]. They are easily incorporated in emulsions, are transparent to visible radiation, and reflection from the particle surface is minimal. For these smaller particles the mechanism of light attenuation is due mostly to Rayleigh scattering for which the intensity of scattered light follows the power law $I_s \sim \lambda^{-4}$. The smaller particles scatter the UVB and UVA wavelengths

to a greater extent than the longer visible light wavelengths. However, TiO_2 also absorbs UVB and UVA light significantly [3].

In its 1999 monograph, the US Food and Drug Administration (FDA) regulated that the term sunblock as used for titanium dioxide in product labeling and promotional flyers should no longer be used. The term "sunblock" erroneously misleads consumers into believing that the product blocks all of the damaging sunlight UV rays.

On absorption of UV light, titania particles catalyze formation of superoxide radical anions ($O_2^{-}\bullet$) and hydroxyl radicals ($\bullet OH$) that can initiate oxidations [4]. The photoactivity of TiO_2 is set by a complex combination of factors, the most critical of which is the very nature of the surface [5], a problem still under active debate and investigation.

An evaluation of the safety of TiO_2 [6] concluded that titania is not mutagenic and hence cannot damage DNA. However, the same study failed to report on the effects of sunlight in the presence of titanium dioxide, or on the particular preparations of TiO_2 that are used in sunscreens. This aspect is significant because sunscreen TiO_2 particles are often coated with compounds (e.g. alumina, silica, zirconia), which in some instances may enhance the photocatalytic activity of TiO_2. As early as 1986, Anpo and coworkers [7] reported the enhancement of activity of TiO_2 in the presence of SiO_2, later confirmed by Anderson and Bard [8], and by Xu et al [9].

We saw earlier that irradiated TiO_2 sunscreen specimens yield hydroxyl radicals that initiate the photodegradation of phenol. Consistent with this, titanium dioxide specimens extracted from sunscreen lotions produced single- and double-strand breaks on plasmid

DNA, and also on nuclei of whole human skin cells. The potential for DNA damage associated with using titanium dioxide (and zinc oxide) as a physical filter in suncare products is real (see e.g., Chapter 7).

A worrying trend in sun protection is the increasing use of physical UV filters (titanium dioxide (TiO_2) and zinc oxide (ZnO), especially in suncare products for children and people with sensitive skin. This increased use of physical sunscreens is due partly to their low potential for producing irritant reactions, but also to the cosmetic efficacy of these materials. With titanium dioxide, cosmetic chemists have formulated products with high Sun Protection Factors (SPF) using only this single active ingredient. Titanium dioxide gives impressive SPF numbers when used in combination with organic sunscreen agents, as well as displaying with UV absorbers a broad absorption spectrum in the UVB (290–320 nm) and UVA (320–400 nm) region [10].

Formulators have also incorporated microfine zinc oxide and, more commonly, microfine titanium dioxide into sunscreen preparations to avoid the decrease of SPF that can occur from the photoinstability of organic UV filters. The lack of photostability of UV organic filters is a common problem for these UV organic absorbers (see Chapter 10). The photoinstability is enhanced when two or more organic ingredients are combined [11]. Related to this problem, the final FDA monograph on the over-the-counter (OTC) sunscreen products provides a list of permitted combinations of approved ingredients and gives the maximal concentration of each ingredient in sunscreens [12]. A most controversial OTC ruling issued by the US Food and Drug Administration was the Final Monograph on:

Sunscreen Drug Product for Over-the-Counter Human Use. The ruling first appeared on August 25, 1978. A tentative final monograph was issued some 15 years later in 1993, and the final monograph was released on May 21, 1999, with many issues remaining unresolved. To be classified in Category I as defined by the FDA [12], all the sunscreens must be tested according to a methodology described fully in the final monograph. These test procedures are based on such factors as the SPF, allergenic tests, and the minimal erythema dose (MED) response of the skin. In effect, the efficiency of a sunscreen is usually tested more with respect to its macroscopic ability to prevent skin erythema and sunburns, than at the molecular and cellular level to ascertain protection against the risk of skin cancer.

To the extent that TiO_2 is photoactive and DNA damage on human skin may follow, sunscreen manufactures must consider the possibility of improving the safety aspect of TiO_2 as a physical sunscreen. Our strategy was to modify and examine TiO_2 samples using a variety of *in vitro* and *in vivo* skin models. The goal of these studies is part of an ongoing effort to prepare a new OTC titania sunscreen product that would be photocatalytically inactive, but one that would provide protection against the damaging UV sunlight radiation. This Chapter explores some ten or so photo-inert TiO_2 specimens for possible implementation in sunscreen lotions. Samples of TiO_2 from several suppliers were modified by a procedure suggested by Serpone [13]; their activity before and after modification are compared using the well characterized photooxidation of phenol as the test reaction (see Chapter 8).

The Chapter also evaluates photo-damage to DNA using various *in vitro* and *in vivo*

skin models and caused by illuminated TiO_2 samples before and after modification. The plasmid nicking assay is employed to investigate whether illuminated TiO_2 inflicts single- and/or double-strand breaks on naked DNA *in vitro* and the extent of the damage induced by the inert TiO_2. The yeast *Saccharomyces cerevisiae* was used to evaluate the cytotoxicity and genotoxicity of TiO_2 specimens on keratinocyte human skin cells to establish *in vivo* whether any observed reactions on naked DNA occurs within the cellular environment. The comet assay was the chosen method to investigate whether this type of DNA damage can be inflicted on human skin cells. There are several methods for measuring strand breaks within cells. The single cell gel electrophoresis assay (comet assay) presents several advantages. First, it is a very sensitive technique with a low detection limit of 0.032 Gy (1 strand break per 2×10^{10} Daltons of DNA) [14], and second it provides a visual method for assessing DNA strand breaks in single cells.

2. EXPERIMENTAL SECTION

2.1 Illumination of DNA in Vitro (Plasmid Nicking Assays)

2.1.1 Materials

Titanium dioxide specimens were tested by biological/biochemical assays. One of these was plasmid nicking assays. This test detects inflicted DNA damage by determining the single- and double-strand breaks effected on DNA by illuminated titanium dioxide. In a plasmid nicking assay, the DNA may exist in three different forms: supercoiled (S), relaxed (R), and linear (L) forms. When DNA damage occurs the number of supercoiled DNA

plasmids diminishes and the relaxed or linear forms arising, respectively, from single- and double-strand breaks appear. Calculation of the intensity of each form *versus* irradiation time provides an estimate of the extent of DNA damage.

All chemicals used for the nicking assays were BDH analytical grade or equivalent. Water (milli-Q) was sterilized by autoclaving at 121 °C and 15 lbs in^{-2} pressure for 15 min prior to use. All glass pipettes, plastic pipettes, and tubes were also sterilized by this method prior to use. DNA was the plasmid pBluescript II SK^- (Stratagene) prepared and analyzed on agarose gels according to the method of Maniatis et al [15]. The *Escherichia coli strain* contained the desired pBluescript II SK^- plasmid; it was prepared and kindly supplied by the Department of Biochemistry, Oxford University (UK).

2.1.2 Methodology

Estimation of the concentration of plasmid DNA prior to use was done using a Beckman DU62 spectrophotometer by measuring the absorbance of the DNA solution at 260 nm (A_{260}) and 280 nm (A_{280}). When the ratio A_{260}/A_{280} is greater than 1.8, the concentration can be estimated using the equation:

$$\text{Concentration } (\mu g\ ml^{-1}) = 50 \times A_{260} \qquad (1)$$

The plasmid DNA so prepared was illuminated in the presence of the different titanium dioxide specimens. Each TiO_2 sample was suspended by sonication and vortexed in water at different concentrations (4%, 2%, 1%, 0.1% w/v) to obtain different final

concentrations of TiO_2. A 25 µl aliquot of each sample was added to 25 µl of plasmid (2–3µg DNA) in 100 mM of sodium phosphate (pH = 7.4). The mixture was then illuminated as droplets (50 µl) on Eppendorf caps placed on a brass block embedded in ice to conserve the DNA at 0°C. Illumination was carried out on a rotating plate to ensure homogeneous irradiation of the samples. Afterward, 10 µl of the sample was collected at appropriate time intervals. The solar simulator [16] consisted of a 250-Watt ozone-free lamp, a WG 320 filter and a quartz lens resulting in an estimated photon fluence between 300 and 400 nm of 12 W m^{-2}. A condensing lens was placed between the lamp output and the dichroic mirror to increase the intensity of light reaching the droplets. Measurement of the lamp output of the solar simulator (see Figure 1 for the nature of lamp output) was done using a cosine diffuser connected by a fiber optic cable to a double grating, scanning spectroradiometer (Bentham Instruments Ltd., Reading, UK). The lamp output was constant for all samples. The bandwidth of the monochromator was fixed at 1 nm; wavelength calibration was achieved using a CL6-H deuterium lamp, which was previously calibrated against NPL reference lamps. The operation of the spectroradiometer was controlled using a Viglen desktop computer.

After illumination the DNA was analyzed by agarose gel electrophoresis. Agarose gels were prepared according to the protocol of Maniatis et al [15]. Gels consisted of 1% w/v of agarose and 0.5x TBE buffer (44.5 mM Tris-HCl; pH = 7.5; 44.5 mM boric acid, and 1.25 mM of EDTA) heated until dissolved, then cast into a slab gel tray and allowed to set. Electrophoresis was performed in GNA 100 or GNA 200 gel tanks (Pharmacia) at 5 V cm^{-1}

(A)

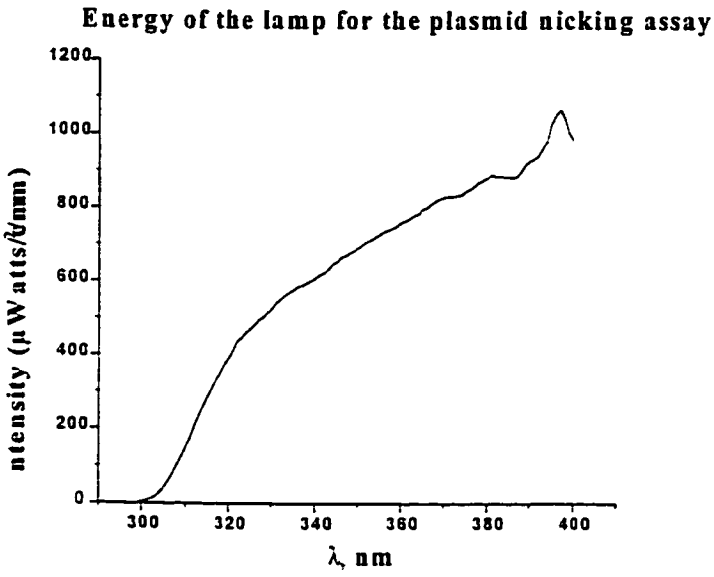

(B)

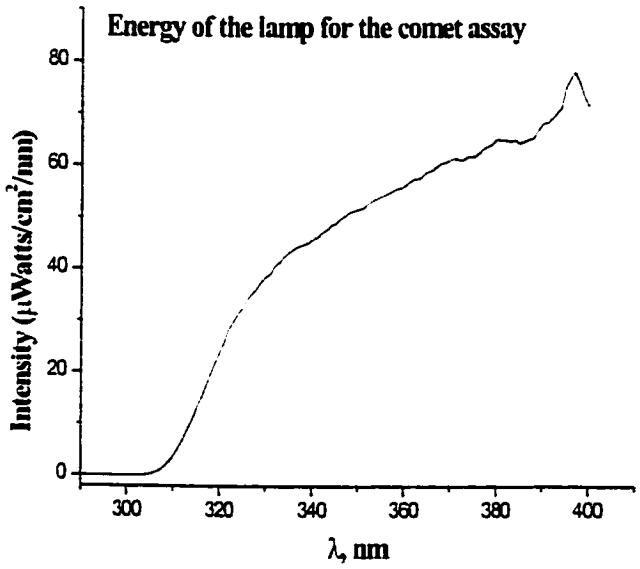

Figure 1. - Lamp spectral output used for (A) plasmid nicking assays, and (B) for comet assays as measured by a spectroradiometer.

for regular gels in 0.5xTBE buffer. The gels were then incubated at ambient temperature for 45 min in 0.5 x TBE buffer containing 0.3 μg of ethidium bromide per milliliter to stain the DNA. Stained DNA was viewed on a 313 nm UV trans-illuminator and photographed on a Polaroid 665 positive/negative instant pack film. Relaxed DNA standards were prepared by depurinating DNA plasmids at pH 4.8 in 25 mM sodium acetate and at 70°C for 20 min. Subsequently, cleavage was done at pH 8 with exonuclease III at 37°C in a solution of 50 mM Tris-HCl, 5 mM of $CaCl_2$ (the Ca^{2+} ions inhibit exonuclease but not cleavage at apurinic sites), and 0.2 mM DTT. Linear standards were obtained by cutting the plasmid with *Eco*RI.

To compare the concentration of DNA in the three forms (supercoiled, relaxed and linear) present in each lane of the agarose gels, it was necessary to scan the photograph negatives of the plasmid nicking gels with a model GS-670 imaging densitometer (Bio-Rad). When DNA damage occurs the number of supercoiled DNA plasmids decreases by a first order process. Every experiment was repeated at least three times. The graphical data reported here are based on the average of the experimental results.

2.2 *Illumination of Yeast Saccharomyces Cerevisiae (Droplet Test)*

2.2.1 Materials

All chemicals used for this test were BDH analytical grade or equivalent. Water (milli-Q), solid media, liquid media and solutions were all sterilized by autoclaving at 121°C and at 15 lbs in^{-2} pressure for 15 min prior to use. All glass pipettes and Petri dishes were also sterilized by this method prior to use.

The yeast strain *Saccharomyces cerevisiae* was the XD83 type, kindly supplied by Dr. John Knowland (Department of Biochemistry, Oxford University, UK).

Yeast cells were grown in the dark in liquid YEPD medium {1 liter of milli-Q Water, 10 g of yeast extract, 10 g of bactopeptone, and 20 g of glucose} harvested in exponential phase overnight. The exponential phase was reached when the cells counted by a hemocytometer was in the range between 1 x 10^6 and 1 x 10^7 cells ml^{-1}.

2.2.2 Methodology

Yeast cells in the exponential phase were exposed to UV light in 0.01M sodium phosphate buffer at pH 7.4 in a Petri dish (dia. 60 mm). The depth of the cell suspension was approximately 2 mm. During light exposure, stirring ensured the homogeneity of the irradiation without changing the turbidity. The light source was a solar simulator consisting of a 250-W ozone-free lamp, a WG 320 filter, and a quartz lens providing an estimated photon fluence between 300 and 400 nm of 10 W m^{-2}. The lamp output was constant for all the samples as determined by a Bentham Instruments spectroradiometer. Titanium dioxide was tested by addition of TiO_2 to the cell suspension to obtain a final concentration of 0.5% w/v; titania was in direct contact with the cells. The samples were irradiated at various time intervals (0, 10, 20, 30, and 40 min). At each time point a droplet (20 µl) was collected and loaded onto a Petri dish containing the solid media, which consisted of 10 g of yeast extract, 10 g of Bactopeptone, 20 g of D-glucose, and 20 g of Agar. Yeast cells that survived were noted after growth at 37°C on a complete solid medium in a Petri dish. The droplet test is a

preliminary test on yeast cells that gauges the genotoxicity of the TiO_2 specimens on yeast cells by noting the yeast colonies that survived at each time point. Various control experiments were performed to ensure the viability of the yeast cells, and the efficacy of the method. In the control experiment (without TiO_2), the cells were left in the dark for a period equal to the times of the irradiation experiment. Another control experiment was carried out by irradiating the cells in the absence of TiO_2 to establish the mortality rate of yeast cells under UV radiation alone. Other control experiments were performed by adding only an organic sunscreen agent such as Padimate-O (50 μM) or Parsol (100 μM). These organic sunscreen active ingredients are known to be genotoxic to yeast cells [16].

The results reported here must be considered as preliminary studies of the effect of TiO_2 partricles on yeast cells. Further experiments on yeast cells to determine the number of genetically altered colonies should be taken up in future studies.

2.3 *Illumination of DNA in Vivo (Comet Assays)*

2.3.1 Materials

The comet assay technique used followed the procedure of Östling and Johanson [17] as modified by Singh et al [18]. The human cells used in comet assays were the human keratinocytes NCTC 2544 kindly donated by Dr. Nigel Cridland (NRPB, England). The keratinocytes were grown to confluent monolayers in NCTC media, made up of 10% fetal calf serum and 1% of penicillin and streptomycin. The flasks were incubated at 37°C under an atmosphere of 5% carbon dioxide. All chemicals and media were purchased from Gibco

BRL Life Technologies, UK.

The cells were harvested in a sterile hood, and were then washed with a PBS solution (0.1 M sodium phosphate; pH = 7.4; 0.1 M of sodium dihydrogen phosphate; pH = 7.4; 2.7 mM of potassium chloride, and 0.137 M of sodium chloride) and a solution of 1 mM EDTA. To detach them from the base of the flasks the cells were treated with 2 ml of freshly prepared, filter sterile, 0.25% trypsin in PBS for 5 min at 37°C. The cells were collected in a sterilin tube and centrifuged at 800 rpm for 5 min. The pellet of cells was resuspended in ice cold PBS to give a final concentration of 2 x 10^6 cells ml^{-1}.

2.3.2 Methodology

The sunlight simulator was the same as the one used for the plasmid nicking assays and for the experiments on yeast cells, namely a 250-Watt ozone-free Xenon lamp with a 28 mm diameter silica window and a 2-mm Schott WG 320 filter placed in front of the window. For illuminations of whole cells, the condensing lens and the dichroic mirror used to increase the light intensity in the plasmid nicking assays were excluded. In this way, the intensity of light was similar to that found under the stratum corneum on sunlight illumination [16]. The diagram in Figure 1B shows the characteristics of the lamp output measured by the spectroradiometer.

Cells illuminated in the presence of titanium dioxide were suspended in PBS and a drop (25 µl) was mixed with 25 µl of 0.025% w/v TiO_2 to give a final concentration of 0.0125% w/v titania in the drop. Ten microliter samples were collected after 0, 20, 40 and

60 min illumination with the solar simulator lamp.

Appropriate slides were prepared after illumination. The 10 µl samples taken from the illuminated system were mixed with 75 µl of 0.8% low gelling temperature agarose (Sigma) at 37°C. The samples were immediately dropped on a 22 mm x 22 mm square of agarose on an agarose-coated slide, after which a cover slip was placed on top of it. The cover slips were removed when the agarose had set. Subsequently, the slides were prepared for electrophoretic experiments. Microscope slides were covered in a cell lysis solution consisting of 0.1 M EDTA, 0.001 M Tris-HCl (pH = 7.5), 2.5 M of sodium chloride, and 1% of Triton X-100 for 1 hr at 4°C in the dark. The slides were then washed twice for 5 min at 4°C in PBS, after which they were covered in alkaline unwinding solution (0.3 M of sodium hydroxide and 1 mM of EDTA) and kept in the dark at 4°C for 40 min. Slides were placed in an electrophoresis tank and covered in 0.003 M sodium hydroxide, and 0.1 mM EDTA at 4°C. Electrophoresis was carried out at 0.67 V cm^{-1} for 25 min. Slides were neutralized in 0.4 M Tris-HCl (pH = 7.4). The nucleoids were stained with 0.01 mg ml^{-1} ethidium bromide.

After electrophoresis, the cells were classified by a comet score. Indeed, after electrophoresis the damaged DNA in the cell's nucleus has the appearance of a comet. These were scored visually using a Zeiss fluorescence microscope. One hundred comets were counted per slide. The comets were classified into one of five Categories (0, I, II, III and IV) according to the appearance and the length of the comet tail. A representation of the comet classes is shown in Figure 2. Photographs of the nucleoids/comets were taken using a digital

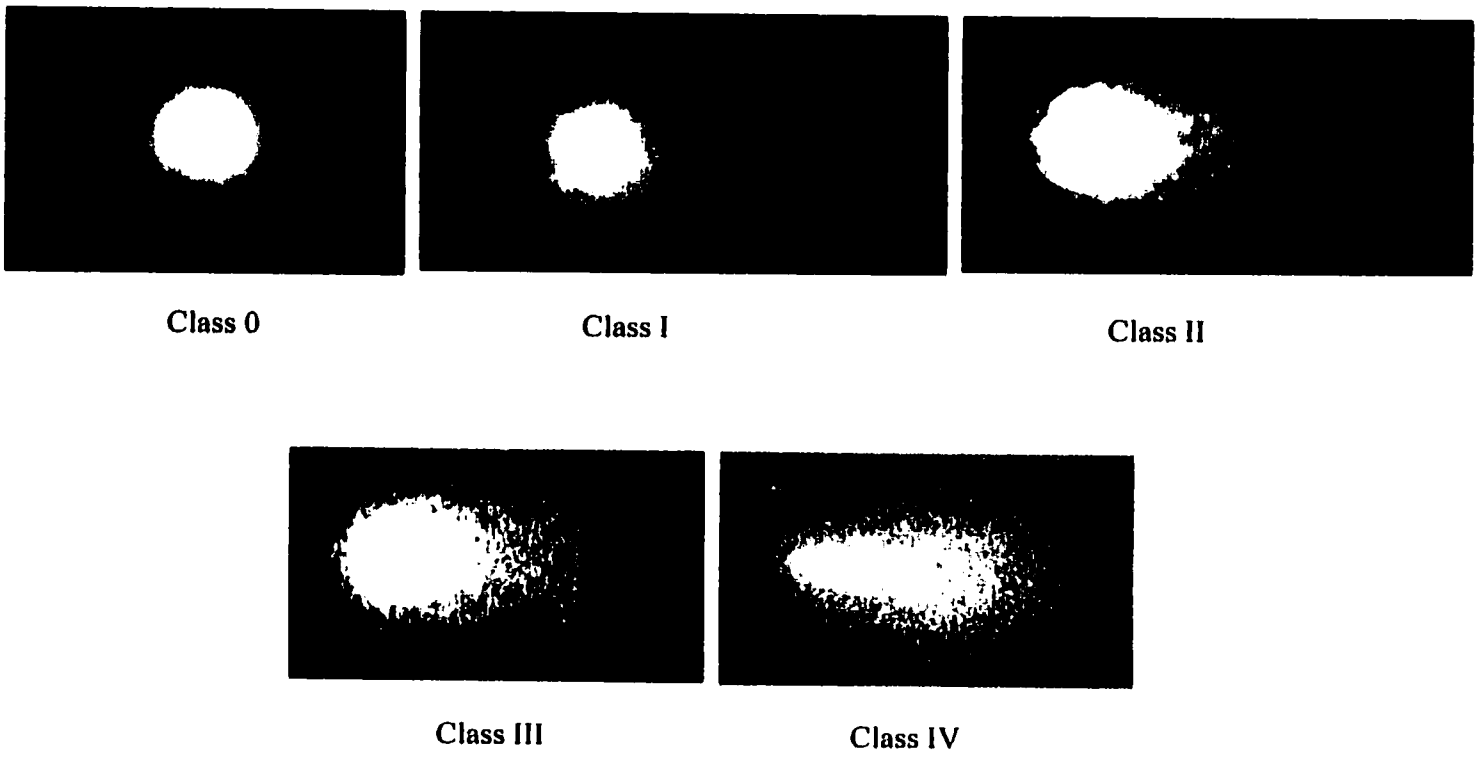

Figure 2. Representation of the five main standard classes of comets

camera.

To quantify the DNA damage, total comet scores were calculated. Raw data obtained from the comet assays were converted into a total comet score (tcs). thus, a comet of class 0 was given a score of 0; one of class I was given a score of 1 and so on up to 4. In a group of 100 cells, the minimum score was obtained when all the comets were of class 0 (tcs = 100 x 0 = 0). The maximum possible tcs scores for 100 comets was obtained when all the comets are of class IV (tcs = 100 x 4 = 400). This method for quantifying the damage has been employed by Reavy and coworkers [19].

3. RESULTS

Since the TiO_2 specimens used in sunscreen lotions have been shown to be photoactive toward the photooxidation of phenol (Chapter 8) and to cause damage to DNA plasmids and human cells (Chapter 7), albeit to different degree, it was important to modify titania specimens to make them completely photo-inactive, while retaining the relevant spectral characteristics of the original state for their safe use in sunscreen lotions. Approximately 20 specimens of TiO_2 were fabricated in a manner that passivated the particle surface so as to eliminate or suppress their photocatalytic activity.

Observation of a significant decrease of the rate of photodegradation of phenol (Chapter 8) suggests that the modification procedure brought about a considerable reduction in the number of hydroxyl radicals produced, the primary cause of the DNA damage. To the extent that the mechanism leading to DNA damage is a very complex process, and species

(e.g. H_2O_2, and $^1O_2$) other than hydroxyl radicals may be involved, the modified titanium dioxide specimens were also tested for damage to DNA plasmids, yeast cells and human cells as evidenced from nicking assays and comet assays.

3.1 Plasmid Nicking Assays

Plasmid DNA was illuminated by UV light alone, and in the presence of each TiO_2 specimen before and after the modification. The experiments with and without titanium dioxide were conducted under otherwise identical experimental conditions of irradiation (calibrated solar simulator; Figure 1A) for a 30-min period. During illumination by light alone the plasmids remained in their supercoiled form. Addition of TiO_2 caused a number of supercoiled plasmids to be converted to the relaxed and linear forms. The modified titanium dioxide specimens behaved differently. Damage (if any) caused by the modified specimens was considerably diminished, and was comparable to the damage inflicted by UV light alone acting on plasmid DNA (used as control).

Figure 3A shows an example of plasmid nicking assays, and illustrates the conversion of supercoiled DNA into its relaxed and linear forms for a variety of RNB specimens (N is a number) and for the corresponding modified RNA samples. The nicking assays tell the story. The modified titania specimens are less damaging to DNA plasmids.

Figure 3B displays the fraction of DNA plasmids remaining in the supercoiled form *versus* illumination time for a 0.005% w/v concentration of TiO_2. When compared to the plasmid DNA control all the samples showed that, after the modification, the irradiated

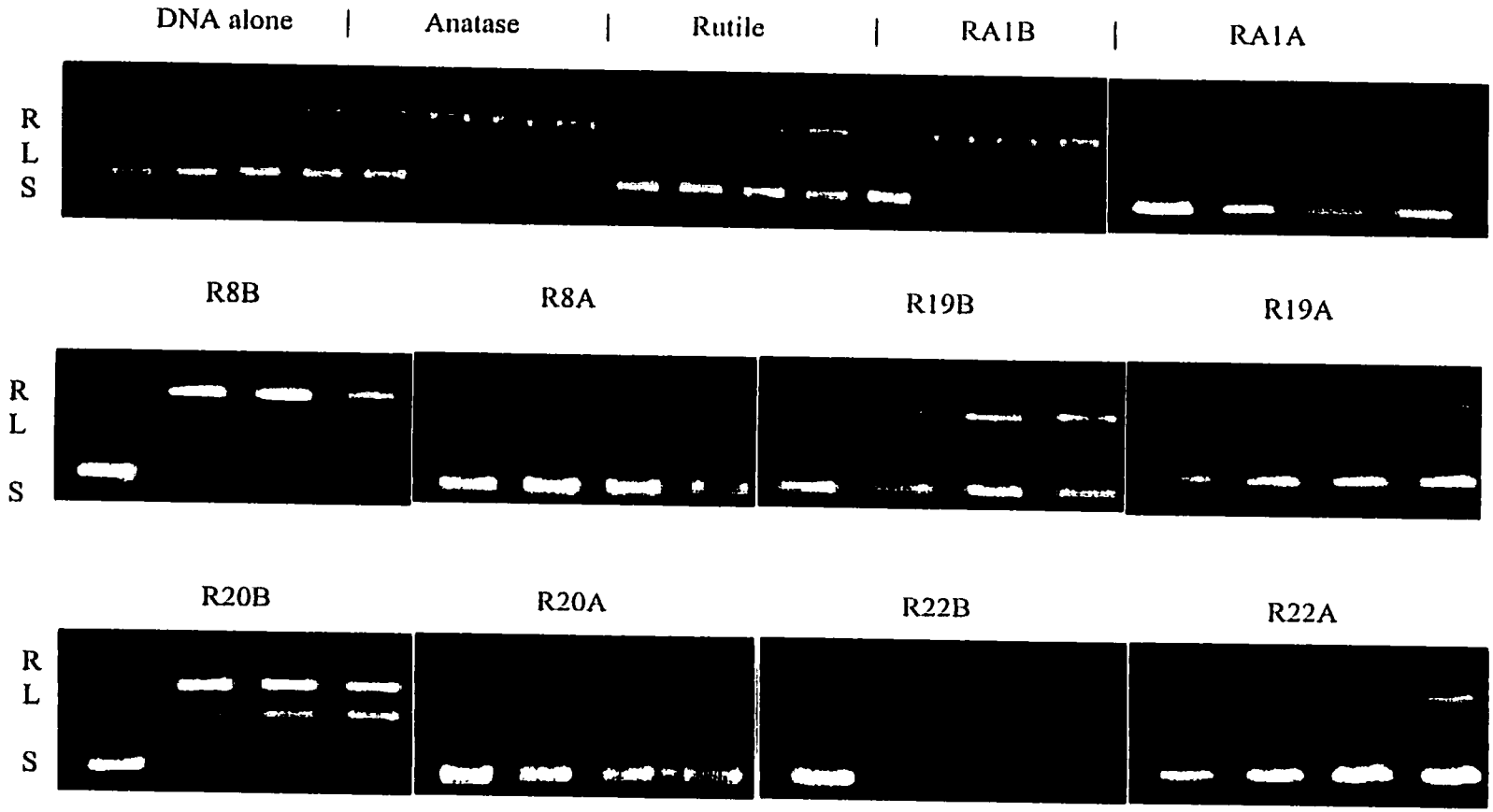

Figure 3A. - Relaxation and migration of supercoiled, relaxed, and linear forms of DNA plasmids caused by various RNB and RNA titanium dioxide specimens before and after modification. Irradiation times were 0, 10, 20, and 30 min.

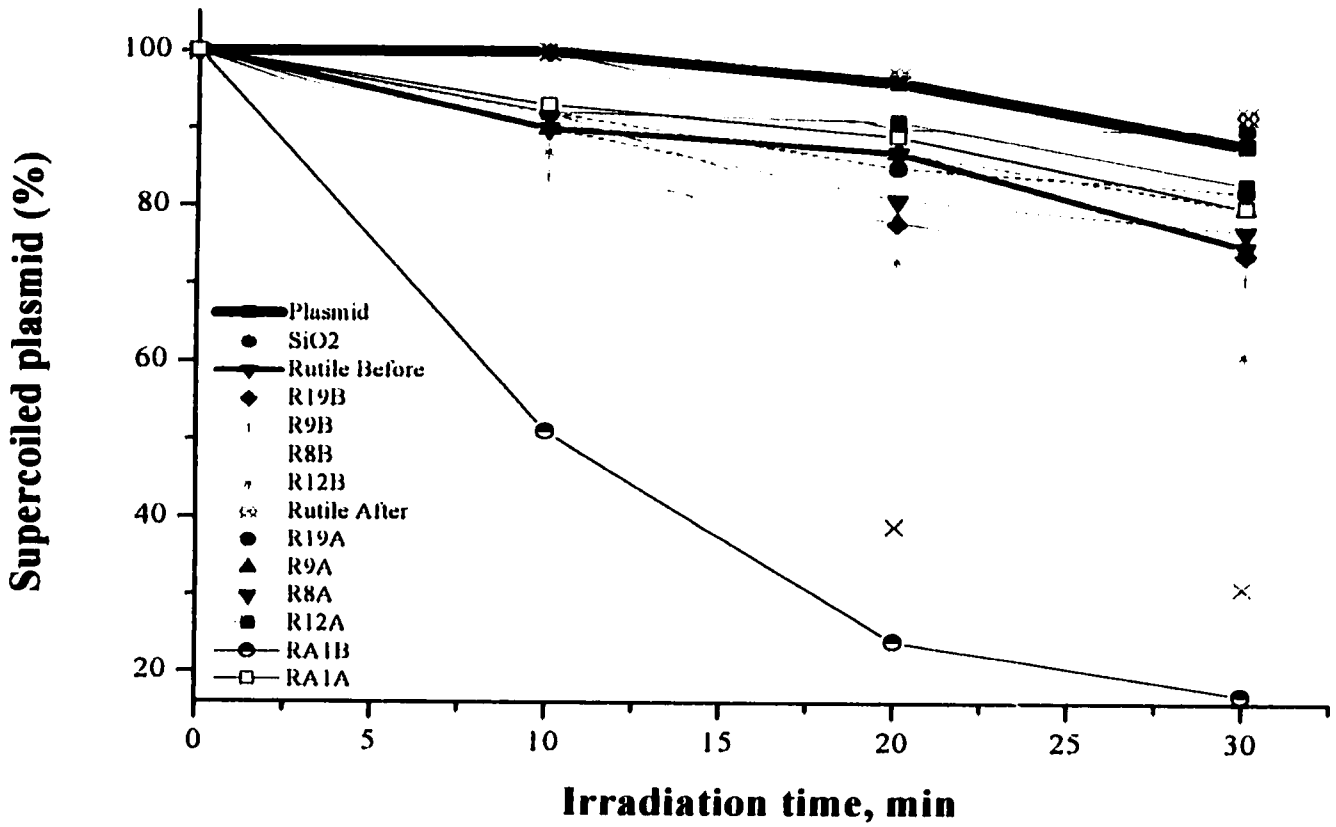

Figure 3B. - Effect of 0.005% w/v of various titanium dioxide specimens before and after modification on the supercoiled form of plasmid DNA. Samples labeled with A refer to modified specimens, and witb B refer to untreated specimens

specimens cause far less damage to DNA than the untreated titania samples. A particular change in DNA plasmids, as evidenced by the single- and double-strand breaks, was displayed by the RA1 and R8 titania specimens. Before modification the RA1B colloids led to near complete disappearance of supercoiled plasmids after 30 min of illumination, whereas irradiation in the presence of RA1A (after modification) only 15% of the supercoiled form were damaged.

Figure 4 displays the results for plasmid DNA, and the effects that treated and untreated rutile TiO_2 together with the modified R19A, R15A and R12A, and SiO_2 specimens have on these plasmids. Note that the scale is expanded relative to that of Figure 3B. The results clearly demonstrate that an increase of the concentration of TiO_2 by an order of magnitude the modified specimens showed relatively no damage compared to the plasmid DNA control and relative to the standard untreated rutile titania typically used as a source of TiO_2 in suncreams. Also, when the inert and inactive silica SiO_2 specimen was exposed to UV light its effect on DNA plasmids was identical to that of modified titanium dioxide samples.

The damage caused by titanium dioxide on plasmid DNA is concentration dependent. Figure 5 displays an increases conversion of supercoiled plasmids to the relaxed form when the concentration of titanium dioxide is increased to 0.5% w/v. Comparing the data in Figure 4 where the concentration is 0.05% w/v to the results in Figure 5, the conversion of supercoiled plasmids by rutile increases by about 30% with increasing concentration of titanium dioxide from 0.05% to 0.5% w/v.

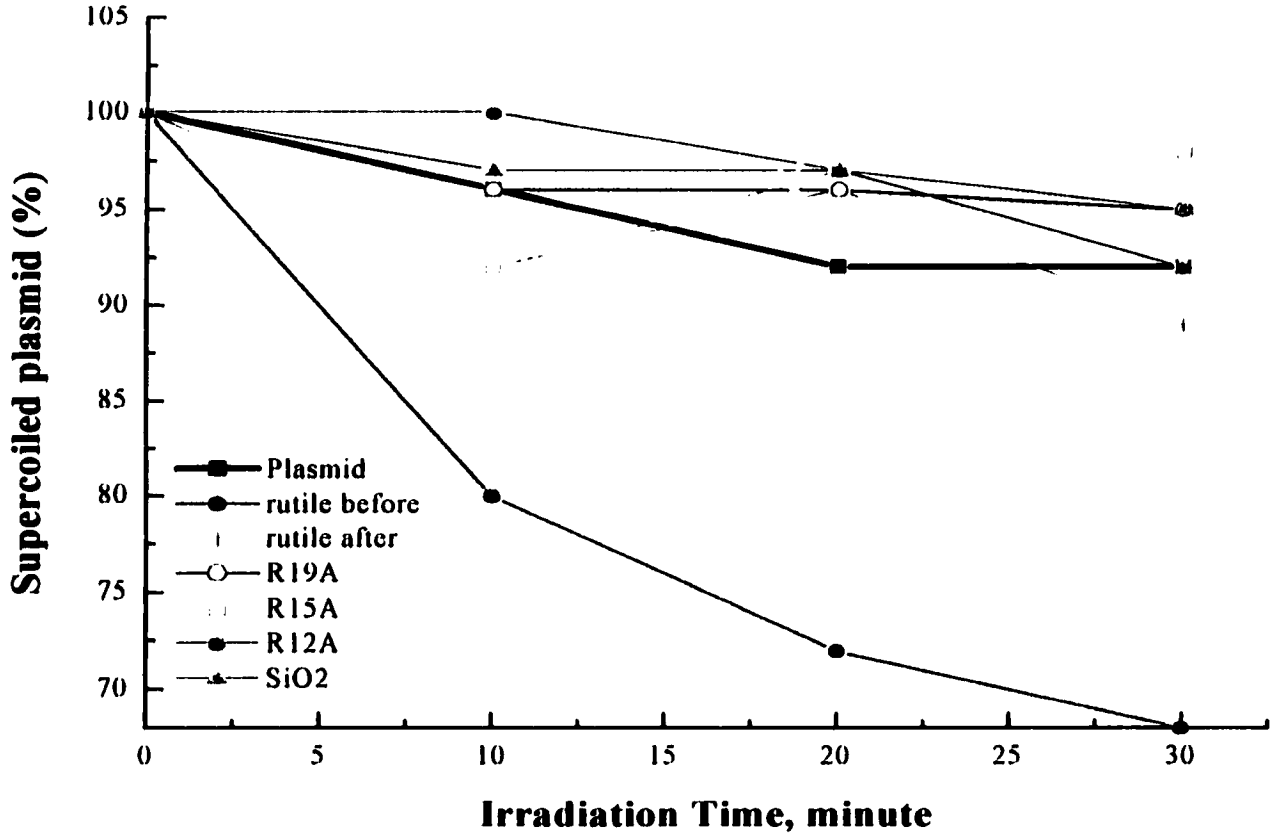

Figure 4. - Plots showing the effect of 0.05% w/v of R19A, R15A and R12A titanium dioxide specimens on plasmid DNA after modification, and comparison with the effects of rutile before and after modification, with silicon dioxide, and with a plasmid DNA control.

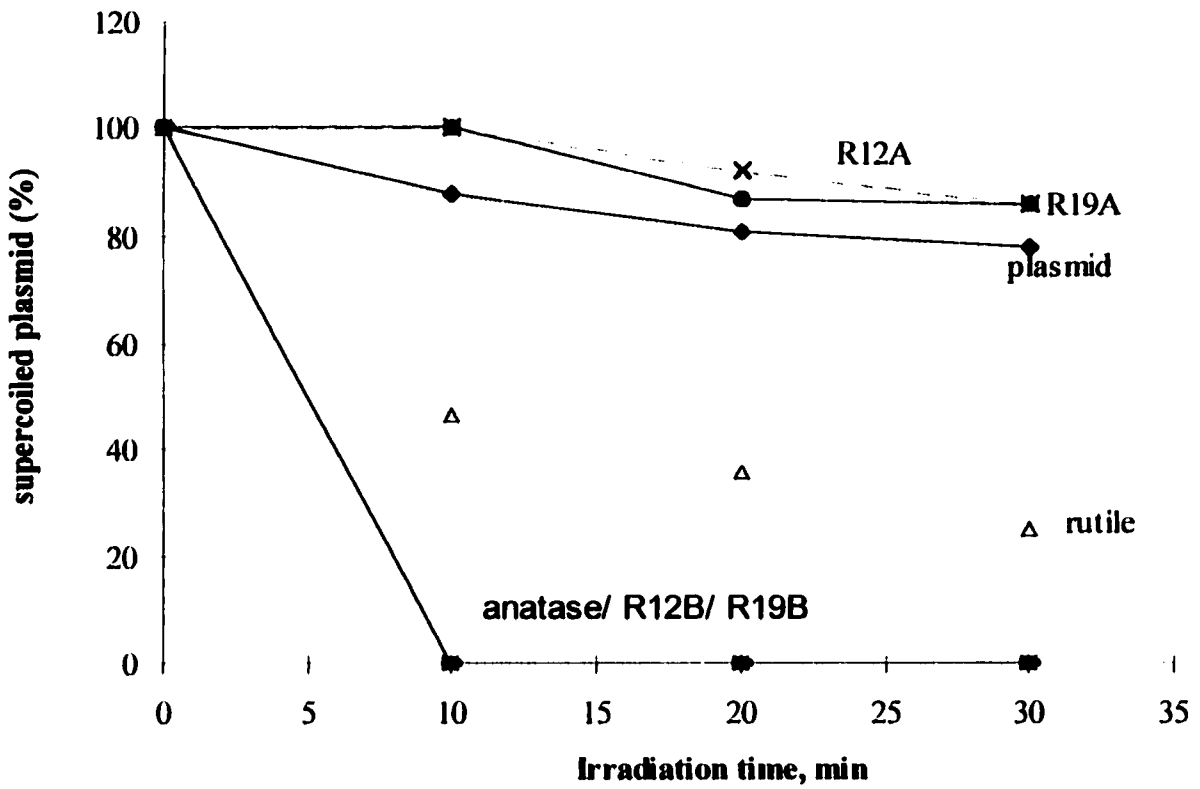

Figure 5. - Effect of 0.5% w/v of titanium dioxide specimens before (R12B and R19B) and after (R12A and R19A) modification together with anatase and rutile TiO_2 on the survival rate of supercoiled plasmid DNA. The plasmid DNA alone is also shown for comparison.

The data shown in Figure 6 confirm the effect of the concentration of TiO_2 on the survival rate of supercoiled plasmids for the rutile and R19A specimens. The concentration of titanium dioxide was increased from 0.5% to 1% to 2% w/v. The concentration dependence is not monotonic above 0.5% w/v probably because of an increase in light scattering by the larger number of titanium dioxide particles at the higher concentrations, thereby attenuating the UV light absorbed by TiO_2. Nonetheless, it is clear from Figure 6 that the modified R19A specimen at a 2% w/v loading inflicts very little damage to plasmid DNA. Other TiO_2 specimens showed similar behavior.

Figure 7 illustrates the low (photo)activity and low damaging effect of the R19A sample (after modification) compared to either the R19B (before modification) or to the Padimate-O sample, a well known organic sunscreen. R19A is completely inactive and appears to protect DNA from the harmful effects of UV radiation. Addition of Padimate-O to DNA plasmids, however, causes considerable damage leading to a near 70% disappearance of the supercoiled plasmids. Yet when R19A is also present with Padomate-O, the damage caused by the latter is unaffected by the inactive R19A titania specimen. The damage is even more severe on addition of the R19B sample, which causes complete destruction of the supercoiled plasmids after 20 min of irradiation. Also shown is the synergy of a physical sunscreen (titania R19) with Padimate-O since both R19B and Padimate-O attack DNA. When R19B and Padimate-O are combined they inflict greater DNA damage than Padimate-O alone, but less than R19B alone. We infer that R19B photodegrades Padimate-O as expected, yet R19B seems so active as to be able to inflict DNA damage and

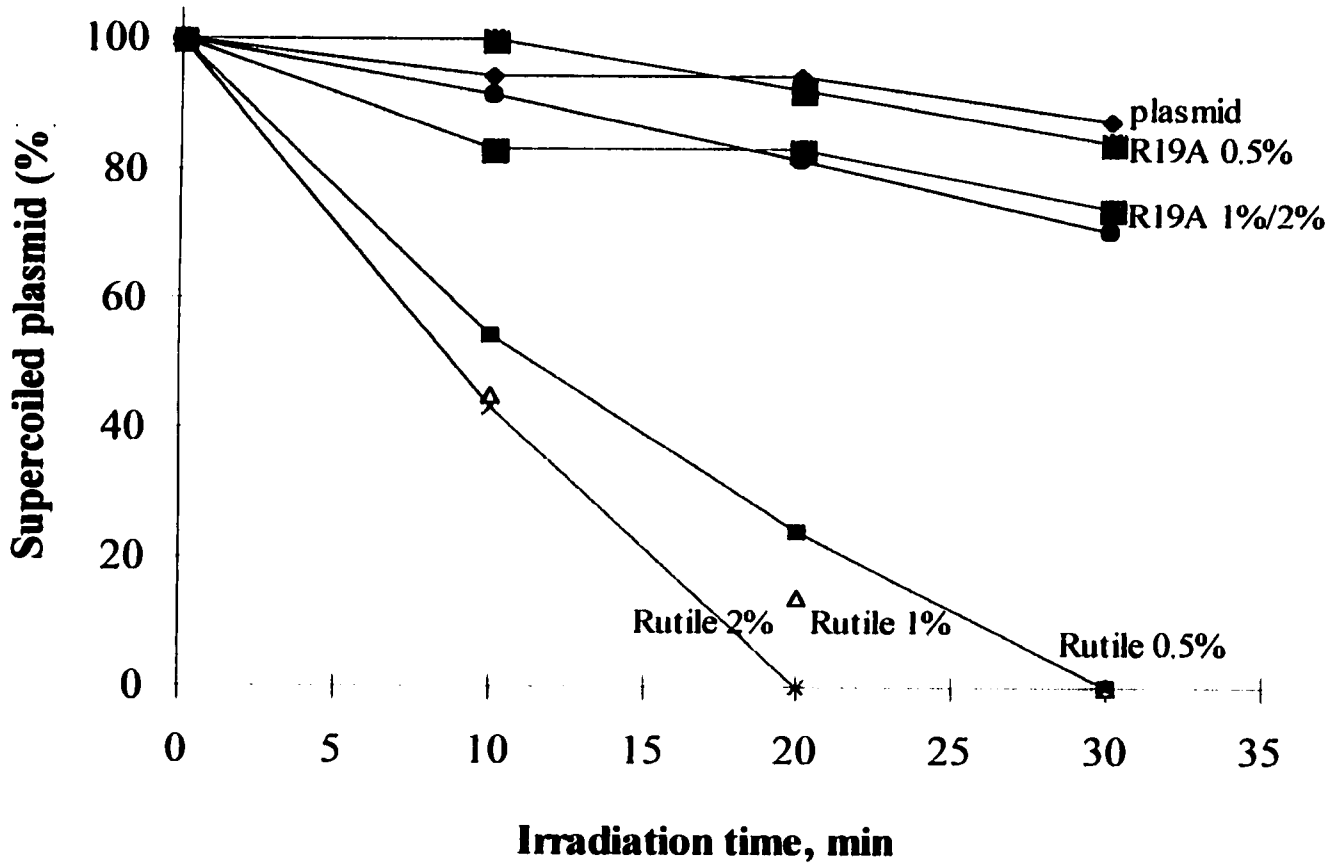

Figure 6. - Concentration dependence of the effect of TiO_2 at various loadings (0.5%, 1% and 2% w/v) on the survival rate of supercoiled plasmid DNA in contact with illuminated R19A and rutile specimens.

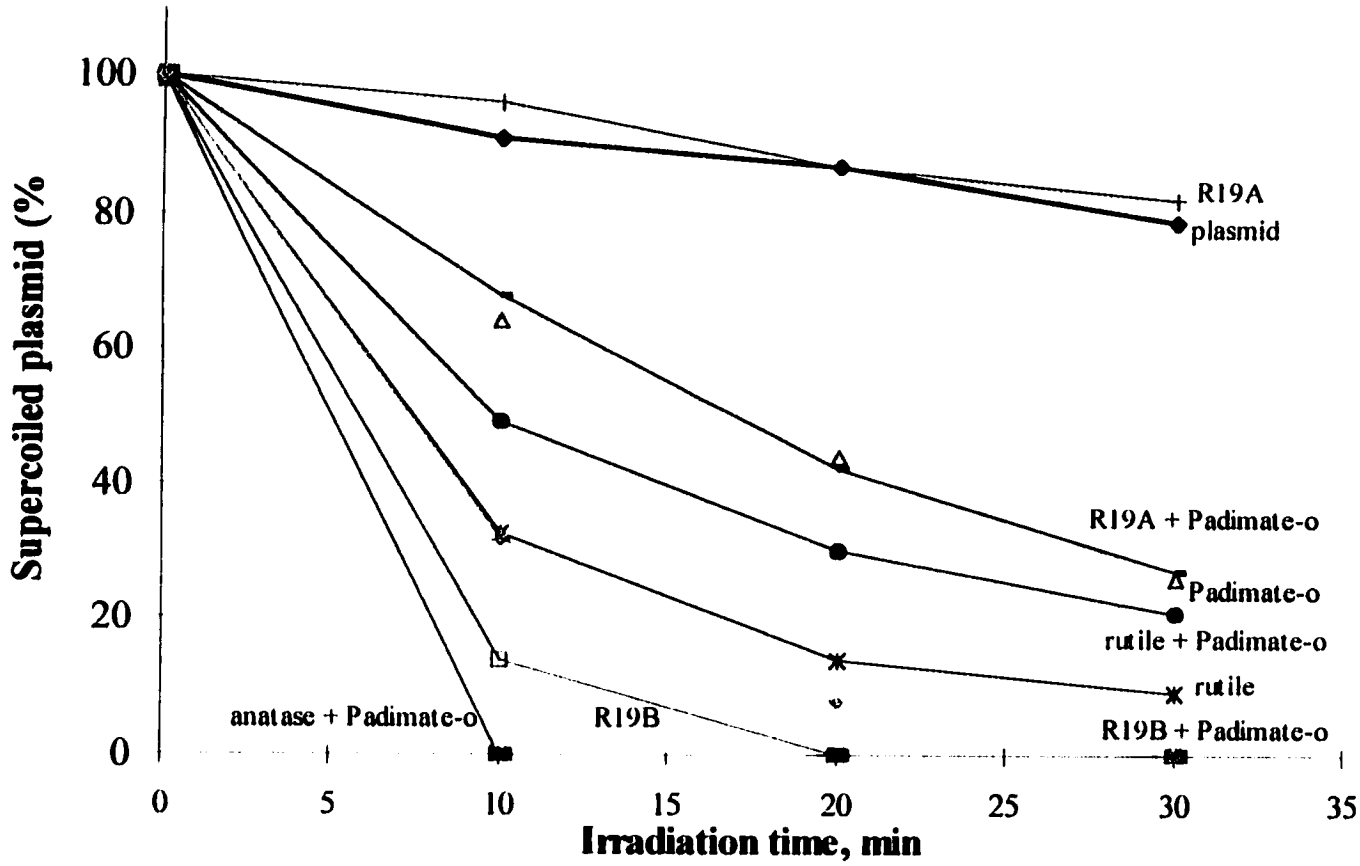

Figure 7. - Effect of 0.1% w/v titanium dioxide specimens (R19A, R19B, rutile and anatase) and Padimate-O (50 μM) alone and in combination on the survival rate of supercoiled plasmid DNA.

attack to Padimate-O at the same time. When both rutile and Padimate-O are present in the mixture and are irradiated, the organic UV filter protects the DNA plasmids somewhat by scavenging some of the •OH radicals produced from irradiated rutile which inflicts the damage to DNA (see Chapter 7). However, Padimate-O appears unable to protect plasmid DNA when anatase titania is also present in the mixture, and expectedly so in view of the overwhelming photoactivity of anatase which produces a considerable number of the very reactive •OH radicals.

In this regard, Chapter 10 reports some preliminary studies on the (photo)stability of organic sunscreens. Padimate-O is photochemically unstable under illumination. What species are produced on irradiation of Padimate-O is unknown since plasmid nicking assays reveal only single- and double-strand breaks in supercoiled DNA owing principally to hydroxyl radicals. It is possible that other radicals or some other very reactive species may be formed in this process, an issue that will be examined during further studies on the photochemistry of organic sunscreen agents in synergy with TiO_2 systems.

3.2 TiO_2 and Yeast cells

Experimental results show that titanium dioxide has no significant effect on the survival rate of yeast cells in the dark, and that the effect of UV light plus titanium dioxide is greater than the effect caused by UV light alone. Experiments with yeast at the exponential phase were performed because this is the phase of fast replication, and this is where the cell wall may be thinner and allow penetration of TiO_2 particles into the cells. Initial experiments

were also repeated in a stationary phase where the cell walls and the membrane are less porous. In this stationary phase modified TiO_2 imparted no killing of yeast cells.

There are several possible mechanisms for cell killing by the photocatalytic process. Yeast cells are made of a cell wall and a plasmalemma (membrane). The thick cell wall is as porous as a sieve with fairly large holes through which compounds can diffuse easily into the cells. Titanium dioxide can either destroy the cell wall or penetrate through the wall into the core of the yeast cell. Actions of the highly oxidizing •OH radicals generated on the surface of illuminated TiO_2 particles are non-selective. Consequently, it is reasonable to expect that the cell wall made of proteins would be oxidized first, followed by •OH radical attack of the membrane. It is also likely that the cell wall in contact with TiO_2 becomes more permeable and may ultimately lead to subsequent cell death. Some workers have found evidence for disruption of the cell wall, of the cell membrane and leakage of the cell content [20,21]. However, there is no electron microscopy evidence to show that the cell wall is in any way disrupted by TiO_2. Clearly, further studies are needed to understand this process.

Figure 8 illustrates the results of the droplet test for the R9A and R9B specimens and compares them to the case when yeast cells are subjected to UV radiation alone and in the presence of two popularly used organic sunscreen agents Padimate-O and Parsol. In the control experiments of yeast cells without titania, the yeast cells did survive after 40 min of irradiation with UVA/UVB light {Figure 8a; note that the concentration of yeast cells on the left hand side is twice the concentration of cells on the right side}.The R9B titania specimen causes more kills than the treated R9A sample. Complete cell death occurred after only 10

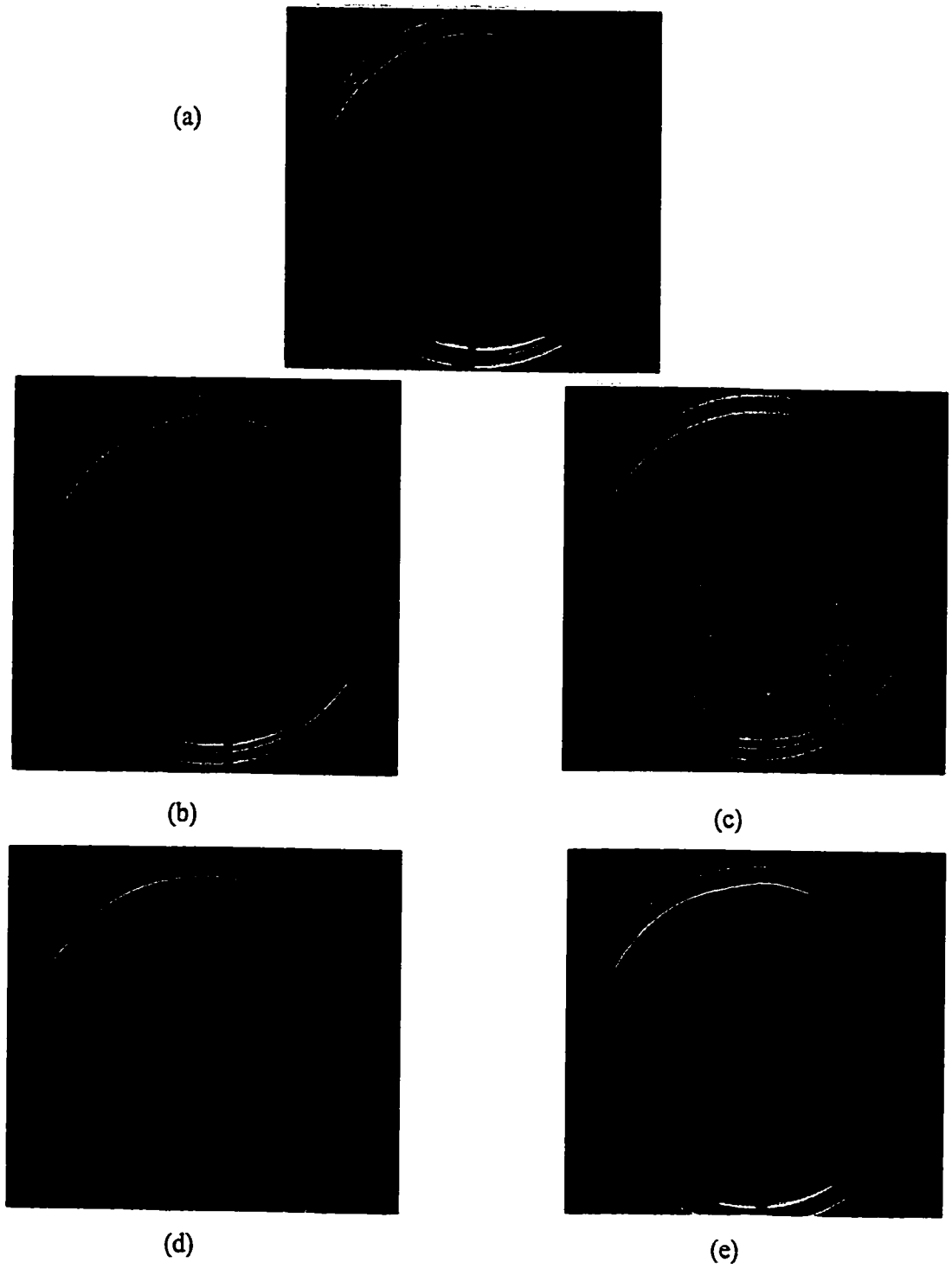

Figure 8. - Survival of yeast cells on illumination for 0, 10, 20, 30, and 40 min. from top to bottom in each dish: (a) yeast cells alone; (b) R9B titania; (c) R9A titania; (d) Parsol; and (e) Padimate-O. The petri dish was divided into two parts to repeat the experiments. Note that the number of yeast cells on the left hand side is twice the number of cells on the right side.

min of illumination with R9B (Figure 8b), whereas all the yeast cells survived even after 40 min of irradiation in the presence of R9A titania (Figure 8c). The organic sunscreens Padimate-O (Figure 8e) and Parsol (Figure 8d) are highly toxic to yeast cells causing cell death almost immediately on irradiation.

In summary, the modified titania specimens are not toxic to yeast cells. We infer again that the number of hydroxyl radicals produced is negligible for these specimens. Nonetheless, the exact mechanism of the kills of yeast cells remains unresolved. Further studies on the genotoxicity of titanium dioxide on yeast cells are programmed to determine the genetic modification (if any) on yeast cells that may be caused by titanium dioxide.

3.3. Comet Assays

Several specimens were tested by the comet assay technique to determine the DNA damage caused by illuminated TiO_2 on whole human skin cells. Treatment of keratinocyte cells with photoexcited titanium dioxide produces comets after only 20 min of irradiation. Figure 9 shows examples of photographs of comets taken with photoexcited TiO_2 specimens. In the dark, TiO_2 specimens cause no damage to DNA. With increasing irradiation time the number and nature of the comets increase; they tend to locate in the upper damage category.

Panel A of Figure 9 illustrates the progress on illumination of keratinocyte cells alone for 0, 20, 40 and 60 min, and displays the extent of damage done to DNA by the UVA/UVB radiation. Panel B depicts the damage caused on irradiation of the keratrinocytes in the presence of the R10B titania specimen, also for 0, 20, 40 and 60 min periods. Clearly R10B

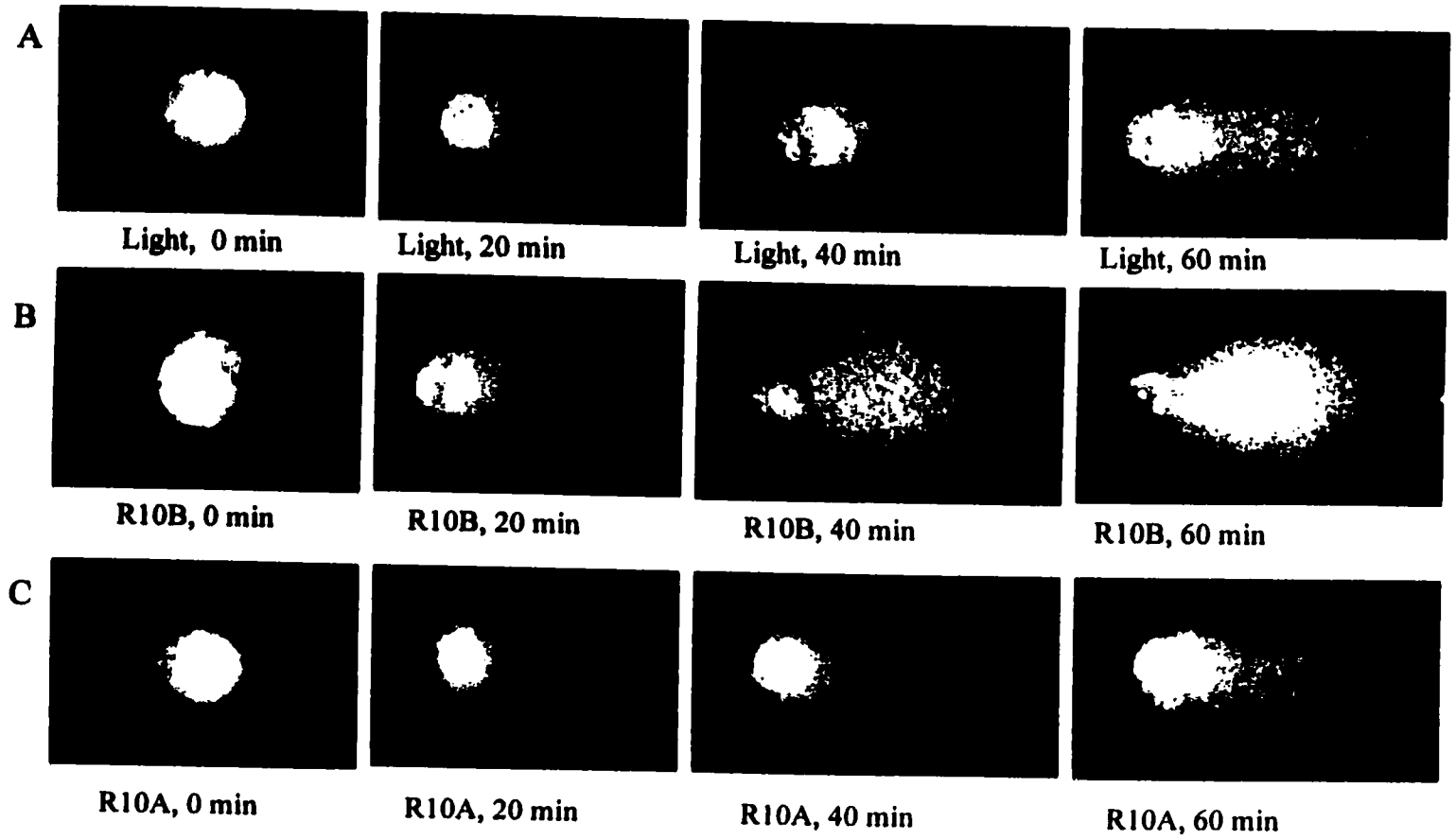

Figure 9. Examples of photographs of typical comets. Panel A illustrates comets by light alone, panel B by photoexcited R10B titania, and panel C by photoexcited R10A titania. (See text for more detail)

engenders far more DNA damage than UV light alone without titania. Compare, for example, the intensity of the comets at 60 min of irradiation for Panels A and B. Panel C summarizes the results of UV illumination of the modified R10A titania specimen in the presence of keratinocytes for otherwise identical irradiation periods. Examination and comparison of the resulting comet after 60 min illumination for the R10A specimen demonstrates that this specimen causes no damage to DNA relative to the R10B sample. In fact the nature of the comets also infers that R10A protects DNA to some extent against the harmful effects of UV radiation {compare Panel C with Panel A}.

Figure 10 summarizes the data from comet assays as a three-dimensional bar chart. It shows the comet class or damage category (0 to IV), the number of comets (out of 100 scored), and the irradiation time. The Figure also illustrates an example of the effect(s) of modified TiO_2 specimens, and how this modification alters the number and category of the comets. Before modification, the R8B specimen irradiated for only 20 min displays some comets of category IV; the number of undamaged comets (category 0) is less than 10%. By contrast, the R8A titania sample under the same irradiation conditions causes less damage and no comets of category IV are evident; the number of comets of category II and III account for about 10%. In addition, if we compare the treatment of keratinocyte cells with R8A to the experiment in which these cells were irradiated with UV light alone (Figure 11), we note that the damage inflicted by R8A is nearly identical to that inflicted by UV light alone. Figure 11 also summarizes the number of comets produced by photoexcited pure rutile. The damage inflicted by rutile on the keratinocyte cells is less than that caused by

(A)

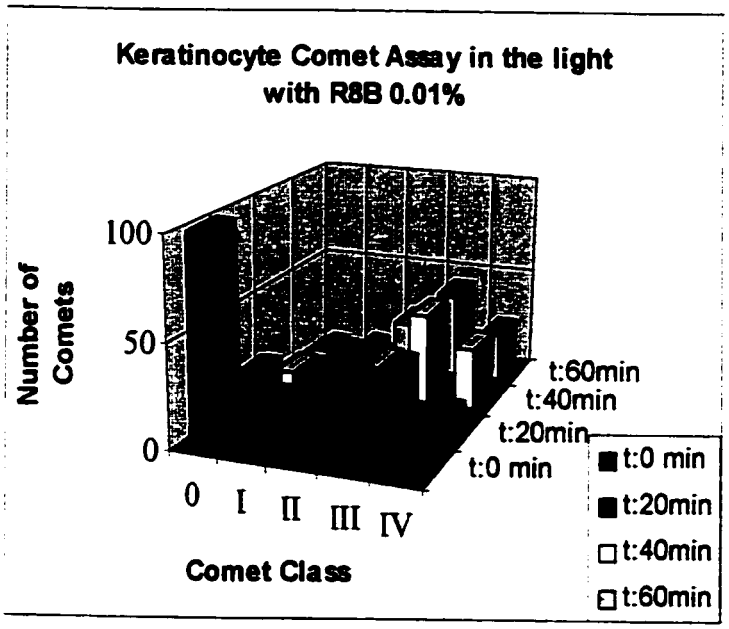

(B)

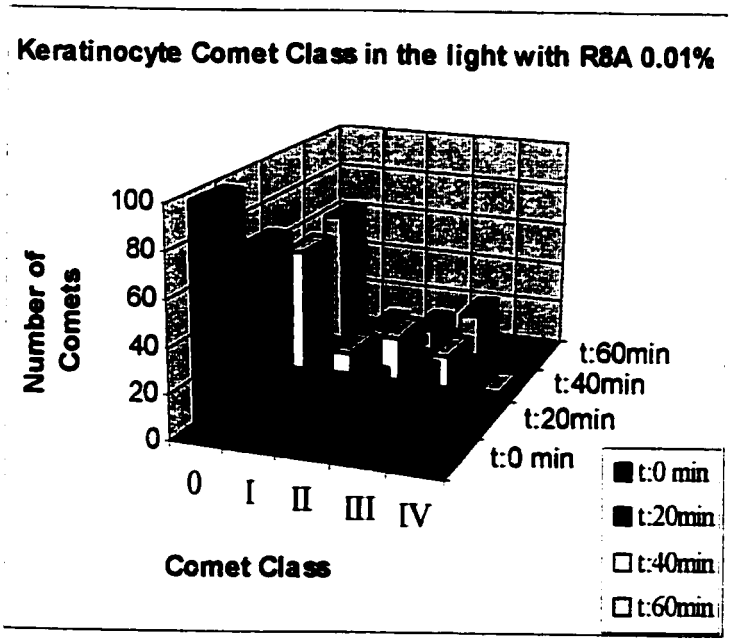

Figure 10. - Bar chart summarizes the results of irradiating keratinocyte cells in the presence of the (A) R8B and (B) R8A titania specimens.

(A)

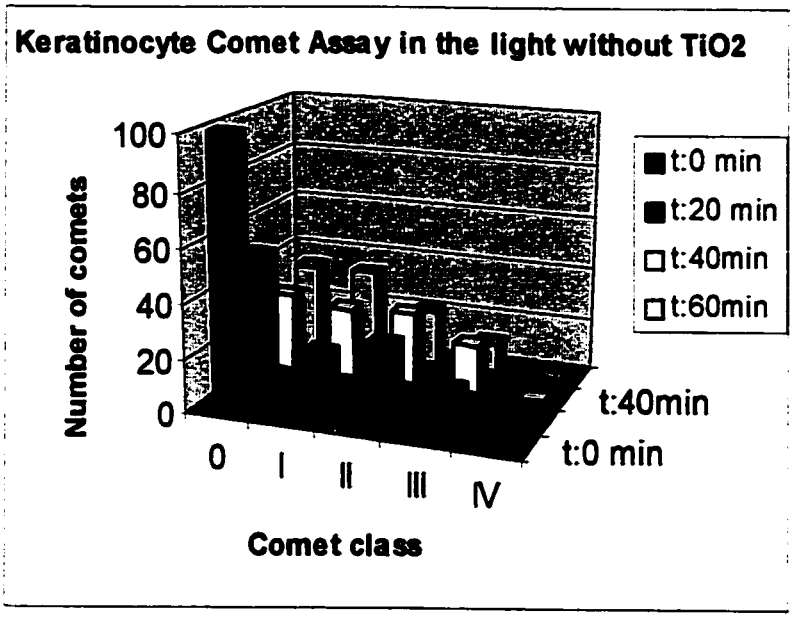

(B)

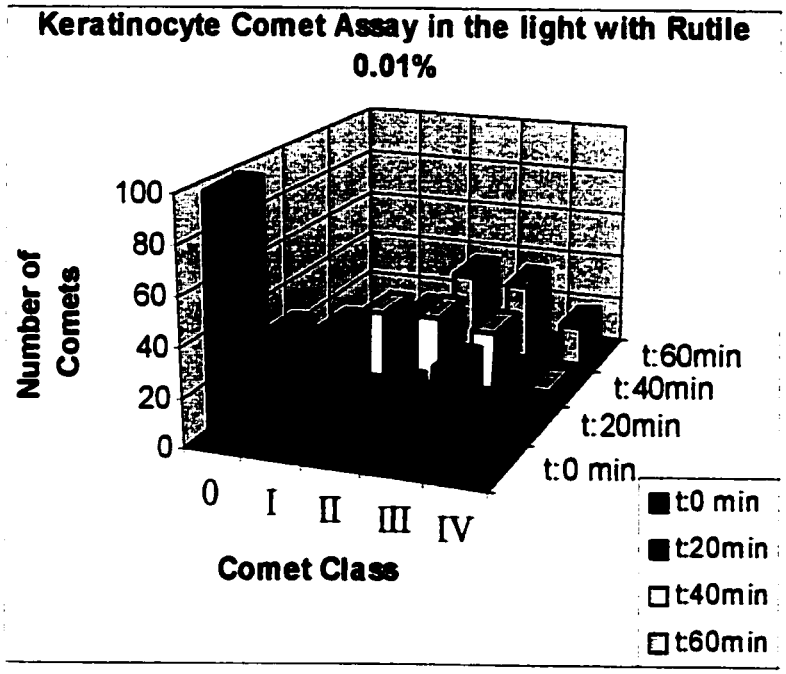

Figure 11. - Bar chart summarizing the effect of UV light alone on keratinocyte cells (A) for times of 0, 20, 40, and 60 min; and (B) for the same time periods but in the presence of rutile titania.

R8B. Note that the R8B specimen contains about 75% anatase. However, some comets of class IV are also formed in the presence of rutile but after ca. 60 min of irradiation.

Figure 12 illustrates the fate of keratinocyte cells when irradiated with UV light in the presence of the TiO_2 specimens R10B and R10A which are 100% rutile. For these specimens the number and the class of comets produced differ from each other. In particular, the R10A specimen inflicts less damage than does R10B. Moreover, the R10A samples maintains a good 50% of undamaged comets after 60 min of UV illumination.

To express the data from the comet assays in a more quantitative format, the data were converted into a total comet score (TCS) defined as the sum of the score (equation 2) of the comets for each class (0 to IV) for which the damage and the comets are classified (see Figure 2 for comets' standards).

$$TCS = [(N^{\circ}_{0\ class} \times 0) + (N^{\circ}_{I\ class} \times 1) + (N^{\circ}_{II\ class} \times 2) + (N^{\circ}_{III\ class} \times 3) + (N^{\circ}_{IV\ class} \times 4)] \quad (2)$$

where N° refers to the number of comets of a given class

A comet of class 0 in a TCS graph gives a score of 0, whereas a comet of class I gives 1, class II gives 2 and so on up to 4. Figure 13 displays TCS/100 cells *versus* irradiation time. It demonstrates that the total comet score TCS for anatase and of all the unmodified specimens is rather high relative to the total comet score obtained with irradiation by UV light alone without TiO_2. By contrast, the modified titania specimens yield a total comet score below the TCS score for irradiation with UV light alone. A standard

(A)

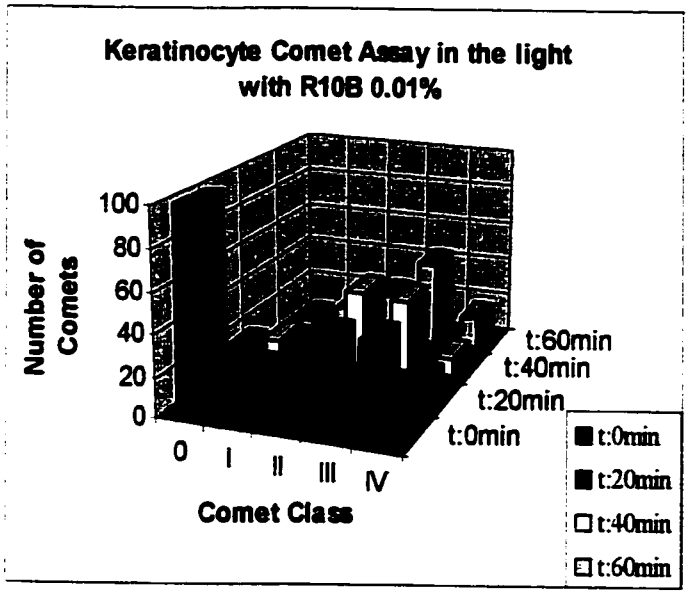

(B)

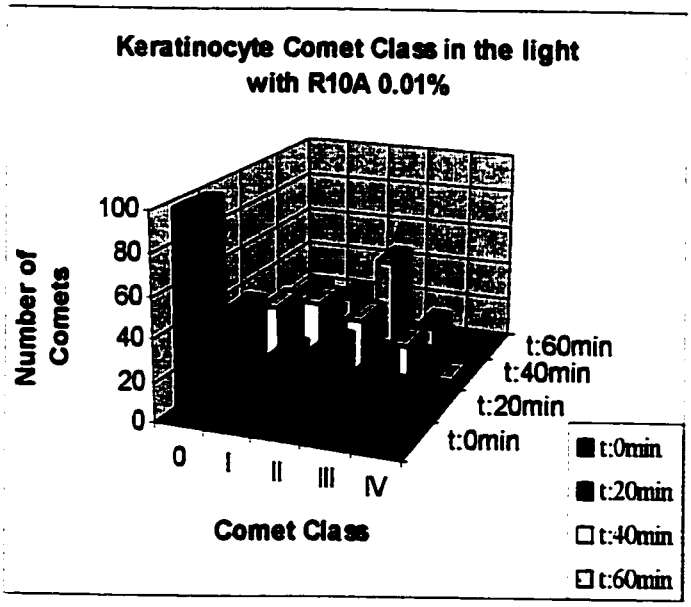

Figure 12. - Bar chart of Keratinocyte comet assay in the light with R10B (rutile), and R10A (rutile modified)

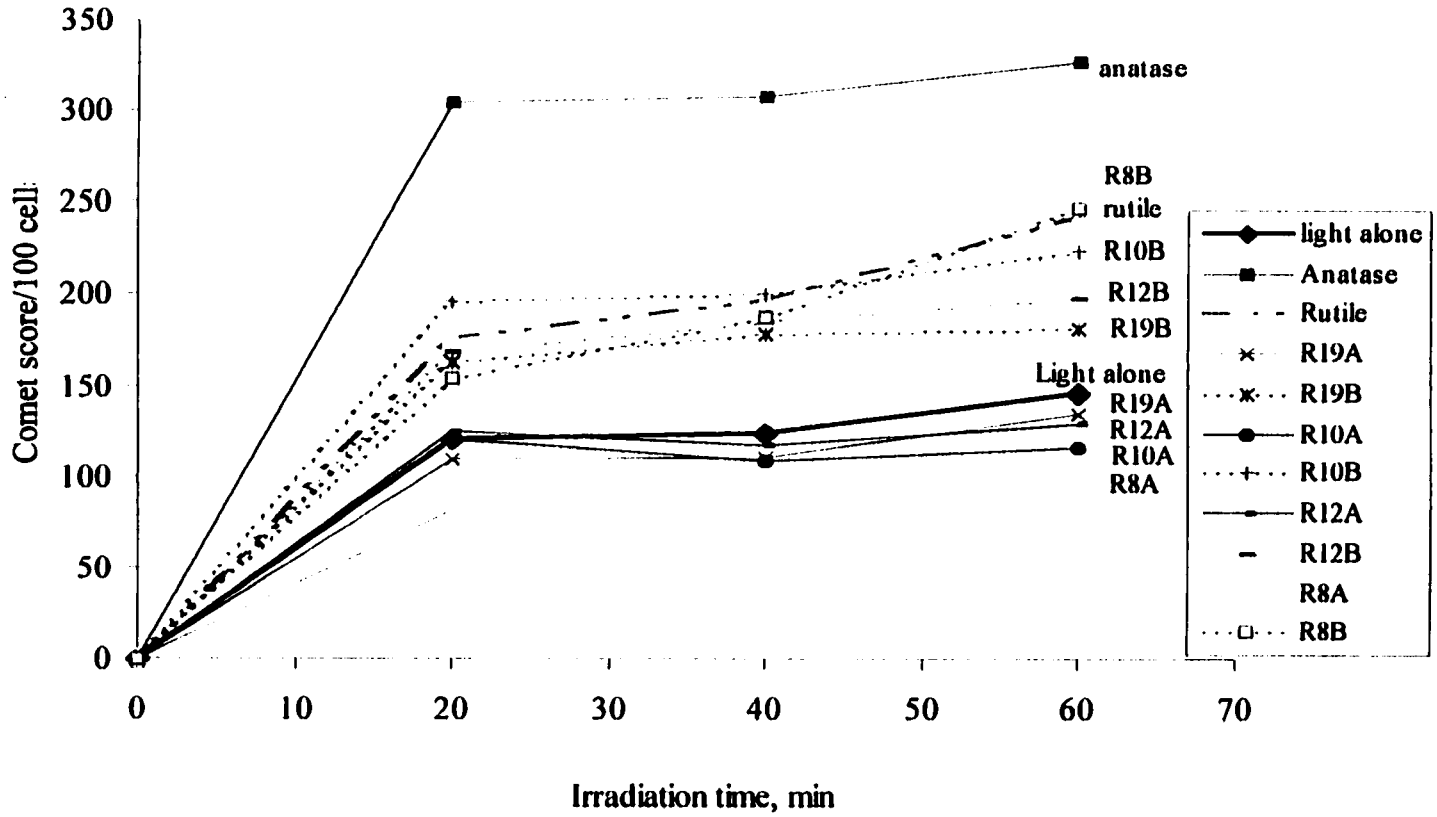

Figure 13. - Total comet score for all the TiO_2 modified and unadulterated specimens.

curve used by Gulston [22] correlates the total comet score to the number of lesions induced by UVC radiation. This standard curve represents the relationship between the UVC dose delivered, the number of lesions induced (originally dimers, but converted to strand breaks) and the total comet score.

4. CONCLUSIONS

This Chapter has examined the effect that passivation of the titanium dioxide particle surface might have on plasmid DNA, whole human skin cells, and yeast cells compared to untreated titania specimens on irradiation with UVA/UVB simulated sunlight. It is demosntrated that the treated titania specimens cause no damage to these *in vitro* and *in vivo* skin models. In fact, the modified specimens protect DNA somewhat from the harmful UVA/UVB radiation. The popular and frequently used organic sunscreen active agents Parsol and Padimate-O have been shown to cause considerable damage to yeast cells, confirming similar work reported on plasmid DNA by Knowland and coworkers [23,24]. Nonetheless, the results presented here indicate that further studies are needed to ascertain the factors that cause the genotoxicity of sunscreen active agents, and how the cells are modified as a result of the transformations reported here.

5. REFERENCES

[1]. D.W. Smithers and J.H. Wood, *Lancet*, **1**, 945 (1952).

[2]. G.M. Murphy, *Photodermatol. Phoroimmunol. Photomed.*, **15**, 34 (1999).

[3]. N. Serpone, A. Salinaro, H. Hidaka, S. Horikoshi, J. Knowland, and R. Dunford, "Beneficial and Deleterious Effects of Solar Radiation", in *Solar Engineering 1998*, J.M. Morehouse and R.E. Hogan, Eds., ASME, New York, 287 (1998).

[4]. N. Serpone, in *Kirk-Othmer Encyclopedia of Technology*, Wiley-Interscience, New York, **18**, 820 (1996).

[5]. D. Lawless, *Ph.D. Thesis*, Concordia University, Montreal (Quebec), Canada, 1992.

[6]. Titanium Dioxide, *IARC Monographs on the Evaluation of Carcinogenic Risks to Humans*, **47**, 307 (1989).

[7]. M. Anpo, H. Nakaya, S. Kodama, and Y. Kubokawa, *J. Phys. Chem.*, **90**, 1633 (1986).

[8]. (a) C. Anderson and A.J. Bard, *J. Phys. Chem.*, **99**, 9882 (1995).
(b) C. Anderson and A.J. Bard, *J. Phys. Chem.*, **101**, 2611 (1997).

[9]. Y. Xu, W. Zheng, and W. Liu, *J. Photochem. Photobiol. A:Chem.*, **122**, 57 (1999).

[10]. (a) J.P. Hewitt, *Parf. Kosm.*, **80**, 36 (1999).
(b) S.R. Spruce, *The Synergy Between Titanium Dioxide and other Materials for use in Sunscreen Formulations*, Florida Sunscreen Symposium, 1995.

[11]. W. Johncock, *Cosmetics & Toiletries*, **114**, 75 (1999).

[12]. *Federal Register* 64, **98**, 27666, United States Food & Drug Administration, Rockville, MD, May 21, 1999.

[13]. N. Serpone, personal communication, 1997.

[14]. M. Gulston, *Ph.D. Thesis*, Oxford University, Department of Biochemistry, 1999.

[15]. T. Maniatis, F. Fritsch, and F. Sambrook, *J. Molec. Cloning: A Laboratory Manual*, Cold Spring Harbor, N.Y., 1982.

[16]. J. Knowland, E.A. McKenzie, P.J. McHugh, and N.A. Cridland, *FEBS Lett.*, **324**, 309 (1993).

[17]. O. Ostling and K.J. Johanson, Biochem. Biophys. Res. Commun., **123**, 291 (1984).

[18]. N.P. Simgh, M.T. McCoy, R.R. Tice, and E.L. Schneider, *Exp. Cell. Res.*, **175**, 184 (1988).

[19]. H.J. Reavy, N.J. Traynor, and N.K. Gibbs, *Photochem. Photobiol.*, **66**, 368 (1997).

[20]. T. Matsunaga, R. Tomoda, T. Nakajima, and H. Wake, *FEMS Microbiol. Lett.*, **29**, 211 (1985).

[21]. D.M. Blake, P.C. Maness, Z. Huang, E.J. Worfrum, and J. Huang, *Separation and Purification Methods*, **28**, 1 (1999).

[22]. M. Gulston and J. Knowland, *Mutat. Res. Gen. Tox. En*, **444**, 49 (1999).

[23]. E. Damiani, L. Greci, R. Parsons, and J. Knowland, *Free Rad. Bio. Med.*, **26**, 809 (1999).

[24]. P.J. McHugh and J. Knowland, *Photochem. Photobiol.*, **66**, 276 (1997)

Chapter 10

SPECTROSCOPY, PHOTOCHEMISTRY AND PHOTOSTABILITY OF ORGANIC CHEMICAL UV ABSORBERS

Summary

This Chapter summarizes studies on the photostability of original commercially available sunscreen emulsions, and on the active ingredients present in the sunscreen lotions. Of all the surveyed properties of sunscreen preparations, special attention must be paid to the possible changes that may occur in sunscreening efficiency under sunlight irradiation. Any change in ultraviolet absorption may have injurious consequences in terms of photoprotection and phototoxicity, since loss of efficiency may occur as a result of some photochemical modification(s) of the screening agent(s) involved. Ingredients used in sunscreen formulations may also photodegrade, and may incur unfavorable interactions with other compounds and solvents used in the formulations. The photodegradation of the active ingredients was investigated in organic solvents of various polarities, as well as in water. The oxygen dependence of the photostability of these compounds was likewise examined. The UV absorption characteristics of active sunscreens were

affected by possible interaction between the UV absorbers and the solvents used in sunscreen formulations, and by photochemical interaction with the ubiquitous molecular oxygen present in sunscreen formulations. In addition, studies were carried out on the photodegradation of two combined active ingredients, in synergy with titanium dioxide. Results show that the photodegradation of the active ingredients is enhanced when titanium dioxide is present.

1. INTRODUCTION

The purpose of sunscreen filters is to prevent skin damage (e.g. burning, skin cancer) while permitting gradual tanning. This is achieved by the chemical sunscreen absorbing UV radiation via electron promotion from a molecular orbital of lower energy to one of higher energy. The energetically excited molecules have a short lifetime and return to their ground state by losing the excess energy in one or a combination of pathways. Energy may be transferred to the neighboring environment in the form of thermal energy, or may decay by fluorescence, phosphorescence, or through a combination of both. Another possible way of losing energy is by chemical reaction. Consequently, a study into the photostability and photochemistry of the original sunscreen emulsions and of the active ingredients present in the sunscreen lotions is of particular interest. Of all the properties studied of the sunscreen preparations, special attention must be paid to the possible changes in sunscreening efficiency under sunlight irradiation.

Any change in ultraviolet absorption may cause injurious consequences in terms of

photoprotection and phototoxicity, as may result from a photochemical modification of the screening agent(s) involved. This photochemical reaction can produce unknown photoproducts whose accumulation on skin may cause some serious damage. Chemical changes can also be brought about in a number of ways such as, for example. photofragmentation and/or photoisomerization. In photofragmentation, the absorbing molecule can dissociate into reactive fragments (e.g., free radicals) or molecular species such as reactive intermediates. Some of the stable photoproducts derived from the active ingredients can be toxic as are the free radicals. Additionally, under the conditions of normal usage, molecular oxygen is ubiquitously present in sunscreen formulations. To the extent that most of the chemical absorbers have the triplet state energies sufficient to lead to energy transfer to molecular oxygen, they can act as photosensitizers and can generate singlet oxygen, $^1O_2$, whose genotoxicity is well known. Accordingly, studies were performed on the photodegradation of the active ingredients in the presence of (air) oxygen, unless otherwise noted. As well, other photochemical interactions may occur between the chemical absorbers and DNA such as for example direct reaction with formation of DNA base adducts. Evidence for the photoaddition of PABA (*p*-aminobenzoic acid) to thymine and thymidine has been reported by Shaw and coworkers [1].

Ingredients used in sunscreen formulation may also incur photodegradation and unfavorable interaction with other compounds and solvents used in the formulations. Studies were also undertaken to determine the influence of four solvents of varying polarity on the photostability of four sunscreen active ingredients commonly present in commercial

suncreams, and on related UV absorption characteristics affected by any possible interaction between the UV absorbers and the solvents used in sunscreen formulations.

The organic sunscreens are almost always used in combination because no single organic sunscreen agent, used at levels currently allowed by the U.S. Food and Drug Administration, can provide a high SPF (Sun Protection Factor). Owing to serious photoinstability and possible unfavorable interaction(s) between the compounds, recent restrictions from the FDA Federal Register Administrations Regulatory Affairs limit the choice of suitable combinations of UV chemical absorbers. However, of all the UV filters commonly used today, only a combination of two, namely octyl methoxycinnamate and the butylmethoxydibenzoylmethane, is not recommended because they are associated with some photoinstability.

In this Chapter we report some preliminarily results on the synergy between two chemical organic standard sunscreens, and on the synergy between the chemical organic sunscreen and the physical sunblock titanium dioxide TiO_2. In the majority of sunscreen lotions, both organic and inorganic active agents are present with their own ability to degrade, to incur chemical change(s), and to interact with the oxygen commonly present in sunscreen lotions to yield free radicals whose nature and extent of damage to skin (and DNA) are matters of some concern. Ideally, no ingredients used in cosmetic product formulations should interact unfavorably with each other.

2. MATERIALS AND METHODS

2.1 SPF Determination and Photostability of Sunscreen Lotions

The Sun Protection Factor (SPF) of sunscreen lotions was measured *in vitro* throughout the ultraviolet spectrum using Transpore™ tape (3M Company, St.Paul, MN). A piece of Transpore tape (4x4 cm^2) was placed over the quartz-input optics of the spectro-radiometer (Bentham instrument with λ resolution of 1 nm). The intensity of radiation transmitted through the tape was determined automatically by recording the photocurrent in 5-nm steps from 290 nm to 400 nm. An appropriate volume of sunscreen to achieve a surface density of 2 μl cm^{-2} was applied to the tape surface by spotting sunscreen ca. 14 mg all over the application area of 7 cm^2. A gloved finger was used to achieve as uniform a thickness as possible with a circular motion for about 10 seconds. Transmission of light measurement was then repeated immediately through the Transpore tape alone and through the sunscreen applied on the Transpore tape. The Transpore tape has a surface that has been found to distribute the sunscreen compounds in a way similar to the uneven topography of human strateum corneum. Accordingly, it is an inexpensive and convenient way used to simulate the distribution of the suncream on the skin, and to evaluate the light transmitted through the sunscreen. The sun protection factor (SPF) was predicted according to the method described by Diffey et al. [2]. From transmission measurement data, equation 1 was employed to

$$SPF = \frac{\Sigma_{290}^{400} E(\lambda)\ \varepsilon(\lambda)}{PF(\lambda)} \qquad (1)$$

estimate the SPF number. Here, $E(\lambda)$ is the spectral irradiance of terrestrial sunlight under some defined conditions (mid-day, mid-summer sunlight for Southern Europe), and $\varepsilon(\lambda)$ denotes the relative effectiveness of UV radiation at a given wavelength λ (nm) to produce delayed erythema on human skin (the so-called erythema action spectrum), both sets of data are taken from published data [2]. The monochromatic protection factor $\{PF(\lambda)\}$ at wavelength λ (nm) is given as the ratio of the transmittance data recorded at this wavelength with no sunscreen applied on a section of the Transpore tape to the transmittance data recorded with the sunscreen applied to another section of the tape.

The photostability test of sun lotions was performed by simulating the exposure to the sun of real sunscreen lotions. We used a solar simulator Xenon lamp (48 W m^{-2}) installed in a Solarbox (Milano Confindustrie) and equipped with a 310-nm cut-off filter. The temperature inside the solarbox was ca. 30 ° C. The sunscreen lotions were mixed with water; however, because of their hydrophobicity the lotions NP1, SN9, and SN10 were first dissolved in a small quantity of acetonitrile with water added later to make up some desired loading. The volume of solution used in the photostability experiments was 400 ml and the reactor was a round 500-ml round pyrex flask with a flat bottom; it was capped during illumination to avoid evaporation of solvents. During illumination, the solution was stirred using magnetic agitation. The optical absorbance change was recorded using a double beam Shimadzu spectrophotometer. The attenuation spectra of the samples were taken at certain time intervals using a 1-cm quartz cuvette; the reference was the same solvent (or solvent mixture) as used for dilution.

Since all the sunscreen lotions are typically labeled as " waterproof" we tested their solubility in water. The water resistance of sunscreen lotions was determined by noting whether a drop (0.1 to 0.2 g) of the suncream could dissolve in 400 ml of water.

The sunscreen lotion NP1 contains Aloe leaf gel, a natural product which appears to cause only slight damage to DNA (see below). The suncreams NP1 and NP2 were analyzed for their ability to inflict DNA damage using Plasmid nicking assays. The appropriate methodology is reported in Chapter 9. To determine the sunscreen properties of the natural product Aloe, 200 mg of the Aloe leaf gel extract in powder form was dissolved in distilled water (200 ml) and then filtered to remove the green organic precipitate. The clear solution was illuminated under a solar simulator and the absorbance change was recorded using the spectrophotometer.

2.2 Spectroscopy, Photostability, and Photochemistry of active ingredients

Four active ingredients present in suncreams were examined: they are (i) Octyl Methoxycinnamate, (ii) Padimate-O, (iii) Oxybenzone, and (iv) Phenylbenzimidazole Sulfonic acid. The light source was an Oriel 1000-Watt Hg/Xe lamp. The emitted radiation from this source was filtered through a water filter to remove IR radiation. The reactor was a 1-cm quartz cuvette located at 12 cm from the light source; the 3-ml irradiated solution was stirred during the experiments. We exposed the air-equilibrated solutions of these compounds to the full UV output of the radiation source (wavelengths greater than 290 nm); the solutions were made-up in four different spectrograde solvents (water, methanol, acetonitrile, and

hexane). The loss of light absorption of each solution was determined at various time intervals after continuous illumination. Unless otherwise noted, the concentration of these active ingredients in all solutions was 8 mg L^{-1}; however, for the Phenylbenzimidazole Sulfonic acid case solutions were saturated in acetonitrile and hexane.

The photodegradation of these four active ingredients was also examined under anaerobic conditions to evaluate a possible dependence of the photoreaction on molecular oxygen. The aqueous solutions of each chemical sunscreen agent was purged with Argon for 30 min prior to illumination by the 1000-Watt light source in order to compare the photostability of the sunscreen agents under anaerobic and aerobic conditions.

We were also concerned about the synergy between two organic chemical filters and synergy between a chemical organic UV filter and a physical sunblock when both are present together in a sunscreen formulation and are illuminated by sunlight. Consequently, we investigated a solution consisting of a typical combination of two chemical organic sunscreen active agents (e.g., Oxybenzone and Octyl Methoxycinnamate), and a dispersion composed of Oxybenzone and titanium dioxide,TiO_2. The solutions were made-up in water under aerobic conditions. The TiO_2 loading was 300 mg L^{-1} and the concentration of Oxybenzone and Octyl Methoxycinnamate was 8 mg L^{-1} in each case. The illumination set-up was the same as the one described above for the photodegradation of the active ingredients. Changes in absorbance was monitored using the Shimadzu double-beam spectrophotometer.

In addition, we estimated the initial quantum yields of photodegradation of some of the active ingredients either in aqueous media or in hexane solutions under air-equilibrated

conditions. The quantum yields were determined by monitoring absorption loss at a single wavelength of excitation and at a single monitoring wavelength. For each experiment the photon flow from the irradiation source was established using Aberchrome-540 actinometry. The procedure and protocol used were suggested by Aberchromics Ltd. of the University of Wales College, Cardiff CF1-3TB, Wales. The concentration of Aberchrome-540 was 32 mg in 25 ml toluene. The increase in absorbance at 494 nm (A) of this dye *versus* illumination time (0, 30, 60 seconds) was used to estimate the photon flow (ρ; equation 2).

$$\rho = \frac{A\ V\ N}{\Phi_c\ \varepsilon\ t} \qquad photons\ s^{-1} \qquad (2)$$

where V is the volume of the irradiated solution (dm^3), N is 6.023×10^{23}, Φ_c is 0.20 in the wavelength range 310 nm to 370 nm, ε is the molar extinction coefficient 8,200 $dm^3\ mol^{-1}\ cm^{-1}$ at 494 nm, and t is the irradiation time is seconds.

3. RESULTS AND DISCUSSION

3.1 Photostability of Sunscreen Lotions

We tested the photostability of some sunscreen lotions available on the market since under exposure to sunlight radiation they must be photochemically stable if they are to serve their intended purpose. Chemical organic sunscreens do achieve that purpose of absorbing the solar energy before it reaches the skin; however, they may do so by converting the stored energy into some photochemical reaction and/or the energy can decay by radiative or non-

radiative paths. A requirement for a safe sunscreen formulation is to convert this stored energy through physical processes into heat. The active ingredients in sunscreen lotions are classified either as UVA absorbers (members of this group are the benzophenones, the anthranilates, and the dibenzoylmethanes) and UVB absorbers (members of this class are the PABA derivatives, the salicylates, the cinnamates and the camphor derivatives). Their relevant chemical structures are illustrated in Figure 6 of Chapter 6.

In general, the active ingredients in sunscreen lotions contain conjugated systems which cause electron delocalization on absorption of a photon of UV radiation. For example, they may contain an aromatic ring conjugated with a carbonyl group and often an electron-releasing group, such as an amine or a methoxyl group, when this group is substituted in the *ortho-* or *para-* position of the aromatic ring. The absorption of UV or visible light by an organic molecule causes excitation of an electron from an initially occupied ground state to a high energy excited state. Molecules in an excited state decay back to the ground state through various radiative or nonradiative decay processes, and/or undergo some photochemical change.

We simulated exposure of sunscreen formulations to the sun using a solar simulator, and monitored the temporal changes in absorption of the emulsions dissolved in either water or organic solvents. The results reported here pertain to the photodegradation of suncreams coded as NP1, SN4, SN5, and SN10. Table 1 gives a brief description of some of the sunscreen lotions and lists their SPF factors, the active ingredients contained in the lotions, and also gives the solubility in water. Table 1 shows that all of the emulsions, except the

Table 1. - Summary of coded active ingredients contained in sunscreen lotions, SPF numbers, and waterproof tests.

SUNSCREEN LOTION CODE	SPF	ACTIVE INGREDIENTS	WATERPROOF
NP1	17	octyl methoxycinnamate	YES
SN1	19	ethyl hexyl *para*-methoxycinnamate; oxybenzone; phenylbenzimidazole sulfonic acid; titanium dioxide	NO
SN2	25	4-methylbenzylidene camphor; butylmethoxydibenzoyl-methane; terephthalydene dicamphor sulfonic acid; titanium dioxide	NO
SN3	25	4-methylbenzylidene camphor; terephthalydene dicamphor sulfonic acid; butylmethoxydibenzoyl-methane; titanium dioxide	NO
SN4	25	4-methylbenzylidene camphor; terephthalydene dicamphor sulfonic acid; butylmethoxydibenzoyl-methane; titanium dioxide	NO
SN5	15+	octyl methoxycinnamate;octyl salicylate; titanium dioxide	NO
SN6	20+	octyl methoxycinnamate; 4-methylbenzylidene camphor; titanium dioxide	NO
SN7	30	titanium dioxide; butyl methoxydibenzoylmethane; triethanolamine salycilate; terephthalylidene dicamphor sulfonic acid	NO
SN8	---	titanium dioxide	NO
SN9	15	titanium dioxide	YES
SN10	25	titamium dioxide; zinc oxide	YES

NP1, SN9 and SN10 systems, are not water-resistant. This water solubility contradicts the waterproof label on the sunscreen bottles. Accordingly, the consumer should beware that

water can easily remove the sunscreens applied on the skin.

For all of the sun lotions we see an optical change in absorbance under simulated sunlight illumination. This demonstrates that the active ingredients in these lotions are not photostable, and shows that they undergo a loss of efficacy in UV sunlight protection and lead to formation of absorbing and/or non-absorbing photoproducts. Figure 1 illustrates the absorbance spectral changes for the sunscreen lotion SN5 under simulated sunlight illumination.

The SN5 lotion degrades during illumination for ca. 3.5 hr as evidenced by the loss of absorbance around 300 nm. This SN5 sunscreen lotion contains titanium dioxide along with two UVB organic filters, namely octyl methoxycinnamate and octyl salicylate. At zero time illumination, the two chemical absorbers act as the major sunscreen filters, since the spectral features of titanium dioxide do not appear to affect their spectral behavior. These combined organic compounds display an absorption band at 310 nm; the inset shows the temporal loss of absorbance at 310 nm. From the SN5 spectra, the TiO_2 loading seems to be rather low; the manufacturer states it is around 0.65% w/w. In lotion SN10, the spectral features of TiO_2 (loading 7.5% w/w) can easily be discerned, and shows some scattering in the visible range (Figure 2). Although SN10 is labeled as containing only ZnO and TiO_2, the spectra also show some organic compound present with a band at 315 nm. Whatever the nature of this organic filter, it degrades fairly rapidly within 155 min.

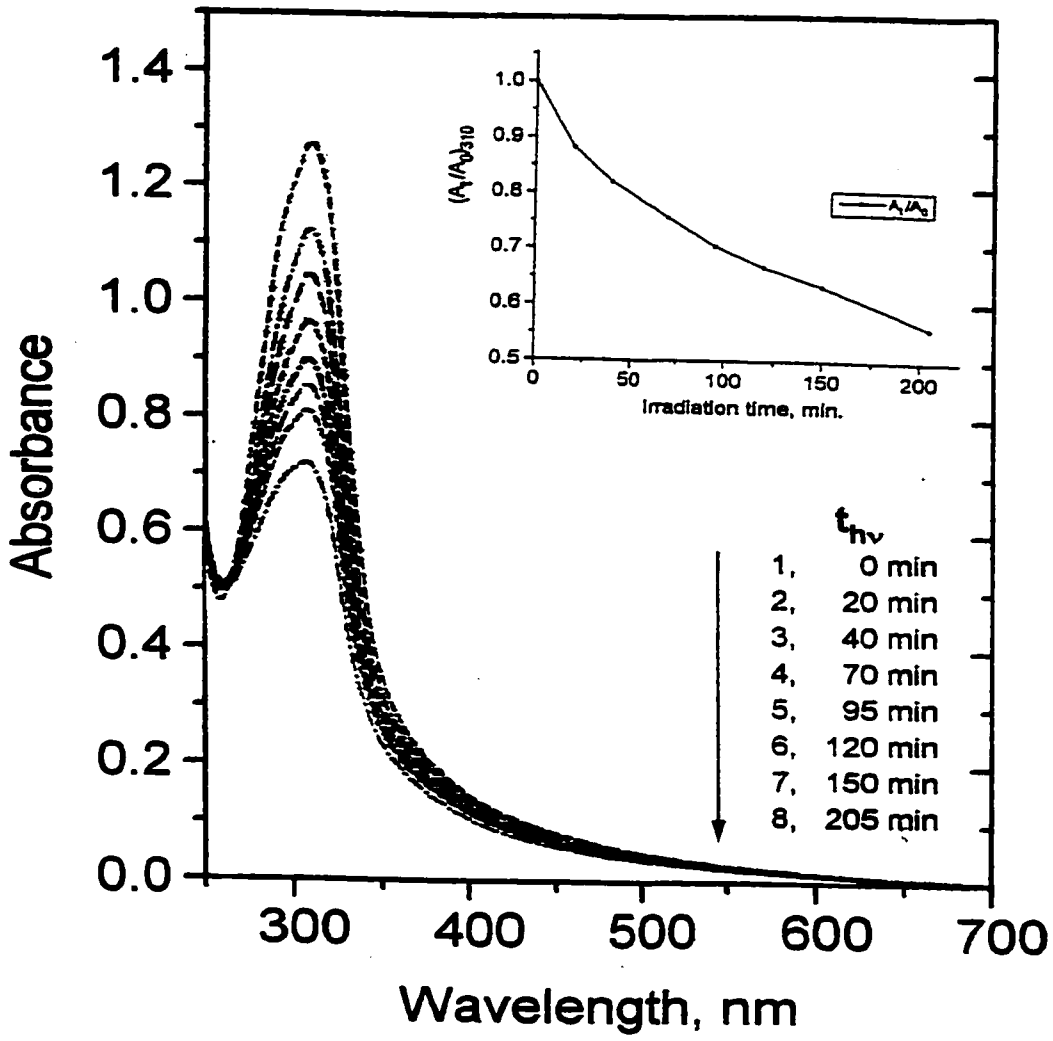

Figure 1. - Absorbance changes taking place during simulated sunlight illumination of the sunscreen lotion SN5; concentration, 0.32 g L^{-1} in air-equilibrated aqueous solutions.

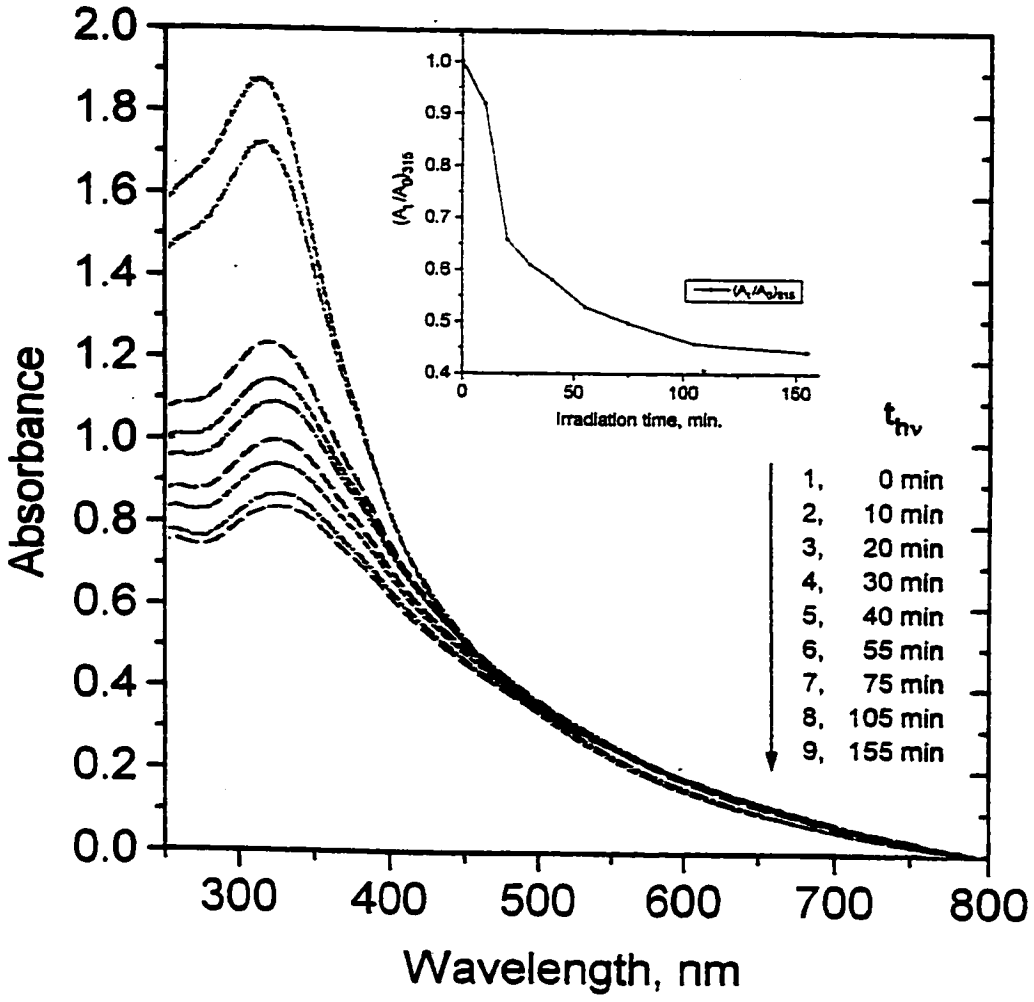

Figure 2. - Absorbance changes occurring in the spectrum of the SN10 sunscream (0.57 g L^{-1} in acetonitrile, air-equilibrated) during simulated sunlight illumination.

Figure 3 illustrates the extent of photodegradation of the SN9 lotion which occurs after about 115 min of simulated sunlight irradiation. This sunscreen lotion is said to contain no chemical filters (organic compounds) as sunscreen agents, only TiO_2 is present to filter out the damaging UV radiation. However, the spectrum reveals there may be some (unknown) organic compound which absorbs around 310 nm, and which undergoes some sort of photodegradation.

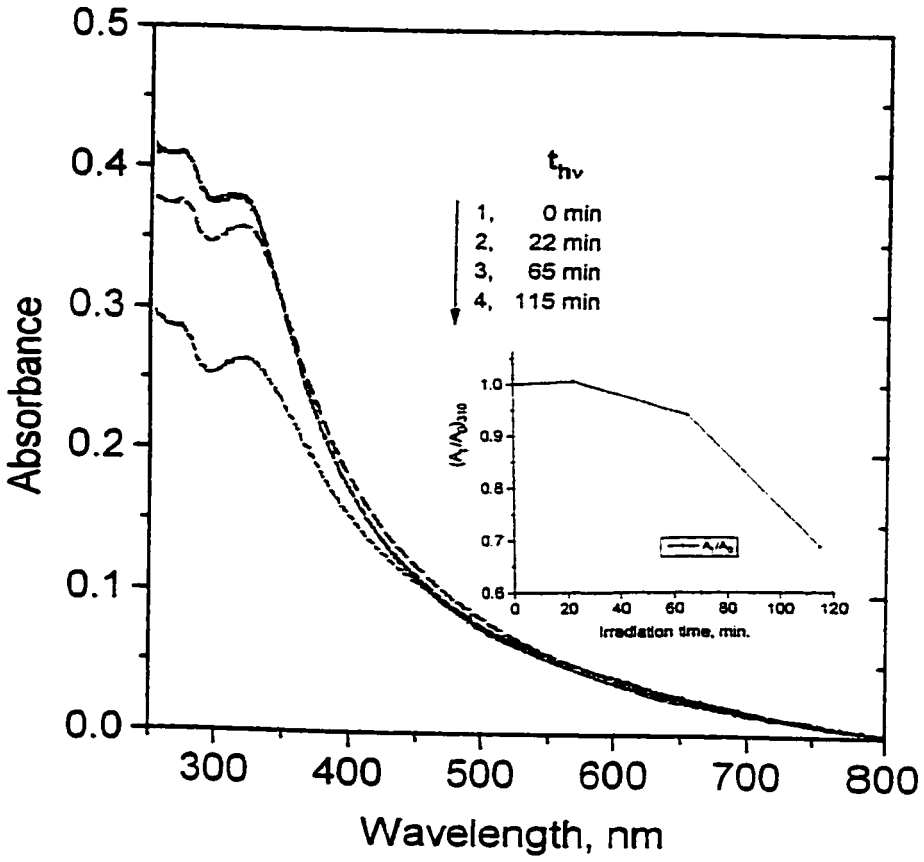

Figure 3. - Absorbance changes taking place in the spectrum of the SN9 suncream (loading, 0.12 g L^{-1} in acetonitrile, air-equilibrated) during simulated sunlight illumination.

Figure 4 illustrates the photodegradation of the sunscreen lotion SN4. This lotion contains a UVA absorber (butylmethoxydibenzoylmethane), and two UVB filters (a camphor derivative and a sulfonic acid compound), together with titanium dioxide - see Table 1. The photodegradation of SN4 leads to a decrease in the absorbance of the lotion. In particular, note the changes occurring at 300 and 360 nm. The spectra also demonstrate an isosbestic point at about 265 nm indicative of formation of a new photoproduct absorbing in the UVB region. The spectrum of titanium dioxide in lotion SN4 is not apparent and does not appear to influence the overall spectra of the combined chemical filters.

Figure 5 shows the temporal spectral changes that occur in the sunscreen lotion NP1 dissolved in water/methanol. This lotion contains titanium dioxide, octyl methoxycinnamate and oxybenzone as the active ingredients. After 2 hrs of irradiation, the absorbance is reduced to half of its original intensity, suggesting that the SPF factor is reduced drastically after two hours. Since one of the main active ingredients is octyl methoxycinnamate (OMC), which undergoes rapid degradation under sunlight exposure (e.g. see below, Figure 8), it is clear that the NP1 lotion is highly photochemically unstable under "real world" conditions. This sunscreen lotion is rather interesting because it is made of organic sunscreens dissolved in an Aloe gel, an original Brazilian plant juice used in cosmetics to heal skin damaged from sunburn. This Aloe gel (NP2) contains a natural UV sunscreen as displayed by the temporal spectra of Figure 6. The Aloe leaf gel also appears to photodegrade under simulated sunlight, albeit very slowly. To determine the anti-radical properties of the Aloe gel, we also tested the NP2 "lotion" for DNA damage using the plasmid nicking assay protocol presented

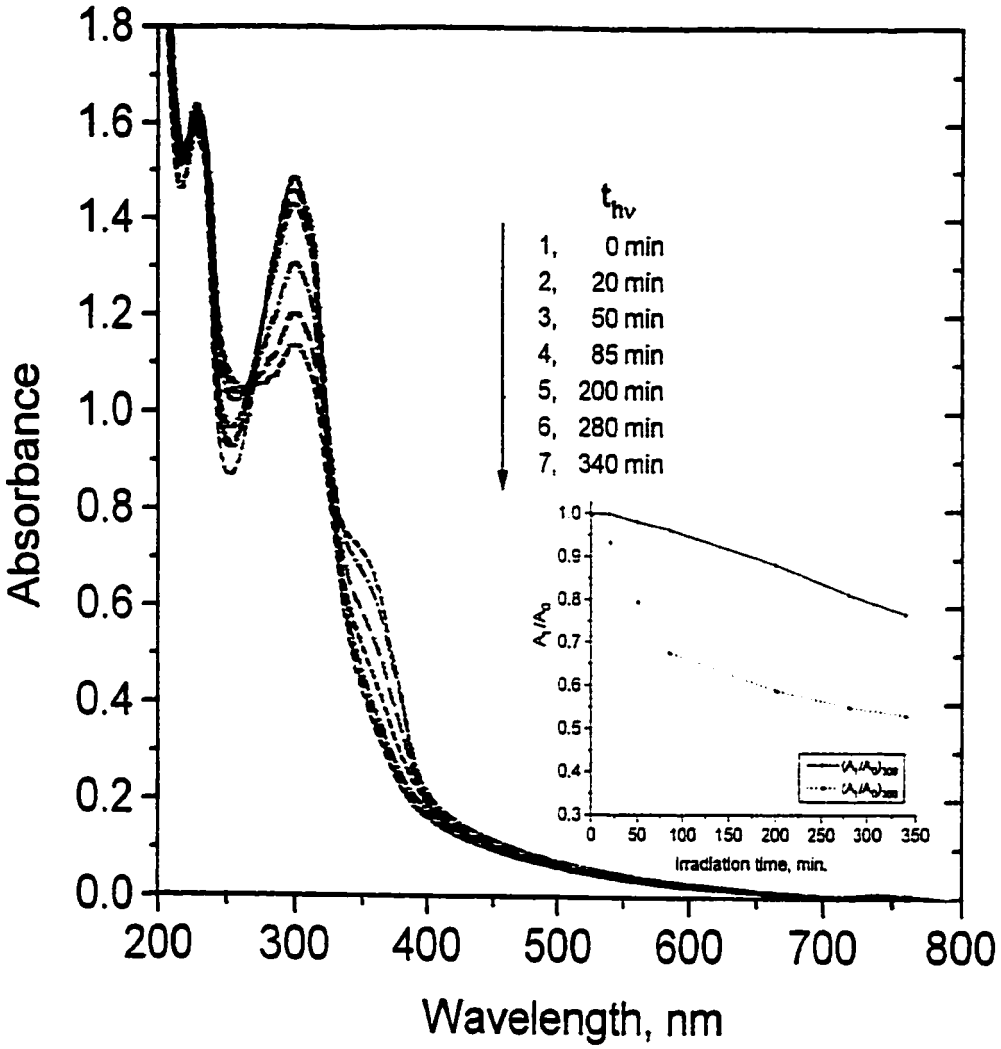

Figure 4. - Absorbance spectral changes occurring in the SN4 sunscream (loading, 0.18 g L^{-1} in water, air-equilibrated) during simulated sunlight illumination.

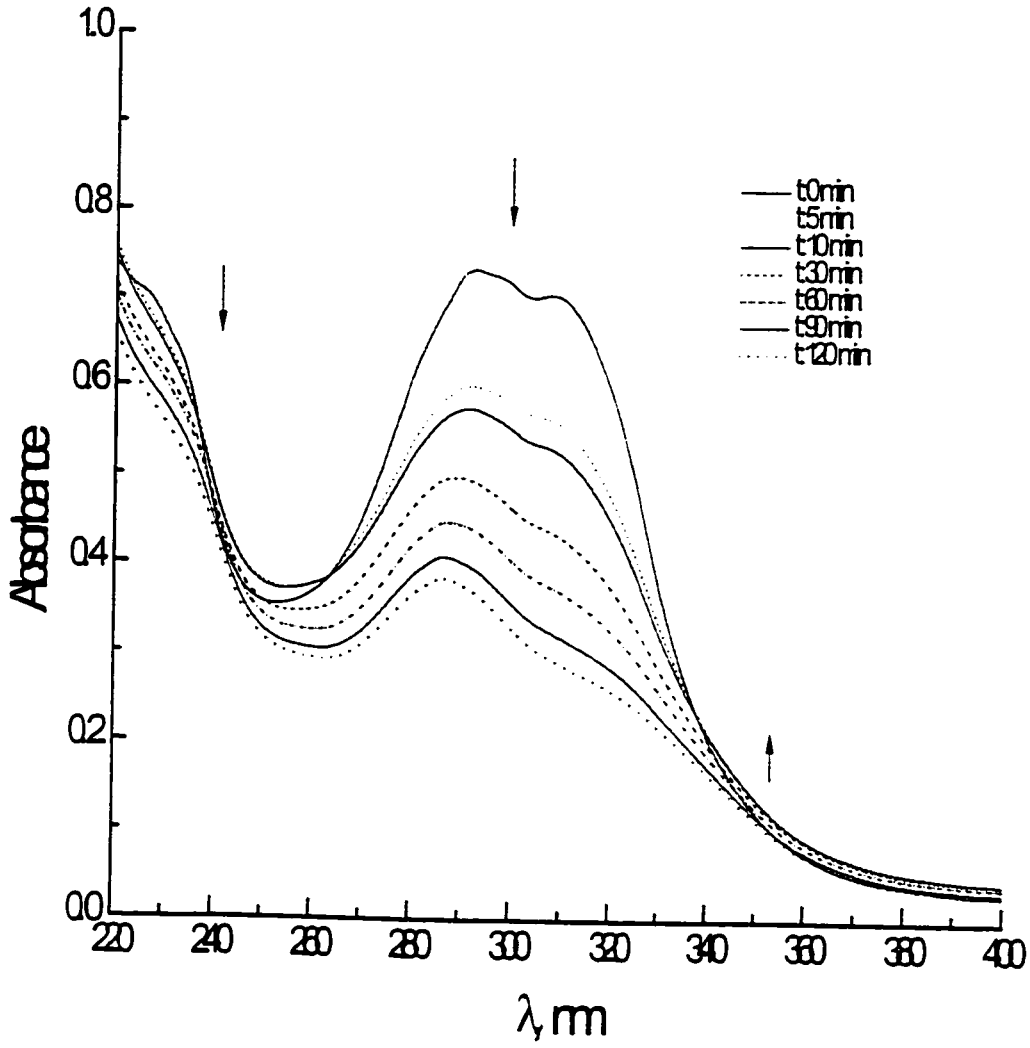

Figure 5. - Irradiation of the NP1 suncream using the solar simulator (concentration, 1 g L^{-1} in 20% methanol/80% water, air-equilibrated).

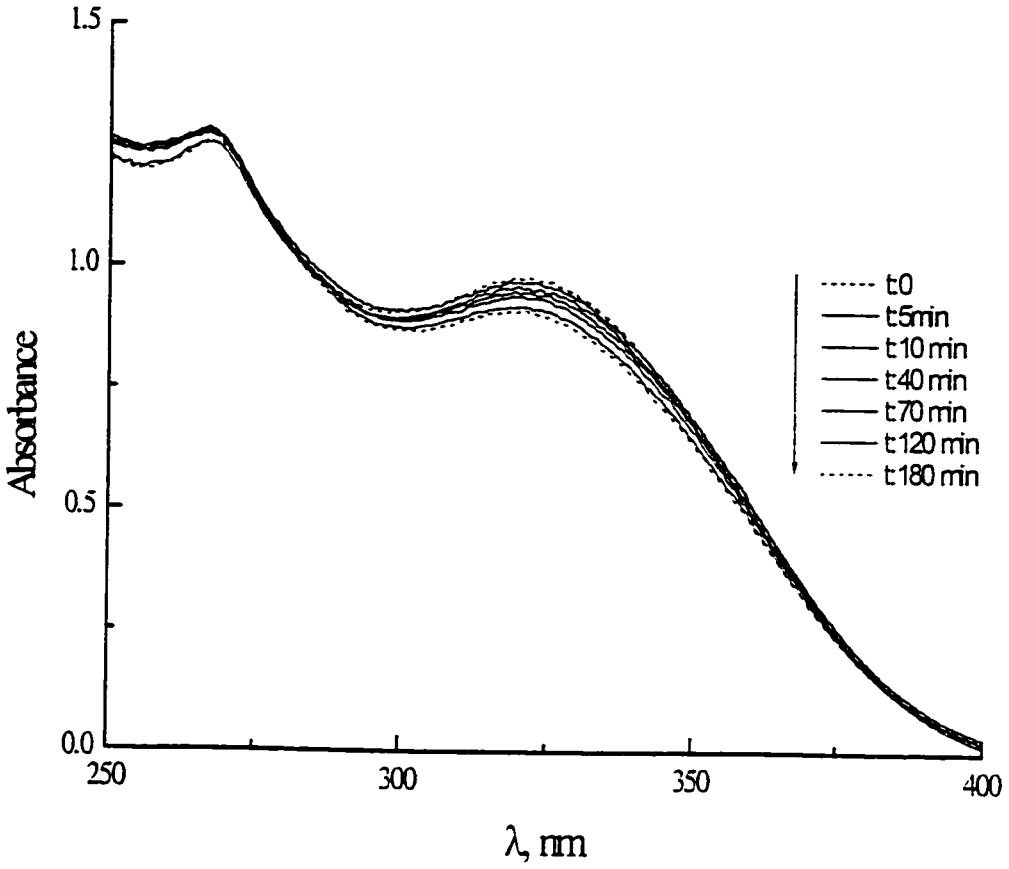

Figure 6. - Absorbance spectral changes for the Aloe plant gel (lotion NP2) in water (concentration, 1g L^{-1}, air-equilibrated) under simulated sunlight illumination.

earlier.

Figure 7 clearly indicates that the NP2 lotion inflicts relatively little, if any, damage to DNA compared to sunscreen lotions previously examined by Knowland and co workers [3,4]. It is interesting to note that the natural product Aloe (NP2) performs better as an anti-radical agent than does vitamin E often used and commercialized in suncare emulsions as a

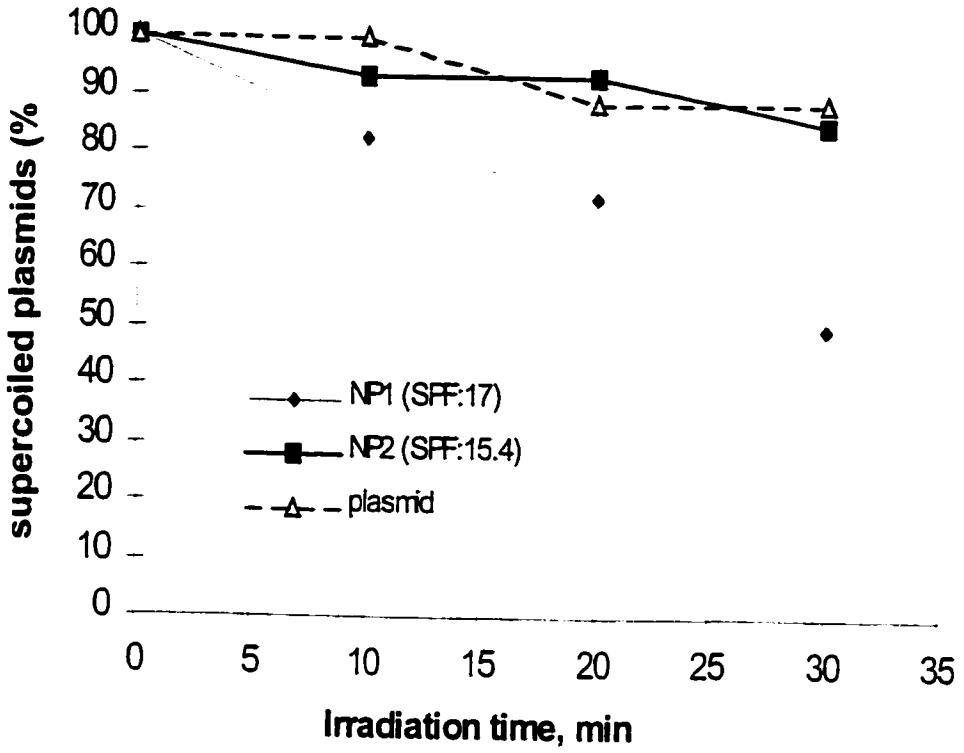

Figure 7. - Survival rate of supercoiled plasmids under exposure to simulated sunlight in the presence of the sunscreen lotions NP1 and NP2 (1/100 dilution in water).

cancer preventing agent [5]. Moreover, Figure 7 also shows the relatively more serious damage caused to DNA by the sunscreen lotion, NP1. As noted above, this NP1 sunscreen lotion contains titanium dioxide as an active sunscreen ingredient, and other natural products as additional active ingredients.

The results presented thus far clearly demonstrate that commercial sunscreen lotions are not photochemically stable. They undergo photodegradation producing unknown

photoproducts that could cause additional damage to skin and to DNA. Moreover, the concentration of the active UV chemical filters decreases on simulated sunlight illumination. This impinges on the relative merits of the SPF factor, which is worth recalling that SPF is defined strictly for UVB radiation only. The sunscreening efficacy of such lotions is therefore questionable. The photodegradation witnessed for these emulsions indicates that the absorbed solar energy is mostly dissipated through photochemical processes, such as photo-fragmentation, photoisomerization, and direct reaction.

Figure 8 shows evidence for an example of such processes of interest on absorption of light by an organic molecule [5]. Absorption loss can be ascribed to photofragmentation or photoisomerization, or to a combination of both processes. In photofragmentation, the absorbing molecule dissociates into reactive free radicals and/or molecular species. This leads to loss of the active ingredients and to a decrease in absorption. Reactive intermediates and various photoproducts formed in illuminated sunscreen lotions [7,8] may be either toxic to DNA or not toxic as in the case of the NP2 lotion.

To the extent that under the normal conditions of sunscreen usage, molecular oxygen (O_2) is ubiquitously present in sunscreen formulations as a result of dissolution from the surrounding air, free radicals and/or molecular species formed from the photofragmentation process can additionally react with molecular oxygen to produce peroxyl radicals. These radicals react with a variety of organic molecules either by H atom abstraction or by addition across unsaturated bonds. For example, peroxidation reactions with cellular lipids lead to formation of hydroperoxide products [9]. Additionally, in some instances generation of

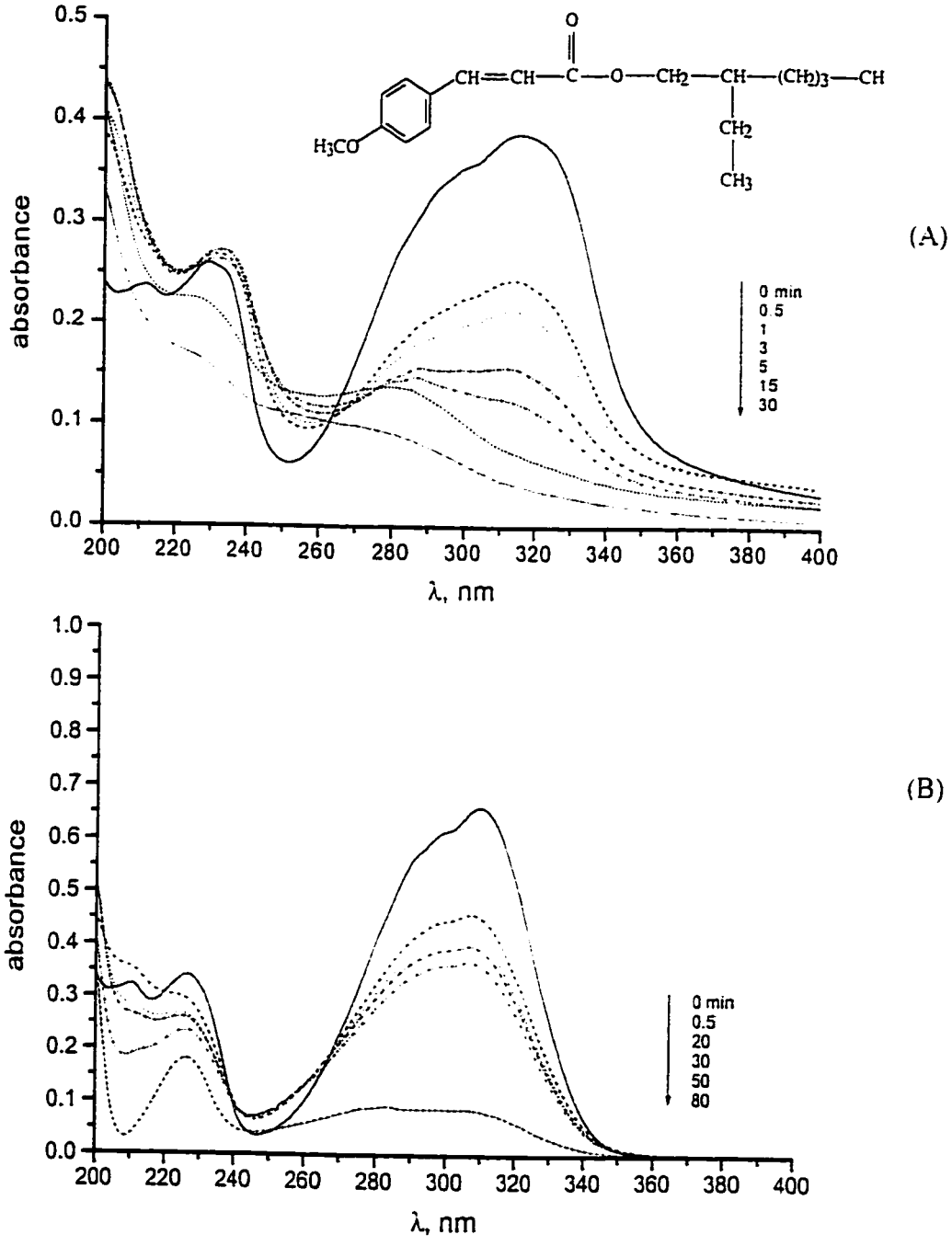

Figure 8. - Illumination of octyl methoxycinnamate (concentration, 8 mg L^{-1}, aerobic conditions): (A) in water, (B) in methanol.

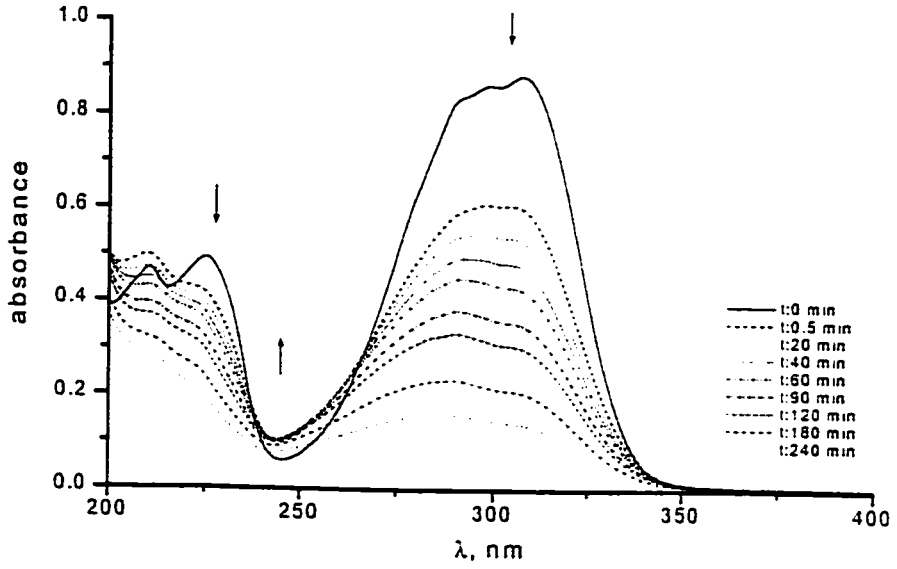

(C)

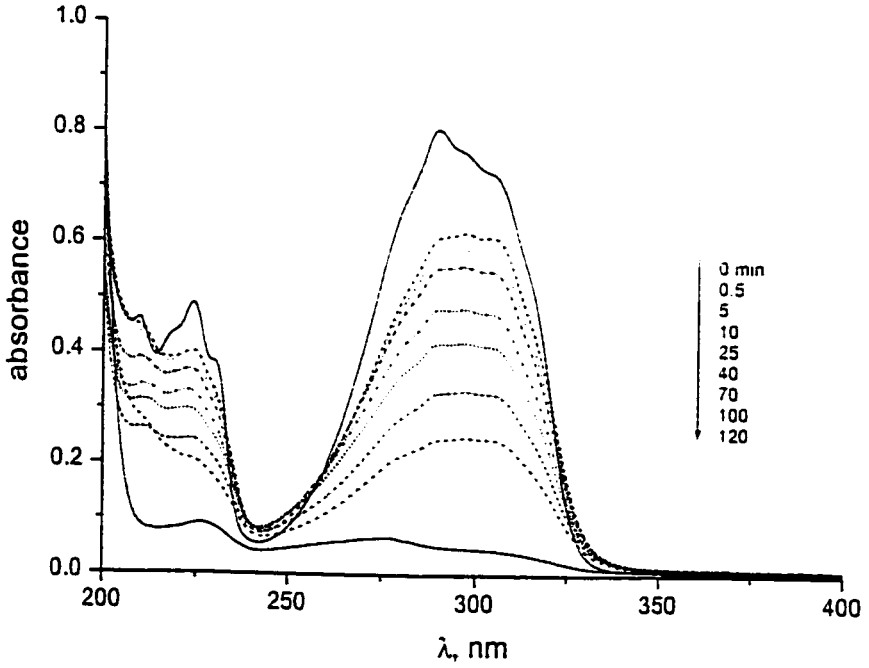

(D)

Figure 8. - Illumination of octyl methoxycinnamate (concentration, 8 mg L^{-1}, aerobic conditions): (C) in acetonitrile, (D) in hexane.

electrons in illuminated titanium dioxide reduce molecular oxygen to form superoxide radical anions ($O_2^{-\bullet}$), which exist in an acid-base equilibrium with hydroperoxyl radicals (HOO•). Superoxide radical anions are selective oxidants and are relatively unreactive toward most biomolecules. However, so-called dismutation/disproportionation reactions involving $O_2^{-\bullet}$ and HOO• (equations 3–5) can lead to rapid formation of hydrogen peroxide [10], which in turn can produce hydroxyl radicals (•OH) through a Fenton-type reaction (equation 6).

$$HOO\bullet + O_2^{-\bullet} + H^+ \rightarrow H_2O + O_2 \quad (3)$$

$$HOO\bullet + HOO\bullet \rightarrow H_2O_2 + O_2 \quad (4)$$

$$O_2^{-\bullet} + O_2^{-\bullet} + 2H_2O \rightarrow H_2O_2 + O_2^{-\bullet} + 2\bullet OH + 2e^- \quad (5)$$

$$H_2O_2 + Fe^{2+} \rightarrow FeOH^{2+} + \bullet OH \quad (6)$$

The •OH species cause considerable damage to DNA inducing strand breaks, cell mutations and cell death. Indirect evidence for the formation of •OH radicals in illuminated solutions containing Padimate-O has been reported by Knowland and coworkers [3]. Evidence for DNA damage due mainly to hydroxyl radicals in illuminated sunscreen lotions containing Padimate-O, Oxybenzone and Octyl Methoxycinnamate were reported by Gulston and coworkers [4].

Loss of absorption in sunscreen lotion can also be caused by some type of

photoisomerization. In particular, the active cinnamate group ingredient [8] and dibenzoyl methane derivatives are known to undergo photoisomerization [11]. The cinnamate absorber photoisomerizes across the ethylenic double bond from the *trans* to the *cis* form. The *cis*-isomer is a less efficient UV absorber, thereby displaying decreased absorbance. Additional decrease in absorbance can also be ascribed to non-absorbing degradation products. Not only can the *trans*-2- ethylhexylmethoxycinnamate photoisomerise, but it can also dimerise with itself through a [2+2]-cycloaddition reaction across the ethylenic double bound. The dibenzoylmethane derivatives photoisomerises showing loss of absorbance in the process of keto/enol tautomerism.

3.2 Spectroscopy, Photostability, and Photochemistry of organic chemical UV absorbers

To the extent that a complete understanding of a photoreaction (e.g., photo-degradation) involving sunscreen lotions requires knowledge of what happens at the molecular level from the absorptive act, together with the isolation and identification of intermediate products, one of the goals of the present study was to obtain some relevant preliminary photochemical data on the sunscreens for future investigations. Four sunscreen active agents were identified from the commercial lotions and chosen for that purpose. They were: (i) 2-ethylhexyl-*p*-methoxycinnamate (also referred to as octyl methoxycinnamate, or as OMC), (ii) the 2-ethylhexyl-ester of N,N-dimethyl-4-aminobenzoic acid- (sometimes denoted as Padimate-O), (iii) 2-hydroxy-4-methoxybenzophenone (or Oxybenzone), and (iv)

the 2-phenylbenzimidazole-5-sulfonic acid (phenylbenzimidazole sulfonic acid). Solutions of these active ingredients in various solvents were subjected to equivalent sunlight exposure under air-equilibrated conditions; temporal absorbance changes were recorded subsequent to illumination at various time intervals. Four solvents with different polarity were chosen to dissolve the active ingredients: water, methanol, acetonitrile, and hexane. To the extent that sunscreen lotions consist of water-in-oil (w/o) or oil-in-water (o/w) emulsions, it was imperative to assess the photostability of these active ingredients and how it changes with the polarity of the solvents. Additionally, it was relevant to simulate sun exposure of these active ingredients dissolved in water and determine/evaluate the oxygen dependence to probe whether the photodegradation proceeds through an oxygen-dependent mechanism.

Table 2 summarizes the UVA and UVB spectral data of these active ingredients depicting the wavelengths of maximum absorption, and the molar absorption coefficient (ε) in the respective solvents used. The active ingredient octyl methoxycinnamate is oil soluble; thus, it is only slightly miscible with water so that a low ε value in water is somewhat tenuous. Nonetheless, the molar absorptivity is reasonably high, and is likely due to a $\pi \rightarrow \pi^*$ transition related to, for example, a C=C-C=O conjugated type structure (see Figure 8A). The absorption maximum of octyl methoxycinnamate in methanol is at 308 nm, blue-shifted to 280 nm in hexane, and red-shifted to 320 nm in water. It would appear that any formulation of non-polar solvents should be avoided with octyl methoxycinnamate since such formulations would display absorption features that would filter out less of the UVB radiation.

Table 2. - UVA and UVB spectral data of sunscreen active ingredients showing the wavelengths of maximal absorption and the molar absorptivity (ε) in solvents of different polarity.

	Octyl Methoxy-cinnamate		Padimate-O		Oxybenzone		Phenylbenzimidazole Sulfonic Acid	
Solvent	λ max nm	ε $M^{-1}cm^{-1}$	λ max nm	ε $M^{-1}cm^{-1}$	λ max nm	ε $M^{-1}cm^{-1}$	λ max nm	ε $M^{-1}cm^{-1}$
Water	320	14,000	311	21,490	321 285	5,870 8,714	302 242	25,990 22,536
Methanol	308	24,070	311	32,730	325 287	9,628 14,857	304 243	27,550 20,962
Acetonitrile	307	32,170	309	33,830	325 287	12,300 18,948	306	saturated solution
Hexane	289	29,090	299	30,270	325 283	12,610 11,757	252 228	saturated solution
From water to hexane	$\Delta\lambda$ = 31 nm		$\Delta\lambda$ = 12 nm		$\Delta\lambda_1$ = 4 nm $\Delta\lambda_2$ = 2 nm		$\Delta\lambda_1$ = 50 nm $\Delta\lambda_2$ = 14 nm	

Figure 8 shows the photodegradation of octyl methoxycinnamate (OMC) in the four different solvents: (A) water, (B) methanol, (C) acetonitrile, and (D) hexane. In all four solvents, the photodegradation of OMC is significant. In hexane (Figure 8C) we observe nearly complete degradation after about 2 hrs of illumination; the estimated quantum yield (Φ) of degradation (excitation wavelength, 313 nm; photon flow, 9.769×10^{15} photons s^{-1}) of this active agent in aqueous media is $\Phi = 4 \times 10^{-2}$, and in hexane $\Phi = 2 \times 10^{-2}$. We infer that OMC degrades rather substantially in both polar and non-polar solvents. According to the work of Morliere and coworkers [8], this loss of absorption results is due mainly to a

trans-cis isomerization process occurring at the double bond since the *cis* isomer is less UV radiation absorbing. Additionally, we noted that in all four solvents the compound displays multiple isosbestic points and formation of new absorbing photoproducts.

Figure 9 summarizes the photodegradation of octyl methoxycinnamate (8 mg L^{-1}) and its dependence on the presence of oxygen in aqueous media. Figure 9A illustrates the spectral variations under aerobic conditions, whereas Figure 9B shows the spectral behavior under anaerobic conditions when the octyl methoxycinnamate system is illuminated with suitable UVA and UVB radiation. Under anaerobic conditions (purging the solution with Argon for ca. 30 min) the absorbance spectrum red-shifts by about 8 nm, and is accompanied by a decrease in intensity. We speculate that owing to the relatively low solubility of octyl methoxycinnamate in water, sparging with argon causes some of the compound to be removed from solution. Comparison of Figures 9A and 9B reveals that OMC photodegrades faster in the presence of oxygen than under anaerobic conditions. Moreover, it also appears that whatever intermediate product is first produced from the initial photodegradation process (band around 230 nm), it too photodegrades under the prevalent conditions. Figure 9B (anaerobic condition) shows a cleaner isosbestic point at 279 nm.

Padimate-O (see Figure 10) manifests a similar behavior to octyl methoxycinnamate displaying a red-shift of the overall absorption band envelope and an increase of the molar absorptivity from a non-polar to a more polar solvent; this influences the efficacy of the sunscreen lotion. The molar absorptivity for Padimate-O is relatively high and highest in non-aqueous solvents (Table 2) . The band is most likely due to a $\pi \rightarrow \pi^*$ transition related

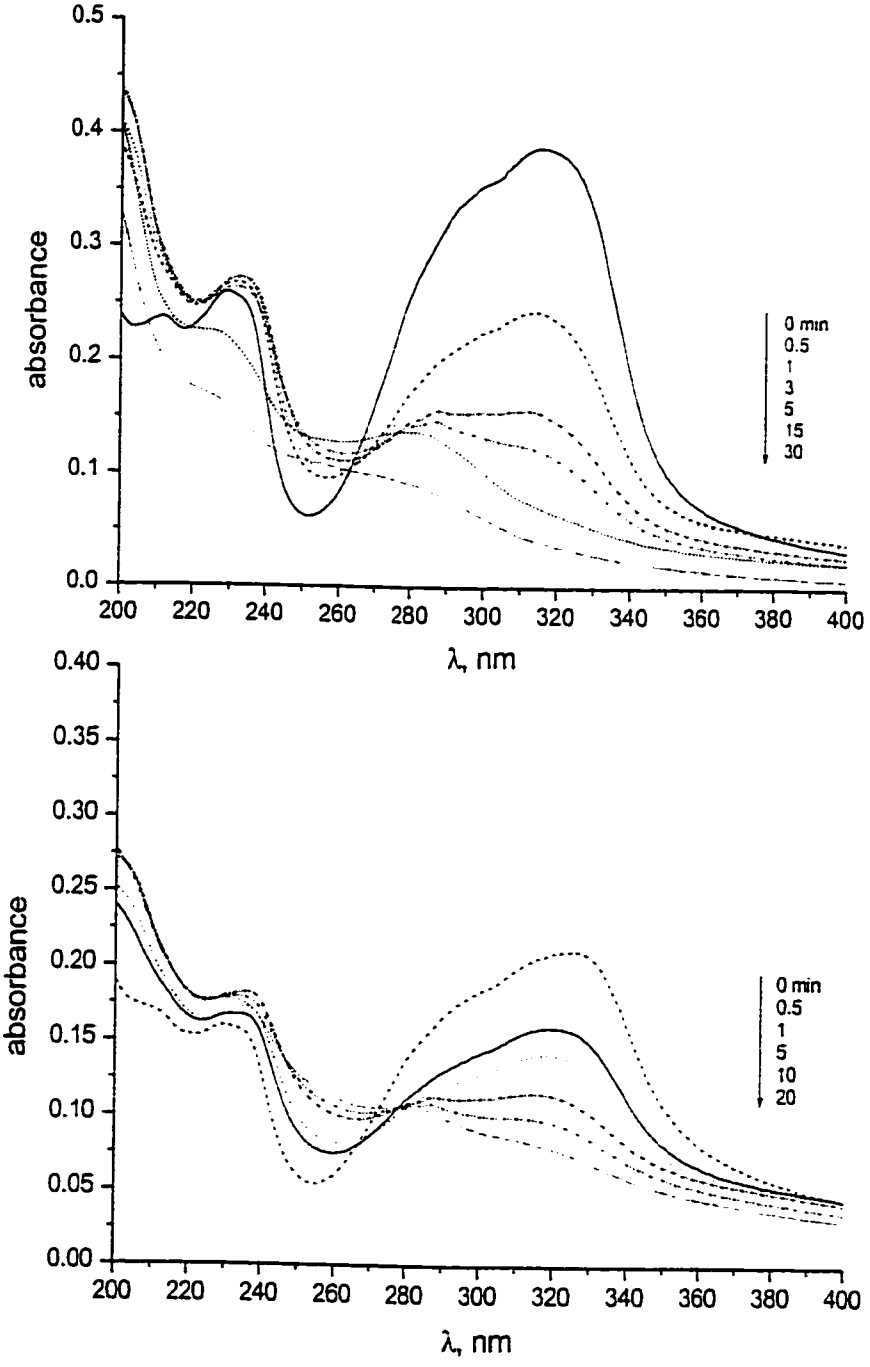

Figure 9. - Illumination of an aqueous solution of octyl methoxycinnamate (8 mg L^{-1}) with the 1000-Watt Hg/Xe lamp: (A) aerobic conditions, (B) anaerobic conditions.

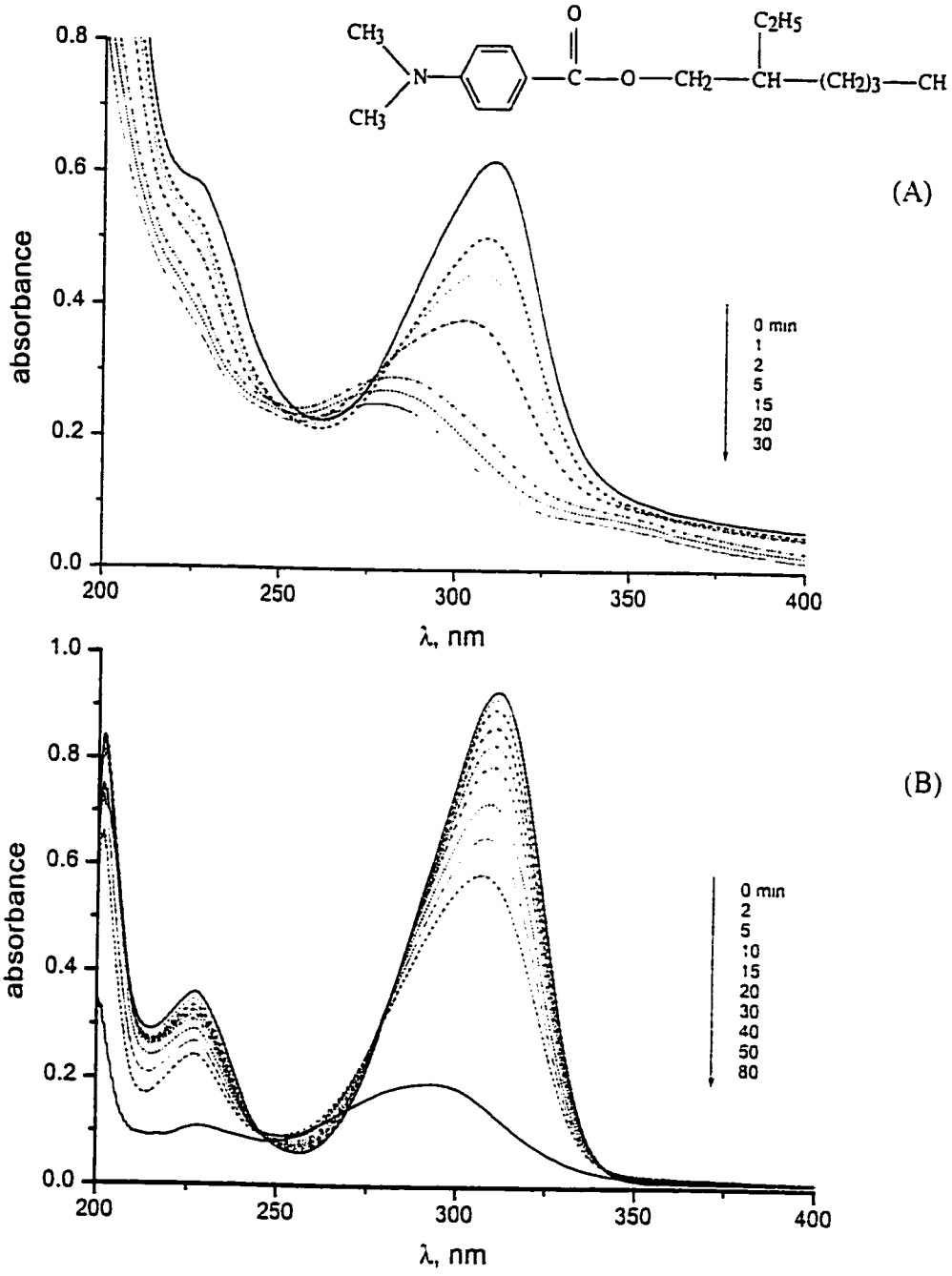

Figure 10 . - Illumination of Padimate-O (loading, 8 mg L^{-1}) under aerobic conditions using the 1000-Watt Hg/Xe lamp: (A) in water, (B) in methanol.

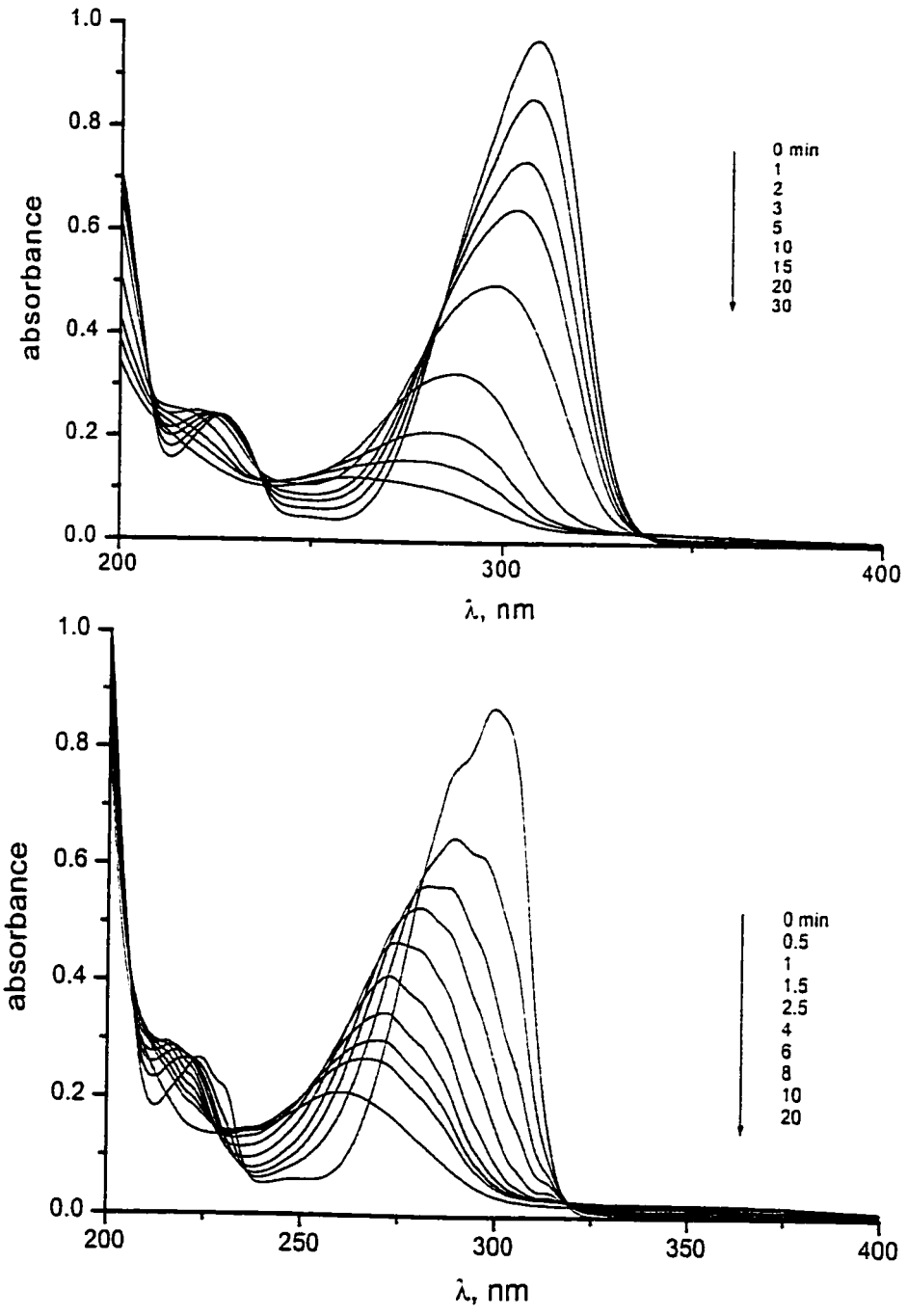

Figure 10. - Illumination of Padimate-O (loading, 8 mg L^{-1}) under aerobic conditions using the 1000-Watt Hg/Xe lamp: (C) in acetonitrile, (D) in hexane.

to the C_6H_5-C=O group conjugation effects (see structure in Figure 10A).

Table 2 also shows that the absorption feature at 299 nm for Padimate-O in hexane is red-shifted in aqueous media by as much as 12 nm. Figure 10 summarizes the photodegradative behavior of Padimate-O in four different solvents of varying polarity: (A) water, (B) methanol, (C) acetonitrile, and (D) hexane. In all four solvents the photodegradation of Padimate-O is significant. In particular, in acetonitrile and in the non-polar solvent hexane (Figures 10C and 10D) complete degradation of Padimate-O occurs after about 20 min of illumination. In water Padimate-O seems to photodegrade more slowly than in hexane; the calculated quantum yield in water (excitation wavelength, 313 nm; photon flow, 1.13×10^{16} photons s^{-1}) is $\Phi = 3.6 \times 10^{-2}$. The spectral variations evident in Figures 10A and 10B suggest that a different photochemistry may be involved during illumination of Padimate-O between a polar and a less-polar solvent. Also note the significant but different blue shifts in band maxima seen between the two sets of spectra illustrated in Figures 10C and 10D for Padimate-O in acetonitrile and hexane, respectively.

Figures 11A and 11B depict the effect of air oxygen when an aqueous solution of Padimate-O is illuminated with UV radiation. Under aerobic conditions, Padimate-O degrades faster (Figure 11A) than in the absence of molecular oxygen (Figure 11B). This calls attention to the possibility that a reaction takes place between appropriate excited state(s) of Padimate-O and molecular oxygen to yield, for example, such species as singlet oxygen, $^1O_2$. Note that Padimate-O is a PABA derivative, an ester of *p*-aminobenzoic acid.

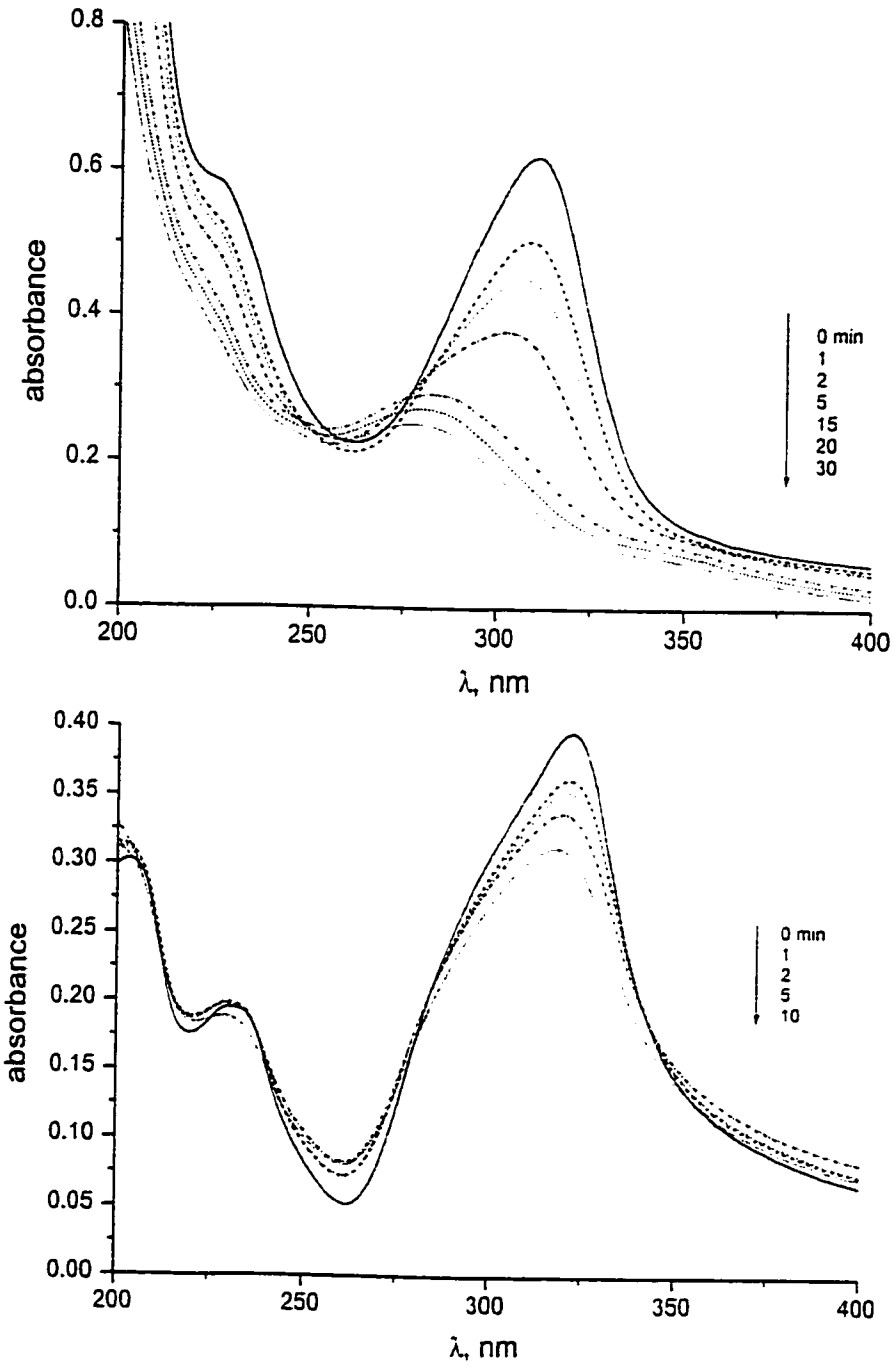

Figure 11. - Illumination of aqueous solutions of Padimate-O (loading, 8 mg L^{-1}) using a 1000-Watt Hg/Xe lamp: (A) aerobic conditions, (B) anaerobic conditions.

Allen and coworkers reported evidence for singlet oxygen generation on illumination of PABA and its derivatives [12].

Figure 12 shows the behavior of Oxybenzone when illuminated in (A) water, (B) methanol, (C) acetonitrile, and (D) hexane. Oxybenzone appears to be most stable in acetonitrile than in the other solvents. It is particularly unstable in methanol, where it photodegrades almost completely after only 2 hrs. Illumination of hexane or acetonitrile solutions of Oxybenzone does not seem to produce new absorbing photoproducts. In hexane, the quantum yield for the initial photodegradation of Oxybenzone is $\Phi = 3.1 \times 10^{-5}$ (excitation at 334 nm; monitored wavelength, 283 nm); the photon flow at 334 nm was 9.769×10^{15} photons s^{-1}. In aqueous media, $\Phi = 1.3 \times 10^{-4}$ nearly an order of magnitude greater than in hexane, under otherwise identical conditions.

Figure 13 describes and compares the oxygen dependence on the photodegradation of Oxybenzone under aerobic and anaerobic conditions. It is evident that under anaerobic conditions (Figure 13B) Oxybenzone degrades much more slowly than under aerobic conditions (Figure 13A).

The oxygen-dependent photodegradation of sunscreen active ingredients may involve such harmful species as singlet oxygen. Indeed, chemical sunscreen UV absorbers make excellent triplet state photosensitizers, transferring energy to another molecule on absorption of sunlight. The photosensitizer, initially in a singlet ground electronic state, is promoted by absorption of a photon to an excited singlet state which then undergoes intersystem crossing to an excited triplet state. Subsequently, energy transfer from this triplet state to oxygen

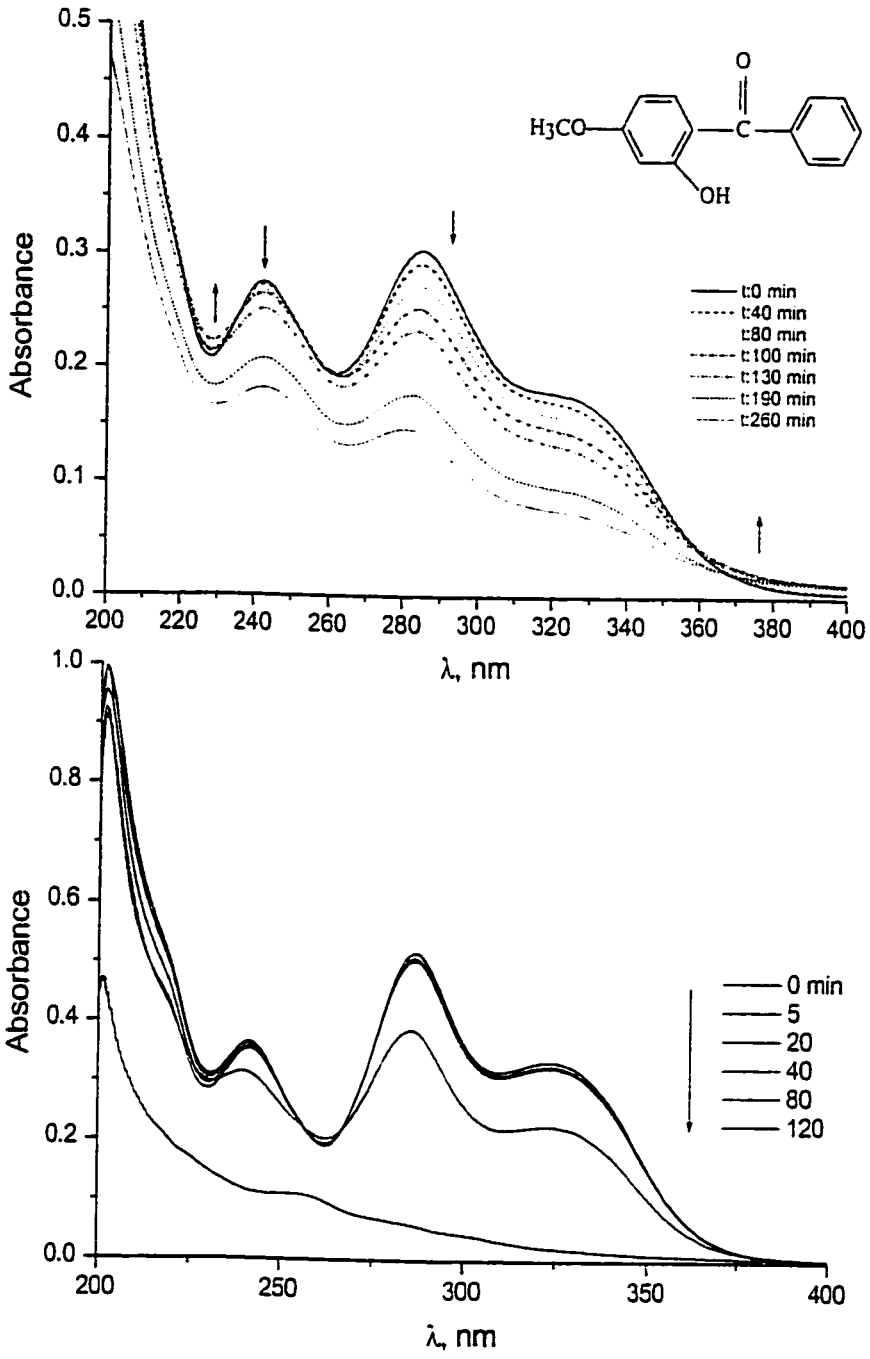

Figure 12. - Illumination of Oxybenzone (8mg L^{-1}; aerobic conditions) using a 1000-Watt Hg/Xe lamp: (A) in water, (B) in methanol.

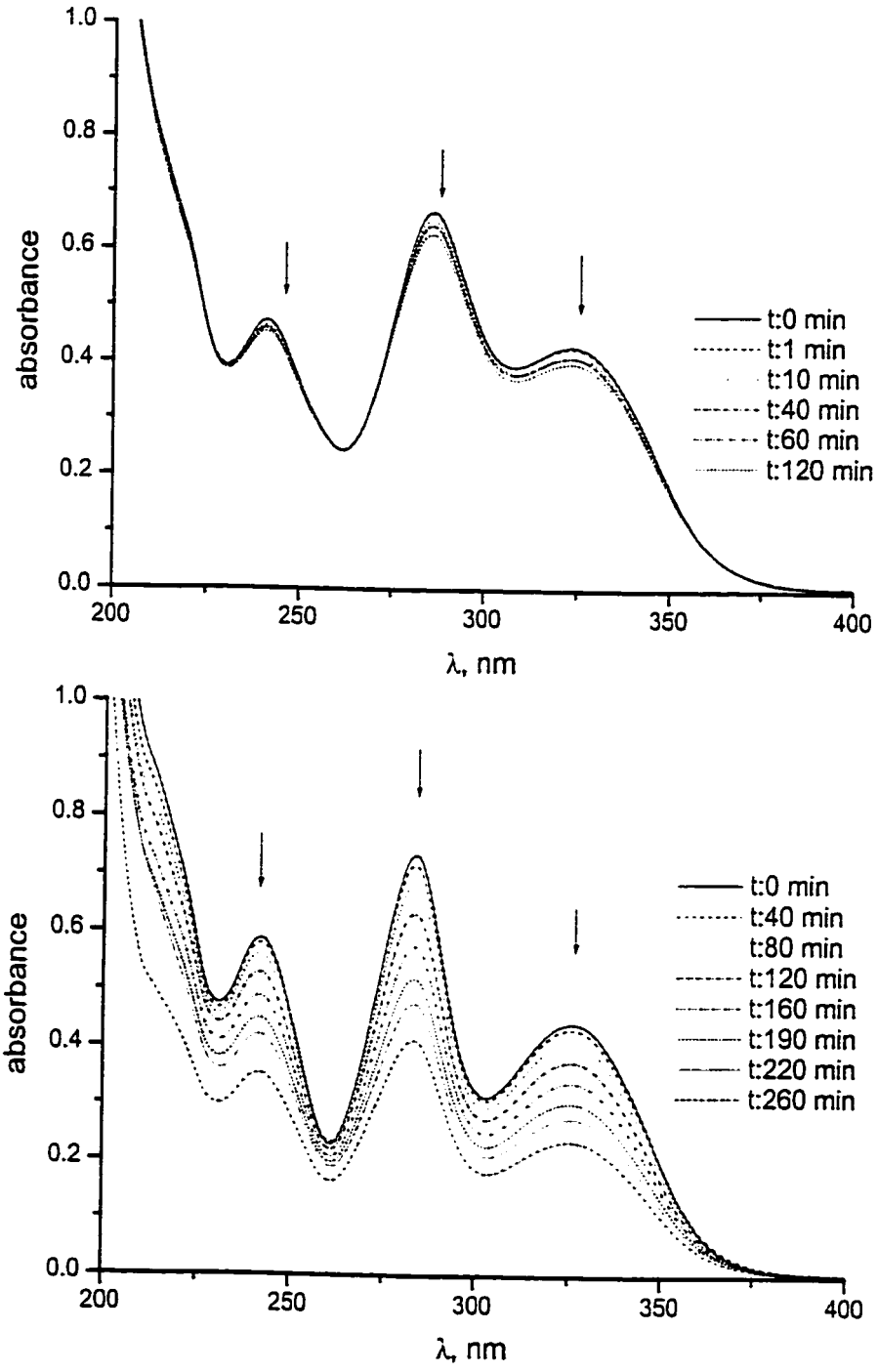

Figure 12. - Illumination of Oxybenzone (8mg L^{-1}; aerobic conditions) using a 1000-Watt Hg/Xe lamp: (C) in acetonitrile, (D) in hexane.

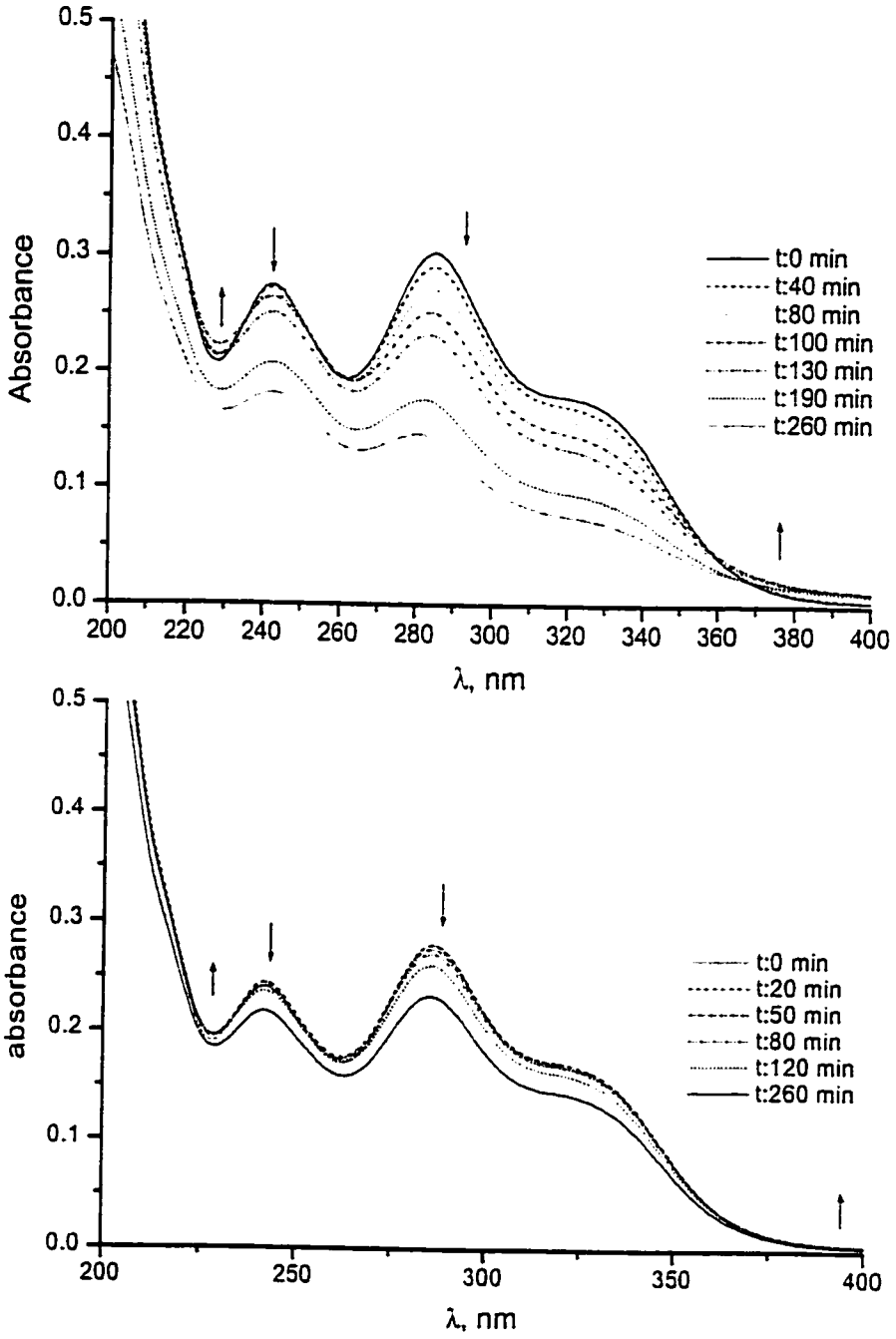

Figure 13. - Illumination of aqueous solutions of Oxybenzone (8 mg L^{-1}) under aerobic (A) and anaerobic (B) conditions using a 100-Watt Hg/Xe lamp.

causes excitation of the triplet ground state of oxygen to its first excited singlet state (see Scheme 1 for the appropriate Jablonski diagram that summarizes many of the photochemical steps for this process).

Singlet molecular oxygen is a significantly more effective oxidant for most organic molecules than ground state molecular oxygen; interactions of $^1O_2$ with singlet ground state organic molecules are spin allowed. The energy required to promote molecular oxygen from its ground state triplet to the excited singlet state is only 22.7 Kcal mol^{-1} [13]. To the extent that triplet state energies of such sunscreens as PABA (75 Kcal mol^{-1}) and octyl methoxycinnamate (57 Kcal mol^{-1}) [14] have enough energy to promote oxygen to its singlet state, formation of singlet oxygen with these chemical sunscreens is indeed energetically favorable. Evidence of singlet oxygen formation has also been reported for other sunscreens, for example Padimate-O [15]. To our knowledge, the energy of the triplet excited state of Oxybenzone has not been reported. However, since the basic structure of Oxybenzone is based on benzophenone, and the triplet state of the latter is 69 Kcal mol^{-1} [14], Oxybenzone is likely to have similar energy for the corresponding triplet state; consequently generation of singlet oxygen on illumination of Oxybenzone is also likely. Allen and coworkers [15], however, report no significant formation of singlet oxygen with Oxybenzone. The spin-allowed absorption spectrum of benzophenone [6] consists of two major bands; one occurs around 280 nm in ethanol corresponding to a $\pi \rightarrow \pi^*$ transition with a high molar absorptivity. This band is not expected to shift significantly from non-polar to more polar solvents. The other absorption band is seen around 325 nm in ethanol; it displays a lower

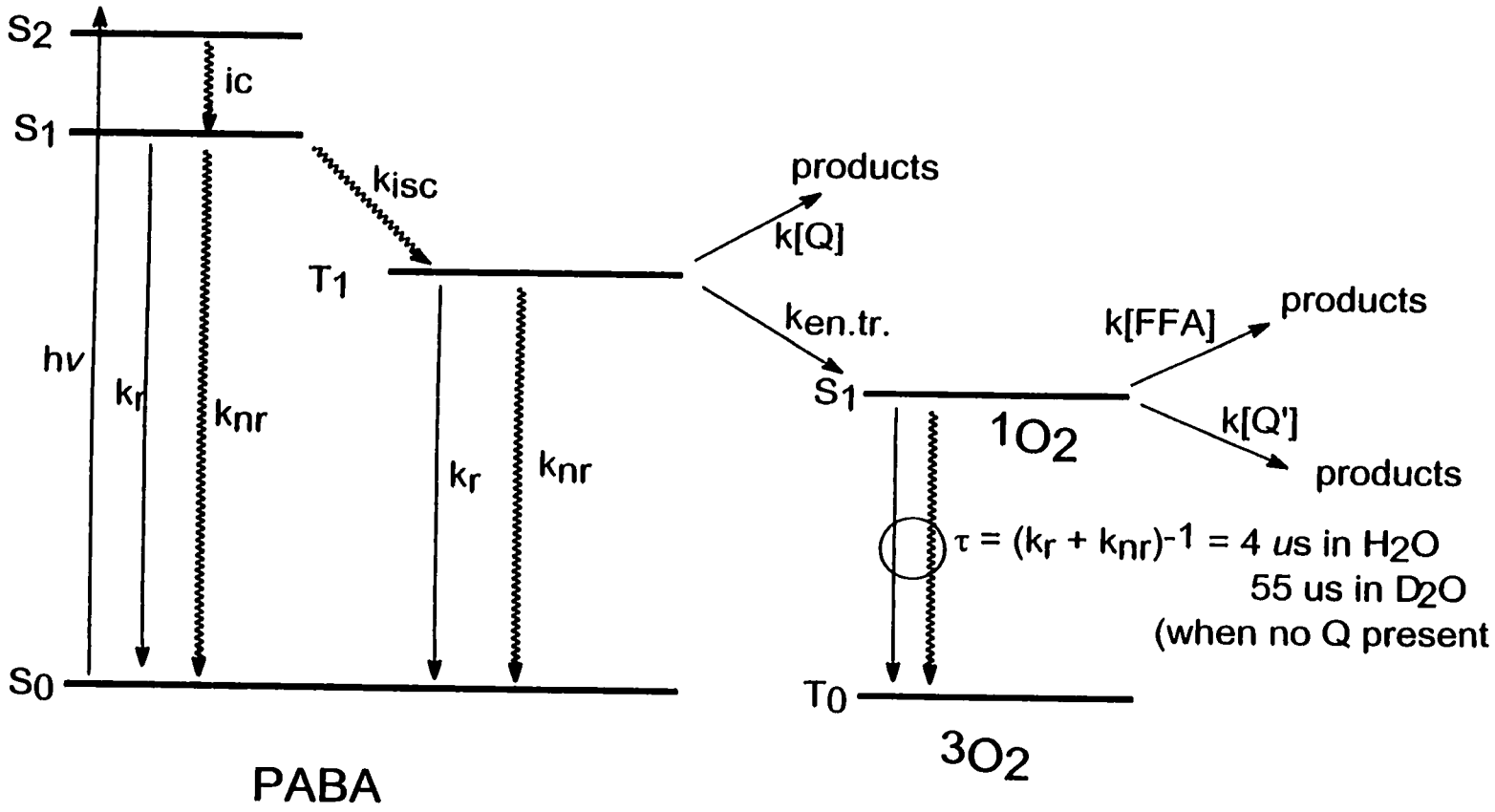
S2
ic
S1
kisc
products
k[Q]
T1
hν
kr
knr
ken.tr.
k[FFA]
products
S1
1O2
k[Q']
products
kr
knr
τ = (kr + knr)-1 = 4 us in H2O
55 us in D2O
(when no Q present
S0
T0
PABA
3O2

Scheme 1

molar absorptivity, and corresponds to a $n \rightarrow \pi^*$ transition. By contrast to the former, this band is expected to red-shift considerably from non-polar to more polar solvents. Consistent with this assertion, inspection of the data of Table 2 indicates that the band for octyl methoxycinnamate occurs at 289 nm in hexane but at 320 nm in water. By comparison, in the case of Oxybenzone the two bands shift position but very slightly when in solvents from highly polar to non-polar characteristics. The results for all four chemical filters of Table 2 are consistent with the notion that the lowest energy band, which shows the greatest red-shift from non-polar solvents to polar solvents is due to promotion from a non-bonding molecular orbital (n) to a molecular orbital of π^* character.

Oxybenzone was the first compound incorporated into sunscreen formulations to offer UVA protection. However, this material presents certain disadvantages. For example, it has limited solubility in water. Additionally, because the molar absorptivity is smaller than for the other sunscreen agents of Table 2, higher concentrations of Oxybenzone are typically needed in formulations to offer the appropriate "protection" against UV radiation. The consequence of this need is that increasing the concentration too often leads to crystallization, and to photoallergenic responses in some individuals [16].

Figure 14 illustrates the temporal course of the photodegradation of the last active ingredient considered in this Chapter 10, namely phenylbenzimidazole sulfonic acid in (A) water, (B) methanol, (C) acetonitrile, and in (D) hexane. Phenylbenzimidazole sulfonic acid is almost insoluble in non-polar solvents. Thus, it should be used in emulsions prevalently aqueous. In aqueous media, the photodegradation of this active agent is particularly fast

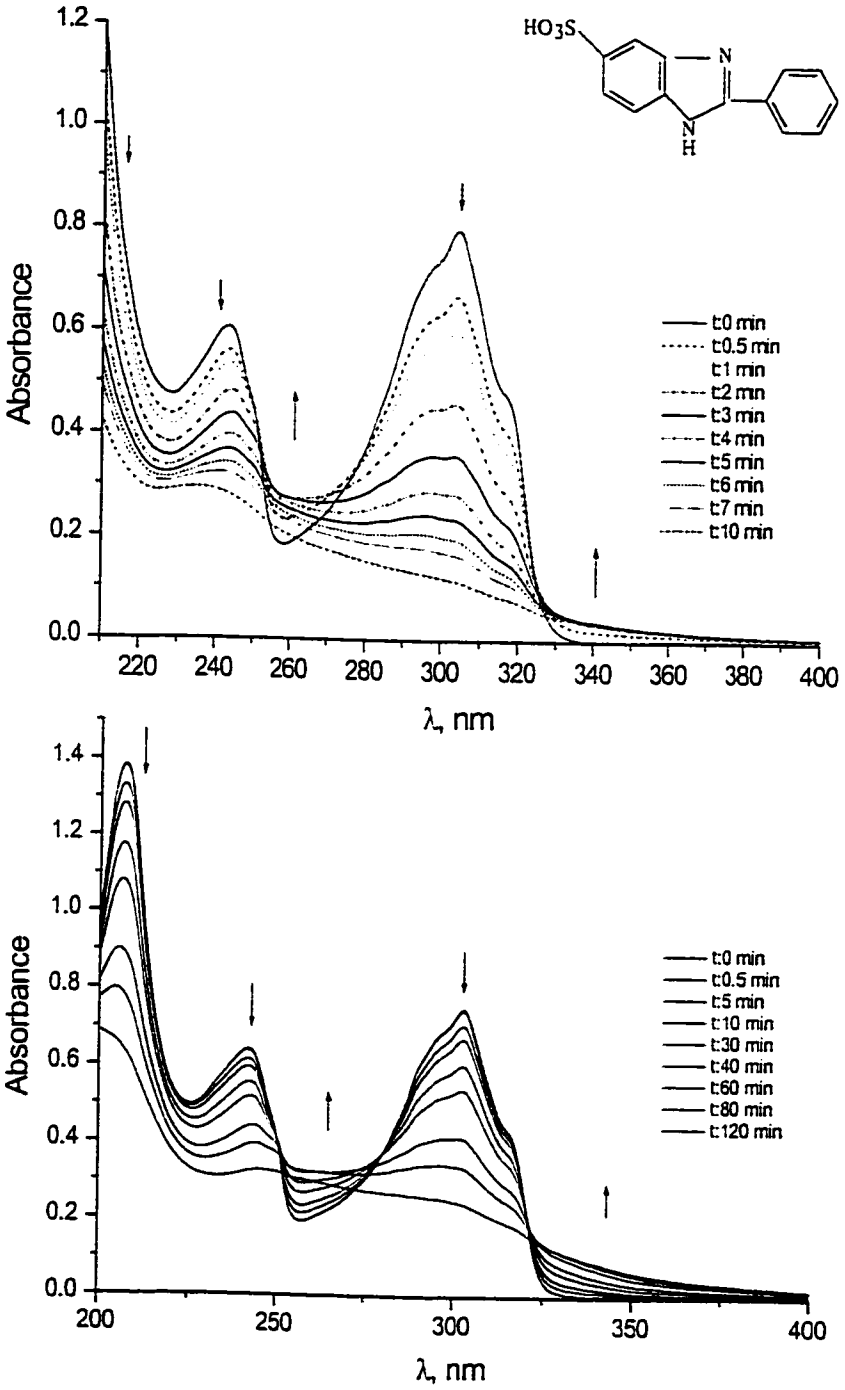

Figure 14. - Irradiation of 2-phenylbenzimidazole-5-sulfonic acid (8 mg L^{-1}) in water (A) and in methanol (B) using a 1000-Watt Hg/Xe lamp source.

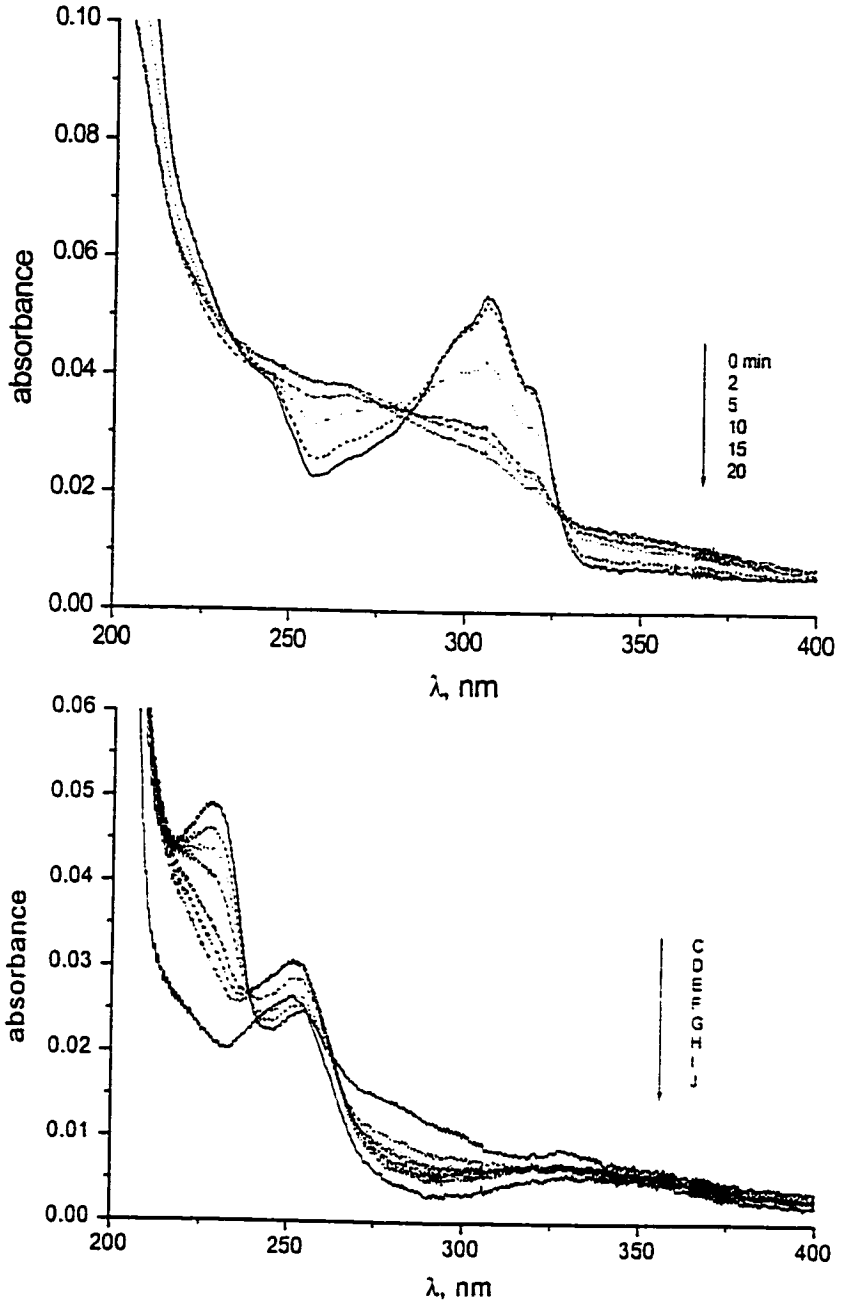

Figure 14. - Irradiation of 2-phenylbenzimidazole-5-sulfonic acid (saturated solutions) in acetonitrile (C) and in hexane (D) using a 1000-Watt Hg/Xe lamp.

(quantum yield not determined). The compound is basically completely degraded after only 10 min of irradiation. In methanolic media, the degradation of this phenylbenzimidazole sulfonic acid is also fairly rapid. Table 2 shows a wavelength shift of $\Delta\lambda = 50$ nm toward the red for the absorption band from 252 nm in hexane to 302 nm in water, whereas the higher energy band displays a smaller wavelength shift of $\Delta\lambda = 14$ nm toward the red from 228 nm in hexane to 242 nm in water. This is consistent with the earlier notion that the more polar the solvent is, the greater will be the effect on the $n \rightarrow \pi^*$ transition. Under aerobic and anaerobic conditions, the photodegradative behavior of this acid in aqueous media shows no substantial differences; compare for example the temporal spectra displayed in Figures 15A and 15B. Nonetheless, there is evidence that illumination of phenylbenzimidazole sulfonic acid does generate singlet oxygen [17].

In as much as a real sunscreen lotion contains more than one active agent, it was imperative that we also assess the synergy in the photochemistry of these chemical filters (and physical filters also) when two or more chemical and physical sunscreens are combined into one single emulsion. Therefore, we prepared and illuminated an aqueous solution (air-equilibrated) of Oxybenzone and octyl methoxycinnamate each at a concentration of 8 mg L^{-1} (see Figure 16). The absorbance of the two compounds is additive; the result is an increase in absorbance compared to the absorbance of the single compound at the same concentration (see Figure 8A, and Figure 12A). Indeed, a single compound could not reach the desired SPF number unless a large amount of any single component were used in the formulation. Note that increasing the amount of sunscreen agent could lead to an increased

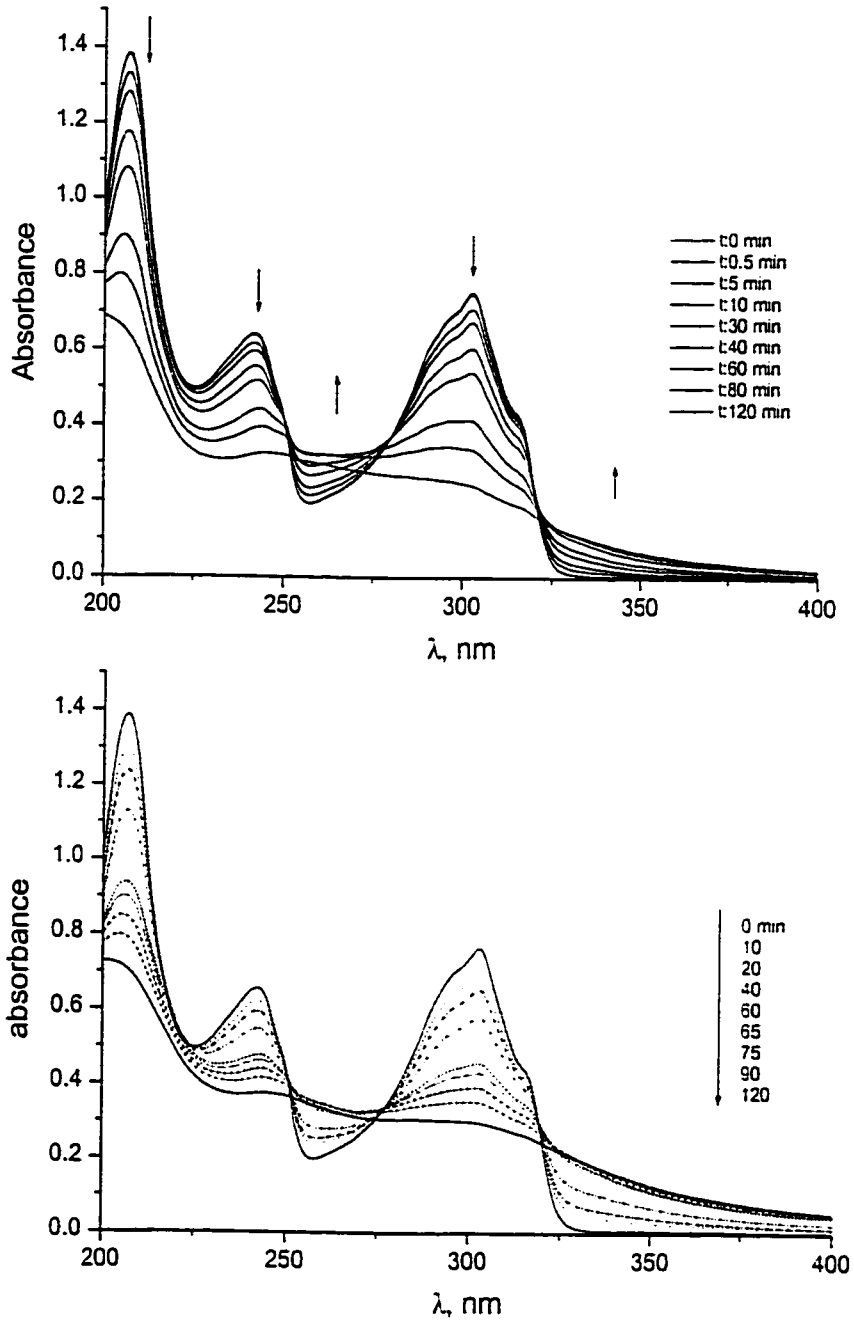

Figure 15. - Illumination of phenylbenzimidazole sulfonic acid (8 mg L^{-1}) in water under aerobic (A) and anaerobic (B) conditions using a 1000-Watt Hg/Xe lamp.

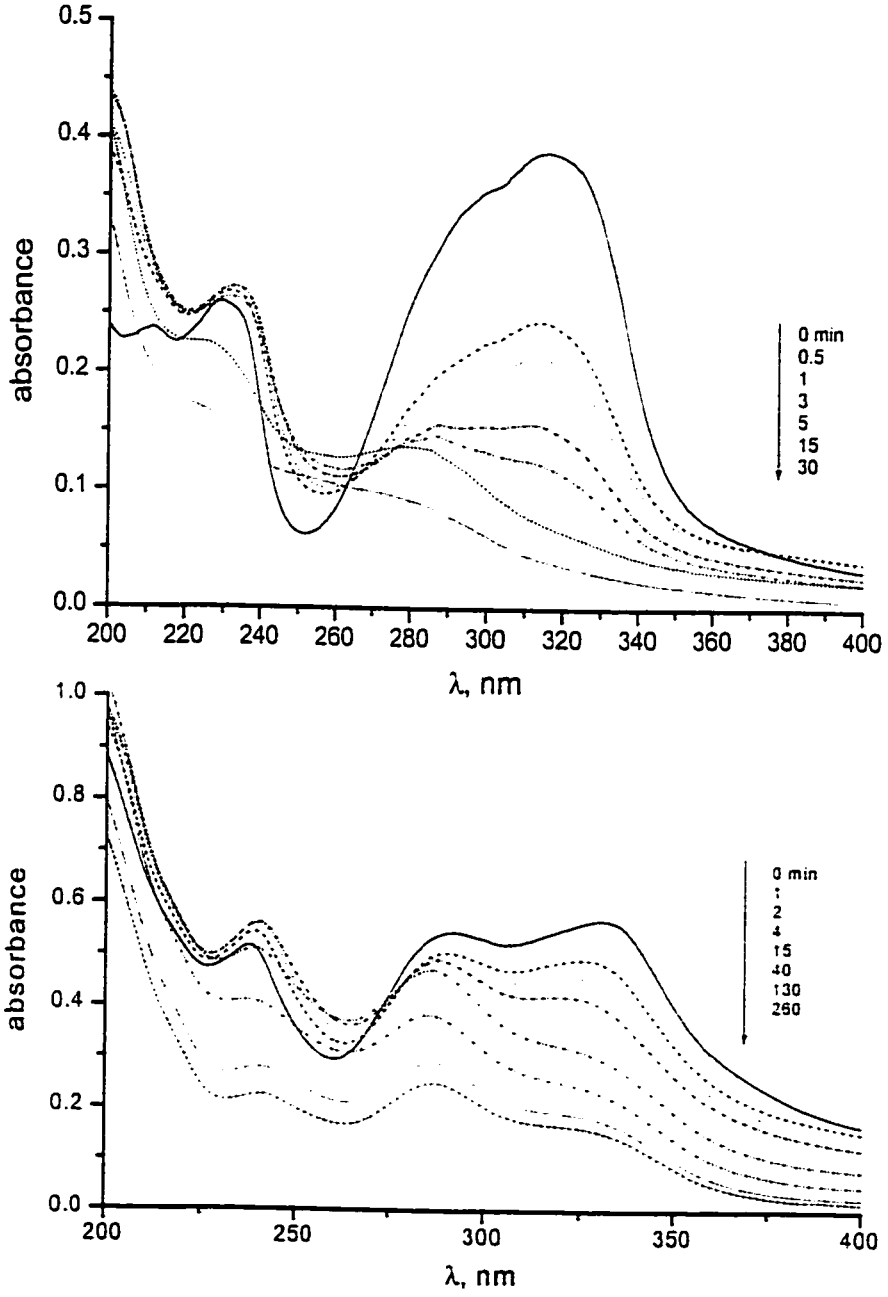

Figure 16. - (A) Irradiation of octyl methoxycinnamate (8 mg L^{-1}) in water under aerobic conditions using a 1000-Watt Hg/Xe lamp. (B) Irradiation of Oxybenzone (8 mg L^{-1}) and octyl methoxycinnamate (8 mg L^{-1}) in water also under aerobic conditions using the same light source.

risk of photo-allergenic effects; other unfavorable drawbacks of increased concentrations are crystallization, cosmetic acceptability, and insolubility. To the extent that Oxybenzone has a molar absorptivity lower than octyl methoxycinnamate, the main sunscreen agent in this mixture is octyl methoxycinnamate, which degrades fairly rapidly. After 15 min of illumination it is almost completely photodegraded leaving Oxybenzone as the sole UV filter. Oxybenzone is more stable, decreasing to half its initial concentration after 260 min of irradiation (see Figure 12A). However, in the presence of octyl methoxycinnamate, the extent of degradation of Oxybenzone is greater than when alone; compare for example the photodegradation of Oxybenzone alone in Figure 12A with that displayed in Figure 16B . Also, additional new photoproducts absorbing in the UVB region appear to be formed when these two standard sunscreen agents are illuminated together; this leads to a more complex photochemistry.

Figure 17 shows the photochemical behavior of Oxybenzone in the presence of TiO_2 particles. To the extent that titanium dioxide is also a common physical sunscreen agent commonly used with other active chemical ingredients, it was instructive to examine the combination of a chemical filter, such as Oxybenzone, and a physical filter such as titanium dioxide under identical illumination conditions. The goal was to assess the photostability of Oxybenzone in air-equilibrated aqueous media under these conditions to compare it to the case where Oxybenzone was alone (Figure 17A) or in combination with another chemical filter (see above and Figure 16B). In the presence of titanium dioxide, Oxybenzone degrades significantly in only 20 min of illumination (see Figure 17B).

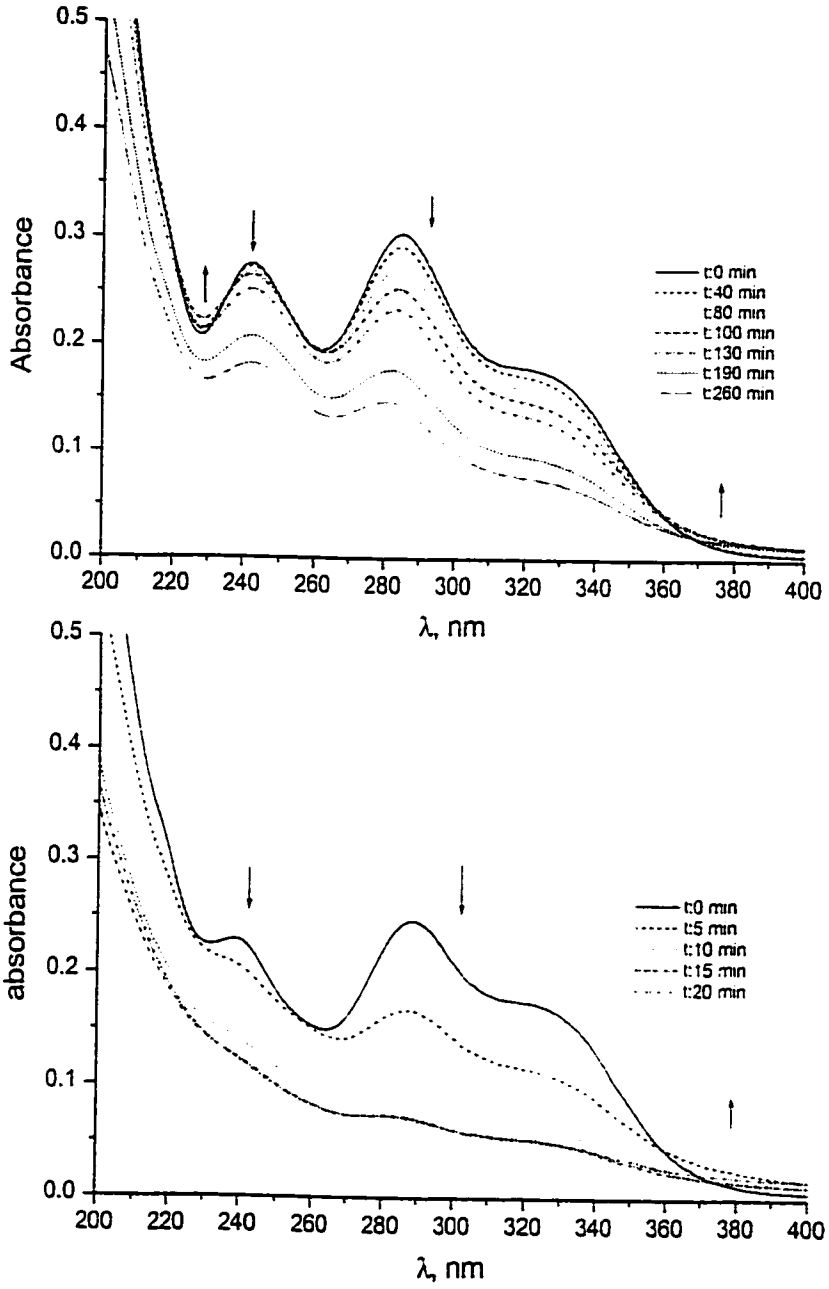

(A)

(B)

Figure 17. - (A) Illumination of Oxybenzone (8 mg L^{-1}) in water under aerobic conditions using a 1000-Watt Hg/Xe light source. (B) Irradiation of Oxybenzone (8 mg L^{-1}) and titanium dioxide (300 mg L^{-1}) also in water under aerobic conditions and under identical illumination conditions.

4. CONCLUDING REMARKS

In this Chapter we have examined the photostability of sunscreen active ingredients, the so-called "chemical filters" so noted in the commercial literature. They were Padimate-O, Oxybenzone, Octyl Methoxycinnamate, and Phenylbenzimidazole sulfonic acid examined in a variety of solvents from very polar to non-polar (e.g., water, mehanol, acetonitrile, and hexane). Photostability of a sunscreen lotions is a prime requirement for a commercial suncream to provide protection against the harmful UVA and UVB sunlight radiation. The results from the study may be summarized thus:

(1) Contrary to claims by sunscreen manufacturers, most of the commercial sunscreen lotions examined (about 10) are not waterproof as often claimed on the product label.

(2) The commercial lotions are not photochemically stable. This will have a dramatic consequence in the SPF number and in the efficacy of the commercial lotion to provide the claimed UV protection.

(3) The sunscreen active ingredients have been shown to be photochemically unstable in neat solvent media of various polarities. They undergo photochemistry, much of which still requires serious systematic studies to ascertain the modes through which the absorbed sunlight energy is dissipated.

It is clear that much remains to be done, first to understand exactly the photochemical changes that a chemical filter undergoes when illuminated with UVA/UVB sunlight under conditions that mimic as close as possible those encountered in usage of the sunscreen lotions. Second, there is a need to find one or more chemical filters that, while providing the needed UV protection, will be photochemically stable, and will be non-toxic to the skin and

to DNA. A physical filter such as zinc oxide and titanium dioxide need to be rendered harmless, that is their photocatalytic activity must be severely curtailed if they are to be used in suncare products.

5. REFERENCES

[1]. A.A. Shaw, L.A. Wainschel, and M.D. Shetlar, *Photochem.Photobiol.*, **55**, 657 (1992).

[2] B.L. Diffey and J. Robson, *J.Soc.Cosmet.Chem.*, **40**, 127 (1989).

[3] J. Knowland, A. McKenzie, P.J. McHugh, and N.A. Cridland, *FEBS*, **324**, 309 (1993).

[4] M. Gulston and J. Knowland, *Mutat. Res.*, **444**, 49 (1999).

[5] E. Damiani, L. Greci, R. Parson, and J. Knowland., *Free Radical Biology & Medicine*, **26**, 809 (1999).

[6] N.J. Turro, *Modern Molecular Photochemistry*, The Benjamin/Cummings, Menlo Park, CA, 1978.

[7] C.F. Chignell, B. Kalyanaraman, and R.P. Mason, *Photochem. Photobiol.*, **32**, 563 (1980).

[8] P. Morliere, O. Avice, and T.S.E. Melo, *Photochem. Photobiol.*, **36**, 395 (1982).

[9] B. Halliwell and J.M.C. Gutteridge, *Free Radicals in Biology and Medecine, 2nd Edn.*, Oxford: Clarendon Press, 1995, pp. 1-20.

[10] D.T. Sawyer, *Oxygen Chemistry*, Oxford University Press, New York, 1991, pp. 120-160.

[11] A. Deflandre and G. Lang, *Cosm.Sci.*, **10**, 53 (1988).

[12] J.M. Allen, C.J. Gossett, and S.K. Allen, *J. Photochem. Photobiol. B*, **32**, 33 (1996).

[13] W.H. Koppenol and J. Butler, *Adv. Free Radical Biol. Med.*, **1**, 91 (1985).

[14] H. Gonzenbach, T.J. Hill, and T.G. Truscott, *Photochem. Photobiol.*, **16,** 377 (1992).

[15] J.M. Allen, C.J. Gosset, and S.K. Allen, *Chem Res. Toxicol.*, **9,** 605 (1996).

[16] E. Knobler, L. Almeida, A.M. Ruzkowski, J. Held, L.Harber, and V. DeLeo, *Arch. Dermatol.*, **125,** 801 (1989).

[17] C. Stevenson and R.J.H. Davies, *Chem.Res.Toxicol.*, **12,** 38 (1999).

Chapter 11

FINAL CONCLUSIONS

"Nothing is final; it's only the beginning"

Titanium dioxide is a metal oxide that finds applications in several different fields. It is used as a high permittivity gate dielectric, as a paint pigment, and as a photocatalyst in pollution abatement; it is also used in medicinal applications, and as an active inorganic sunscreen agent to block UVA and UVB radiation in suncare products. The major focus of this thesis was lay principally on examining titanium dioxide as a photocatalyst in Heterogeneous Photocatalysis and as a physical inorganic sunscreen active agent. On the one hand, trough heterogeneous photocatalysis titanium dioxide is being exploited to detoxify polluted ecosystems, thus a very beneficial and desirable application. On the other hand, when titanium dioxide is used in sunscreen lotions, it inflicts serious damage to skin and to DNA. Undeniably, the use of titanium dioxide in suncream formulations remains a controversial issue. Major obvious concerns led us to explore the role of titanium dioxide in

both applications, which in the semiconductor world of titanium dioxide would play the dual role of Dr. Jeckyll and Mr. Hyde.

To protect the skin from UVA and UVB radiation, commercial sunscreens typically employ chemical filters in combination with physical filters (e.g. TiO_2 and ZnO) for protection against the harmful effects of UVA and UVB sunlight radiation. However, ultrafine TiO_2 particles irradiated with (simulated) sunlight has been demonstrated to be harmful to supercoiled plasmid DNA because of the hydroxyl radicals photogenerated on illuminated TiO_2 [1] (see Chapter 7). Indeed, TiO_2 causes single- and double-strand breaks in DNA, and photoexcited TiO_2 specimens extracted from commercial sunscreens show similar DNA damage and similar strand breaks in nuclei of whole human skin cells In the majority of sun lotions, both organic chemical filters and titanium dioxide (so-called) micronized particles are present. The former can photodegrade to produce free radicals, incur chemical changes, and interact with molecular oxygen to yield reactive oxygen species. It was imperative therefore to probe, through some preliminary studies, the photostability of chemical organic sunscreens, and to investigate any potential synergy between the organic active ingredients and titanium dioxide. The results show that the chemical suncreen agents are not photochemically stable. Similar investigations on about ten commercial sunscreen lotions show similar behavior: they are not photostable, a point that impinges seriously on the meaning of Sun Protection Factors (SPF numbers) and on the efficacy of the suncream to provide the UV protection manufacturers claim they do. In fact, in the presence of titanium dioxide the photodegradation of the chemical filters is considerably enhanced (Chapter 10).

Over the last two decades, application of titanium dioxide in heterogeneous photocatalytic processes has been examined and explored extensively as a potentially viable alternative technology to classical technologies for both environmental detoxification and for energy production. This technology employs illuminated semiconductor particulate materials, e.g. TiO_2, as photocatalysts to produce both reducing and highly oxidizing species on the particle surface poised to unleash redox processes in aqueous media, many of which would not otherwise occur by normal chemical means. Indeed of all the metal oxides, TiO_2 has been explored extensively in heterogeneous photocatalysis as a means to abate and detoxify polluted waters, air and soils.

Heterogeneous photocatalysis describes a process whereby illumination of a semiconductor particulate (e.g. TiO_2) with UV-visible light suitable to its bandgap energy ($\geq E_g$) ultimately generates thermalized conduction band electrons (e^-) and valence band holes (h^+) which, subsequent to their separation and other competitive photochemical and photophysical decay channels (see below), are poised at the particulate/solution interface ready to initiate redox chemistries. The energy level at the bottom of the conduction band (LUMOs) reflects the reduction potential of the photo-electrons, whereas the uppermost level of the valence band (HOMOs) is a measure of the oxidizing ability of the photo-holes. The flatband potenial, V_{fb}, fixed by the nature of the material and by proton exchange equilibria, determines the energy of the two charge carriers at the interface. Hence, reductive and oxidative processes for adsorbed couples with redox potentials more positive and more negative than the V_{fb} of the conduction and valence bands, respectively, can be driven by

surface-trapped e^- and surface-trapped h^+ carriers. Figure 1 illustrates a very simplistic fraction of the complex sequence of events that can take place in a semiconductor photocatalyst.

Irradiation of the semiconductor particle TiO_2 generates a bound electron/hole pair (the exciton), which can either recombine or dissociate to give a conduction band electron and a valence band hole. These separated charge carriers may also recombine, migrate to the

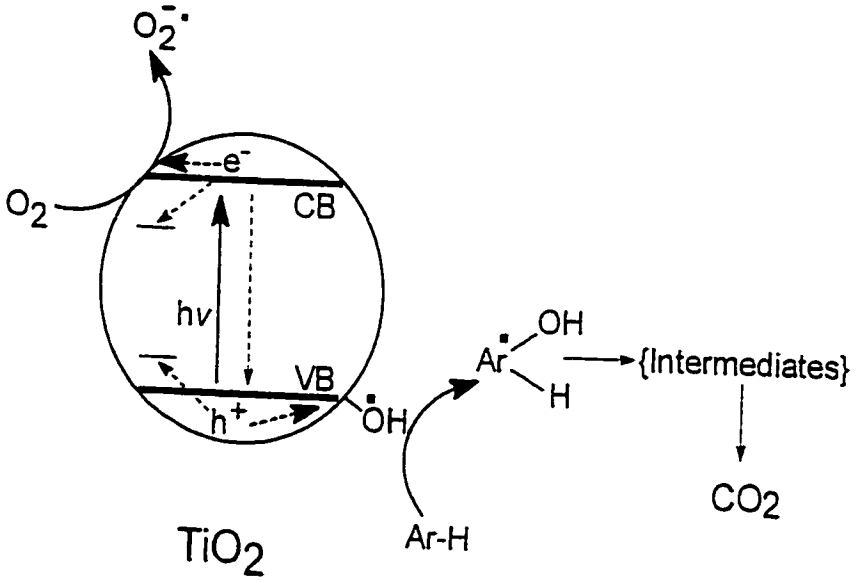

Figure 1.- Sequence of photophysical and photochemical events taking place upon irradiation of a TiO_2 particle in an air-equilibrated aqueous dispersion with $h\nu$ greater than E_g together with secondary reactions of the oxidized Ar-H to total mineralization to CO_2.

surface while scanning several shallow traps (anion vacancies and/or Ti^{3+} for the electrons; and oxygen vacancies or other defect sites for the hole). On the surface, both charge carriers

scan the surface visiting several sites to reduce pre-adsorbed electron acceptors (A_{ads}) and to oxidize pre-adsorbed electron donors (D_{ads}) in competition with surface recombination of the surface trapped electrons and holes (e^-_{st} and h^+_{st}) to produce light emission and/or phonon emission. In an air-equilibrated aqueous dispersion, oxygen is omnipresent on the particle surface and acts as an electron acceptor, whereas surface-bound OH^- groups and H_2O molecules act as electron donors to yield the strongly oxidizing •OH radicals. At concentrations of organic pollutants normally found in the environment (a few tens of mg L^{-1}) the •OH radicals are the primary oxidizing entities to produce, in the case of an aromatic substance, the corresponding •OH-adduct (a cyclohexadienyl radical [5]) that ultimately breaks down into a variety of intermediate products on the way to total mineralization to carbon dioxide.

The function of photo-excited semiconductor particles then is to act as pools of electrons and holes which can be exploited in several multi-electron transfer processes [4]. Reactions 1 to 6 summarizes the main steps:

$$TiO_2 \xrightarrow{h\nu} TiO_2(e^-/h^+) \rightarrow e^-_{cb} + h^+_{vb} \quad \text{(generation/separation)} \quad (1)$$

$$e^-_{cb} + h^+_{vb} \rightarrow e^-_{tr} + h^+_{tr} \quad \text{(lattice and/or surface trapping)} \quad (2)$$

$$e^-_{cb} + h^+_{vb}\,(\text{and/or } h^+_{tr}) \rightarrow \text{recombination} \quad (h\nu' \text{ and phonon emission}) \quad (3)$$

$$e^-_{cb}\,(\text{and/or } e^-_{tr}) + h^+_{vb} \rightarrow \text{recombination} \quad (h\nu'' \text{ and phonon emission}) \quad (4)$$

$$e^-_{tr} + h^+_{tr} \rightarrow \text{recombination} \quad (h\nu''' \text{ and phonon emission}) \quad (5)$$

$$Ti\text{-}{}^{\bullet}OH + RH \rightarrow \rightarrow \rightarrow \ldots\text{.photooxidations} \quad (6a)$$

$$e^-_{tr} + \text{compound} \rightarrow \rightarrow \rightarrow \text{....photoreductions} \qquad (6b)$$

where e^-_{tr} is a trapped electron (e.g., as Ti^{3+}) and h^+_{tr} is a trapped hole denoted here [3.6] as a surface-bound •OH radical, i.e. as Ti-•OH. Close examination of the field disclosed serious gaps in our understanding of the basic elements that underlie heterogeneous photocatalysis.

Issues that required a collective fundamental understanding of heterogeneous photocatalysis are the description of (i) photocatalysis, (ii) quantum yields, and (iii) turnover numbers, rates and frequencies.

In spite of the large and excellent body of literature demonstrating the utility of TiO_2 in heterogeneous photocatalysis, understanding the (primary) events in photocatalysis has lagged somewhat behind. Therefore, this thesis addresses some of the issues that have been objects of some debate in heterogeneous photocatalysis. For example such issues as: (i) a description of process efficiencies (Chapters 2 and 3); (ii) a description of what photocatalysis means and what turnover quantities symbolize (Chapter 4); and (iii) the spectral dependency of quantum yields and photonic efficiencies, together with wavelength selectivity of photocatalyst (Chapter 5). This latter study demosntrates that the "classical" view of the band model of semiconductors needs to be revisited to accomodate the new findings reported herein.

One of the major issues has been the lack of an appropriate protocol to compare the activities of different photocatalysts in different heterogeneous systems. The quantitative

description and characterization of photo-induced processes in such heterogeneous systems remained a matter of considerable interest but also one of controversy. In this regard, a protocol for measuring quantum yields of heterogeneous photocatalytic processes, Φ, was developed and in this thesis (Chapters 2 and 3) and later proposed to the International Union of Pure & Applied Chemistry (IUPAC) for adoption as a standard protocol [2,3].

A few parameters had been suggested earlier for the characterization of photocatalytic activities in heterogeneous systems. One was the photonic efficiency ξ which expresses the ratio between the rate of molecules formed or degraded in the system, dN_r/dt (molecules s^{-1}) to the rate of incident photons impinging on the system, $dN_{hv}(inc)/dt$ (photons s^{-1}) at some given wavelength (some workers had incorrectly taken ξ to be equivalent to the quantum yield). In other words, photonic efficiency is a reaction rate normalized to the photon flow from the light source that describes how many molecules are transformed per photon incident on the system.

Another parameter used to characterize the photochemical activity of heterogeneous systems is of course the more fundamental quantum yield (Φ: equation 7) of the photo-

$$\Phi = \frac{\dfrac{dN_r}{dt}}{\dfrac{dN_{hv(abs)}}{dt}} \qquad (7)$$

reaction defined in homogeneous photochemistry as the ratio between the rate of molecules

formed or converted in the system, dN_r/dt (molecules s^{-1}) to the rate of photons actually ***absorbed*** by the system, $dN_{h\nu}(abs)/dt$ (photons s^{-1}) at some given wavelength. Thus, Φ represents how many molecules are transformed per photon actually absorbed. The essential difference between photonic efficiency ξ and quantum yield Φ in heterogeneous photochemistry is that not every incident photon will necessarily act upon the heterogeneous system and initiate the chemical transformation. Consequently, and especially for weak absorption of light, although the photonic efficiency may be close to 0, the quantum yield may nevertheless reach high values. Appropriate determination of the fraction of absorbed light in heterogeneous systems had rendered the measurements of quantum yields a complex issue.

Using the above definition of photonic efficiencies and quantum yields, in the course of our studies it became imperative to assess the spectral dependence of the parameters for the photodegradation of phenol and 4-chlorophenol based on theoretical findings by Dr. Emeline of this laboratory. Indeed, we suspected that the quantum yields of loss of phenol and chlorophenol were spectrally dependent in spite of the conventional band model of semiconductors which predicted rapid thermalization of the photogenerated charge carriers to the lowest energy levels in their respective conduction and valence band states. The results reported in Chapter 5 and elsewhere [4]) contrast with expectations based on the classical band model. The experimental results clearly point to the need for a reconsideration of the band model to take into account the existence of conduction band states and valence band states that may not communicate effectively with each other within their respective

bands. Lack of this communication bears on the various factors that affect the properties of charge carriers , and consequently on the photocatalytic process.

The conventional band model defines the semiconductor in terms of two bands: the valence band which is typically composed of $2p$ orbitals of the oxide O^{2-} ions in a metal oxide semiconductor, and of a conduction band typically made up of the n d orbitals of the M^{x+} ions. These two bands are separated by a forbidden band gap (E_{BG}) within which there may exist surface states (ss). These bands are also thought to consist of a very large number of closely spaced energy levels, such that when the semiconductor is illuminated with light of energy greater than the bandgap energy E_{BG} to generate free charge carriers, these carriers are expected to thermalize rapidly to the lowest energy level of the conduction band (CB) for electrons and to the "lowest energy level" of the valence band (VB) for the holes.

Conventional wisdom has always dictated that whatever the ensuing redox reactions may be, they will take place from the lowest energy levels of a given charge carrier and thus there should be no spectral dependence of the quantum yields, or whatever other parameter is employed to assess the efficiencies of photons. The conventional band model of semiconductors alluded to earlier and based on the concept of continuity of carrier states within the solid's valence and conduction bands, which infers fast thermalization of the hot carriers, requires revisiting.

We also addressed (see Chapter 4) the usage of and provided a kinetic description of the three turnover quantities: turnover number (TON), turnover rate (TOR) and turnover frequency (TOF) [5]. As they bear on the (photo)catalytic activity of a given material in

heterogeneous solid/liquid or solid/gas (photo)catalysis we examined these quantities to quantify catalytic activity of TiO_2 and similar (photo)catalysts. Unlike the requirement to determine TOF, the quantities TON and TOR require knowledge of the number of active sites on the (photo)catalyst's surface. Most significant, these turnovers depend on the nature of the active state of the (photo)catalyst, and hence on how the active centers are described. In heterogeneous (photo)catalysis, one of the prime difficulties with describing the turnover rate and turnover number is how to specify the number of surface active sites. It has become common practice to substitute this quantity by the specific surface area of the catalyst particle (BET surface area procedure by physical adsorption of nitrogen or argon at low temperature). However, the BET surface area reflects the number of adsorption sites and not necessarily the number of catalytically active sites. Indeed, an active site will have a finite lifetime for various processes, determined by such factors as inactivation through poisoning by impurities.

In as much as the key to change the activity of photocatalysts hinges on the number and types of surface active sites on metal oxide surfaces, we modified homemade TiO_2 colloids and several other titania specimens obtained from various commercial sources to produce photo-inactive TiO_2 systems. Their photo-activity was probed using the photooxidation of phenol, and damage caused to DNA plasmids, to human cells and to yeast cells (see Chapter 9). Considering that titanium dioxide particle can reflect, scatter, and absorb at all UV wavelengths, that they have high SPF numbers, and exceptional cosmetic acceptability, we had sokme degree of success in inactivating titanium dioxide specimens for

the sole purpose to employ them as safer physical sunscreen active agents, than what is presently employed in commercial sunscreen lotions. The results provided here do demonstrate that these modified titanium dioxide specimens are inconsequential in their potential toxicity when illuminated in contact with plasmid DNA, whole human skin cells and yeast cells. The survival rate of these three probes is remarkable.

REFERENCES

[1] R. Dunford, A. Salinaro, L. Cai, N. Serpone, S. Horikoshi, H. Hidaka, and J. Knowland, *FEBS Letts.*, **418**, 87 (1997).

[2] N. Serpone and A. Salinaro, *Pure Appl.Chem.*, **71**, 303 (1999).

[3]. A. Salinaro, A.V. Emeline, J. Zhao, H. Hidaka, V.K. Ryabchuk and N. Serpone, *Pure Appl.Chem.*, **71**, 321 (1999).

[4] A.V. Emeline, A. Salinaro, and N. Serpone, *J. Phys. Chem. B*, **104**, 11202 (2000).

[5] N. Serpone, A. Salinaro, A.V. Emeline, and V.K. Ryabchuk, *J.Photochem. Photobiol.A:Chem.*, **130**, 83 (2000).